Petrographic and Geochemical Study of the Hybrid Rock Unit Associated with the Current Lake Intrusive Complex

A THESIS
SUBMITTED TO THE FACULTY OF
UNIVERSITY OF MINNESOTA
BY

Matthew Ryan Chaffee

IN PARTIAL FULFILLMENT OF THE REQUIREMENTS
FOR THE DEGREE OF
MASTER OF SCIENCE

Advisor
Dr. James Miller

June 2015

Acknowledgements

I would like to thank my advisors, Dr. Jim Miller and Dr. Pete Hollings, for all their guidance, support, and, most importantly, patience through the entirety of this project. I would also like to thank Magma Metals, LLC for the great opportunity to work on the Current Lake Intrusive Complex and for the analytical funding necessary for the completion of this thesis. I would like to further extend my gratitude to Al MacTavish and Dr. Geoff Heggie for the help, support, and insights they contributed to this project. I would like to thank my mother and father, Lenna and Jerry, for their guidance and support throughout my life and for encouraging me to pursue my passions. I also thank my wife, Steph Theriault, whom I met while attending UMD, for her support and encouragement, which included constant reminders to keep working toward completing this project. Lastly, I want to thank my family and friends who have helped or supported me in some way over the past few years while I worked on this project.

Abstract

The Current Lake Intrusive Complex (CLIC) is one of several ultramafic to mafic intrusions associated with the Midcontinent Rift that host Ni-Cu-PGE deposits. Geophysical surveys and drilling have outlined a six kilometer-long mafic to ultramafic, chonolith-shaped intrusion that is composed primarily of wehrlite to dunite and has intruded into granitic (Current Lake Zone or CLZ) and metasedimentary rocks (Beaver Lake Zone or BLZ) of the Quetico Subprovince.

Initial core logging conducted by Magma Metals (now Panoramic Resources Ltd.) noted the occurrence of a zone of texturally and mineralogically heterogeneous, intensely altered, inclusion-bearing, mafic to intermediate intrusive rocks located at the margins of the main mineralized body. These intrusive rocks were initially referred to as the Hybrid Rock unit (HRU), and due to subtle differences in color, were subsequently spilt into the “red hybrid” and “gray hybrid” units.

Observations from core logging and petrography of the “red hybrid” show it to be an intensely altered and hematized, locally poorly mineralized, vari-textured (prismatic to subophitic), fine- to medium-grained, quartz gabbro to lesser quartz ferrodiorite. The mineralogical, textural, and chemical characteristics of this rock type are similar in both the CLZ and BLZ, with the exception that the BLZ contains large, chlorite-mantled quartzite and granitic xenoliths and has more abundant interstitial quartz. Some of the “grey hybrid” rocks were found to be very similar to “red hybrid” rocks and were thus renamed the Heterolithic Quartz Gabbro (HQG) unit in both the CLZ and BLZ.

Further petrographic investigations of the non-HQG “grey hybrid” rocks indicated a mineralogical and textural resemblance to the CLIC rocks as they were moderately to intensely altered, fine- to medium-fine grained, intergranular to subpoikilitic quartz-bearing feldspathic wehrlite to melagabbro in the BLZ and gabbro to melagabbro in the CLZ. Consequently, the non-HQG “grey hybrid” rock were renamed the Melagabbro unit in both the CLZ and BLZ. In both zones, the Melagabbro unit is observed as the marginal phase of the CLIC rocks.

The principal goals of this study were to document the mineralogical, textural, chemical, and alteration attributes of the HQG and Melagabbro units, the nature of their lithologic heterogeneity, and transition into the CLIC rocks, as well as to establish the petrogenetic relationship, if any, between the HQG and Melagabbro units to the CLIC rocks.

Evaluation of lithogeochemical data indicate that despite the intense felsic contamination and hydrothermal alteration, the trace element characteristics of the HQG unit are consistent with having similar parental magma as the CLIC rocks. These data also indicate that the granitic and metasedimentary country rocks of the Quetico Subprovince are a reasonable source of contamination. These results and the contact relationships between the HQG unit and the CLIC rocks are best explained by a two-stage model of emplacement. First, as the HQG unit was emplaced it incorporated abundant country rock xenoliths, becoming strongly contaminated, and extensively hydrothermally altered. Then, the CLIC mafic magma was emplaced into the HQG unit, likely by reaming out and inflating the semi-molten core of the HQG intrusion.

Table of Contents

List of Tables

List of Figures

Appendices

1.0 Introduction

The Current Lake Intrusive Complex (CLIC) is one of several mineralized ultramafic to mafic intrusions associated within the Midcontinent Rift (MCR) that host Ni-Cu-PGE deposits (Heggie, 2005; Hollings et al., 2007b; Ware et al., 2008; Rossell, 2008; Ding et al., 2010; Goldner, 2011; Foley, 2011; Miller and Nicholson, 2013). Largely unexposed in the Current Lake area, about 50 kilometers northeast of Thunder Bay, Ontario, the CLIC was discovered by Magma Metals Ltd. (now Panoramic Resources Ltd.) in 2001 when ultramafic glacial boulders with disseminated sulfides were located along the shores of Current Lake (MacTavish and Smyk, 2010; Goodgame et al., 2010). An aeromagnetic survey was conducted in July 2006, showing a linear anomaly beneath Current Lake (Panoramic Resources LTD, 2014). Drilling began in December 2006 and confirmed the presence of Ni-Cu-PGE mineralization hosted by an ultramafic intrusion (Panoramic Resources LTD, 2014).

The aeromagnetic survey and subsequent drilling of over 620 holes, as of April 2011, revealed that the CLIC is a six-kilometer-long, mafic-ultramafic, tube-like intrusion (chonolith) emplaced in the metasedimentary and granitoid rocks of the Archean Quetico Subprovince (Panoramic Resources LTD, 2014). Over the course of drilling, it was discovered that a heterogeneous intrusive rock unit commonly occurs at the margins of the mineralized ultramafic intrusion. This occurrence was called the Hybrid Rock unit (HRU). The close spatial relationship between the HRU and the CLIC raised the obvious question as to whether these two intrusions were petrogenetically

related. If they were, this suggested that the occurrence of the HRU could be used as an exploration indicator of nearby ultramafic mineralization.

1.1 Geologic Setting

The CLIC was emplaced during an early phase of 1.1 Ga MCR magmatism in the vicinity of an unconformity between granitic and metasedimentary rocks of the Archean Quetico Subprovince and flat-lying sedimentary rocks of the Mesoproterozoic Sibley Group. The CLIC occurs on the southwestern margin of the Nipigon Embayment (Fig. 1.1), a northwest-trending aulocogen that has been cited by some (e.g., Van Schmus, 1992) as a possible failed third arm of the MCR. Within the Nipigon Embayment, sedimentary rocks of the Sibley Group were intruded by several extensive diabase sills (Nipigon Sills) and smaller ultramafic intrusions, both of which are related to early rift magmatism (~1112-1106 Ma) based on U-Pb age dating and paleomagnetic polarity (Hart et al., 2005; Heaman et al., 2007; Hollings et al., 2007b, 2007c).

The Quetico Subprovince represents one of several east-west trending subprovinces in the Archean Superior Province (Fralick et al., 2006). It is bounded by crustal-scale faults and bordered by the Wabigoon Subprovince to the north and the Wawa Subprovince to the south (Fig. 1.1). The Quetico consists of dominantly detrital metasedimentary rocks, granitic intrusions, and associated migmatite. The metamorphic grade of this subprovince displays a symmetrical distribution, with higher grade (amphibolite) rocks located near the central axis and lower grade (greenschist) rocks near the bordering Wabigoon and Wawa Subprovinces (Card and Poulsen, 1998). U-Pb ages of zircons from the Quetico Subprovince cluster around 2.7 Ga (Davis et al., 1990).

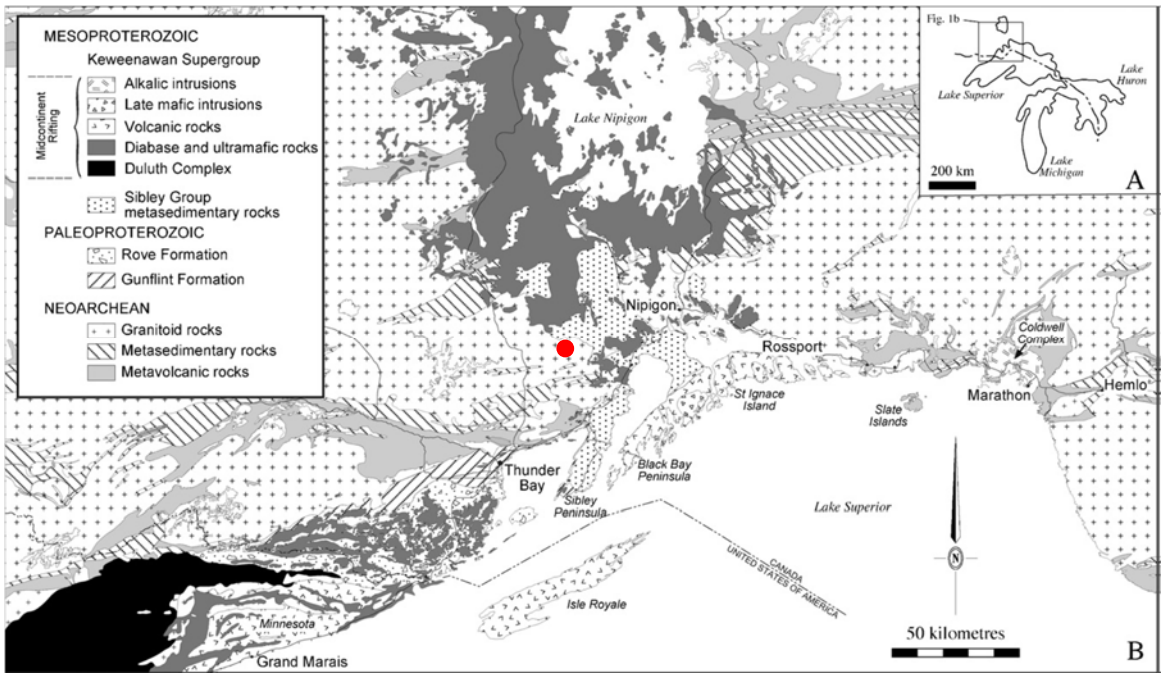

Figure 1.1 – General geology of the Thunder Bay area showing the location of the CLIC (red dot). From Hollings et al. (2010).

The Mesoproterozoic Sibley Group is located along the northern coast of Lake Superior and in the Lake Nipigon area (Fig. 1.1). It is a flat-lying, unmetamorphosed sedimentary succession consisting of a mixture of siliciclastic and chemical sedimentary rocks (Metsaranta, 2006). The sedimentary environment of deposition for the Sibley Group is interpreted to be lacustrine with a gradual transition into a saline playa lake environment (Fralick et al., 2000). Geochronological studies and field relationships constrain the depositional age range of the Sibley sediments between 1339 and 1537 Ma (Franklin, 1978; Davis and Sutcliffe, 1985).

The CLIC is an early ultramafic intrusion associated with the MCR. Studies have shown that the 1.1 Ga MCR, which is well exposed in the Lake Superior region (Fig. 1.2), is one of the best-preserved large igneous provinces of Precambrian age (Miller,

2007). The full extent of the MCR is known from its arcuate 2,500 km-long magnetic and gravity anomaly that crosses several geologic provinces (Van Schmus, 1992). The rift arcs across Late Archean (2.8-2.6 Ga) granite-greenstone terranes of the Superior Province in the Lake Superior region, with the western arm extending south to Kansas, crossing various Paleoproterozoic terranes, and the eastern arm passing beneath the Michigan Basin, abruptly ending at the Grenville Front.

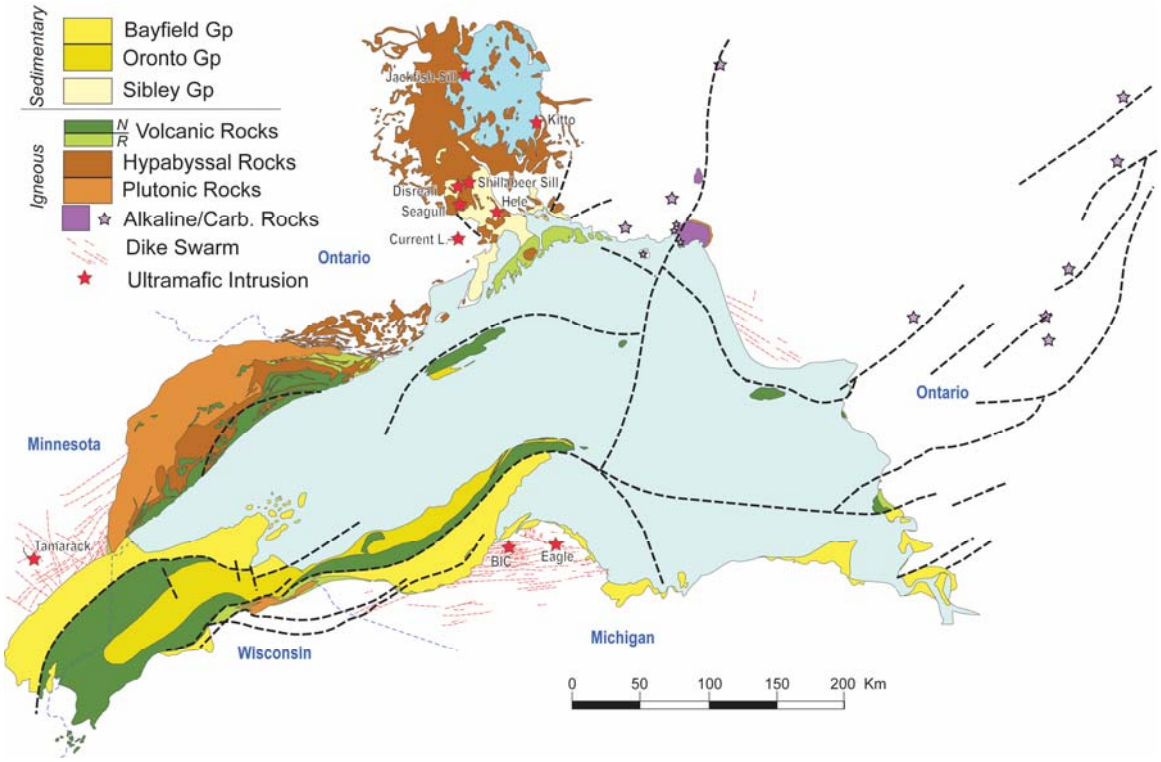

Figure 1.2 – Geology of the MCR in the Lake Superior region showing the distribution of ultramafic intrusions including the CLIC (Current L.). Modified from Miller and Nicholson (2013).

The MCR consists of predominantly mafic volcanic and intrusive rocks that were emplaced within an approximately 25 m.y. period (Nicholson et al., 1997; Heaman et al.,

2007). Mafic magmatism has been attributed to the upwelling and decompression melting of a starting mantle plume (Hutchinson et al., 1990; Nicholson and Shirey, 1990; Cannon, 1994; Shirey, 1997), though this interpretation has recently been challenged (Hollings et al., 2012; Hollings and Heggie, 2014). Felsic rocks comprise 5-20% of the rift fill and are represented by rhyolite flows and large granophyre intrusions (Green, 1982). Radiogenic isotope compositions of felsic rock have been interpreted to be formed via partial melting of pre-rift crust (Vervoort et al., 2007).

Geochemistry of the MCR igneous rocks, constrained by U-Pb zircon ages and magnetic polarity, have led to the interpretation that rift magmatism can be divided into at least four stages (Miller and Vervoort, 1996; Nicholson et al., 1997; Vervoort et al., 2007; Miller and Nicholson, 2013):

1) Early magmatic stage (1110-1106 Ma): dominated initially by the emplacement and eruption of primitive mantle-derived, mafic to ultramafic magmas during reversed magnetic polarity. As will be discussed below, the CLIC magmas were generated during this phase of the early stage of MCR magmatism. The initial emplacement of primitive magmas quickly gave rise to evolved and contaminated mafic magmas and the appearance of felsic crustal melts. Intrusive rocks of these evolved magmas are represented by the ferrogabbroic Logan and Nipigon Sills, the early gabbroic and felsic series of the Duluth Complex, and the alkaline to mafic rocks of the Coldwell Complex (Fig. 1.2).
2) Latent magmatic stage (1106-1100 Ma): characterized by a hiatus in mafic magmatism and only minor felsic volcanism. During this stage, magnetic polarity

shifted from reversed to normal, though an extra reversal may have occurred based on the sequence observed in the Mamainse Point volcanics in eastern Lake Superior (Fig. 1.2; Klewin and Berg, 1990). Miller and Vervoort (1996) suggest that this stage represents a period of extensive magma underplating and continued melting of the lower crust that lead to the production of felsic melts. The development of felsic liquids created density and rheologic barriers that promoted underplating of mafic magmas.

3) Main magmatic stage (1100-1094 Ma): occurred during a period of normal magnetic polarity and is characterized by renewed magmatic activity throughout the MCR. During this stage, volcanism involved variably differentiated, but uncontaminated mafic compositions, as well as intermittent felsic eruptions (Green, 1982). Concurrent with this volcanism was the emplacement of tholeiitic mafic magmas that formed the anorthositic and layered series of the Duluth Complex, the Beaver Bay Complex, the Mellen Complex, and other hypabyssal intrusions (Fig. 1.2; Miller and Severson, 2002; Miller and Green, 2002). Intrusive felsic magma, generated by crustal melting, were also emplaced to create large granophyre intrusions (Vervoort et al., 2007).
4) Late magmatic stage (1094-1086 Ma): characterized by the waning of flood-basalt volcanism. Soon after the termination of volcanism many of the graben-bounding normal faults were inverted into reverse faults in response to Grenville tectonism (Cannon, 1994).

With many mafic to ultramafic intrusions in the Nipigon Plate area yielding U-Pb ages on baddeleyite and zircon as old as 1120 Ma (Heaman et al., 2007; Hollings et al., 2010), Miller and Nicholson (2013) recently proposed a fifth magmatic stage, which they termed the initiation stage occurring between 1120 and 1110 Ma. This stage was interpreted as being related to crustal upwelling associated with the initial starting plume impact and suggested that any volcanic rocks erupted during this stage were largely eroded before a central graben developed and thus able to preserve the volcanic edifice. However, Hollings and Heggie (2014) have recently questioned the validity of the plume model stating the absence of primary ultramafic magmas and lack of radiating dike swarms suggest that a passive rifting model may be more appropriate for the MCR.

In the Thunder Bay-Lake Nipigon area, rocks associated with the MCR include volcanic units of the Osler Group, mafic sills of the Nipigon and Logan suites, and a collection of small ultramafic-mafic intrusions (Hollings et al., 2007a, 2007b, 2010). Most volcanic rocks and all intrusions are associated with the initiation or early stages of MCR magmatism as they are reversely polarized and yield U-Pb ages between 1120 and 1107 Ma (Heaman et al., 2007; Hollings et al., 2010).

The Osler Group is located on the northern coast of Lake Superior along the Black Bay Peninsula (Figs. 1.1 and 1.2). It consists predominantly of variably evolved tholeiitic basalt flows and minor rhyolites (Lightfoot et al., 1991; Hollings et al., 2007a). Most of the sequence is reversely polarized, but the uppermost sequence has normal polarity and evidently erupted during the main magmatic stage of the MCR. The lowermost 100 m of the Osler Group contain abundant sandstones and conglomerates of

the Simpson Island Formation, which unconformably overlies the sedimentary rocks of the Sibley Group (Hollings et al., 2007a).

Hollings and coworkers (Hollings et al., 2007b, 2007c, 2010, and 2012) recognized five distinct geochemical groups among the diabase sills emplaced in the Thunder Bay-Nipigon area during the early stages of the MCR. Heaman et al. (2007) have reported ages generally ranging between 1120-1108 Ma, but have discovered some intrusions as old as 1150 Ma that they attribute to MCR magmatism. The sills commonly intrude into the Sibley Group sedimentary rocks, but some are floored in Archean rocks of the English River, Wabigoon, and Quetico Subprovinces (Hart and MacDonald, 2007).

Prior to the sill complexes, small ultramafic-mafic intrusions, commonly displaying Ni-Cu-PGE sulfide mineralization, were emplaced (Fig. 1.2). In the Nipigon Embayment area, these intrusions include the Seagull, Disraeli Lake, Hele, Kitto, and Current Lake (Heggie, 2005; Hart and MacDonald, 2007; Hollings et al., 2007b) and are described as plug-, sill-, and tube-like in shape (Hart and MacDonald, 2007). Typically, the rocks display cumulate textures and are composed of peridotite cores with margins of olivine gabbro to olivine melagabbro (Hollings et al., 2007b). Emplacement of the ultramafic intrusions, along with the mafic sills, appear to have been structurally controlled by a series of north and northwest trending faults (Hart et al., 2005). Disseminated to massive Ni-Cu-PGE-enriched sulfide is most concentrated in the marginal and feeder zones of these intrusion implying that mineralization was triggered by country rock contamination (Miller and Severson, 2002; Miller and Green, 2002).

Of these intrusions, the Seagull is the most studied and can be divided into an upper mafic and lower ultramafic component (Heggie, 2005). The upper unit consists of alternating gabbroic and pyroxenitic rocks, whereas the lower unit is predominately peridotite. PGE-enriched Cu-Ni sulfide mineralization of the Seagull is confined to the lower unit. U-Pb ages date extracted from baddeleyite indicate emplacement of the ultramafic intrusion during the early magmatic stage. Specific ages for the various intrusions include: 1109 ± 1.5 Ma for Disraeli, 1112.8 ± 1.4 Ma for Seagull, 1106.6 ± 1.5 Ma for Hele, and 1117.5 ± 3.7 Ma for Kitto (Heaman et al., 2007).

Similar Ni-Cu-PGE mineralized mafic to ultramafic intrusions associated with early magmatism of the MCR are found elsewhere in the Lake Superior region (Fig. 1.2). These include the Eagle and Bovine Igneous Complex (BIC) in Upper Michigan (Ware et al., 2008; Rossell, 2008; Ding et al., 2010; Foley, 2011) and Tamarack in Minnesota (Goldner, 2011). All of these intrusions were emplaced into sulfidic argillites and arenites of the Paleoproterozoic Animikie Basin. The major lithologies of the intrusions consist of lherzolite, wehrlite, pyroxenite, gabbronorite, and gabbro.

All these early ultramafic intrusions share several features in common besides their significant Ni-Cu-PGE mineralization (Miller and Nicholson, 2013). One is that they are dominated by olivine and olivine-pyroxene cumulates. The principal pyroxene is clinopyroxene in some intrusions such as BIC and Seagull, but is both clinopyroxene and orthopyroxene in others such as Eagle and Tamarack. Plagioclase and Fe-Ti oxide become cumulus phases in the upper differentiated parts of the Tamarack, BIC, and Seagull intrusions (Heggie, 2005; Goldner, 2011; Foley, 2011). Another common feature

is the significant abundance of primary amphibole and biotite. Collectively, these attributes indicate that the intrusions were formed from volatile-enriched, sulfide-saturated mafic parent magmas (Heggie, 2005; Goldner, 2011; Foley, 2011). Sulfur isotope data indicate that the sulfide was derived largely from contamination by Paleoproterozoic and Archean crustal sources (Ripley and Li, 2009)

1.2 Discovery and Exploration of the Current Lake Intrusive Complex

In 2001, Graham Wilson and Gerald Harper discovered glacially-transported, mineralized peridotite boulders along the western shore of Current Lake (Goodgame et al., 2010). Samples collected from these boulders assayed up to 9.5 g/t Pt+Pd+Au, 1% Cu and 0.3% Ni. In 2005, Magma Metals Limited[1] optioned the claims from Wilson and Harper. In May 2006, several more mineralized peridotite boulders were discovered along the eastern shore of Current Lake. This discovery led to the beginning of an ongoing drilling project in December 2006. The first drill hole intersected 10.5 meters of disseminated mineralization averaging 1.4 g/t Pt, 1.3 g/t Pd, 0.5% Cu, and 0.3% Ni (Goodgame et al., 2010). Subsequent geophysical surveys and roughly 145,000 meters of drilling have outlined a 6 kilometer long mafic-ultramafic magma conduit showing a core of mineralization that widens out to a more sheet-like intrusion at its southeastern extent (Figs. 1.3 and 1.4).

In plan view, the CLIC has been divided into the following regions: the Current Lake Zone (CLZ), the Bridge Zone, the Beaver Lake Zone (BLZ), the Beaver Lake East

[1] Panoramic Resources (Perth, Australia) acquired Magma Metals Ltd. in mid-2012.

Zone, 437 Zone, and the Southeast Anomaly (Fig. 1.3). In cross section, the CLZ, Bridge Zone, and BLZ display the chonolithic form of its mineralized ultramafic core (Fig. 1.4).

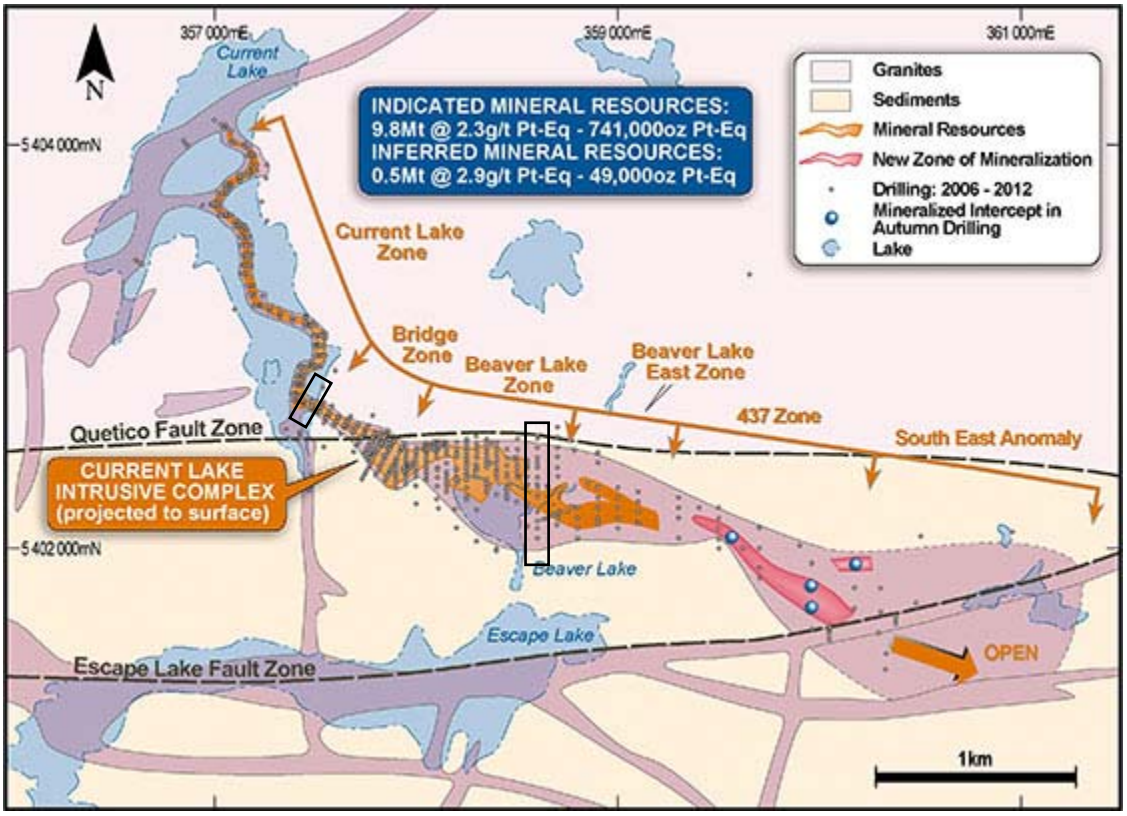

Figure 1.3 – Schematic geological map of generalized geology and drilling density of the CLIC and related intrusions. The CLIC is divided into several zones based on intrusion shape and country rock. Black rectangles outline the locations of drill core sampled for this study from the CLZ and the BLZ (Panoramic Resources Ltd., 2014).

A.

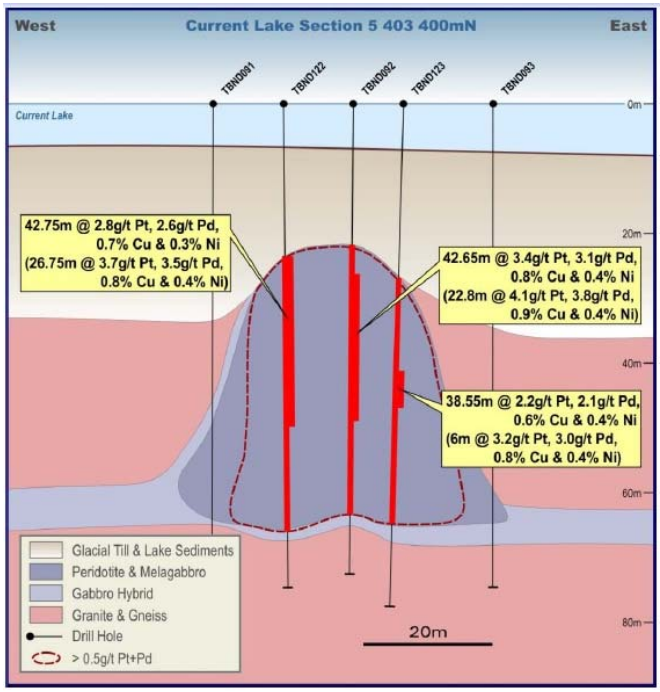

B.

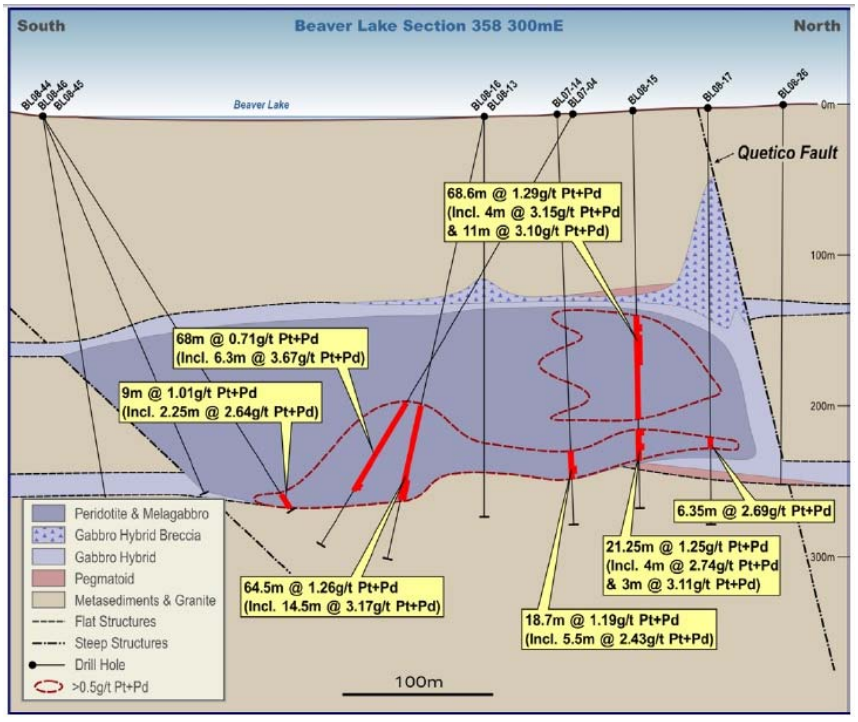

Figure 1.4 – Cross sections of the CLIC in the CLZ (A) and the BLZ (B) showing general lithologies and areas of mineralization. From Magma Metals' old website: http://media.corporateir.net/media_files/IROL/19/198021/ currentlake.jpg)

The main lithologies of the CLIC are feldspathic dunite, lherzolite, and olivine melagabbro (Goodgame et al., 2010). Feldspathic dunite, which makes up the core of the CLIC (Fig. 1.4), consists of 50-70% olivine (typically altered to serpentine), 10-25% plagioclase, 4-12% clinopyroxene, and orthopyroxene, and approximately 5% magnetite. Lherzolite contains more olivine and pyroxene, less plagioclase and little to no serpentine. Melagabbro consists of 40-70% olivine, commonly altered to serpentine, 10-25% plagioclase, 4-12% clinopyroxene, and 5% magnetite (Goodgame et al., 2010). Sulfide minerals include pyrrhotite, chalcopyrite, pentlandite, pyrite, cubanite, and violarite. The main platinum group minerals are moncheite, michenerite, and platarsite (Goodgame et al., 2010).

Commonly in close spatial association with the mineralized ultramafic rocks of the CLIC is a structurally and lithologically complex network of intrusive rocks, including altered and locally inclusion-rich, mafic to intermediate rock types, Magma Metals termed this intrusive network the HRU, which is the focus of this study. It typically occurs marginal to the main ultramafic chonolith, but often forms subhorizontal "wings" that project hundreds of meters away from the main body (Fig. 1.4). Like the main CLIC chonolith, the HRU is interpreted to have intruded along sub-horizontal structures in the Archean metasedimentary rocks and granites, and assimilated large amounts of country rock. Contact relationships between the HRU and rocks of the CLIC can be irregular, gradational, or sharp. Hybrid rocks near contacts with country rocks commonly show strong hematite alteration.

1.3 Goals and Objectives

The principal goals of this study were:

1. Document the mineralogical, textural, chemical, and alteration attributes of the HRU, the nature of its lithologic hetereogeneity, and its transition into the main mineralized ultramafic intrusion of the CLIC; and
2. Establish the petrogenetic relationship, if any, between the HRU and the CLIC ultramafic rocks.

The first of these goals was accomplished largely by re-logging core, petrographic study, and lithogeochemical analysis of HRU samples collected from drill core that profile the CLIC in the CLZ where the country rock is granite, and in the BLZ where the country rock is metasedimentary (Fig. 1.3). The second goal was addressed by evaluating macro- and microscopic characteristics of the contact relationship between the HRU and the mineralized ultramafic intrusion of the CLIC, as well as comparing their geochemical attributes.

Some specific questions that were addressed by this study are:

- Recognizing that the HRU is an intensely altered, heterogeneous intrusive unit, what were its original igneous rock types?
- What are the types and possible origins of inclusions that occur within the HRU?
- Was the HRU formed in a single or multiple emplacement event?
- What was the parental magma composition(s) of the HRU and to what extent was it modified by country rock contamination and hydrothermal alteration?
- What do the contact relationships between the HRU and the mineralized

ultramafic intrusion imply about their emplacement histories?

- Factoring in the contamination and alteration of the HRU, could it be petrogenetically related to the mineralized ultramafic intrusion?

2.0 Methods

In order to address the goals and objectives and answer the petrogenetic questions posed above, several methods of investigation were utilized including core logging, transmitted light petrography, scanning electron microscopy, and lithogeochemical analysis. The zoning of igneous lithologies in the HRU and CLIC (e.g., Fig. 1.4) was studied macroscopically by detailed core logging of portions of ten drill cores containing intersections of the HRU; six from the CLZ and four from the BLZ. Transmitted light petrography was used to determine the primary and secondary mineralogical, textural, and alteration characteristics of the HRU unit and its transition into the ultramafic intrusion. Due to intense alteration that typically involved very fine-grained phases, the energy dispersion spectrometer-equipped scanning electron microscope (EDS-SEM) at the University of Minnesota Duluth (UMD) was used to assist in identification of primary and secondary minerals not readily identified with standard petrography. The SEM was also used to determine the compositions of unaltered primary mineral phases and identify any cryptic variations of pyroxene and olivine that may be present. Whole rock geochemical analyses were obtained from a commercial laboratory (Acme Labs, Vancouver, BC) in order to evaluate the parental magma of the HRU, its extent of contamination, and genetic relationship with the CLIC. These methods are described in more detail below.

2.1 Core Logging and Sampling

Ten drill cores were selected for re-logging and sampling for the petrographic

study, mineral chemical analysis, and lithogeochemistry. With the assistance of Magma Metals staff, cores were selected that profiled the HRU on either side of the Quetico Fault and intersected significant and representative sections of the HRU. Six cores profile the narrow CLZ near its transition into the Bridge Zone and four traverse the BLZ (Fig. 1.3). Although the HRU is the primary focus of this study, samples were also collected from the intruded granitic and metasedimentary rocks of the Quetico Subprovince and the margins of the ultramafic rocks of the CLIC.

Magma Metals logs were used as guides to aid in the re-logging efforts. Samples were collected that typified the major mineralogical and textural characteristics of the HRU. Samples were also strategically selected from contacts and areas of distinct grain size differences. A total of 123 half core samples were collected. Core logs and macroscopic descriptions are reported in Appendix A.

2.2 Petrographic Study

From the 123 core samples collected, 139 thin section billets were cut and shipped to Quality Thin Sections in Tucson, Arizona to be made into unpolished thin sections for petrographic investigation by transmitted light. Sixty-nine of these thin sections were later polished at Lakehead University in Thunder Bay, ON for investigation under reflected light and for SEM-EDS analyses. The features analyzed by transmitted light petrography include mineral mode, habit, and internal features (exsolution, zoning, twinning); bulk rock textures (absolute and relative grain size, foliation, overgrowth/corona relationships); and alteration assemblages and intensities. Mineral modes were based on visual volume estimates. Complete transmitted light petrographic descriptions are

reported in Appendix B and elements of this database are summarized in figures shown in Chapters 3 (Results) and 4 (Discussion).

Modal rock names for intermediate, mafic, and ultramafic rock types were assigned based on the classification schemes proposed by Miller et al. (2002) for use with the Duluth Complex (Fig. 2.1). As previously stated, modal percentages of minerals were visually estimated and subsequently normalized to the appropriate classification scheme. Mineral grain sizes were also visually estimated using the following classification: very fine (<0.2mm), fine (0.2-0.8mm), medium-fine (0.8-1.5mm), medium (1.5-3mm), medium-coarse (3-7mm), and coarse (7-12mm).

A)

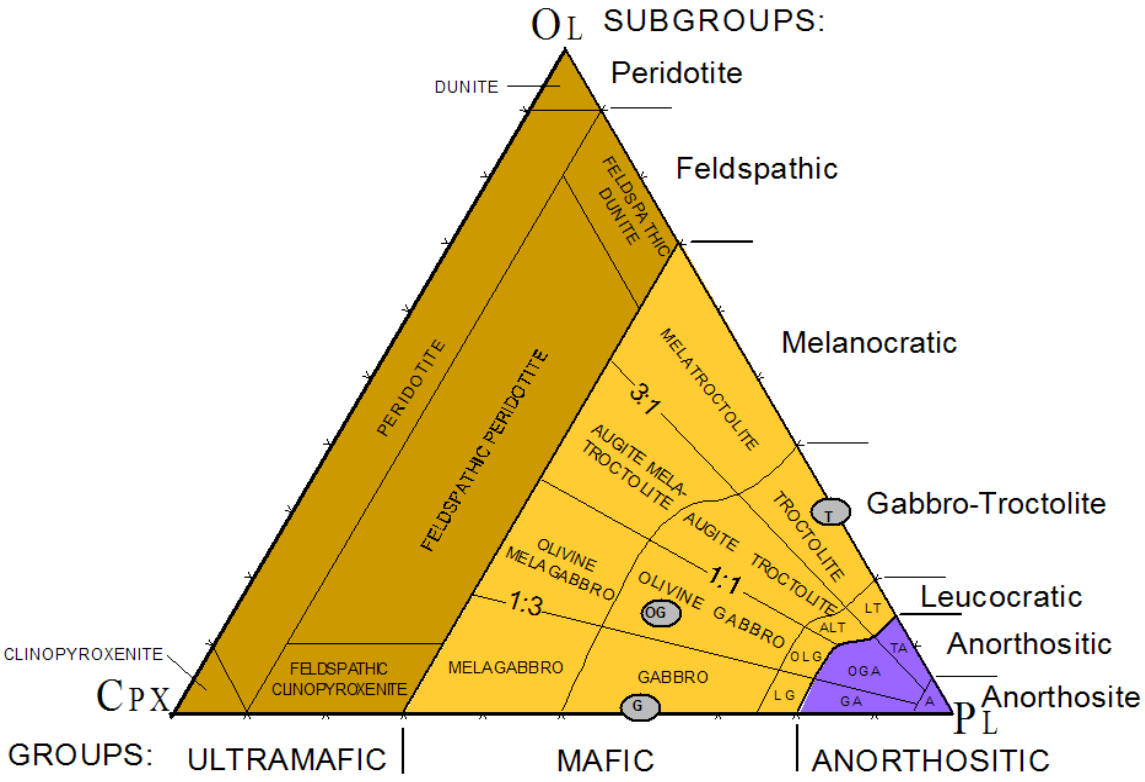

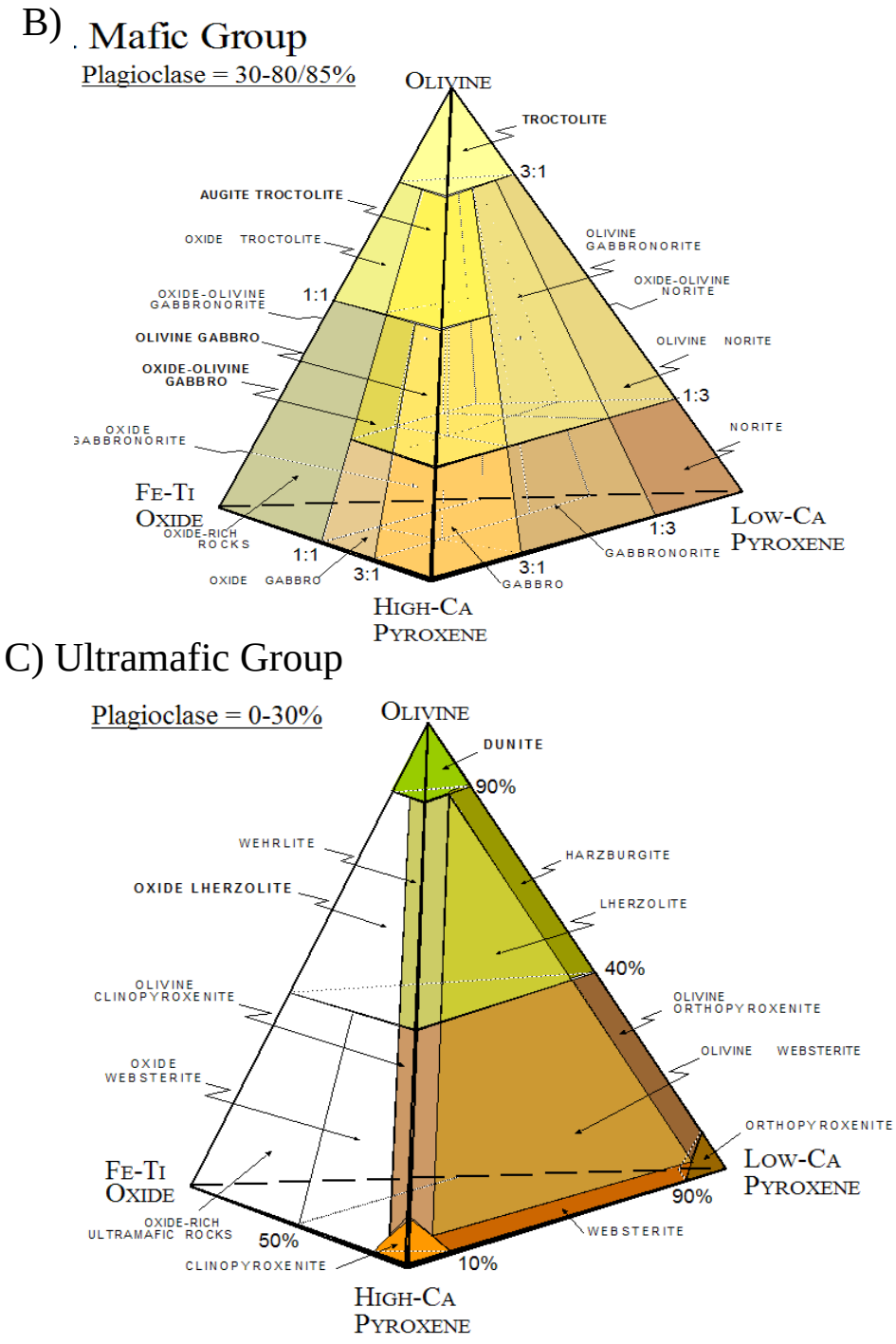

Figure 2.1 – Modal rock type classification schemes. A) General modal classification scheme based on relative abundances of plagioclase, olivine, and pyroxene that

distinguishes the ultramafic, mafic and anorthositic groups based largely on plagioclase abundance. T, OG, and G identify experimentally determined cotectic proportions for mafic magmas saturated in Pl+Ol, Pl+Ol+Cpx, and Pl+Cpx, respectively. B) Modal rock types in the mafic group (Pl % = 80/85-30%) based on relative abundances of olivine, clinopyroxene, orthopyroxene, and Fe-Ti oxide. C) Modal rock types in the ultramafic group (Pl% <30%) based on relative abundances of olivine, clinopyroxene, orthopyroxene, and Fe-Ti oxide. From Miller et al. (2002).

2.3 Scanning Electron Microscopic Analysis

Scanning Electron Microscopic analyses were acquired to assist in identification of primary mineral phases and their alteration assemblages that could not be readily resolved in the petrographic study. Samples containing primary pyroxene and olivine were also analyzed to qualitatively assess the parental magma composition(s) of the CLIC. As previously noted, analyses were conducted at UMD using the JEOL JSM-6490LV SEM-EDS.

Of the 69 polished thin sections, 41 were analyzed and include samples from nine of the ten drill cores. Samples were chosen that best represented the various mineralogies and textures, contained unknown mineral assemblages, and/or contained sulfide minerals. The selected thin sections were coated with an average of 20 nanometers of carbon using a Denton vacuum carbon coater. Applying a conductive carbon coat to the sample surface allows for the dissipation of electrons, which would otherwise accumulate on the surface and result in sample charging and electron beam deflection. An accelerating voltage of 15 Kv was used for the electron beam. Each sample was analyzed at a working distance of 10 millimeters and a spot size of 58-60 in order to achieve 30% deadtime for each mineral

phase analyzed. Prior to each use, the EDS spectrum was calibrated to a thin piece of copper tape attached to the sample holder. After calibration, four to five areas of each thin section were carefully analyzed using the “point and shoot” method for a 10 second count time in order to acquire the spectrum required to identify each distinct mineral phase.

The EDS was also used to acquire standard-less analyses, which yielded semi-quantitative major element compositions of augite and olivine. Six samples from cores TBND-60, TBND-125, BL08-78, and BL09-146 were selected for mineral analysis, due to the known presence of unaltered augite and olivine. Operating conditions for these analyses were identical to those reported above with the exception of a 60 second count time rather than 10 seconds. As before, prior to each use, the EDS was calibrated using a thin piece of copper tape. After calibration, ten analyses were acquired of augite and olivine grains, where present. Complete mineral chemical analyses collected for this study are tabulated in Appendix C.

2.4 Lithogeochemical Analysis

Fifty-two representative samples were selected from the 139 samples collected from the ten drill cores for lithogeochemical analyses. Drill core TBND-60 was selected as the representative core for the CLZ and BL08-78 was selected for the BLZ as they each best characterize the overall stratigraphy, mineralogical, and textural features of the HRU in each zone. In total, eight samples were selected from TBND-60 and eleven from BL08-78, with one or more samples chosen from each rock type that best represent that lithology. The remaining thirty-three samples were selected from the other eight cores, which included three chilled samples, two granitic, and three metasedimentary samples

from the Quetico country rocks.

All samples were submitted to Acme Laboratories in Vancouver, British Columbia. Samples were crushed, split, and pulverized to 200 mesh. Pulps of each sample were analyzed for select major and trace elements using ICP-MS methods. In addition, 30 gram splits were analyzed for platinum, palladium, and gold by fire assay fusion with an ICP-MS finish. All data reported by Acme Labs are tabulated in Appendix D.

Upon completion of these analyses by Acme, the leftover pulps from all 52 samples were returned to UMD to acquire major element compositions and calculate loss on ignition (LOI) for each sample using X-ray fluorescence analysis. LOI was calculated by measuring two grams of ground sample into a porcelain crucible and cooked at 925°C for 45 minutes in a muffled furnace. Samples were then removed from the furnace and placed into a dessicator to cool for approximately twenty minutes. Once the samples had cooled, they were reweighed. The LOI was then calculated using the following equation:

$$[(\text{Crucible} + \text{Sample}_{wet} - \text{Crucible} + \text{Sample}_{dry}) / \text{Initial Sample}] \times 100$$

After calculating the LOI, 1.6 grams of that sample was mixed with 6.4 grams of lithium borate flux (1:5 ratio) in a platinum/gold crucible. The sample+flux mixture was then placed into a Claisse Fluxor, heating the mix to 1200° C, which melted the flux and allowed for the pulped sample to be dissolved into the resultant liquid. The molten material was poured into a platinum/gold mold and cooled to form the glass bead (or disk) necessary to conduct XRF analyses. This method was repeated for each of the 52 ground samples. The prepared samples were then loaded five at a time with one standard

into the Rigaku S.Max X-ray fluorescence spectrometer and analyzed for their major element oxide compositions. It is important to note that robust analytical protocols, at the time analysis was being conducted, had not been well established for the XRF analyzer used at UMD. All XRF analyses are tabulated in Appendix E.

3.0 Results

Core logging (Appendix A) and petrographic observations (Appendix B) provided detailed macro- and micro-scopic characterization of the HRU, their mineralogical and textural attributes, and their relation to the country rock and mineralized ultramafic intrusion. SEM-EDS results and analysis has aided in primary and secondary mineral identification (Appendix C). Whole rock lithogeochemical data (Appendix D & E) was used to evaluate the parental magma compositions of the various lithologies and their genetic relationship to one another. Observational and analytical data from the CLZ and the BLZ will be reported separately in this chapter and compared in the discussion chapter.

3.1 Current Lake Zone Geology

Six drill cores profiling the CLZ were investigated for this study (Figs. 1.3 and 3.1). Described below are the macro- and microscopic attributes of the main rock types and their contact relationships identified from core logging, petrographic observations, and some mineral chemical analyses. Previous core logging by Magma Metals identified four principal rock units in the six drill holes selected to represent the CLZ of the CLIC. Those rock units are the hybrid gabbro unit (red and grey varieties), peridotite, and, melagabbro (Fig. 1.4A). Based on the greater mineralogic and textural detail revealed mostly from microscopic observations in this study (e.g., Figs. 3.2 and 3.3), it became clear that the rock units distinguished by Magma Metals, based largely on macroscopic characteristics, needed to be renamed and redefined. As such, the main rock units

comprising the CLZ defined in this study are defined as Heterolithic Quartz Gabbro (HQG), Melagabbro, and Wehrlite units. The range of modal, textural, alteration, and inclusion attributes of these redefined CLZ rock units, and the host Archean granite, are summarized in Table 3.1.

Table 3.1 – Attributes of general rock units identified in CLZ drill core.

First row indicates the rock units designated in Magma Metals drill core logs. The second row gives the rock units defined in this study followed by their mineralogical, textural, alteration and inclusion attributes observed from re-logging, petrographic, and SEM-EDS studies.

Rock Units – *Magma Metals*	*Granite*	*Red Hybrid*	*Grey Hybrid*	*Melagabbro*	*Peridotite*
Rock Units - This Study	**Granite**	**Quartz Gabbro**	**Melagabbro**		**Wehrlite**
Rock Types	Granite	Quartz Gabbro, Quartz Leucogabbro, Quartz Ferrodiorite	Gabbro, Melagabbro, Feldspathic Wehrlite		Wehrlite Feldspathic Wehrlite
Color	Red, Pink	Red, Grey	Grey, Green		Dark Green, Black
Grain Size	Coarse	V. Fine to Medium	Fine to Medium		Medium to Coarse
Dominant Minerals	Potassium feldspar, Quartz	Plagioclase, Pyroxene, Quartz	Plagioclase, Clinopyroxene, Olivine		Clinopyroxene, Olivine, Plagioclase
Bulk Texture	Equigranular	Subprismatic to Subophitic; Mottled	Subpoikilitic		Plagioclase-poikilitic
Alteration *Intensity* – Mineralogy	*Moderate* - Hematite, Sericite, Calcite	*Intense to Complete* - Chlorite, Sericite, Albite, Rutile, Ilmenite, Titanite, Hematite, Calcite	*Moderate* - Sericite, Albite,		*Weak to Moderate* - Actinolite, Chlorite, Talc, Serpentine, Magnetite, Sericite
Inclusions?	None	Quartz and Potassium Feldspar	Quartz		None

Figure 3.1 shows the vertical and the relative lateral distribution of the rock units defined in Table 3.1 in six drill cores investigated to characterize the CLZ (TBND-60,

TBND-125, TBND-136, TBND-124, TBND-95, and TBND-023). Plotted in Figures 3.2 and 3.3 are the petrographic attributes observed in core TBND-60. The modal and textural attributes in the lower section of core TBND-124 are plotted in Figures 3.9 and 3.10. The TBND-60 core was chosen for detailed examination because it profiles all three units observed in the upper part of the CLZ and best displays the contact relationships between the three rock units. Core TBND-124 was chosen because it best shows the relationship between the mineralized Wehrlite core and the flanking Melagabbro unit without the overlying HQG unit.

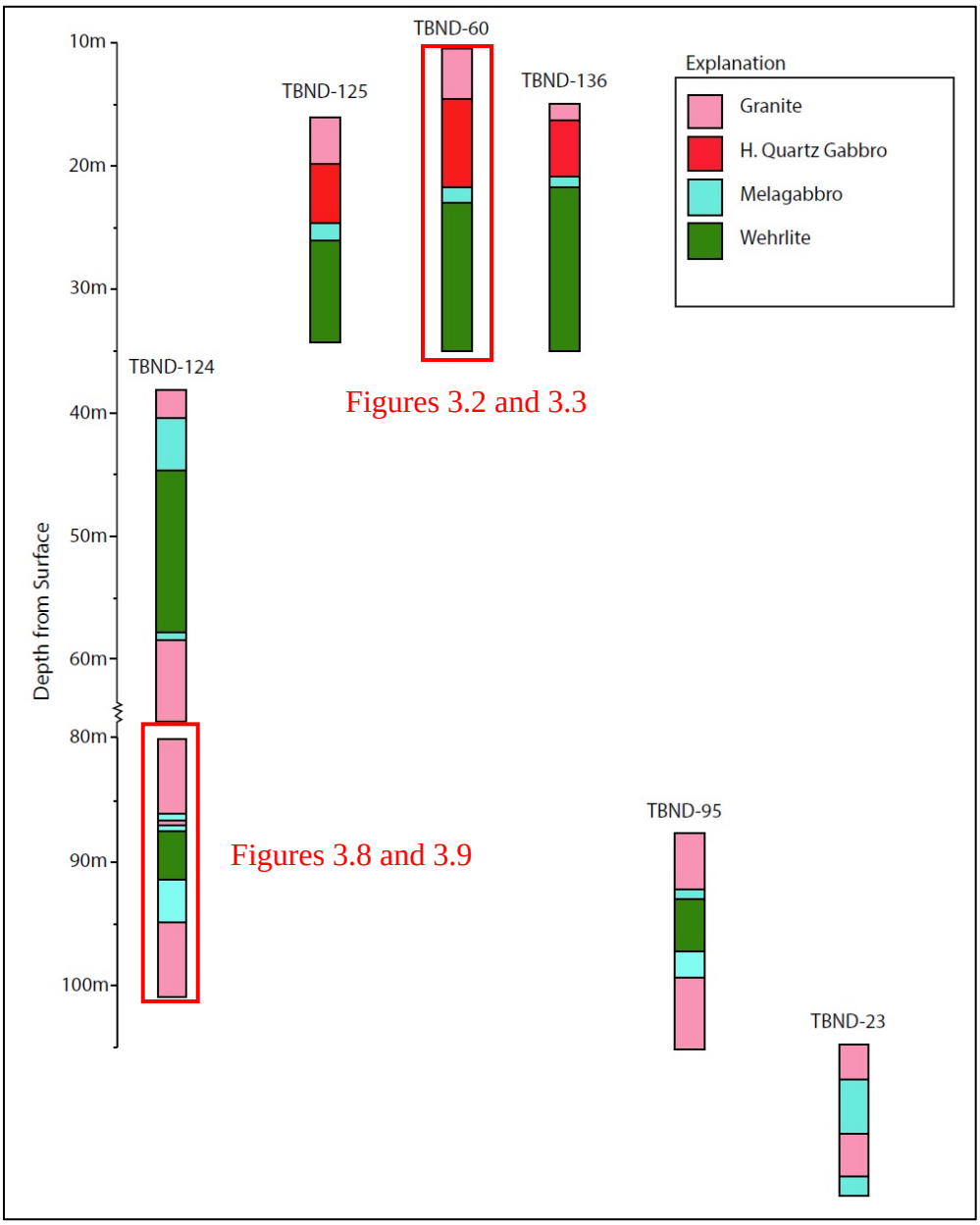

Figure 3.1 – Distribution of rock units identified in drill cores re-logged from the CLZ for this study. The red outlines identify cores that were singled out for detailed examination and the figures where that data is plotted. The vertical distribution of rock units is to scale, but the horizontal position of each drill core, while in proper order, is not to scale. Lithologic logs for all CLZ cores are given in Appendix A.

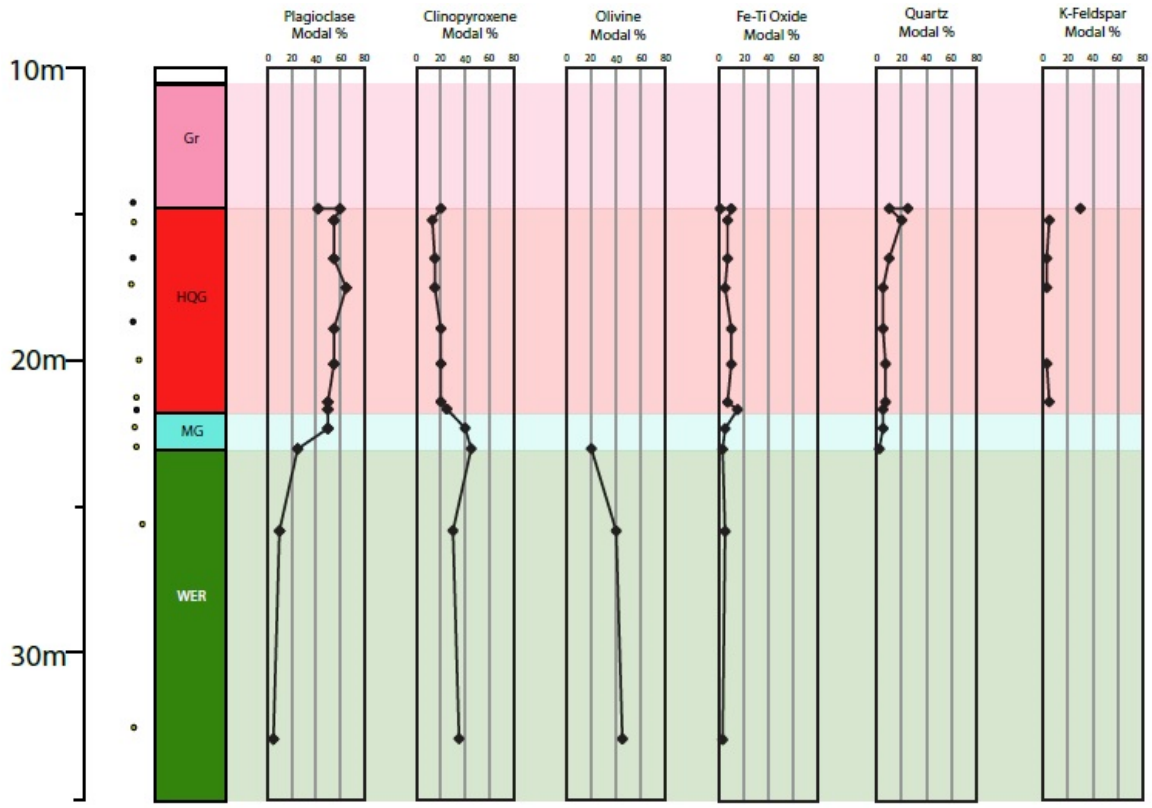

Figure 3.2 – Stratigraphic variation in modal abundances in TDND-60 of plagioclase, clinopyroxene, olivine, Fe-Ti oxides, quartz, and potassium feldspar (0-80% in intervals of 20)**.** Abundances based on visual estimates. The lithologic log for TBND-60 is given in Appendix B.

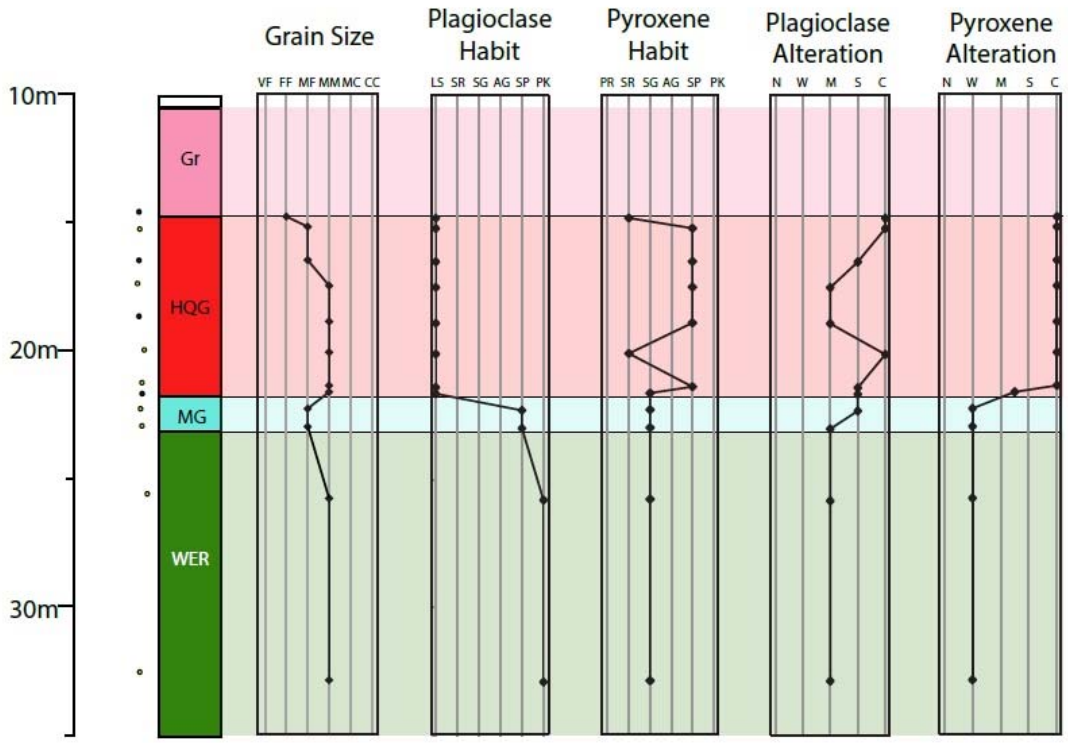

Figure 3.3 – Stratigraphic variation of grain size, plagioclase, and pyroxene habit and alteration in drill core TBND-60. The grain size codes are: VF-very fine, FF-fine, MF-medium fine, MM-medium, MC-medium coarse, CC-coarse and are based on size distributions defined by Miller et al. (2002). Crystal habit codes are: LS-lath shaped, PR-prismatic, SR-subprismatic, SG-subhedral granular, AG-anhedral granular, SP-subpoikilitic, PK-poikilitic. Alteration codes are: N-not altered, W-weakly, M-moderately, S-strongly, C-completely. The lithologic log for TBND-60 is given in Appendix B. NOTE: The pyroxene habits reported on this figure represent the dominant habit and not the only crystal habit present.

3.1.1 Granitic Country Rock

Granitic rocks make up the majority of country rock in the CLZ. Equigranular granite to granodiorite comprises the uppermost rock type of in TBND-60, TBND-125, and TBND-136, and the upper and lowermost type in cores TBND-124, TBND-95, and

TBND-023 (Fig. 3.1). It is typically red to grey in color and consists of coarse-grained crystals of uniform size. The dominant mineral assemblages in the samples investigated for this study consist of red to pink potassium feldspar, quartz, white to grey plagioclase (not always present), and ~3% fine-grained micas and oxides (Fig. 3.4A).

Potassium feldspar is the most abundant mineral in the granitic country rock, ranging between 55 and 75%, typically exhibiting anhedral to subhedral tabular habit. Hematite alteration can be observed in plane-polarized light as a reddish brown staining around the margins or throughout the crystals. Though much of the potassium feldspar is intensely altered, it is very common to see microcline twinning still preserved, making it easily distinguishable from plagioclase, which usually occurs as inclusions or 'lamellae' within potassium feldspars.

Quartz is typically anhedral granular in habit and ranges from 20 to 35% in mode, but also occurs as elongate grains with sutured grain boundaries. Plagioclase is more abundant in the lower intervals, ranging between 10 and 25%, but can be as high as 40%, and exhibits an anhedral lath-shaped habit. Other common minerals are iron oxides, ranging between 1 and 5%, and micas, the most common being muscovite ranging between 3 and 8%.

Textural features include prismatic and micrographic textures between potassium feldspar and quartz that typically occur near the contacts between the granites and the intrusive rocks of the CLIC. Sulfides are rarely observed in the granites, only appearing in TBND-023 as pyrite crystals within fractures.

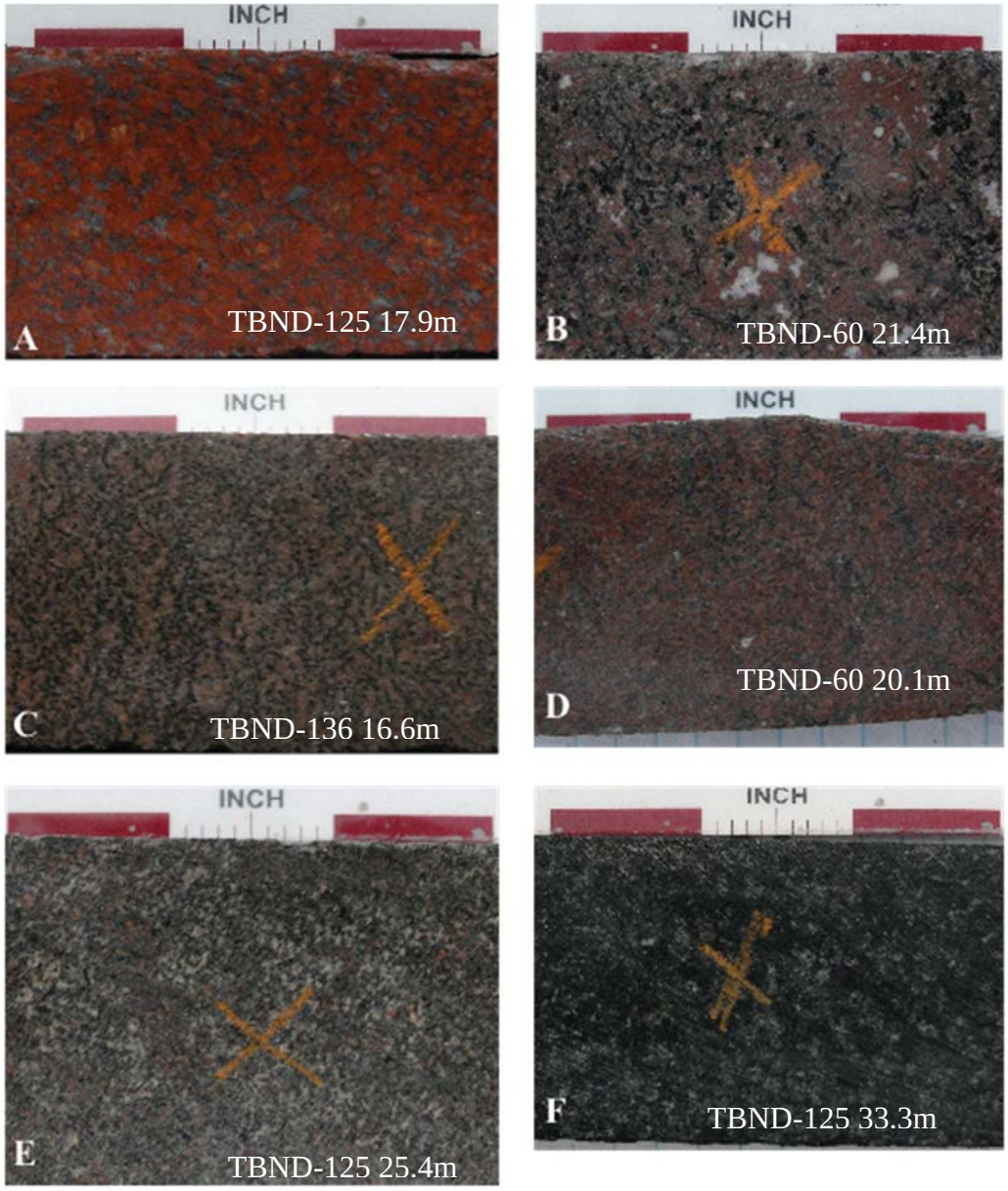

Figure 3.4 – Core photographs illustrating the common rock types from the CLZ. A) Equigranular red granite country rock; B) Mottled, subophitic quartz gabbro (HQG unit); C) Subprismatic ferrodiorite (HQG unit); D) Subprismatic, ferrodiorite (HQG unit); E) Quartz-bearing gabbro with subpoikilitic plagioclase (HQG unit); F) Wehrlite with subhedral granular pyroxene (grey splotches) (Wehrlite unit)

3.1.2 Heterolithic Quartz Gabbro (HQG) Unit

Intensely altered, quartz-bearing, gabbroic to ferrodioritic rocks, previously logged as the red hybrid unit, make up a 4- to 7-meter-thick lithologic unit at the upper contact of the CLIC in the three CLZ cores observed in this study (Fig. 3.1). It is characterized by a moderate to deep red color, variations in altered prismatic to anhedral granular pyroxene (now chlorite and magnetite), and mottled textures (Figs. 3.3 and 3.4 B-D).

The most common modal rock type comprising this unit is potassium feldspar-bearing quartz gabbro, but it ranges from quartz ferrodiorites to quartz leucogabbro. Mineralogically, these rocks are consistent in terms of modal abundances (Figs. 3.2 and 3.5). The primary minerals are plagioclase, pyroxene, iron-titanium oxides, quartz, potassium feldspar, and apatite

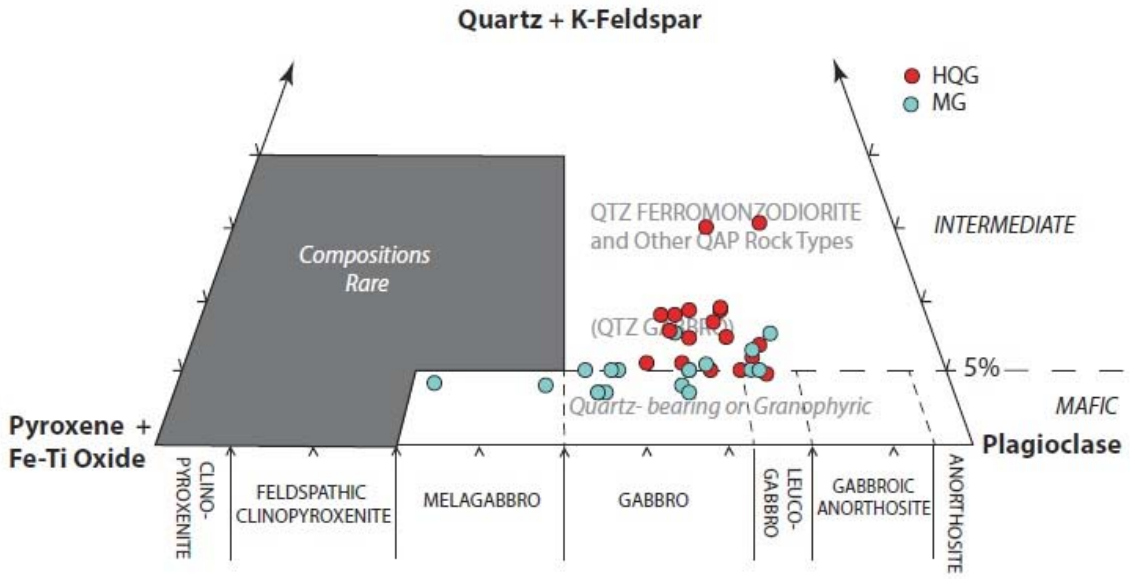

Figure 3.5 – Modal compositions of rock samples from the CLZ HQG unit based on relative proportions of plagioclase, pyroxene+Fe-Ti oxide, and quartz + K-feldspar. Figure based on recommendations by Miller et al. (2002) for distinguishing mafic (gabbroic) rocks from intermediate (dioritic) rocks. Mafic rock modifiers "quartz-bearing" and "granophyric" are used when Qtz>Ksp and Qtz<Ksp respectively. Intermediate rock types should be named base on their relative proportions of Qtz-Ksp-Pl (QAP classification). The term "quartz gabbro" is used rather than quartz ferrodiorite when Qtz+Ksp>5%, Qtz>>Ksp, and pyroxene has an anhedral granular to subophitic habit (pyroxene in ferrodiorites tend to be subprismatic to prismatic).

Plagioclase typically exhibits lath-shaped crystal habits (Figs. 3.3 and 3.6A), ranging between 50 and 70% modal abundance (Figs. 3.2 and 3.5), and strongly to completely altered to sericite, saussurite, and/or albite (Figs. 3.3 and 3.6). Pyroxenes are also strongly to completely altered to chlorite, with calcite and titanite blebs (Figs. 3.3 and 3.6), but can be recognized by their distinctive crystal habits (Fig. 3.3), which include subprismatic (Fig. 3.6C), subophitic (Fig. 3.6A and B), and anhedral granular (Fig. 3.6D).

Despite their textural variability, the modal abundance of pyroxene remains relatively constant, ranging between 15 and 25% (Figs. 3.2 and 3.5). The common Fe-Ti oxides identified, using SEM-EDS analysis, are titanomagnetite, magnetite, ilmenite, and rutile (Fig. 3.6). Titanomagnetite is the primary oxide, occurring as anhedral granular, subhedral granular, and skeletal crystal habits. Ilmenite occurs as exsolution lamellae in titanomagnetite as well as acicular crystal habits. Rutile rarely occurs, but when present, it is usually with other oxides as anhedral granular habits. Modal abundances for all oxide varieties were estimated to range between 2 to 15% and typically exhibit bladed to

anhedral granular crystal habits with skeletal crystal habits towards the basal contact with the Melagabbro Unit (Fig. 3.6D).

A distinctive macroscopic feature of the HQG unit is the presence of centimeter-sized red granophyre patches that impart a mottled texture to the rock (Figs. 3.4B and 3.6B). Observations made by transmitted light and SEM-EDS analysis show these patches to be interstitial, micrographic quartz and hematized potassium feldspar. Potassium feldspar, in the CLZ, always occurs with quartz, never by itself, and exhibits anhedral granular crystal habits and commonly ranges between 2 and 5% modal abundance. Quartz, in addition to micrographic texture, also appears as single crystals that exhibit anhedral granular to subpoikilitic habits and ranges in modal percentage from 5 to 20%.

Other notable minerals are apatite and calcite. Apatite typical occurs in trace amounts as very fine-grained needles within plagioclase feldspar. Calcite is much more common, from trace to 15% modal abundance, and occurs as anhedral grains associated with quartz/granophyre inclusions. Calcite also occurs as an alteration phase of plagioclase and clinopyroxene.

The basal contact of this unit with the Melagabbro Unit is gradational on a scale of 10’s of centimeters and is marked by an abrupt increase in mafic and oxide phases and an abrupt decrease in quartz and feldspar (Fig. 3.2). It is important to note the gradual decrease in modal abundance of quartz from the upper contact with the granites towards the basal contact with the Melagabbro Unit (Fig. 3.3).

The contact between the HQG rocks and quartz-bearing gabbros of the Melagabbro unit is characterized by an abrupt decrease in plagioclase abundance and an increase in clinopyroxene (Fig. 3.2). Texturally, the contact is marked by an abrupt decrease in grain size from medium-grained to medium fine-grained, a change in plagioclase habit from predominantly lath-shaped to subpoikilitic/poikilitic, an abrupt shift in clinopyroxene habit from subophitic to subhedral granular (Fig. 3.3), and the intensity of clinopyroxene alteration drastically changes from strongly to completely altered in the HQG unit to very weakly altered in the Melagabbro unit. Additionally, potassium feldspar is absent in the Melagabbro unit.

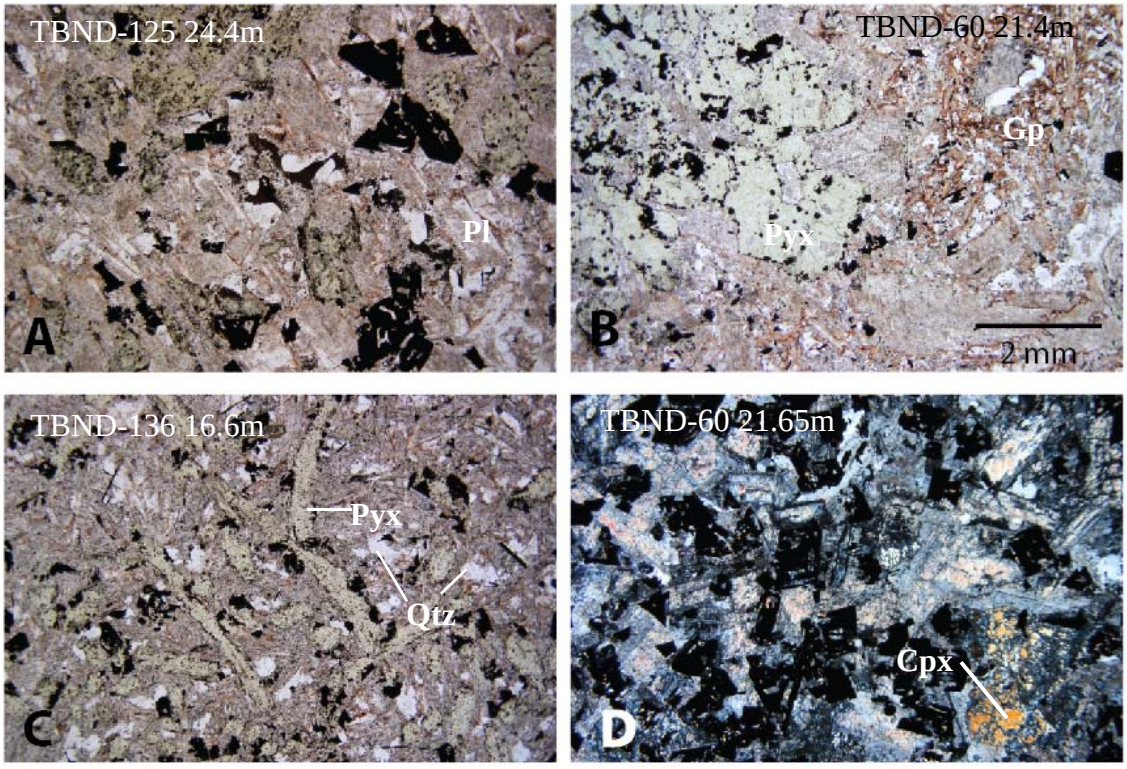

Figure 3.6 – Photomicrographs of the HQG unit showing its various textures and crystal habits: A) Subophitic pyroxene (altered to chlorite) - PPL, skeletal oxides, and albitized and sericitized, lathy plagioclase; B) Subophitic pyroxene

(Pyx), mottled patch of micrographic quartz and hematized potassium feldspar (Gp) - PPL; C) Subprismatic pyroxene, skeletal oxides, anhedral quartz - PPL; and D) Skeletal oxides, subpoikilitic plagioclase, anhedral granular clinopyroxene (strongly altered to chlorite) - XPL. 2mm scale bar applies to all photographs.

3.1.3 Melagabbro Unit

The Melagabbro unit of the CLZ (Table 3.1) always occurs marginal to the Wehrlite unit, but is only found in contact with the HQG unit in the upper part of the CLIC (Fig. 3.1). This unit includes what Magma Metals termed the Melagabbro unit and most occurrences of what they called the grey hybrid (Table 3.1). The mineralogical and textural occurrences of this unit are subtly different depending on whether it is in contact with the HQG unit (Figs. 3.2 and 3.3) or not (Figs. 3.7-3.9)

Where it occurs below the HQG unit in the upper CLZ, the Melagabbro unit is 1 to 1.5 meters thick and composed of grey, fine- to medium fine-grained, quartz-bearing gabbro to feldspathic olivine clinopyroxenite (Fig. 3.7). Most lithologies are medium fine-grained, but fine-grained gabbroic anorthosite and some quartz-bearing gabbro occur where the Melagabbro unit is in direct contact with the granite country rock. Texturally, this unit contains subprismatic to subhedral granular pyroxene and subpoikilitc to poikilitic plagioclase (Figs. 3.3, 3.4E, 3.8, and 3.10A-B).

Olivine, which is only present near the contact with the Wehrlite unit, is completely altered to talc and serpentine+iron oxide, but is recognizable as subhedral granular psuedomorphs that make up as much as 20% of the modal mineralogy (Fig. 3.10C). The most common Fe-Ti oxide minerals in this unit are titanomagnetite and ilmenite, commonly as exsolution lamellae and acicular crystal habits. Collectively, the

oxides make up 3-5% of the total mineral assemblage and exhibit acicular to skeletal crystal habits (Fig. 3.10B). Sulfide minerals, mainly pyrite and some pyrrhotite, make up 2-3% modal abundance and exhibit anhedral granular to poikilitic habits.

Anhedral granular quartz also appears in this unit in minor abundances (0-5%) and occurs interstitially to all other mineral phases. Carbonate is even less common, typically exhibiting anhedral crystal habits and, when present, makes up approximately 5% modal abundance. Primary amphibole and biotite are also present in some instances, exhibiting anhedral to subhedral habits and occur in trace amounts to as much as 3% abundance. Alkali feldspar is not observed in the Melagabbro unit.

Where the CLZ Melagabbro unit is in direct contact with granite country rock, it is composed of a very fine-grained quartz gabbro. The dominant minerals are plagioclase, clinopyroxene, Fe-Ti oxides, quartz, and carbonate. Plagioclase is the most abundant mineral, ranging from 55 to 65%, and exhibits lath shaped crystal habits throughout the unit.

Clinopyroxene, often altered to chlorite, typically exhibits subophitic to subprismatic crystal habits and ranges between 15 and 20% modal abundance. Fe-Ti oxides, the most common being magnetite with some ilmenite needles, ranges between 7 and 15% modal abundance and exhibits anhedral granular, skeletal and prismatic habits. Quartz appears in smaller abundances, 2 to 5%, and typical exhibits a poikilitic habit. Carbonate also appears throughout this unit in trace amounts to 5% abundance and typically exhibits anhedral granular habits.

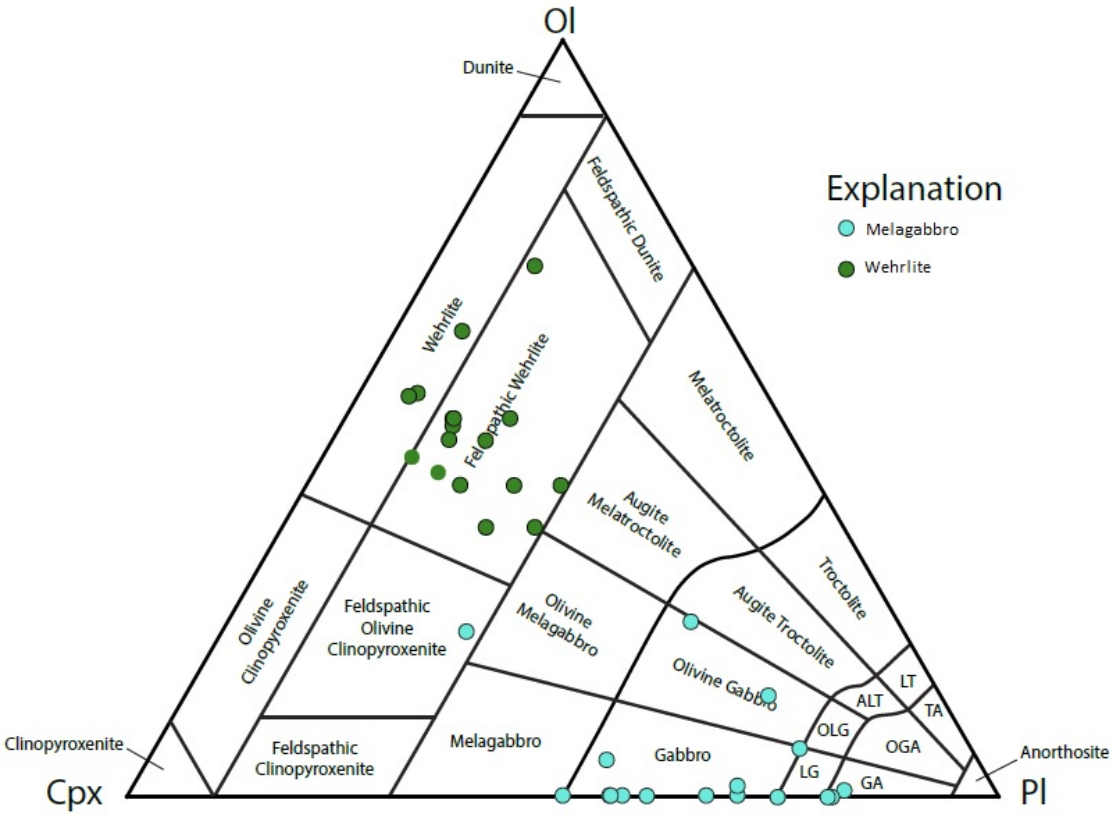

Figure 3.7 – Modal abundances of olivine, clinopyroxene, and plagioclase of samples from the Melagabbro (blue) and Wehrlite (green) units of the CLZ. Classification scheme after Miller et al. (2002).

The contact between the Melagabbro and HQG units exhibits an abrupt mineralogical and textural change. Overall grain size changes from medium-grained to medium fine-grained. Plagioclase abruptly changes across the contact from predominantly lath-shaped to sub-poikilitic, and the alteration intensity from intensely to moderately altered. Clinopyroxene slightly increases in modal abundance across the contact, along with abrupt transitions in crystal habit, sub-ophitic to subhedral granular, and alteration intensity, completely to weakly altered.

Quartz is present throughout the Melagabbro unit, however potassium feldspar becomes absent at the contact with the HQG unit. This contrasts with the texturally and compositionally sharp contact between the Melagabbro unit and the granitic country rock (Figs. 3.8 and 3.9).

The contact between the Melagabbro and Wehrlite units can be described as diffuse, TBND-60, or gradational, TBND-124. The diffuse contact relationship observed in TBND-60 is primarily characterized by the continued decrease in modal plagioclase and transition from sub-poikilitic to poikilitic. Modal clinopyroxene decreases slightly, but maintains a subhedral granular habit and weak alteration intensity. Quartz gradually decreases in modal abundance from ~5% to ~2% and completely disappears at the contact which is commonly coupled with the appearance of olivine.

This contact relationship differs slightly in TBND-124 as it is more gradational in nature. As with above, plagioclase gradually decreased in modal abundance, but the habit transitions from lath-shaped to poikilitic. Clinopyroxene changes from anhedral to subhedral granular habits, slightly increases in modal abundance, and transitions from strong/completely altered to weakly altered. Olivine appears in small abundances (~5-10%) and gradually increases across the contact. Quartz completely disappears at the contact.

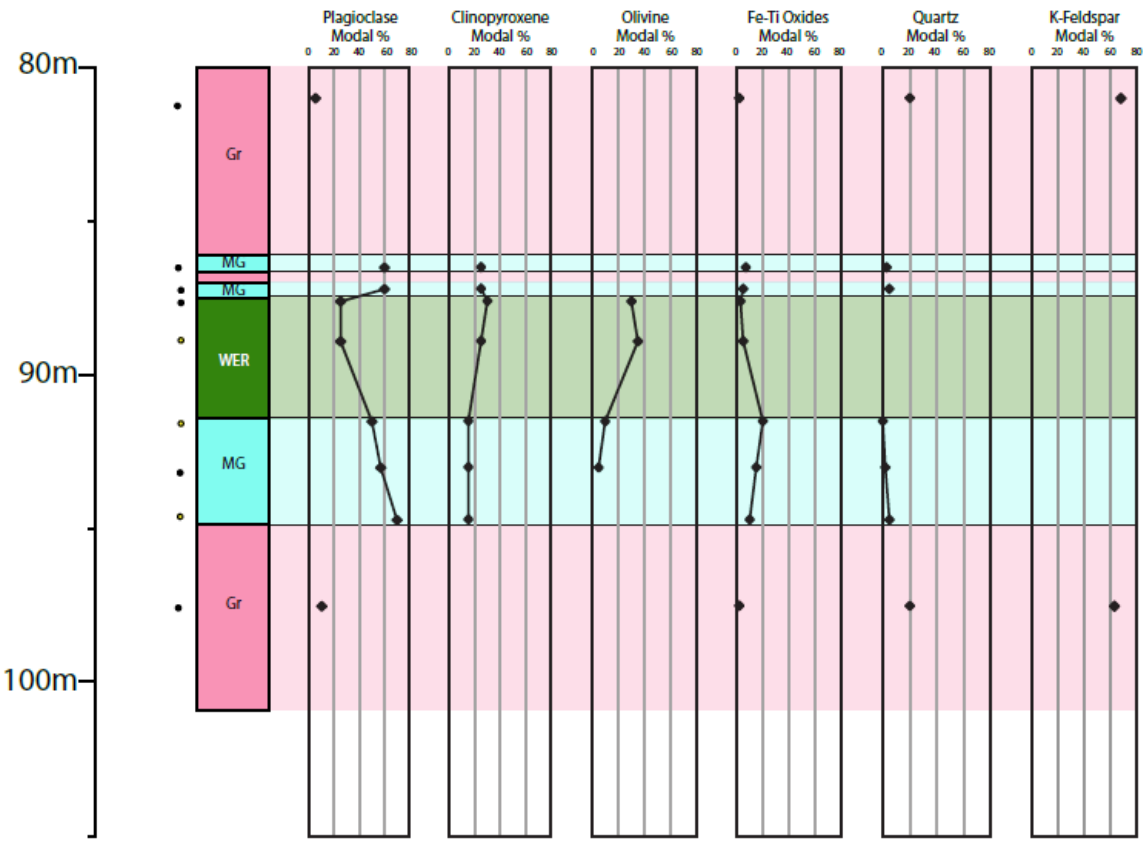

Figure 3.8 – Stratigraphic variation of modal abundances in TBND-124 of plagioclase, clinopyroxene, olivine, Fe-Ti oxides, quartz and potassium feldspar (0-80%) (See Fig. 3.1 for the location within the hole).

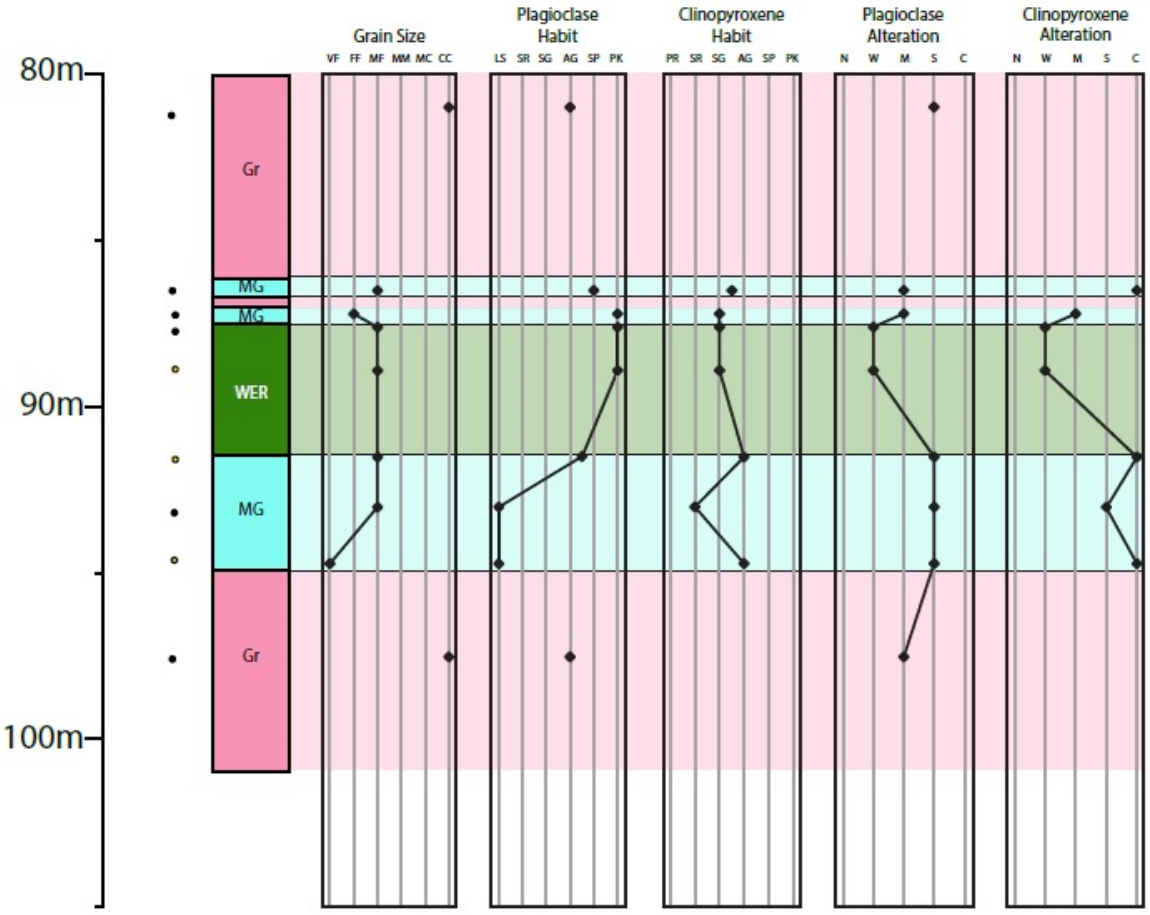

Figure 3.9 – Stratigraphic variation of grain size, plagioclase habit and alteration, and pyroxene habit and alteration, in TBND-124 (see Fig. 3.1 for location within hole). The grain size codes are: VF-very fine, FF-fine, MF-medium fine, MM-medium, MC-medium coarse, CC-coarse and are based on size distributions defined by Miller et al. (2002). Crystal habit codes are: LS-lath shaped, PR-prismatic, SR-subprismatic, SG-subhedral granular, AG-anhedral granular, SP-subpoikilitic, PK-poikilitic. Alteration codes are: N-not altered, W-weakly, M-moderately, S-strongly, C-completely. The log for core TBND-124 can be found in Appendix B. NOTE: The pyroxene habits reported on this figure represent the dominant habit and not the only crystal habit present.

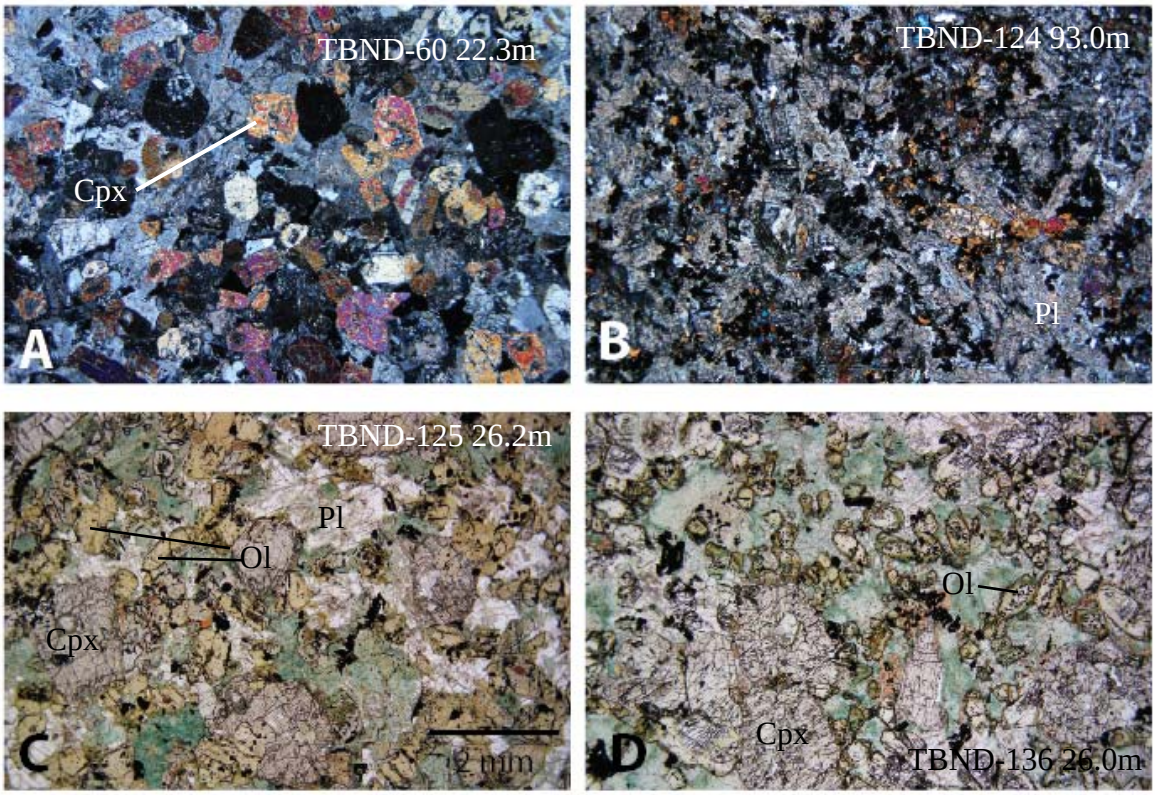

Figure 3.10 – Photomicrographs of samples from the Gabbro and Wehrlite units of the CLZ showing the characteristic textures and crystal habits. A) Subpoikilitic plagioclase with subhedral granular clinopyroxene (Gb unit), B) Quartz gabbro with lath-shaped plagioclase, subophitic clinopyroxene and skeletal to acicular oxides (Gb unit), C and D) Wehrlite with subhedral olivine (strongly altered to serpentine and talc), subhedral granular clinopyroxene, and poikilitic plagioclase (Wehrlite unit). All photos in XPL. Scale in C applies to all photomicrographs.

3.1.4 Wehrlite Unit

Previous logging of the CLIC by Magma Metals identified the main mineralized intrusive body as the peridotite unit. As this rock unit is largely composed of olivine and clinopyroxene (Fig. 3.7), it is termed the Wehrlite unit in this study. The Wehrlite unit

was observed in all cores from the CLZ profile except TBND-23. In drill core, it consistently occurs as a dark green to black, homogeneous, medium fine- to medium-grained, intergranular ultramafic rock with rare to moderate amounts (up to 25%) of interstitial plagioclase.

The dominant modal rock types are feldspathic wehrlite to wehrlite (Fig. 3.7), with the majority of the feldspathic wehrlite rocks occurring near the contacts with the Melagabbro unit (Figs. 3.2 and 3.8). The primary mineral assemblage for this unit, in order of decreasing abundance, consists of olivine, clinopyroxene, plagioclase, Fe-Ti oxides, amphibole, and sulfides. Olivine ranges in mode between 30 and 60% and occurs as subhedral to euhedral granular primocrysts typically completely or partially enclosed within larger clinopyroxene grains (Fig. 3.10 C and D). Olivine grains near contacts with the gabbro unit are commonly intensely to completely altered, however they are easily distinguished by the granular shapes of their pseudomorphs and alteration mineral assemblages (talc, serpentine, and oxide corona). Clinopyroxene occurs as anhedral granular to subpoikilitic oikocrysts ranging between 15 and 35% modal abundance. Poikilitic to subpoikilitc plagioclase, where present and unaltered, occurs in modal abundances between 5 and 25%. Oikocrysts up to 4 mm in diameter enclose chadacrysts of clinopyroxene and olivine (Fig. 3.10C).

Other less abundant minerals include Fe-Ti oxides, amphibole, and sulfides. The most common oxides include titano-magnetite and ilmenite. Collectively, the Fe-Ti oxides make up 2 to 7% modal abundance and range in habit from bladed (ilmenite), to subhedral granular (magnetite). Sulfide minerals consist dominantly of pyrrhotite,

chalcopyrite, and pentlandite with rare amounts of galena. Disseminated sulfide ranges from 2 to 8% in modal abundance and commonly occur as subpoikilitic to anhedral granular masses interstitial to silicate and oxide phases. Primary brown to green pleochroic amphibole is also present, typically away from the gabbroic margins, and ranges from trace amounts to 3% modal abundance. It exhibits anhedral to subhedral crystal habits. Subhedral granular biotite occurs in up to 2% abundance and is commonly spatially associated with amphibole and as rims on oxide. Trace to rare apatite occurs as needles in plagioclase.

3.2 Beaver Lake Zone

Previous core logging conducted by Magma Metals in the BLZ of the CLIC identified four principal rock units: schist and metasedimentary country rocks, red hybrid rocks, grey hybrid rocks, and peridotite. These units are similar to those defined in the CLZ with the exception of the metasedimentary, rather than granitic, country rock. The same redefined units in the CLZ identified by core re-logging and petrographic studies are also recognized in the four cores investigated in the BLZ (BL08-75, BL08-78, BL09-146, and BL09-147; Fig. 3.11). As in the CLZ, the unit previously defined as the gray hybrid is actually comprised of the HQG and the Melagabbro units. One significant difference between the two CLIC zones is the nature of the HQG, which in the BLZ is characterized by abundant inclusions of quartzite and granite. This and other attributes of the BLZ units are summarized in Table 3.2.

Table 3.2 – Attributes of rock units identified in BLZ

First row indicates the rock units designated in Magma Metals drill core logs. The second row gives the rock units interpreted in this study followed by the mineralogical and textural attributes recognized from re-logging and petrographic observations.

Rock Units – *Magma Metals*	*Metasediment*	*Red Hybrid*	*Grey Hybrid*	*Melagabbro Pyroxenite*	*Peridotite*
Rock Units- ***This Study***	**Metasediment**	**Quartz Gabbro**		**Melagabbro**	**Wehrlite**
Rock Types	Metasiltstone Schist	Quartz Gabbro, Quartz Leucogabbro, Quartz Ferrodiorite, Quartz Monzodiorite		Gabbro, Feldspathic Wehrlite, Feldspathic Clinopyroxenite	Wehrlite, Feldspathic Wehrlite
Color	Grey	Red, Grey		Grey, Green	Dark Green, Black
Grain Size	Coarse	V. Fine to Medium		Fine to Medium	Medium to Coarse
Dom Minerals	Potassium Feldspar, Quartz, Muscovite	Plagioclase, Pyroxene		Plagioclase, Clinopyroxene, Olivine	Clinopyroxene, Olivine, Plagioclase
Bulk Texture	Foliated	Sub-Ophitic, Mottled		Sup-Ophitic	Poikilitic
Alteration	Moderate	Intense to Complete		Moderate	Weak to Moderate
Inclusions	None	Quartz, Potassium Feldspar		Quartz	None
Other		Calcite		Calcite	

Figure 3.11 shows the vertical distribution of the rock units defined in this study collected from four drill cores investigated to characterize the BLZ (BL08-75, BL08-78, BL09-146, and BL09-147). All four cores traverse the three CLIC units, however, core BL08-78 was chosen for detailed examination (Figs. 3.12 and 3.13) because it profiles the greatest lengths of the three CLIC units observed in the BLZ. Summarized below are the modal and textural characteristics of rock units of this hole and the other three drill

cores investigated from the BLZ. Core logs and petrographic summaries of the BLZ cores are reported in Appendices A and B, respectively.

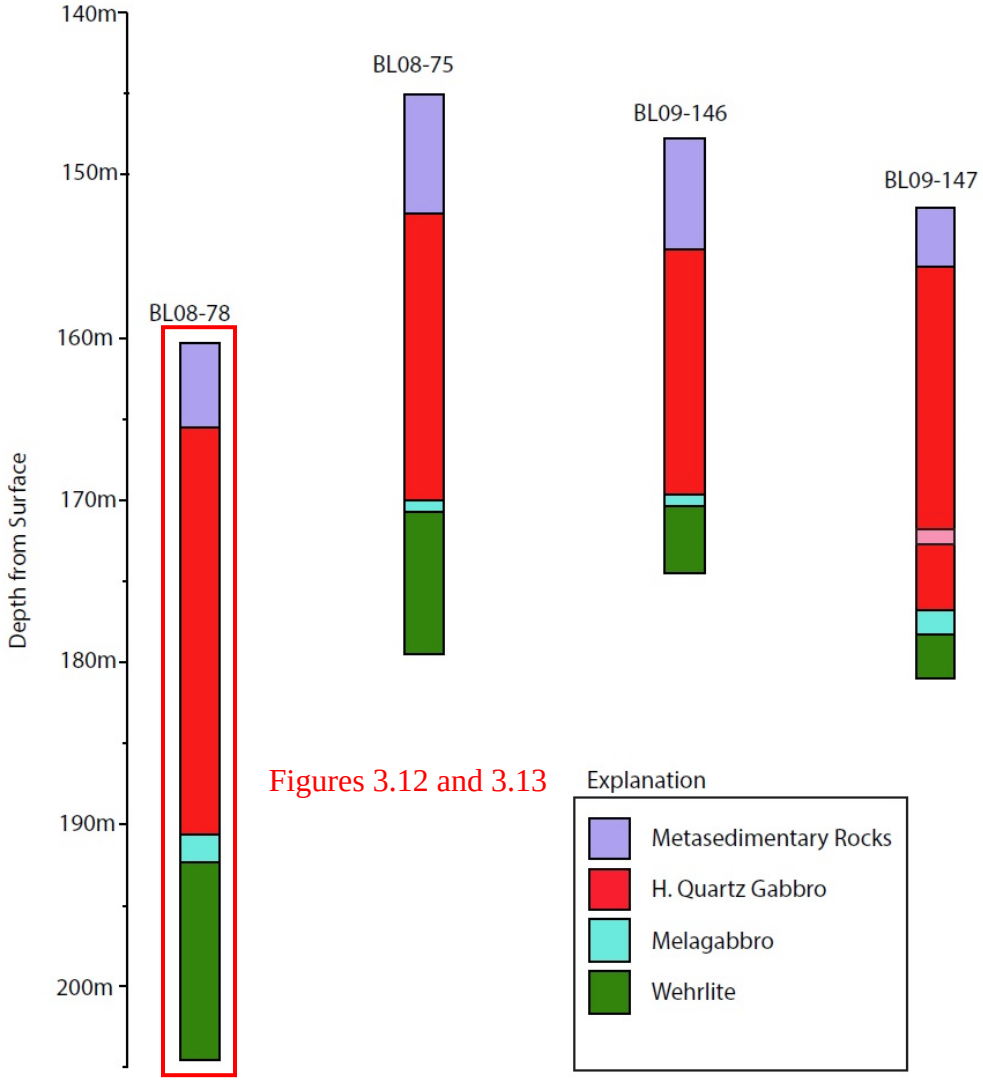

Figure 3.11 – Distribution of rock units identified in drill cores re-logged from the BLZ for this study. The thickness of the units is to scale and the lateral ordering of the cores are correct, but are not to scale. See Appendix A for logs of all cores.

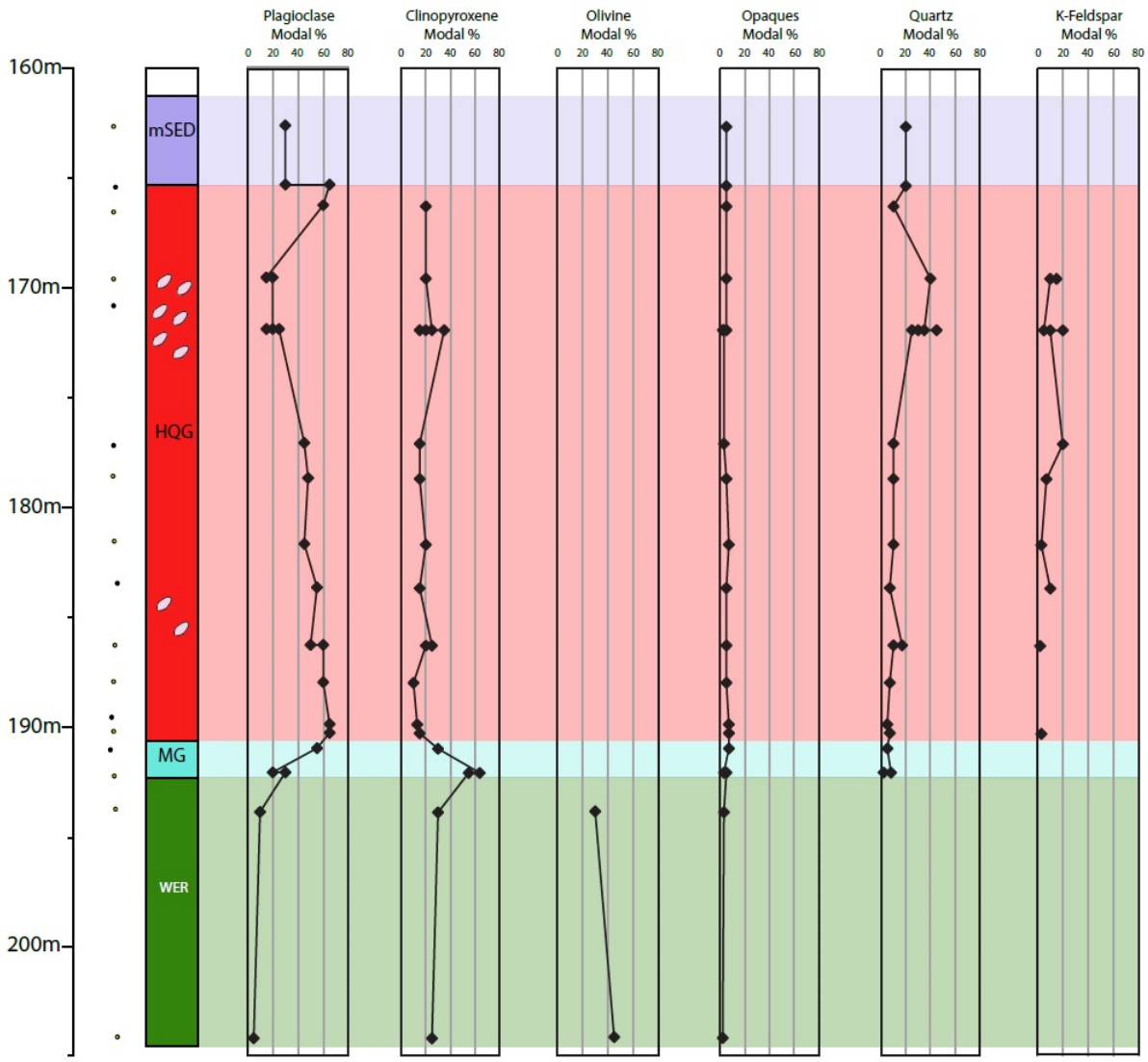

Figure 3.12 – Variation of visually estimated modal abundances in BL08-78 of plagioclase, clinopyroxene, olivine, opaques (Fe-Ti oxides and sulfides), quartz, and potassium feldspar in BLZ units.

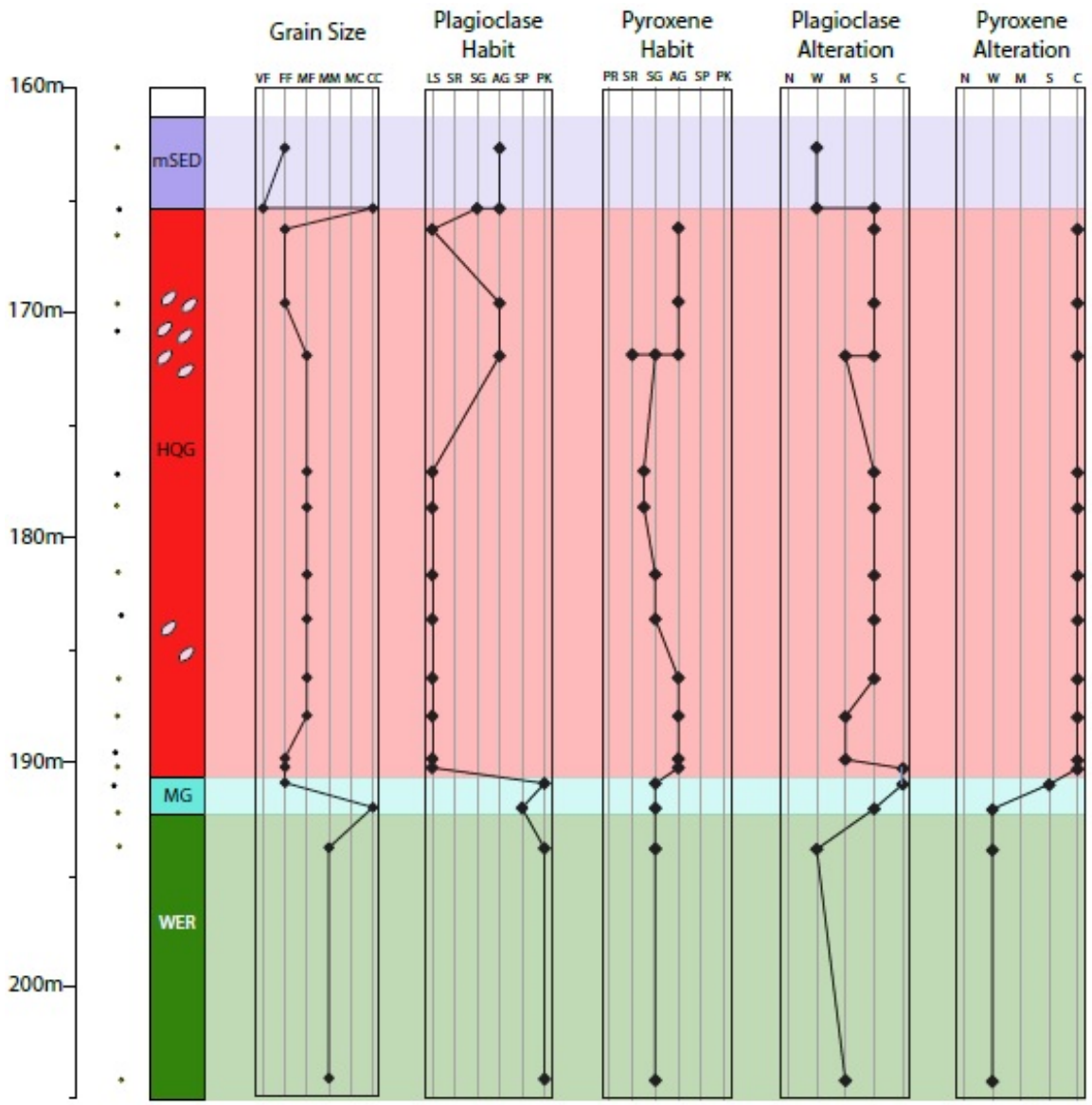

Figure 3.13 – Variation of grain size, and plagioclase and pyroxene crystal habits and alteration intensities in BLZ units from drill core BL08-78. The grain size codes are: VF-very fine, FF-fine, MF-medium fine, MM-medium, MC-medium coarse, CC-coarse and are based on size distributions defined by Miller et al. (2002). Crystal habit codes are: LS-lath shaped, PR-prismatic, SR-subprismatic, SG-subhedral granular, AG-anhedral granular, SP-subpoikilitic, PK-poikilitic. Alteration codes are: N-not altered, W-weakly, M-moderately, S-strongly, C-

completely. NOTE: The pyroxene habits reported on this figure represent the dominant habit and not the only crystal habit present.

3.2.1 Metasedimentary Country Rock

The country rocks of the BLZ consist primarily of schists and metasiltstones. These rocks are very fine- to fine-grained, and commonly exhibit well-developed foliation (Fig. 3.14A). Mineralogically, this unit consists primarily of plagioclase, potassium feldspar, quartz, and mica (as biotite, muscovite and chlorite). Micas are typically well foliated and surround granoblastic feldspars and quartz. Garnet also appears in trace amounts as fine-grained porphyroblasts. The contact between metasedimentary rocks and the HQG unit of the CLIC is abrupt. This is similar to the contact between granitic country rock and the HQG unit in the CLZ.

3.2.2 Heterolithic Quartz Gabbro Unit

Underlying the country rock in the BLZ cores (Fig. 3.11) is a 15 to 26 meter interval of texturally and mineralogically variable, inclusion-rich mafic intrusive rocks that are similar in most respects to the HQG unit of the CLZ and are therefore grouped into the same HQG unit. However, there are several unique features observed throughout this unit that are not found in the CLZ-HQG unit. The most notable is the common occurrence of rounded, irregular-shaped, quartz-rich and granitic inclusions mantled by a thin (1-3 mm) rind that is rich in chlorite (Fig. 3.14C-D). The inclusions range in size from 0.2 to 3 cm (Fig. 3.14C, D, and F). Another feature unique to the BLZ, is the presence of calcite-filled amygdules, most notably seen in drill hole BL08-75 in the upper

14 m of the HQG (Fig. 3.14C). A distinctive feature of the BLZ-HQG unit, also found in the CLZ-HQG unit, are intervals that exhibit red mottling, which are hematized patches of potassium feldspar and quartz that occur interstitially to primary mafic minerals (Fig 3.10E-F).

As observed in drill core, grain size throughout most of the unit is medium fine-grained, but grades to very fine-grained at the upper contact and fine-grained at the lower contact with the Melagabbro unit (Fig. 3.13). Lath-shaped plagioclase comprises about half the composition of the HQG unit and is easily identifiable by its light tint due to being moderately to strongly altered. Although clinopyroxene is completely altered to chlorite and actinolite, its pseudomorphs show subprismatic to prismatic, in some cases poikioprismatic, habits near the upper and lower contacts with the metasedimentary rocks and the Melagabbro unit, respectively. Internally, dark green clinopyroxene psuedomorphs typically display subhedral granular habits (Figs. 3.10E-F and 3.13). Sulfide mineralization occurs as disseminations sporadically through the unit and, when present, it makes up 3-5% modal percent. Lastly, rock types gradually transition to more mafic compositions, as distinguished by their darker color and increase in modal Fe-Ti oxides, near the basal contact.

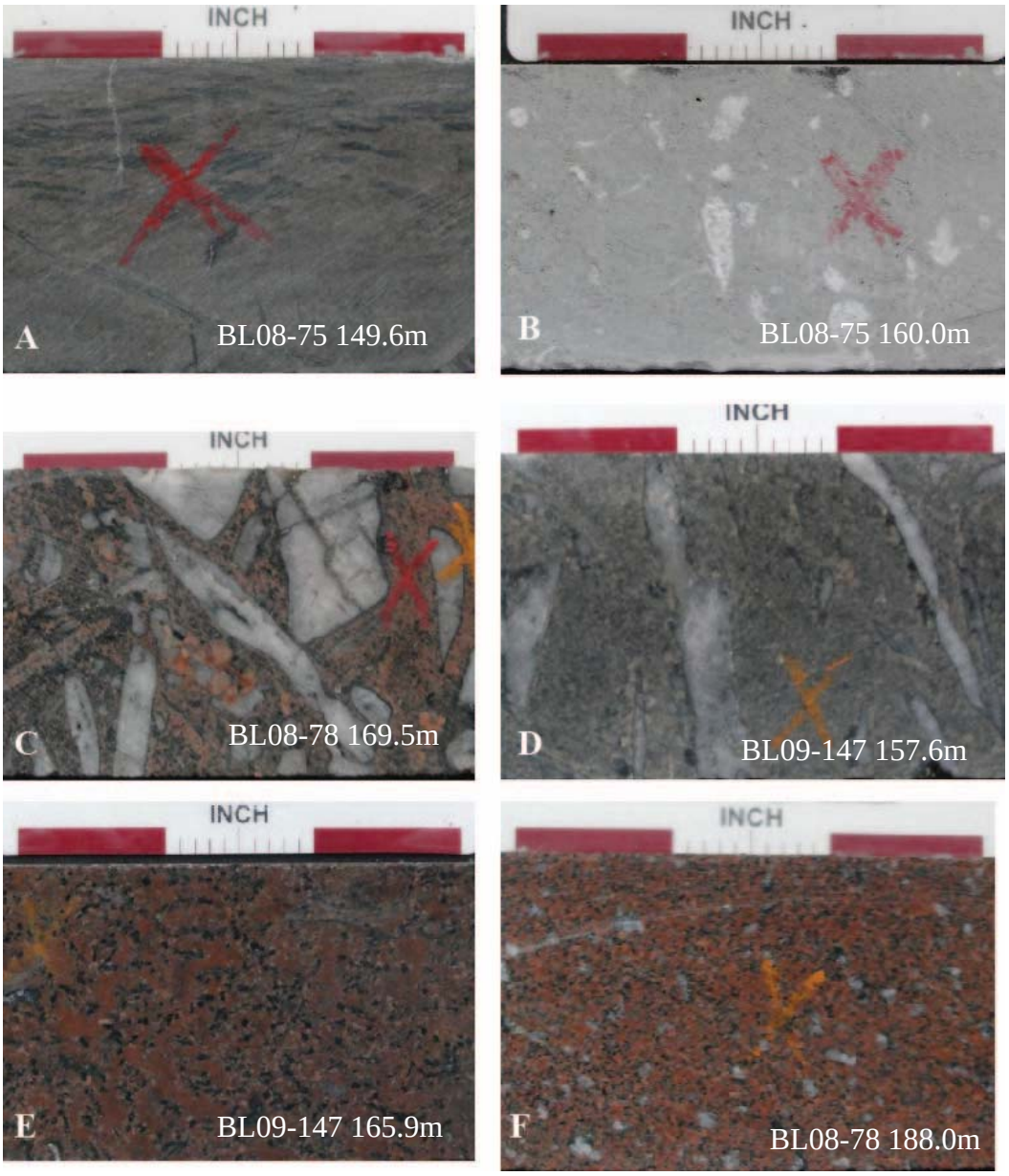

Figure 3.14 – Photographs of BLZ core samples from metasedimentary country rock (A) and the HQG unit (B-F). A) Fine-grained foliated texture of metasiltstone; B) Large calcite amygdules; C) Large chlorite mantled, granitic and quartz-rich inclusions with red fine grained “groundmass”; D) Large quartz-rich inclusions in a grey, fine grained “groundmass”; E) Mottled texture, red patches of hematized potassium feldspar; F) Medium grained anhedral quartz inclusions in a medium fine, equigranular hematized quartz gabbro.

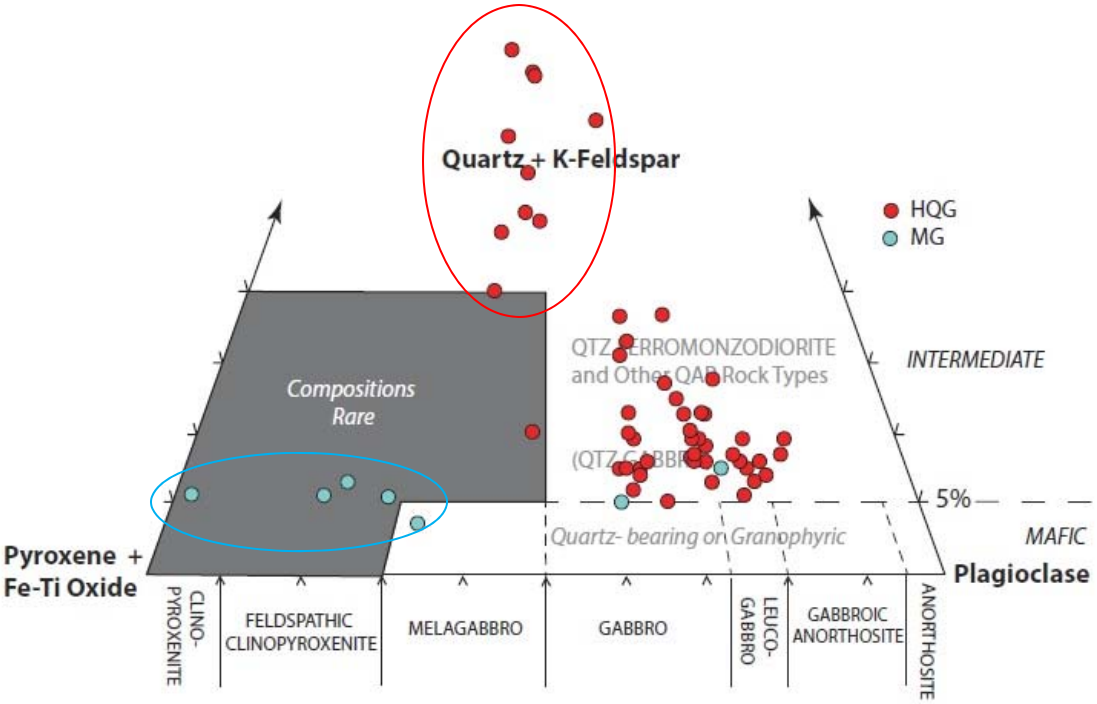

Figure 3.15 – Modal compositions of the samples from HQG unit in the BLZ based on relative proportions of plagioclase, pyroxene + Fe-Ti oxide, and quartz + K-feldspar. Figure based on recommendations by Miller et al. (2002) for distinguishing mafic (gabbroic) rocks from intermediate (dioritic) rocks (see Figure 3.5 for more explanation). The red points indicate samples that qualify as HQG rocks – quartz gabbro, quartz leucogabbro, quartz ferromonzodiorite, quartz ferrodiorite. The samples highlighted by the red circle contain abundant quartz-rich and granitic inclusions. The blue points indicate samples that belong to the Melagabbro unit, which includes ultramafic compositions that contain ~5% quartz (blue circle).

As determined by petrographic analysis, the dominant modal rock types comprising the HQG in the BLZ include quartz gabbro, quartz leucogabbro, quartz ferrodiorite, and quartz ferromonzodiorite (Fig. 3.15). The dominant primary minerals are plagioclase, pyroxene, iron-titanium oxides, quartz, potassium feldspar, and apatite.

Plagioclase typically exhibits lath shaped crystal habits (Fig. 3.13), ranging between 45 and 65% in modal abundance (Fig. 3.12), and is strongly albitized, sericitized, and sauseritized (Fig. 3.13). Though the plagioclase habit and modal percentage remains relatively consistent throughout the unit, the crystal habit changes to anhedral granular and decreases in abundance when there is an increase in potassium feldspar and/or quartz (Figs. 3.12 and 3.13).

Pyroxene is completely altered to chlorite throughout the HQG unit in the BLZ. Pyroxene pseudomorphs exhibits a variety of crystal habits, including prismatic to subprismatic and poikio-prismatic near the margins of the unit (Fig 3.14E and F, Fig. 3.16D) and anhedral granular in the center (Fig. 3.13C). Despite their textural variability, pyroxene modal abundance remains relatively consistent, ranging between 15 and 25%; but is as high as 40% modal abundance where large quartz inclusions occur at ~172 m in BL08-78 and ~165 m in BL09-146 (Fig. 3.12).

The common Fe-Ti oxides identified, using a combination of petrography and SEM-EDS analysis, are titano-magnetite and ilmenite (Fig. 3.15B). Modal abundances for all oxide varieties were estimated to range between 2 to 8% and typically exhibit prismatic to anhedral crystal habits as well as skeletal in some samples. Titano-magnetite often exhibits exsolution lamellae that consist of ilmenite and, at times, rutile.

As previously noted, a common textural component, similar to the CLZ, is the presence of a red mottled appearance. Observations made by transmitted light and SEM-EDS analysis indicate that these mottled areas are comprised of interstitial, micrographic quartz and hematized potassium feldspar clots that enclose primary plagioclase,

pyroxene, and oxide (Figs. 3.14D and E and 3.16E). In addition to being micrographically intergrown, potassium feldspar and quartz also occur as anhedral granular to subpoikilitic crystals throughout other areas of the HQG unit (Fig. 3.16C). Feldspar ranges between 2 and 15% modal abundance, while quartz ranges in mode from 5 to 20% (Fig. 3.12).

Unique to the HQG unit in the BLZ is the presence of large quartz-rich and granitic inclusions. These inclusions consist primarily of deformed, elongate polycrystalline masses of nearly pure quartz grains displaying sutured grain boundaries. The masses are typically rounded to subangular and are commonly mantled by chlorite, potassium feldspar, and granophyre (Fig. 3.14C). In the intervals that contain large quartz inclusions, the modal abundance of quartz and potassium feldspars in the matrix increases, and plagioclase modal abundance decreases (Fig. 3.12). These inclusions occur together in cores BL08-78 and BL09-147 where the quartz-rich inclusions are much more abundant than the granitic inclusions. There are intervals containing only quartz-rich inclusions, including the upper 4 meters of the HQG in BL09-147 and the core of the HQG in BL09-146. Quartz-rich and granitic inclusions are absent in the HQG in BL08-75 where the upper 15 meters contain coarse-grained calcite amygdules (Fig. 3.14B). In contrast to intervals with the quartz-rich and granitic inclusions, the modal percentages of all mineral phases remain relatively constant in the presence of the calcite amygdules.

The contact between the HQG unit and the underlying Melagabbro unit is sharp in terms of changes in texture, mineral abundances, and alteration intensities. Plagioclase abruptly decreases in modal abundance and changes from lath-shaped to

subpoikilitic/poikilitic. Conversely, clinopyroxene increases abruptly in mode and transitions from anhedral granular to subhedral granular and occasionally subprismatic and subophitic textures. Alteration intensities of clinopyroxene also abruptly decrease from completely altered to strongly altered and continues to decrease downward through the Melagabbro unit. Another transitional indicator is the abrupt disappearance of potassium feldspar and the appearance of olivine (Figs. 3.12 and 3.13).

3.2.3 Melagabbro Unit

Sandwiched between the HQG unit and the main mineralized Wehrlite unit in the BLZ is a 1- to 2-meter thick interval of grey, fine- to medium fine-grained mafic to ultramafic rocks. Disseminated sulfide mineralization is present in 2 to 5% modal abundance, throughout the Melagabbro unit.

Based on estimated modal abundances from the petrographic study, the dominant modal rock types in the melagabbro unit of the BLZ include oxide-bearing gabbro, feldspathic clinopyroxenites, and feldspathic wehrlites (Fig. 3.17). All Melagabbro unit rock types from the BLZ also contain 2-8% quartz and would thus be modally described as “quartz-bearing.” It is clear when comparing modal data in Figures 3.17 vs. 3.7 that the Melagabbro unit rocks from the BLZ are distinctly more ultramafic than Melagabbro unit rocks in the CLZ. Despite this modal difference, the textural aspects of Melagabbro unit rocks from both the BLZ and the CLZ are very similar (compare Figs. 3.13 and 3.3/3.9, respectively). Moreover, the relationship of the Melagabbro unit to the HQG and Wehrlite units are the same in both the BLZ and CLZ.

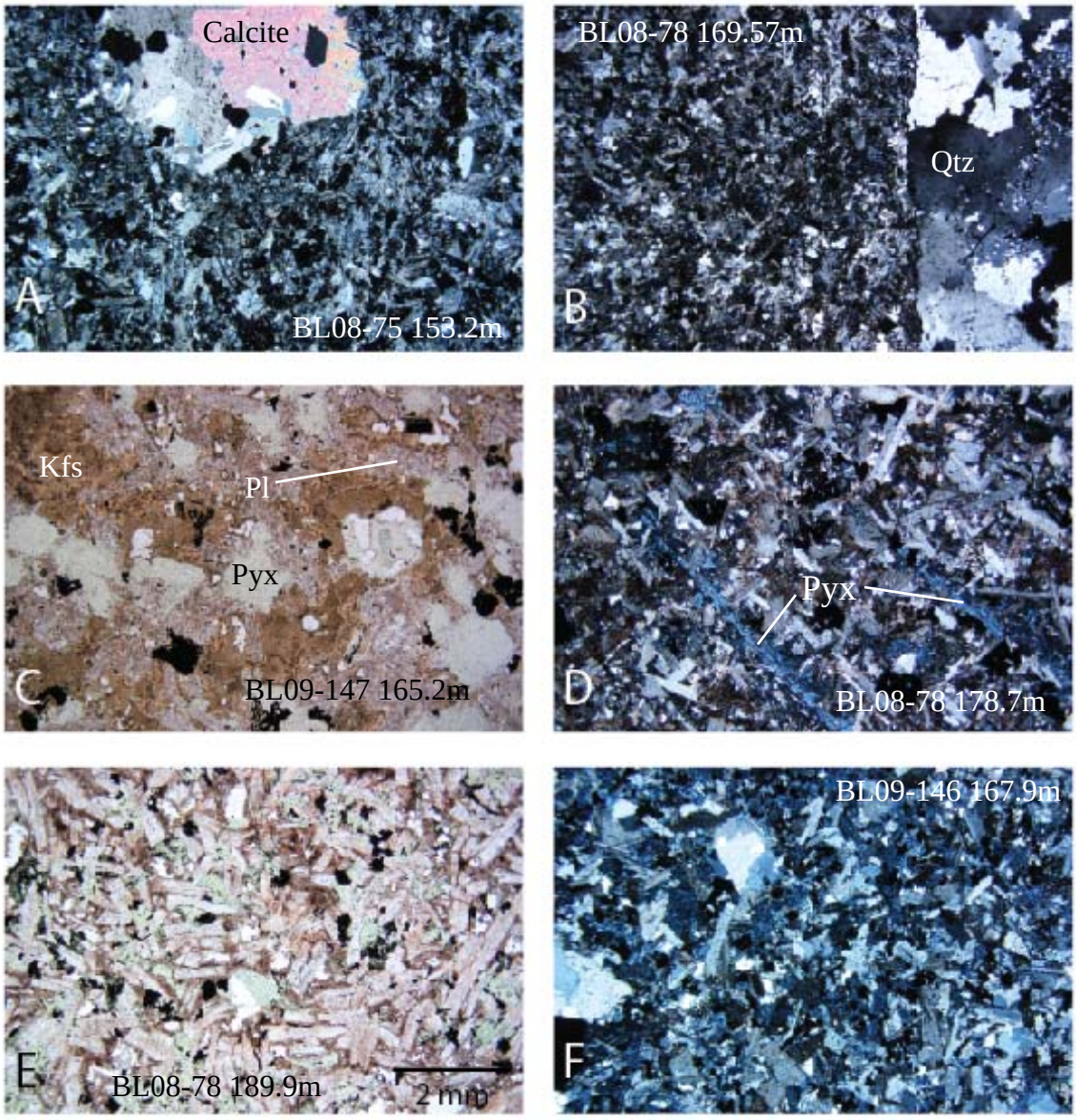

Figure 3.16 – Photomicrographs of textural characteristics of in the BLZ HQG unit.

A) Fine-grained quartz gabbro with calcite amygdule, B) Fine-grained quartz gabbro with large quartz-rich inclusion, C) Mottled texture in quartz monzodiorite with anhedral granular potassium feldspar and quartz, chloritized anhedral granular pyroxene, and lathy plagioclase, D) Poikilo-prismatic pyroxenes, lath-shaped plagioclase in a quartz ferrodiorite, E) Lathy plagioclase with interstitial quartz and hemitized potassium feldspar in a quartz gabbro F) Equigranular plagioclase and pyroxene, and quartz inclusions with calcite in a quartz gabbro.

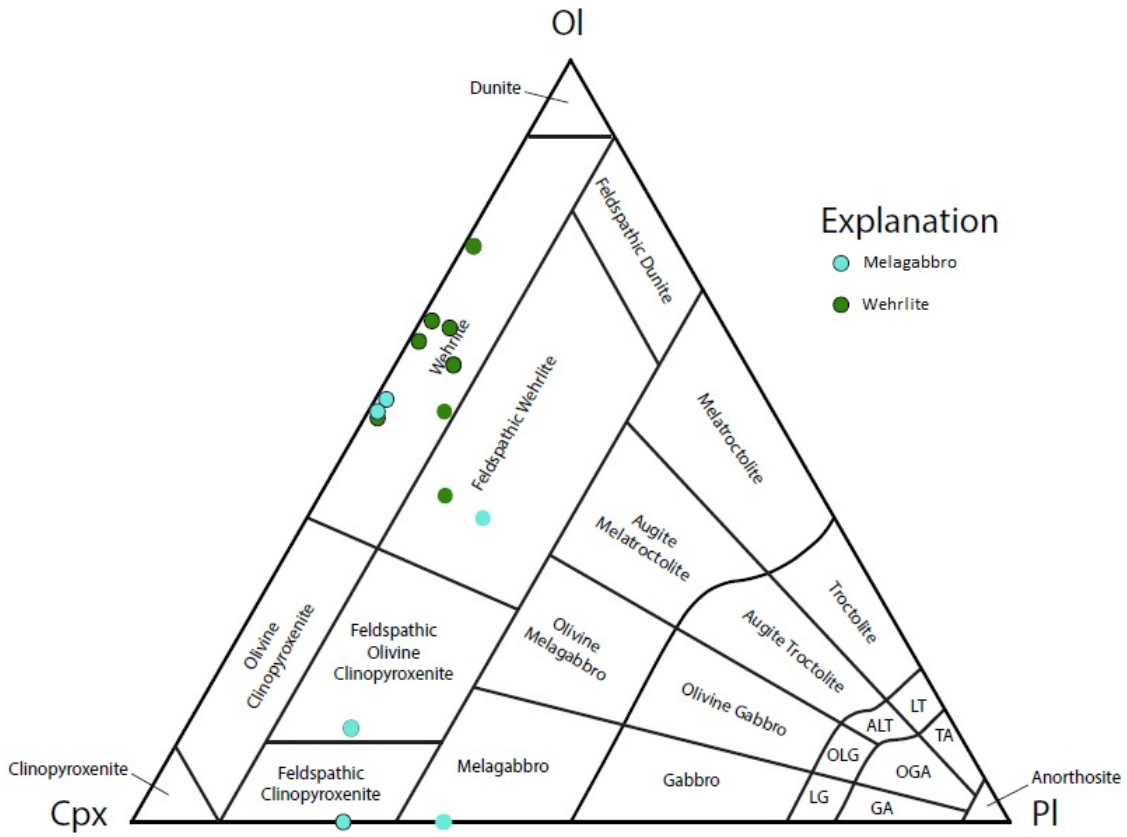

Figure 3.17 – Modal abundances of olivine, clinopyroxene, and plagioclase of samples from the Melagabbro (blue) and Wehrlite (green) units of the BLZ. Classification scheme after Miller et al. (2002).

Downward from the HQG/Melagabbro unit contact in BL08-78 from the BLZ (Figs. 3.12 and 3.13), plagioclase displays an abrupt decrease in modal abundance from 55% to 20% and a change in habit from subpoikilitic to poikilitic. Conversely, clinopyroxene shows an abrupt increase in modal abundance, from 25% to as high as 65% and consistently exhibits subhedral granular crystal habit. Plagioclase and clinopyroxene in the other cores exhibit similar crystal habits and abundances as in BL08-78. Olivine in the Melagabbro unit is typically completely altered, however, its

subhedral granular crystal habit is well preserved. Olivine mode ranges from 10 to 65%. Fe-Ti oxides are much less abundant, 2 to 5%, and commonly exhibit poikilitic and skeletal habits. Quartz is observed interstitial to primary mafic phases and gradually decreases in modal abundance downward from 8 to 2% (Fig. 3.12).

As in the CLZ, the contact between the Melagabbro and the Wehrlite units are gradational over a few centimeters. In drill core BL08-78 (Figs. 3.12 and 3.13), the contact is marked by a rapid decline in modal abundance and alteration intensity of poikilitic plagioclase, commonly becoming absent in the Wehrlite unit. Clinopyroxene remains subhedral granular across the contact. However, after peaking at 35-60% at the base of the Melagabbro unit, clinopyroxene abruptly decreases to 25-35% in the Wehrlite unit (Fig. 3.12). Alteration intensity of clinopyroxene also drastically decreases to weakly altered at the Wehrlite contact (Fig. 3.13). Olivine mode increases to as much as 65% at the base of the Melagabbro unit before decreasing to approximately 45% deeper in the Wehrlite unit (Fig. 3.12). Lastly, though quartz is present in the Melagabbro unit, it is completely absent in the Wehrlite unit.

3.2.4 Wehrlite Unit

Core logging and sampling of the four cores investigated from the BLZ ended in well mineralized, dark green to black, medium/fine- to medium-grained ultramafic rock, which petrographic studies showed to be feldspathic wehrlite to wehrlite (Fig. 3.17). These rocks collectively compose the Wehrlite unit. In core, these rocks are typically medium fine-grained and intergranular near the upper contact and grade to medium- to coarse-grained with depth. The dominant minerals are medium-grained, subhedral

pyroxene that enclose fine-grained olivine crystals. Plagioclase also occurs interstitially to pyroxene and olivine. Sulfide mineralization typically consists of pyrrhotite and chalcopyrite, with trace amounts of galena. Sulfides range from 2 to 3% modal abundance and commonly occur as poikilitic blebs and disseminations. Other minerals include magnetite and chlorite.

Petrographic observations and modal estimates indicate that the dominant modal rock types are feldspathic wehrlite and wehrlite (Fig. 3.16), with the majority of the feldspathic wehrlite compositions occurring near the contact with the Melagabbro unit (Fig. 3.12). The primary mineral assemblage for the Wehrlite unit consist of olivine, clinopyroxene, plagioclase, Fe-Ti oxides, and sulfides. Olivine ranges between 25 and 65% (Fig. 3.12) and occurs as fine- to medium fine-grained, subhedral to euhedral granular primocrysts completely or partially enclosed within larger clinopyroxene grains. Olivine, near the Melagabbro unit margins is generally more abundant and intensely to completely altered to serpentine and talc, whereas unaltered olivine is typically present further from the margin.

Clinopyroxene occurs as medium-grained, subhedral granular typically ranging between 20 and 30% modal abundance (Figs. 3.12 and 3.13). Plagioclase ranges between 5 and 10% modal abundance and occurs exclusively as poikilitic oikocrysts up to 4cm across enclosing clinopyroxene and olivine. Fe-Ti oxides make up 2 to 5% modal abundance (Fig. 3.12) and range in crystal habits from bladed to subhedral granular to anhedral granular.

3.3 Lithogeochemistry of CLIC Units

A total of 52 samples were collected from drill holes profiling the CLIC for geochemical analysis and assay. Two cores, TBND-60 and BL08-78m, which most completely represent CLIC geology of the CLZ and BLZ, respectively, were sampled extensively so as to provide a geochemical representation of each of the major lithologic units in each zone. The remainder of the samples were selected from the other drill cores to obtain a more complete representation of the different units. Of the 52 samples, 26 were collected from each zone, eight samples were collected from TBND-60 and 11 from BL08-78. As explained in Chapter 2, all samples were analyzed for their major and trace element geochemistry and assayed for precious metals (Pt, Pd, and Au). The final results are displayed in the following figures and tabulated in Appendices D and E.

Due to the intense alteration of rocks in the HQG unit (Figs. 3.3 and 3.13), trace elements were heavily relied upon to characterize the geochemical characteristics of the rocks associated with the CLIC. Primitive mantle-normalized multi-element spider plots show very similar smooth patterns for the major rock units in the CLZ and BLZ with an even enrichment of increasingly more incompatible elements (Fig. 3.18). Negative Nb anomalies are observed in most rock types with $Nb/Nb^{*}_{(cn)}$ values ranging between 0.31 and 0.82 (only three samples show positive anomalies).

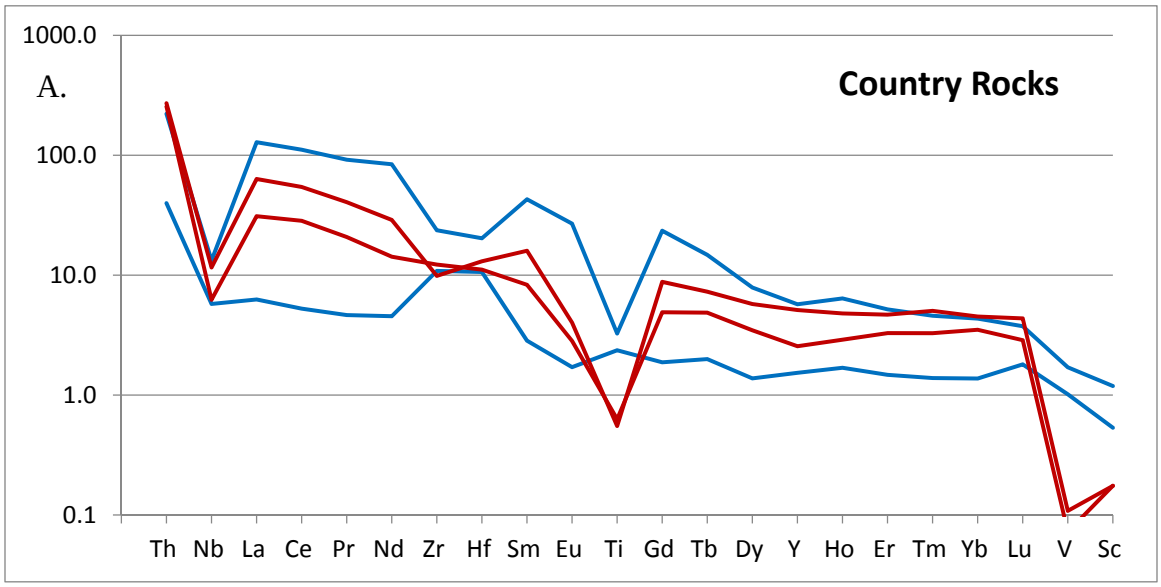
A.
Country Rocks
1000.0
100.0
10.0
1.0
0.1
Th Nb La Ce Pr Nd Zr Hf Sm Eu Ti Gd Tb Dy Y Ho Er Tm Yb Lu V Sc

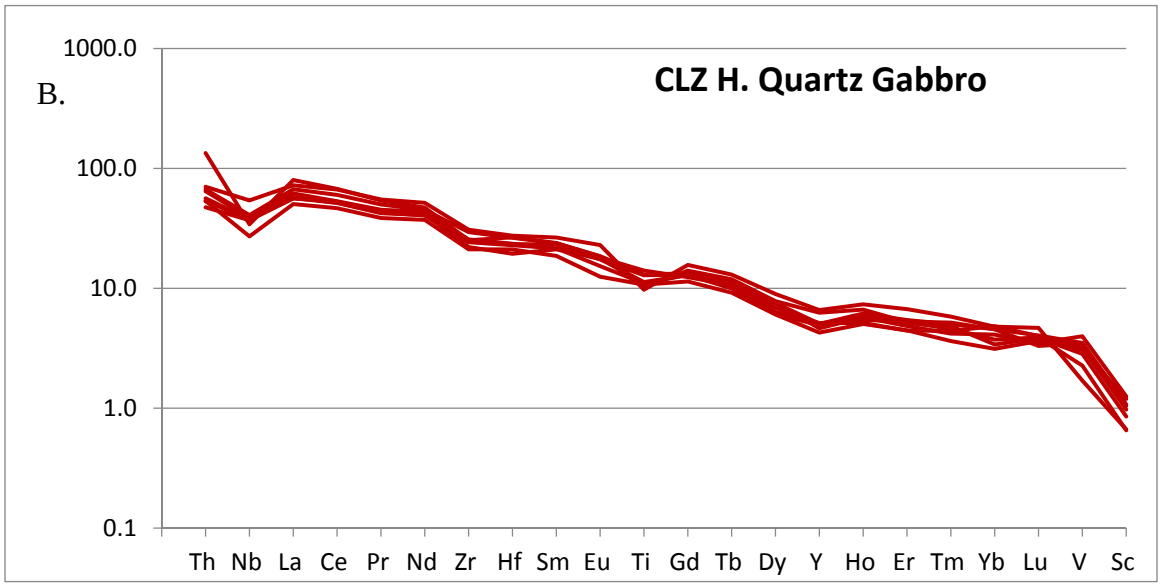
B.
CLZ H. Quartz Gabbro
1000.0
100.0
10.0
1.0
0.1
Th Nb La Ce Pr Nd Zr Hf Sm Eu Ti Gd Tb Dy Y Ho Er Tm Yb Lu V Sc

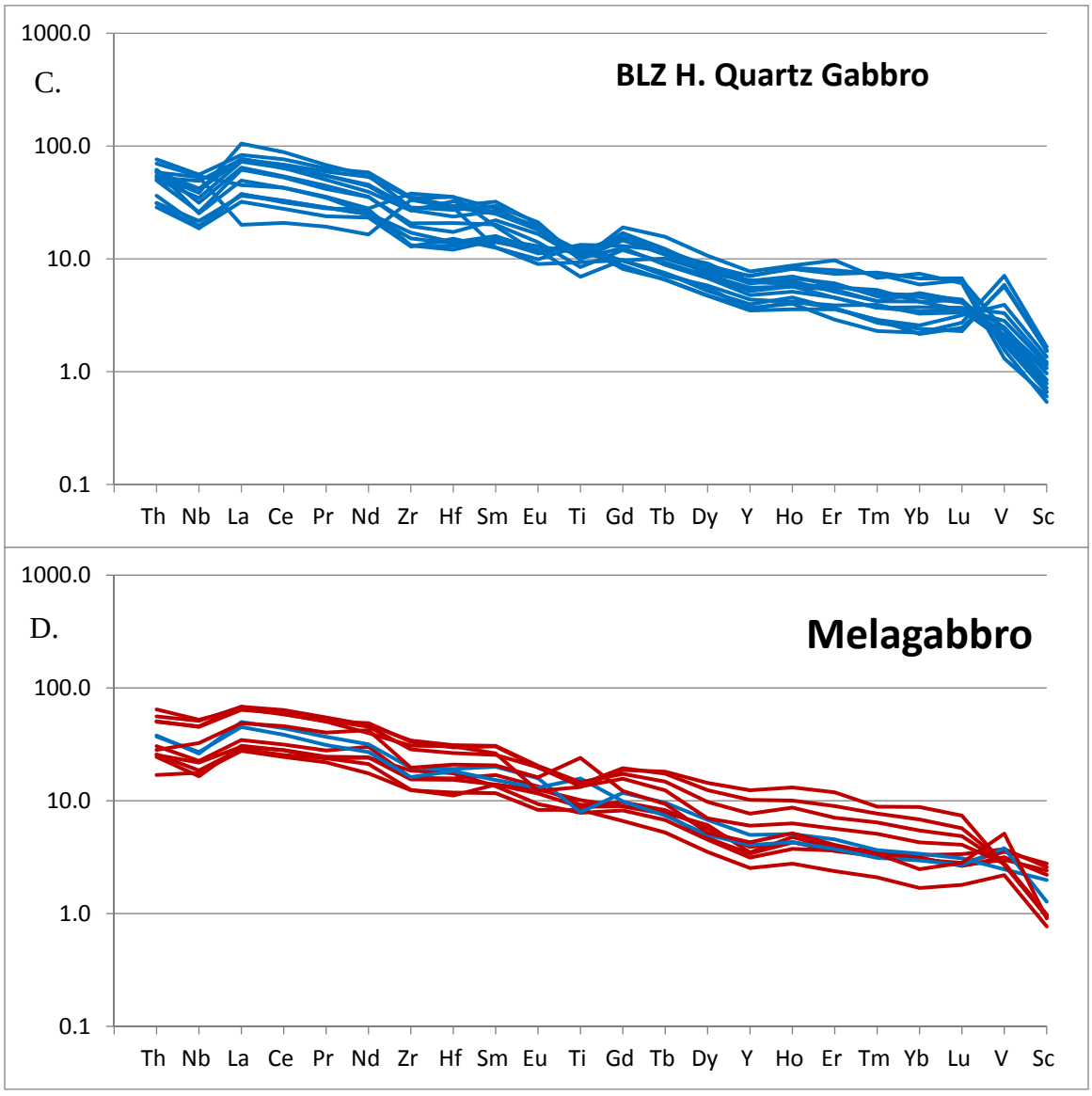
C.
BLZ H. Quartz Gabbro
1000.0
100.0
10.0
1.0
0.1
Th Nb La Ce Pr Nd Zr Hf Sm Eu Ti Gd Tb Dy Y Ho Er Tm Yb Lu V Sc
D.
Melagabbro
1000.0
100.0
10.0
1.0
0.1
Th Nb La Ce Pr Nd Zr Hf Sm Eu Ti Gd Tb Dy Y Ho Er Tm Yb Lu V Sc

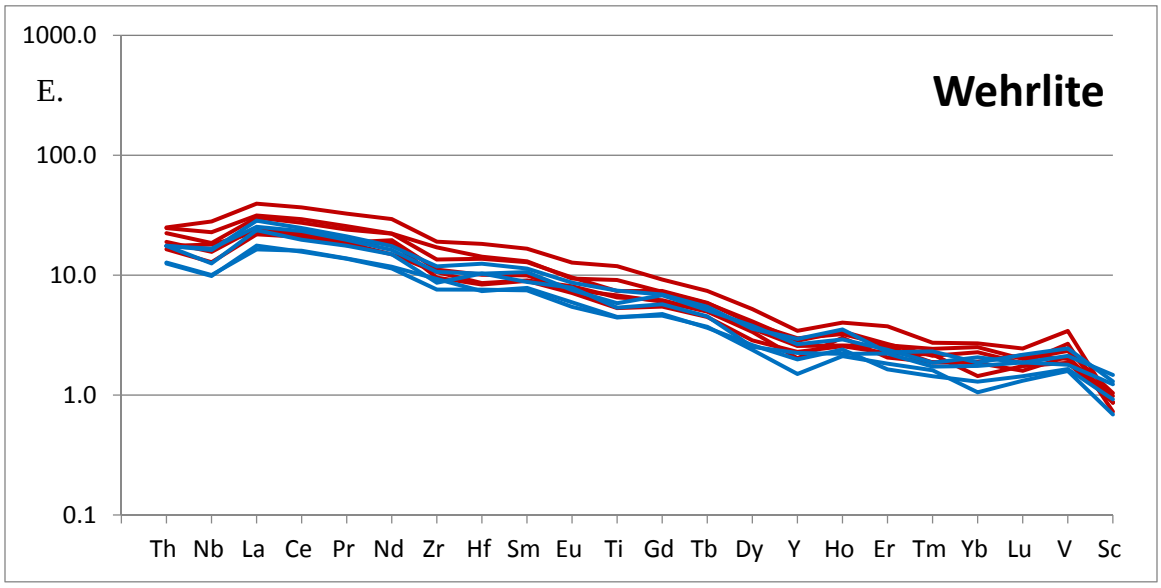

Figure 3.18 – Primitive mantle-normalized spider diagram of trace elements for the major units identified for the CLIC. Samples collected from the CLZ are shown as red lines; BLZ samples are shown as blue lines. (A) Country Rock; (B & C) HQG unit (2 panels); (D) Melagabbro unit; (E) Wehrlite unit; Normalized values after Sun and McDonough (1989).

4.0 Discussion

The observational and analytical data generated through core logging, petrographic studies, SEM-EDS, and lithogeochemistry can now be interpreted to address the primary goals and objectives of this research. The most important goal was to determine the petrogenetic relationship between what was initially identified as the "HRU" and the main mineralized ultramafic rock types comprising the CLIC. However, as discussed in the preceding chapter, petrographic observations more clearly identified the rock types comprising the HRU, resulting in a reinterpretation of rock unit subdivisions originally defined by core logging alone (Tables 3.1 and 3.2). In both the CLZ and the BLZ, the CLIC was subdivided into three main lithologic units: 1) HQG unit, occurring at the margins and outliers of the CLIC; 2) Melagabbro unit, occurring as a marginal phase of the main mineralized ultramafic intrusion; and 3) a Wehrlite unit forming the main mineralized ultramafic intrusion of the CLIC. Although the Melagabbro unit in the CLZ and BLZ are modally distinct (Figs. 3.7 and 3.16), they are geochemically similar (Fig. 3.18), occupy similar structural positions in the CLIC, and are thus interpreted to be petrologically equivalent (this will be discussed in section 4.2);

These new lithological designations along with the other pieces of analytical data have allowed for a better evaluation of the emplacement and crystallization history of the CLIC. Additionally, the data will aid in determining the number and composition of parental magmas as well as the role of country rock contamination in the formation of the CLIC.

4.1 Emplacement History of the CLIC

Integrating the petrographic and lithogeochemical data, it is clear that the three rock units comprising the CLIC in both the CLZ (Table 3.1) and the BLZ (Table 3.2) represent two distinct intrusive phases of emplacement: an early phase represented by the emplacement of the now heavily contaminated HQG unit followed by a later phase of emplacement of the interior zone of the mineralized Wehrlite unit mantled by the Melagabbro unit.

Evidence supporting the interpretation that the HQG unit is a separate, early intrusive phase relative to the Melagabbro and Wehrlite units comes, first and foremost, from the observation that the HQG unit is never found in direct contact with the Wehrlite unit, despite being commonly in direct sharp chilled contact with the country rock and in narrowly gradational contact with the Melagabbro unit in both the CLZ and BLZ (Figs. 3.1 and 3.11).

The intrusive, narrowly gradational HQG-Melagabbro contact is evident in a number of macroscopic and microscopic features. This is particularly apparent downward across the 10-20 cm thick HQG-Melagabbro contact zone profiled in drill hole TBND-60 from the CLZ (Figs. 3.2 and 3.3). Distinct observations of this occurrence include:

- Modal plagioclase decrease from ~50% to ~25% with a complimentary increase in clinopyroxene from ~20% to ~45% (Fig. 3.2);
- Plagioclase habit abruptly changes from lath shaped to subpoikilitic whereas pyroxene habit changes from variable (subophitic, subprismatic, and anhedral granular) to consistently subhedral granular (Fig. 3.3);

- Fe-Ti oxide mode increases slightly (5% to 15%) and anhedral granular habits are joined by skeletal and acicular habits (Figs. 3.2 and 3.5B)
- The degree of plagioclase and pyroxene alteration decreases from strong to complete in the HQG unit to moderate in the Melagabbro unit (Fig. 3.3).
- Micrographic potassium feldspar disappears completely (Fig. 3.2).

In the BLZ, the transition from quartz gabbro in the HQG unit into feldspathic wehrlite in the Melagabbro unit is a much more pronounced shift in relative concentration than observed in the CLZ, though textural changes are comparable. The downward changes observed at the HQG-Melagabbro contact over a distance of 20 cm in drill hole BL08-78 include:

- Modal plagioclase decreases from ~65% to ~20% with clinopyroxene showing a complimentary increase ~15% to ~65% (Fig. 3.12).
- Plagioclase habit changes from lath-shaped to poikilitic and pyroxene from variable (subprismatic, subprismatic/subophitic, subhedral, and anhedral granular; Fig. 3.17C-D) to consistently subhedral granular in the Melagabbro unit (similar to CLZ; Fig. 3.13)
- Degree of plagioclase and pyroxene alteration decreases from strong to complete in the HQG unit to moderate in the Melagabbro unit (similar to CLZ; Fig. 3.13).
- Abrupt loss of potassium feldspar and micrographic quartz+potassium feldspar and decrease in quartz from 10% to 5% (Fig. 3.12).

As a result of the abrupt modal and textural changes observed along the HQG-Melagabbro contact, it is concluded that the Melagabbro unit intruded into the more evolved and altered gabbros and intermediate rocks of the HQG unit. Additionally, the lack of a clear chill zone along with a moderate degree of alteration in the Melagabbro unit at the contact with the HQG unit suggests that the HQG unit was still quite hot, volatile-rich, and potentially partially molten when the second pulse of magma was emplaced.

4.2 Petrogenetic Relationship between the Melagabbro and Wehrlite Units

As previously mentioned, the main mineralized ultramafic cumulates of the CLIC have been grouped into the Wehrlite unit, though only a limited number of samples from the margin of the main mineralized ultramafic intrusion were investigated in this study. Marginal to this unit, grey, predominantly mafic, rocks were observed by Magma Metals and termed the “grey hybrid.” Additional core logging and petrographic analysis conducted in this study resulted in the reclassification and renaming of some of the “grey hybrid” rocks as the Melagabbro unit (present in both the CLZ and the BLZ).

While the narrowly gradational contact between the Melagabbro and HQG units suggest that the Melagabbro intruded into the HQG unit, the more gradational transition from the Melagabbro unit into the Wehrlite unit results is consistent with the Melagabbro unit being a marginal phase of the main mineralized intrusion. However, it is necessary to address the distinctly different modal compositions of the Melagabbro unit in the CLZ (Fig. 3.7) and BLZ (Fig. 3.16).

Based on visually estimated volume proportions of olivine, clinopyroxene, and plagioclase, the majority of CLZ-Melagabbro samples (Fig. 3.7) are modally classified as gabbro, with a lesser amounts classified as leucogabbro, olivine gabbro, melagabbro, and feldspathic olivine clinopyroxenite. In contrast, BLZ-Melagabbro samples (Fig. 3.16) are modally classified as having a more ultramafic composition including werhlite, feldspathic werhlite, olivine clinopyroxenite, feldspathic olivine clinopyroxenite, feldspathic clinopyroxenite, and melagabbro.

Despite these differences in modal classification, the Melagabbro units in both zones share many common feature which include:

- Spatial positions within the CLIC: located always marginal to the Wehrlite unit and either in direct chilled contact with the country rock or narrow gradational contact with the HQG unit;
- Primary mineral assemblages: despite proportional differences, the types of minerals present are identical, including plagioclase, clinopyroxene, olivine (appearing away from the contact and modally increasing into the Wehrlite unit), and Fe-Ti oxide, with minor sulfide, amphibole, biotite, and apatite. Minor quartz is also locally present in both units as individual anhedral granular crystals;
- Textures and alteration intensities of primary minerals: both zones consist of subpoikilitic to poikilitic plagioclase and subhedral granular clinopyroxene with weak to strong alteration intensities; when olivine is present, it is has subhedral granular texture and is intensely altered, becomes less so as it grades into the Wehrlite unit;

- Trace element geochemistry: identical primitive mantle normalized patterns (Fig. 3.18).

These commonalities suggest that the CLZ- and BLZ-Melagabbro units are likely comagmatic. A plausible explanation for the significant difference in relative mineral abundance is differences in cooling rate, which ultimately may be related to the size of the intrusion and whether the Melagabbro/Wehrlite magma was emplaced into a precursor HQG intrusion or into country rock. As apparent by the distribution of units in the CLZ (Fig. 3.1), much of the Melagabbro unit is in direct contact with granitic country rock. Along with the smaller size of the CLIC in the CLZ, rapid cooling at these granitic, country rock contacts would explain the greater abundance of plagioclase, as well as the very fine to fine grain size and lathy habit at the contact. In contrast, where the Melagabbro unit is located between HQG and the Wehrlite unit (e.g., drill hole TBND-60 in the CLZ (Figs. 3.2 and 3.3) and BLZ (Figs. 3.11, 3.12, and 3.13) plagioclase is typically more medium-fine to medium-grained and subpoikilitic to poikilitic in habit. Slower cooling where Melagabbro/Wehrlite magmas intruded into the initial and still hot HQG intrusion would promote crystallization of only high temperature liquidus phases (olivine and clinopyroxene) resulting in plagioclase crystallizing poikilitically from trapped liquid between the mafic primocrysts.

Following the assumption that the CLZ- and BLZ-Melagabbro units are comagmatic, it may be reasonable to then interpret the Melagabbro unit as a more rapidly cooled marginal zone of the main ultramafic intrusion, as evident by the gradational

contact between the Melagabbro and Wehrlite units (Figs. 3.2, 3.3, 3.8, 3.9, 3.12, and 3.13). This diffuse and/or gradational nature of the contact is seen through the steady coarsening of primary mineral phases when transitioning into the Wehrlite (Figs. 3.3, 3.10, and 3.13). Simultaneously, modal plagioclase continues to decrease with its crystal habit transitioning from subpoikilitic (or lath-shaped where the Melagabbro unit is in direct contact with country rock) to poikilitic (Figs. 3.8, 3.9, 3.12, and 3.13).

In addition to the mineralogical and textural evidence, comparisons of trace element lithochemical data also support the Melagabbro unit as a marginal phase. Comparing Wehrlite and Melagabbro data on primitive mantle-normalized spider diagrams (Fig. 4.1), it is apparent that both units share parallel slopes and similar patterns. Additional, as seen in Figure 4.1B, the Melagabbro unit samples contain higher concentrations of incompatible elements relative to the Wehrlite unit data. This further supports the conclusion that the Melagabbro unit is more representative of rapid cooling of the parent magma whereas the lower trace element abundances of the Wehrlite unit samples are consistent with being cumulates of that same magma.

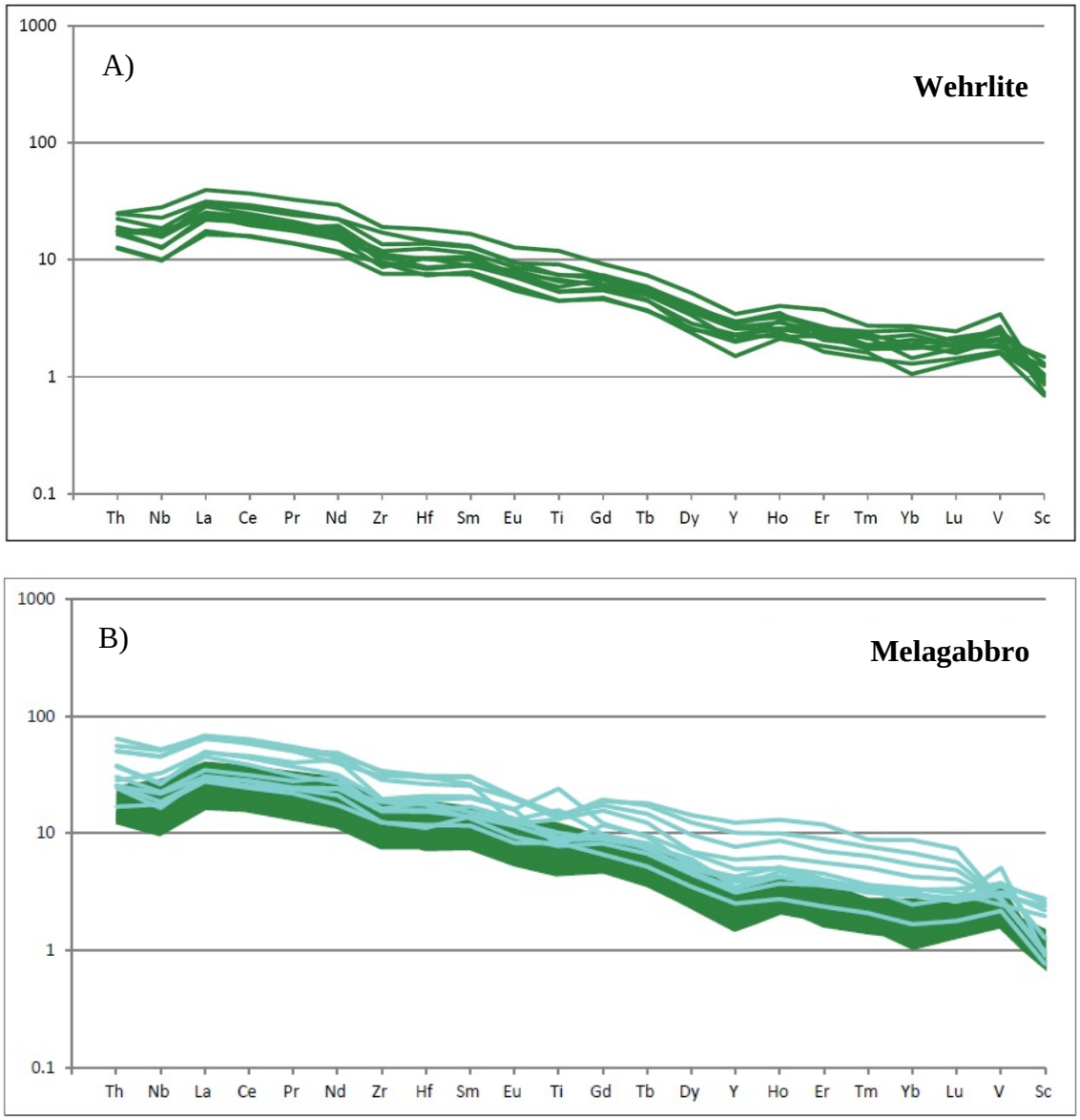

Figure 4.1 – Primitive mantle-normalized spider diagrams of Wehrlite and Melagabbro units. A) Wehrlite unit samples. B) Melagabbro unit samples (lt. blue) over a mask of Wehrlite data (green). Normalization values from Sun and McDonough (1989).

4.3 Parental Magma of the CLIC

Given the differences in the mineralogy, texture, internal structures, and alteration displayed by the two main intrusive phases of the CLIC, it may be expected that distinct parental magmas were involved in their formation. However, given the role contamination may have played in the origin of the HQG unit and the close spatial (and potentially temporal) relationship between the two intrusive phases, it seems possible that both intrusive phases are related to a common parental magma that was intensely contaminated in the early intrusive phase. Immobile trace element geochemistry was utilized to determine if the intrusive phases were related to a common parental magma.

4.3.1 Evaluation of Trace Element Data

In Figure 4.2, a spider diagram of primitive mantle-normalized incompatible element concentration of HQG unit samples are compared to the data field for Melagabbro unit samples. The HQG unit data exhibits similar patterns and nearly identical slopes to the Melagabbro unit sample. The co-parallel spidergram plots of the HQG and Melagabbro units (Figure 4.2) clearly support the idea that both intrusive phases were derived from a common parent magma.

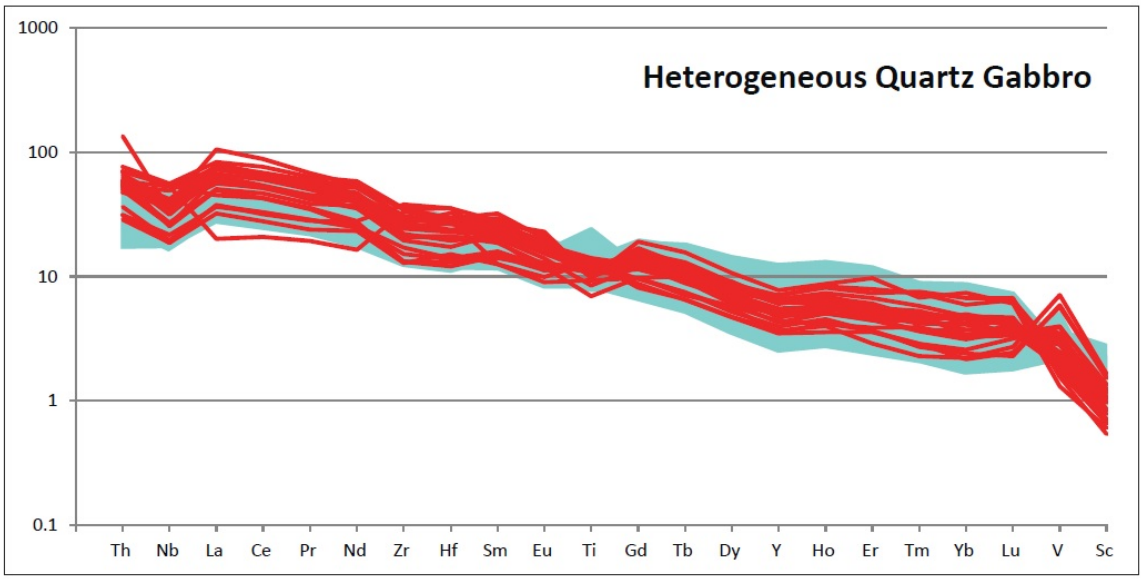

Figure 4.2 – Primitive mantle-normalized incompatible trace element spidergrams comparing the HQG unit (red lines) **to the Melagabbro unit** (lt. blue mask). Normalization values from Sun and McDonough (1989).

To evaluate the potential of country rock contamination of the CLIC parental magma, La/Sm and Nb/Nb* ratios for all CLIC units and country rocks were plotted in Figure 4.3. This bivariate plot identifies distinctive, but overlapping, fields for the HQG, Melagabbro, and Wehrlite units. Additionally (and except for a few data points), the Wehrlite and Melagabbro data fields completely overlap, further evidence to support that the Melagabbro unit is a marginal phase of the Wehrlite unit. However, samples from the HQG unit define a broader distribution of trace element ratios that extend from the Melagabbro-Wehrlite field toward the compositions of granite. This supports the interpretation that both the HQG unit was sourced from the same parental magma (speculated to correspond with the red star in Fig. 4.3) that later formed the Melagabbro/Wehrlite units and it was strongly and variably contaminated by country

rock compositions (brown arrow in Fig. 4.3). This contamination will be discussed in more detail below.

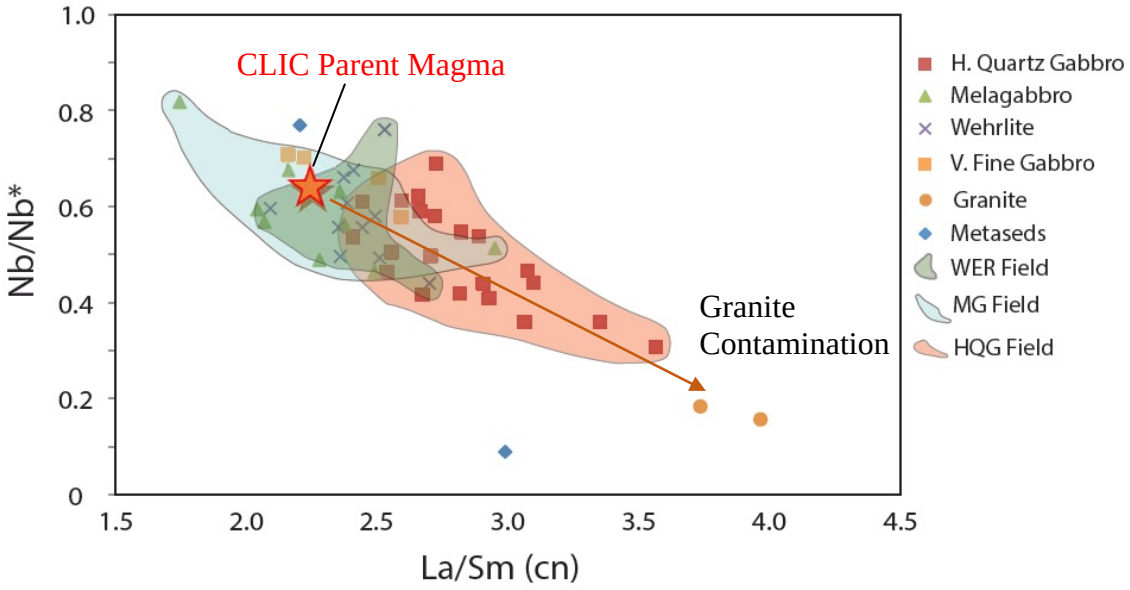

Figure 4.3 – Bivariate trace element ratio graph of La/Sm(cn) versus Nb/Nb* for all CLIC rock units and metasedimentary (BLZ) and granitic (CLZ) country rock. Also shown are fields of the three principal CLIC rock units which significantly overlap. Data from the HQG unit displays a linear trend which projects toward the granite samples. The red star is a speculative parental magma composition for all CLIC lithologies and the brown arrow indicates a possible mixing line between this composition and granitic contaminants. Normalizing values from Sun and McDonough (1989).

4.3.2 Evaluation of Very Fine Grained ("Chilled") Gabbro Compositions as Approximate CLIC Parental Magma

After determining that the HQG and Melagabbro/Wehrlite units are genetically related to the same, but variably contaminated, parental magma, the next question to address is the actual composition of that magma. Since the high trace element

concentrations of the HQG and Melagabbro units likely represent rapidly crystallized phases of the CLIC, it is possible that the least contaminated of these compositions may approximate the parental magma composition. However, due to the intense contamination and alteration present in most rocks of the HQG unit, it is unlikely to contain a fine-grained sample that would qualify as an uncontaminated “chill” of CLIC parental magma composition. Therefore, the best candidates for possible chills are the very fine-grained Melagabbro unit samples from the CLZ that are in direct contact with granitic country rocks (Figs. 3.1, 3.8, and 3.9). Although these samples are typically strongly altered and contain (xenocrystic) quartz, they represent the best approximation of major element composition of the CLIC parental magma. The speculated parental magma composition in Figure 4.3 was estimated based on the average values of the four Melagabbro unit “chill” samples (termed very fine grained gabbro).

Four very fine-grained, quartz-bearing gabbro samples collected at the contact between the Melagabbro unit and the granitic country rock in the CLZ are of particular interest as potential parental magma candidates. These samples, along with being very fine-grained, have a distinctive felty texture which resulted from an abundance of prismatic plagioclase, anhedral granular clinopyroxene, and acicular Fe-Ti oxides (Fig. 4.4). On a normalized trace element spider diagrams, these fine-grained rocks show similar patterns and slopes to the Melagabbro unit (Fig. 4.5) as well as the HQG and Wehrlite units (Fig. 3.18), More importantly, the fine-grained Melagabbro unit samples contain significantly elevated incompatible trace element values, which is more representative of a liquid composition (Fig. 4.5). These mineralogical, textural, and

geochemical attributes give strong support to the interpretation that these rocks represent the rapidly cooled parental magma of the CLIC.

A.

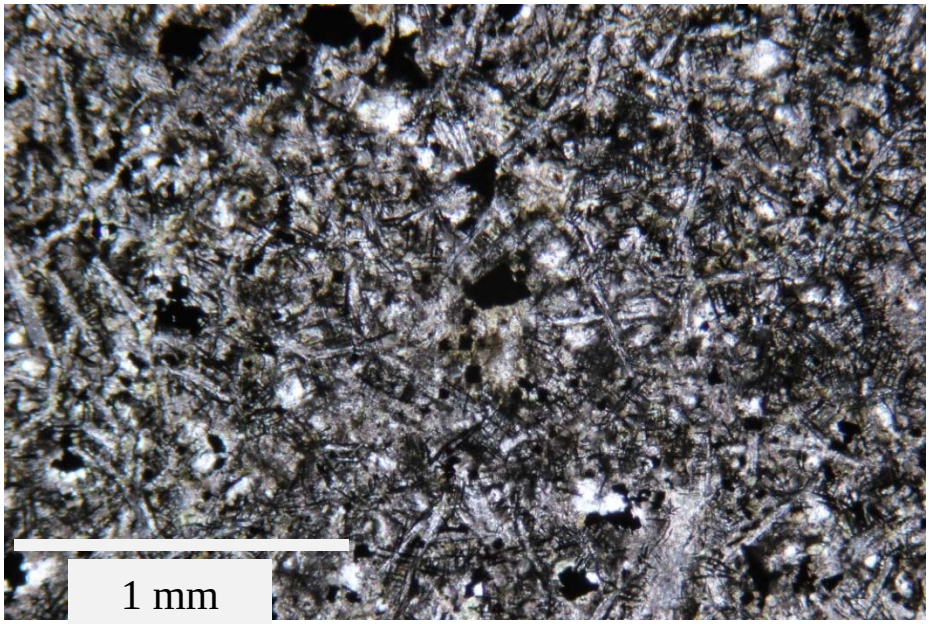

B.

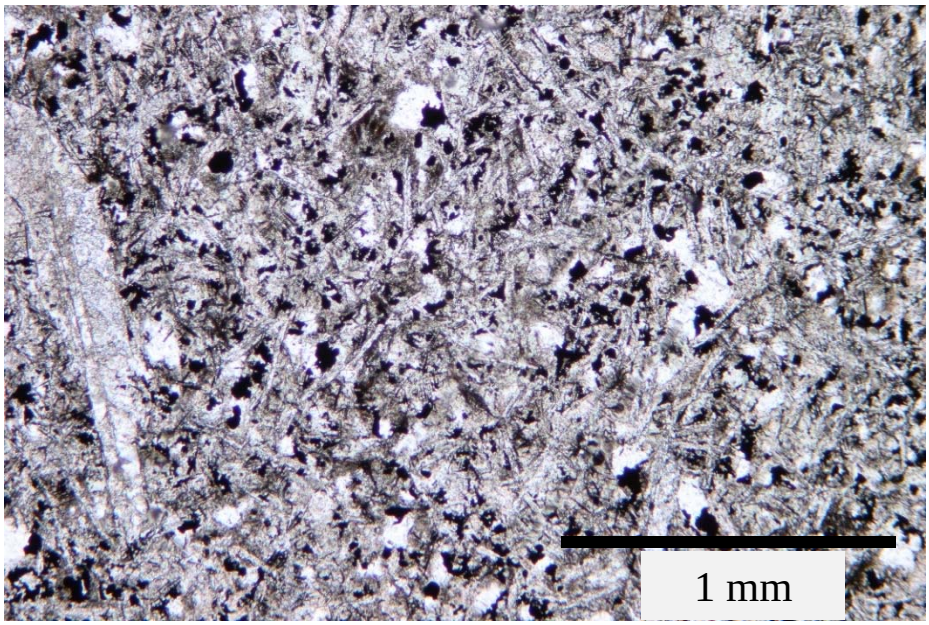

Figure 4.4 – Photomicrographs of very fine-grained, felty-textured gabbro samples collected from the margins of the Melagabbro unit where it is in direct contact with granitic country rock (see Fig. 3.1). A) TBND-124 (94.7m) and B) TBND-95 - 99.1m. Both images were taken in PPL.

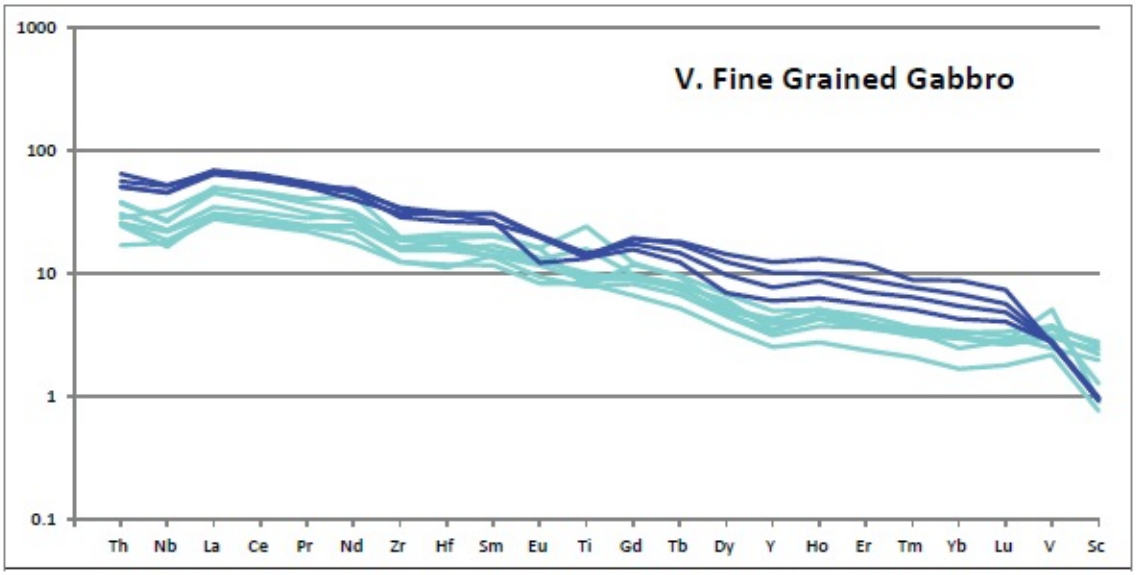

Figure 4.5 – Primitive mantle-normalized spider diagrams of samples from the Melagabbro unit (lt. blue). The four fine-grained gabbro samples that may approximate chilled magma compositions are shown dark blue. Normalization values from Sun and McDonough (1989).

PELE (a variation of MELTS developed by Boudreau, 1999) can be used as an independent test of the plausibility of the fine-grained Melagabbro unit samples approximating the parental magma. PELE can establish the mode and compositions of phases expected to crystallize from a cooling magma at a set pressure and oxygen fugacity. If the fine-grained gabbro are a valid choice, PELE should show a mineral paragenesis of extensive olivine crystallization followed by clinopyroxene, plagioclase, and Fe-Ti oxide as implied by cumulus and post-cumulus phases observed in the Wehrlite unit.

Table 4.1 shows the major elemental compositions of the four “chill” samples and the average of all four. Note that the loss on ignition totals are large, reflecting the altered

state of the samples. These compositions were renormalized to 100 wt. %, distributing FeO and Fe_2O_3, assuming QFM oxidation conditions, and adding 2 wt. % H_2O (a reasonable assumption given the abundance of primary biotite and amphibole in the Wehrlite unit).

The liquidus temperature for various phases calculated by PELE using equilibrium crystallization conditions are shown in the lower part of Table 4.1. All runs show protracted crystallization of olivine starting at liquidus temperatures ranging from 1090 to 1190°C. However, most compositions indicate crystallization of plagioclase and Fe-Ti oxide before clinopyroxene, which is not observed in the Wehrlite unit. Only sample TBND-124 94.7 shows a mineral paragenesis close to what is observed, olivine crystallizing at 1090°C, followed by clinopyroxene, plagioclase, and Fe-Ti oxide, all with liquidus temperatures between 1020 and 1000°C. Interestingly, the results show that sample TBND-95 99.1 does not crystallize clinopyroxene at all, but is the only sample where orthopyroxene arrives late.

The variability in the PELE results, coupled with the observed alteration and possible crustal contamination of these samples raises questions as to their validity as representations of the CLIC's parental magma. Another possible issue is that the major element compositions for these and other CLIC samples were analyzed by an XRF analyzer at UMD for which robust analytical protocols have not been well established, potentially resulting in inaccurate and/or unusable major element data.

Table 4.1 – Major element compositions of four fine-grained gabbro samples and their average from the CLZ speculated to be an approximate representation of the CLIC parent magma.

Sample ID	TBND-124 94.7	TBND-023 115.9	TBND-95 99.1	TBND-023 107.5	Average Chill
SiO_2	45.7	47.26	45.56	50.56	**46.35**
TiO_2	2.68	2.81	2.69	3.1	**2.82**
Al_2O_3	14.84	15.64	15.07	16.27	**15.46**
Fe_2O_3	12.3	15.64	10.9	14.59	**12.44**
MnO	0.09	0.11	0.09	0.16	**0.11**
MgO	4.33	3.85	6.75	4.9	**4.96**
CaO	7.37	6.03	5.07	6.03	**6.13**
Na_2O	3.97	4.52	3.14	4.55	**4.05**
K_2O	0.5	0.42	0.3	0.84	**0.52**
P_2O_5	0.4	0.45	0.42	0.54	**0.45**
LOI(~H_2O)	7.07	5.15	8.68	5.58	**6.62**
Sum	99.25	98.20	102.36	103.43	**100.81**
Mg#	43.65	41.47	50.45	49.73	**46.33**
PELE Model Liquidus Temperatures (Equil. Xtal @ 1.5 Kb, fO_2~ QFM, H2O~3%)					
Olivine	1090	1080	1190	1120	**1120**
Clinopyroxene	1010	930	-	920	**940**
Plagioclase	1020	1020	1000	1010	**1010**
Ti-Magnetite	1000	990	990	950	**990**
Apatite	940	950	940	960	**950**
Orthopyroxene	-	-	870	-	**-**
Gas	950	930	970	930	**960**

With the validity of the four “chill” samples in question, a different approach may be necessary to determine the composition of the parental magma. Early MCR intrusions of the Nipigon Plate area (Disraeli, Seagull, and Hele; Hollings et al., 2007b) may have been produced by similar parental magma, and therefore a comparison of the CLIC’s immobile trace element geochemistry with those early intrusions might provide a robust

analogue. The incompatible elements pattern were plotted on primitive mantle normalized spider diagrams for the ultramafic rocks from Disraeli, Seagull, and Hele intrusions against the Wehrlite unit (Fig. 4.6). Both the Disraeli and Hele peridotite data consist of similar patterns and slopes as the Wehrlite unit, suggesting they were derived from similar parental magma compositions. Although the peridotites of the Seagull intrusion yield a similar slope to the Wehrlite unit, there are a variety of patterns present that make it difficult to accurately compare the two intrusions. However, a much cleaner comparison is evident between the olivine gabbros of the Seagull intrusion and the CLIC (Fig. 4.7).

Bivariate plots of $La/Sm_{(cn)}$ versus Nb/Nb* were used to compare the CLIC with the Disraeli, Seagull, and Hele intrusions (Fig. 4.8). The data from Disraeli, Seagull, and Hele plot close to or within the CLIC field. However, most importantly, the three other intrusions show a similar increasing $La/Sm_{(cn)}$ trend with decreasing Nb/Nb* values, compared to that of the CLIC. This enforces the conclusion that these intrusions were produced by magmas of similar composition as well as implying similar crustal contamination source. This is not surprising given that Disraeli, Seagull, and Hele also intruded into the Quetico Subprovince.

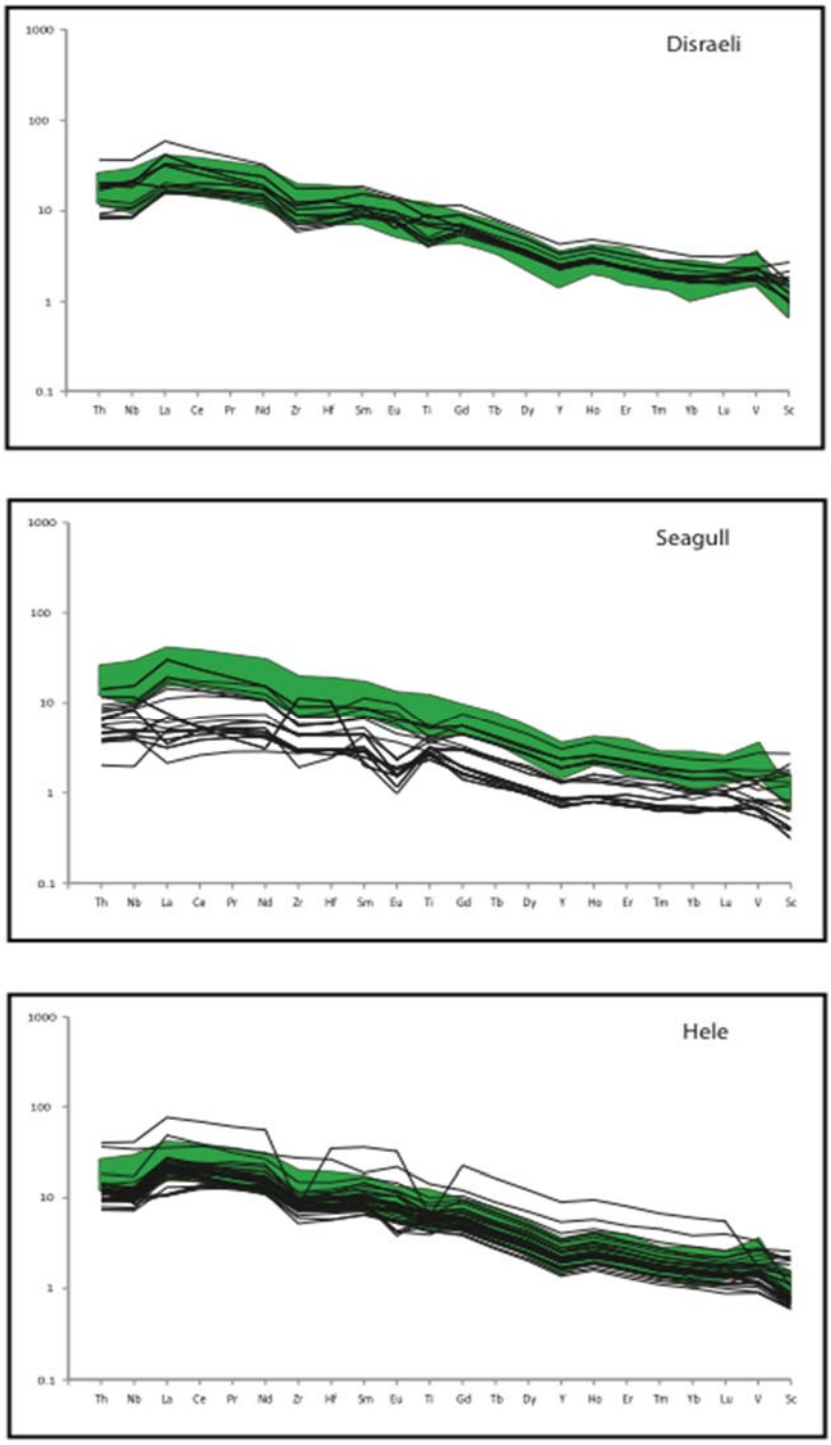

Figure 4.6 – Primitive mantle normalized trace element diagrams of peridotite samples from Disraeli, Seagull, and Hele compared to data from the Wehrlite unit of the CLIC outlined by a green "mask." Values were normalized after Sun

and McDonough (1989). Disraeli, Seagull, and Hele data reported in Cundari (2012).

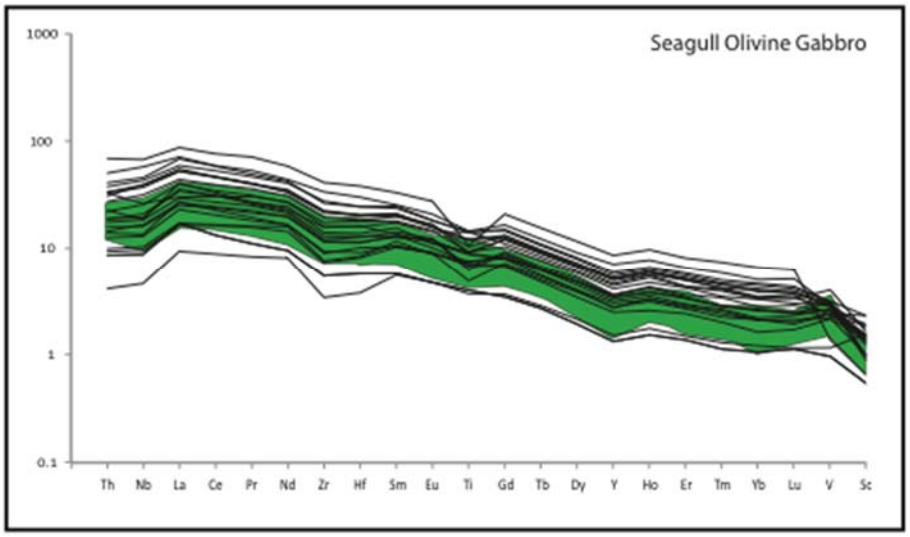

Figure 4.7 – Primitive mantle normalized trace element spider diagram of olivine gabbro data from the Seagull intrusion compared to data from the Wehrlite unit of the CLIC, represented by the green "mask." Values were normalized after Sun and McDonough (1989). Seagull data from Heggie (2005).

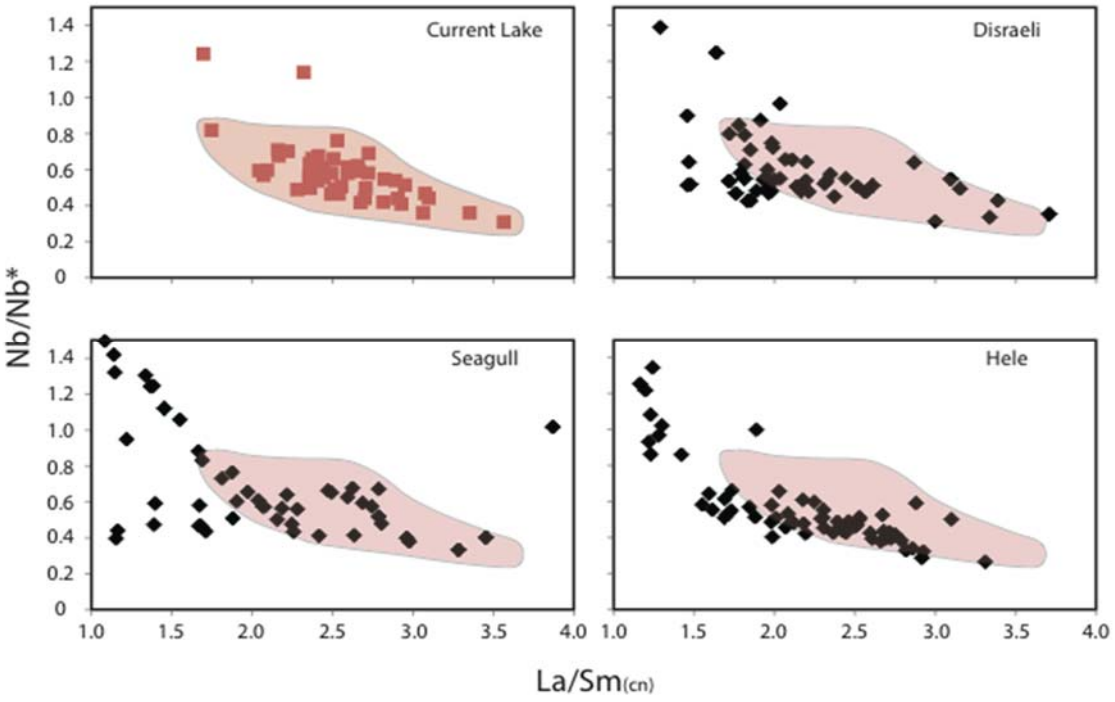

Figure 4.8 – Bivariate plots of La/Sm(cn) versus Nb/Nb* comparing the CLIC to the Disraeli, Seagull, and Hele intrusions (Cundari, 2012). Field is extent of CLIC data. Normalization values from Sun and McDonough (1989).

As previously stated, the similarities in the lithogeochemistry between the CLIC and the three other Nipigon Plate intrusions provides additional evidence that they were derived from similar mafic parent magmas. Of the three, the Seagull intrusion has been the most intensely studied. Calculations made by Heggie (2005) for the parental magma composition of the Seagull intrusion, along with evidence of limited crustal contamination were interpreted to be similar to that of modern plume-related ocean island basalt (OIB) lavas. Similarly, Hollings et al. (2007a) indicated that the high incompatible element abundances with light rare earth element (LREE) enrichment and heavy rare earth element (HREE) fractionation of these intrusions are comparable to the most primitive basalts at the base of the Osler Group Volcanics. Therefore, it is interpreted that

those basalts show similar incompatible element patterns as modern OIBs, which were produced by an enriched mantle plume (Hollings et. al. 2007b). Considering the resemblance between the trace element signatures of the rocks of the CLIC and those of other intrusions associated with the early stages of the MCR, it is concluded that the parental magma of the CLIC was likely derived from an enriched mantle plume source similar to that of modern OIBs.

4.4 Evaluating Country Rock Contamination

One of the primary objectives of this study has been to evaluate the extent of contamination in the HQG unit. Another major objective was to determine how contamination differs between the CLZ and BLZ where the country rock differs. As an ancillary benefit, the nature of the contamination may provide a means of determining the direction of flow of the CLIC chonolith.

4.4.1 Mineralogical and Textural Evidence of Contamination in the Heterolithic Quartz Gabbro Unit

Observations made during drill core logging and petrographic analysis yield the first clue as to a potential source of contamination, including the mineralogical and textural components of the large quartz-rich and granitic inclusions of the BLZ (Figs. 4.9 and 4.10) and the interstitial micrographic quartz and potassium feldspars (Figs. 3.5A and 3.14C). Figure 4.9A shows two examples of the large granitic inclusions, consisting primarily of hematized potassium feldspars and chlorite-mantled, irregularly shaped quartz. Like the granitic inclusions, the quartz-rich inclusions only occur in the BLZ and consist of irregular quartz grains that typically exhibit sutured grain boundaries, wavy

extinction, and are usually mantled by chlorite, potassium feldspar, and granophyre (Fig. 4.10A and B). In addition to the large inclusions, micrographic quartz and potassium feldspar occur as red patches (Figs. 3.4B and 3.14E), as well as interstitial to mafic mineral phases in the HQG unit. However, quartz and potassium feldspar do not always occur together in this manner. Quartz, for example, is also observed as single, fine-to-medium-grained, anhedral to subpoikilitic crystals. Potassium feldspar, which only occurs as micrographic intergrowths with quartz and is less abundant in the CLZ, can also be observed as medium-fine to medium-grained, anhedral granular crystals in the BLZ (Fig. 3.16C). These textural relationships imply that quartz and potassium feldspar crystallized from a felsic liquid that incompletely mixed with a mafic magma that had crystalized the mafic mineral phases.

The presence of these inclusions potentially indicate that the contamination of the HQG unit may have been derived from crustal granites, likely the Quetico granites. Though the granitic inclusions may provide the strongest case for the Quetico granites being the source of contamination, they are far less abundant than the large, quartz-rich inclusions (Fig. 4.9B). These quartz-rich inclusions may be the residual products of partially melted Quetico granites, where potassium feldspar is completely melted and separated from quartz. This anatectic melt then re-crystallizes at or near the margins of what later becomes an inclusion (Fig 4.9B and 4.10A). Quartz, on the other hand, only partially melts, as evident by the presence of granophyre and interstitial quartz in the “ground mass” between the restite inclusions (Fig. 4.10A). The remaining, un-melted quartz undergoes thermal metamorphism, which results in the sutured recrystallized

appearance and wavy extinction of individual quartz grains (Fig. 4.10B). Another possibility is that the inclusions were derived from quartz veins in the Quetico metasedimentary rocks that did not completely melt, as it is more difficult to melt pure quartz, but may react with the mafic magma to make a form a granophyric and/or chlorite mantle on the margins of the inclusions.

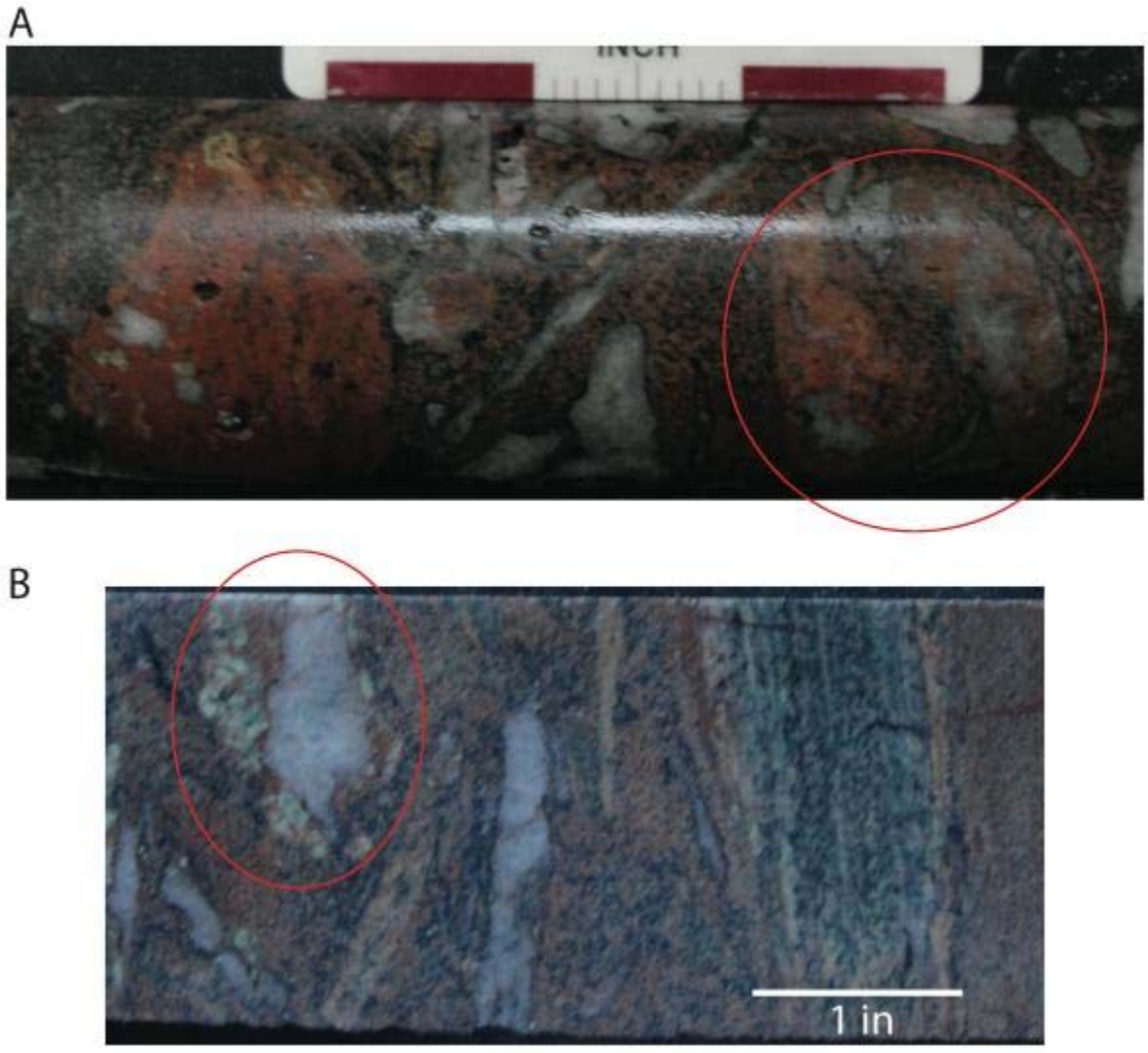

Figure 4.9 – Country rock inclusions in the HQG unit from the BLZ. A) Two large granitic inclusions, as well as several quartz-rich inclusions (BL08-78 169.5) and

B) Massive quartz and, less abundant, granite gneiss inclusion (BL08-78 171.92). The red circle indicates a quartz inclusion mantled by potassium feldspar.

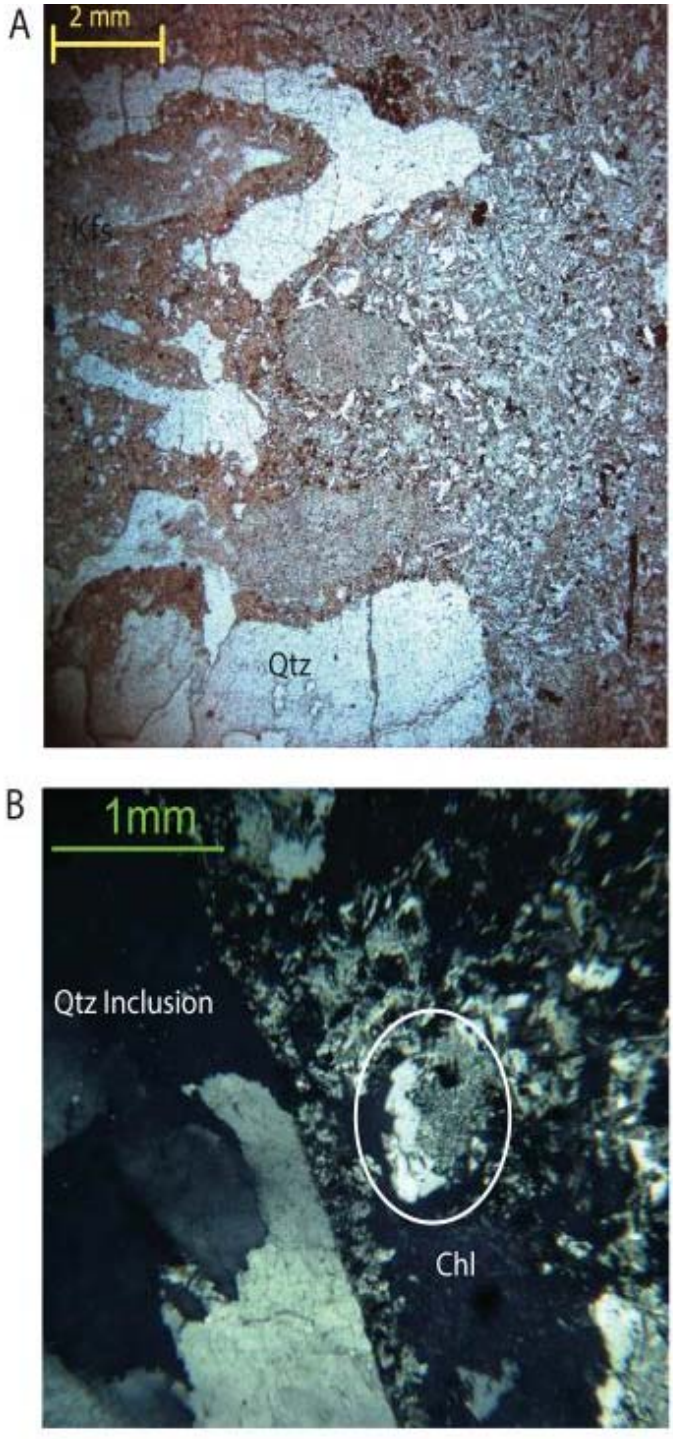

Figure 4.10 – Microphotographs of quartz-rich and granitic inclusions. A) Sample BL08-78 171.92a, showing hematized potassium feldspar surrounding quartz, and B) Sample BL09-147 157.6 showing a quartz-rich inclusion mantled by chlorite, potassium feldspar, and granophyre (circled). Notice the irregular quartz grains with sutured grain boundaries of the quartz-rich inclusion.

4.4.2 Trace Element Evidence for Contamination

As implied by Figure 4.3, trace element geochemistry can also indicate the source and location of crustal contamination. The HQG unit samples plotted in Figure 4.3 show a trend of decreasing Nb/Nb* and increasing $La/Sm_{(cn)}$ toward two data points representing granite samples collected for this study. To more robustly evaluate the contamination of the HQG unit by granite country rock implicit in this diagram, additional geochemical data from Cundari (2012) of Quetico granites and metasedimentary rocks were plotted (Figure 4.11). As evident in this figure, the additional data enforces the interpretation that the Quetico granites are the primary source of the contamination of the HQG unit. Additionally, some of the Quetico schist data plot within the vicinity of the Quetico granites, which implies that the metasedimentary rocks may be an additional source of crustal contamination.

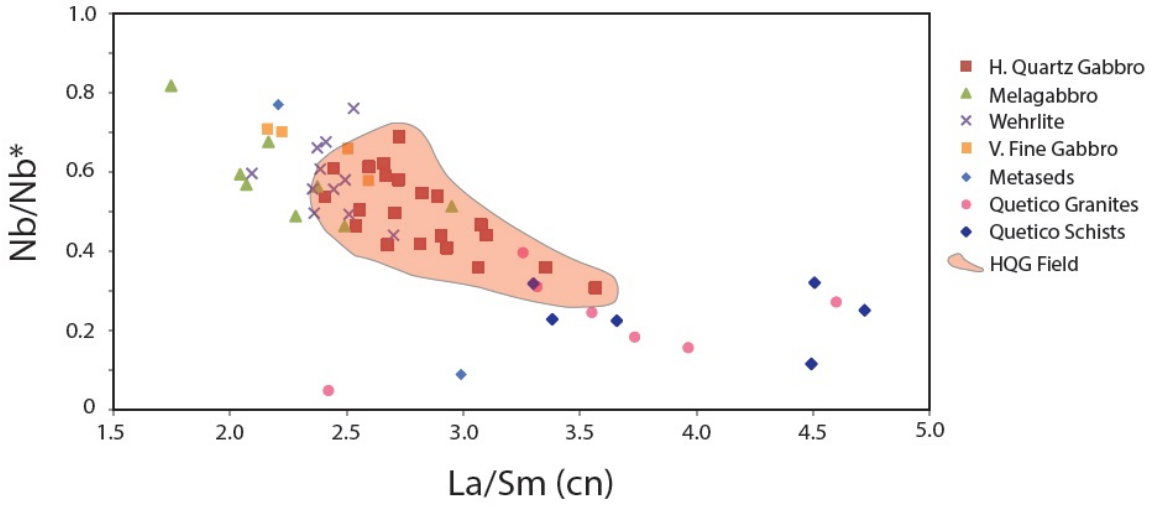

Figure 4.11 - Bivariate trace element ratio graph of $La/Sm_{(cn)}$ versus Nb/Nb* with additional geochemical data from the Quetico Subprovince **(**from Cundari, 2012).

4.5 Model for the Emplacement, Contamination, and Crystallization of the CLIC

With the comagmatic relationship between the HQG unit and the Melagabbro/Wehrlite units clearly established, and the probable parental magma estimated to be similar to other MCR intrusions in the area, a two-stage emplacement model for the CLIC can be proposed (Fig 4.12).

The first intrusive pulse, emplacing the HQG unit, was likely strongly controlled by pre-existing structures in the Quetico Subprovince (Fig. 4.12A) resulting in a subhorizontal orthogonal pattern of intrusions (Heggie et al., 2012). This first phase of mafic magma emplacement (Fig. 4.12B) was accompanied by extensive assimilation of the country rock, probably by partial melting of Quetico granites and some metasediments. Because of the small size of the intrusions, in relatively cold country rock, mafic and antectic felsic magmas did not completely mix, resulting in the

mineralogically and texturally heterogeneous HQG unit crystallizing from the walls inward (Fig. 4.12C).

The second pulse of primitive magma, derived from the same source as the initial pulse, utilized the same structural weaknesses and the semi-molten interior of the first intrusive phase to ream out and expand the CLIC chamber, especially in the BLZ, and offshoot dykes and sills (Fig. 4.11D). This second pulse, when fully crystallized, became the Melagabbro margin and the Wehrlite core (Fig 4.11E). Intermingling of felsic melts present in the semi-molten HQG intrusion with the second pulse mafic magmas resulted in contamination of the marginal part of the second intrusion (the Melagabbro unit).

Knowing the effects that rapid cooling and quenching has on the crystallization of the Wehrlite unit, coupled with the evidence that the HQG unit was derived from the same magmatic source, sheds light on the crystallization history of the HQG unit. As alluded to in previous sections, upon its emplacement, the original magma of the HQG was significantly contaminated by assimilation/partial melting of the granites and possibly the metasedimentary rocks of the Quetico Subprovince (country rock), thus adding a felsic liquid component to the intruding mafic liquid. However, rather than creating a hybrid magmatic composition through mixing, the two liquid components remained compositionally segregated. This is likely result of the significant difference in viscosity between high-silica felsic melt and more fluid mafic magma. Additionally, the inherent temperature differences would have initially created a thermal disequilibrium between the mafic and felsic magmas, which ultimately caused a thermal shock to the mafic component, resulting in rapid cooling and the formation of mafic mineral phases

similar to those observed in the chilled Wehrlite rocks. In turn, this produced felty textured plagioclase as the dominant mineral, subhedral to poikio-prismatic clinopyroxene, and acicular to euhedral Fe-Ti oxides (Fig. 4.13). After the mafic liquid component had fully crystallized, the residual felsic magma crystallized in the pore space between the mafic phases and in irregular pockets to produce micrographic potassium feldspar and quartz. The consequence of these phenomena was the rapid cooling of two liquid components that, although thermally and compositionally separate, led to the formation of the hybridized rock unit, known as the HQG unit.

A)

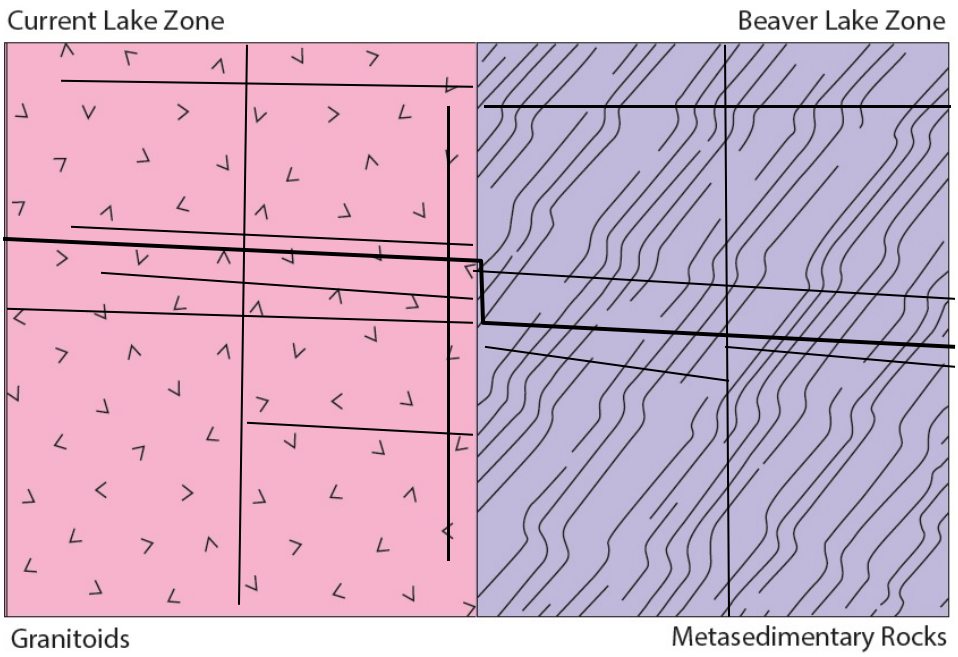

B)

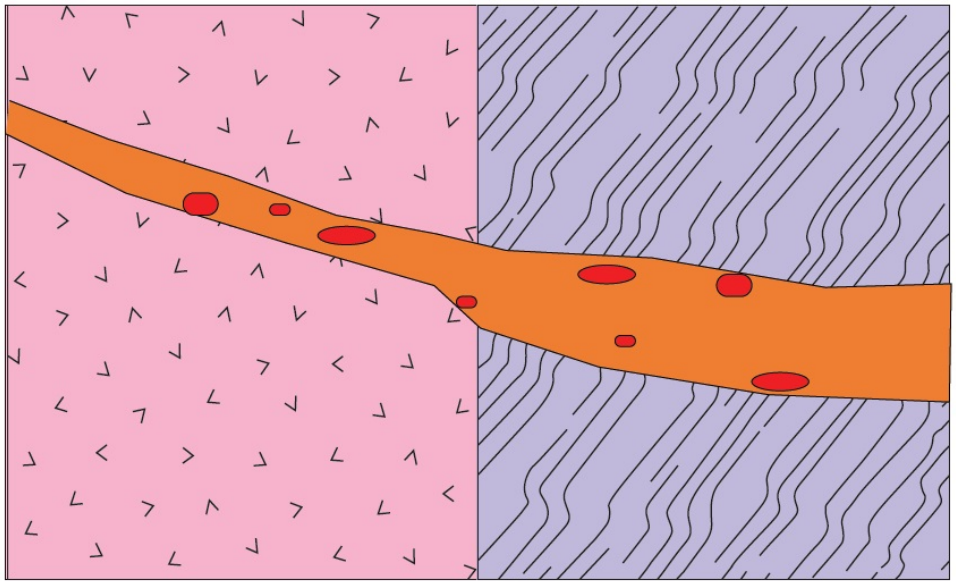

C)

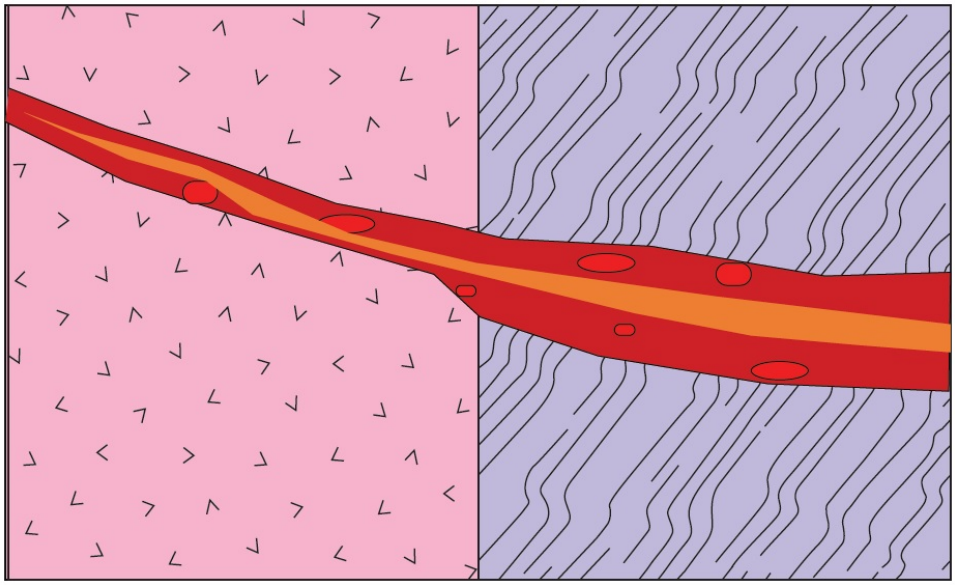

D)

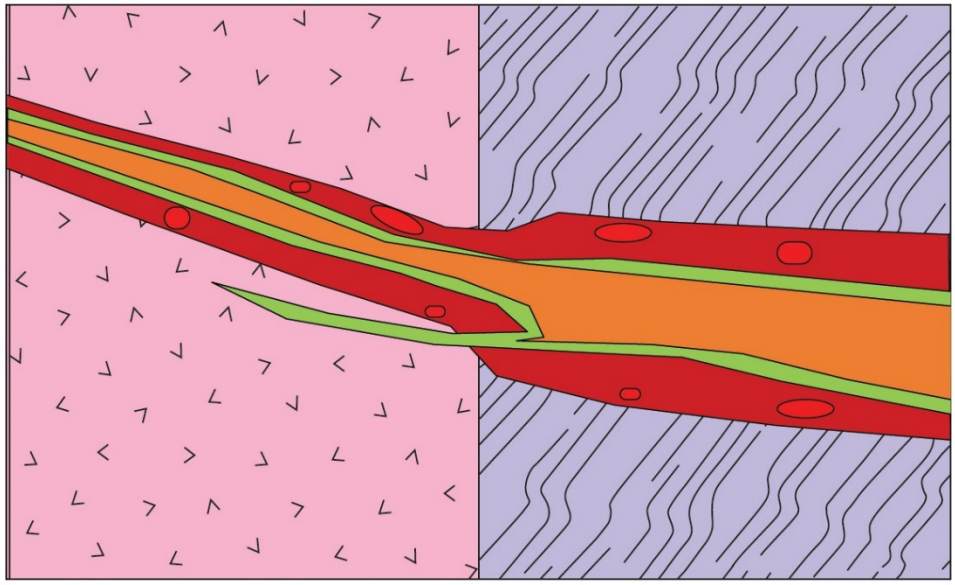

E)

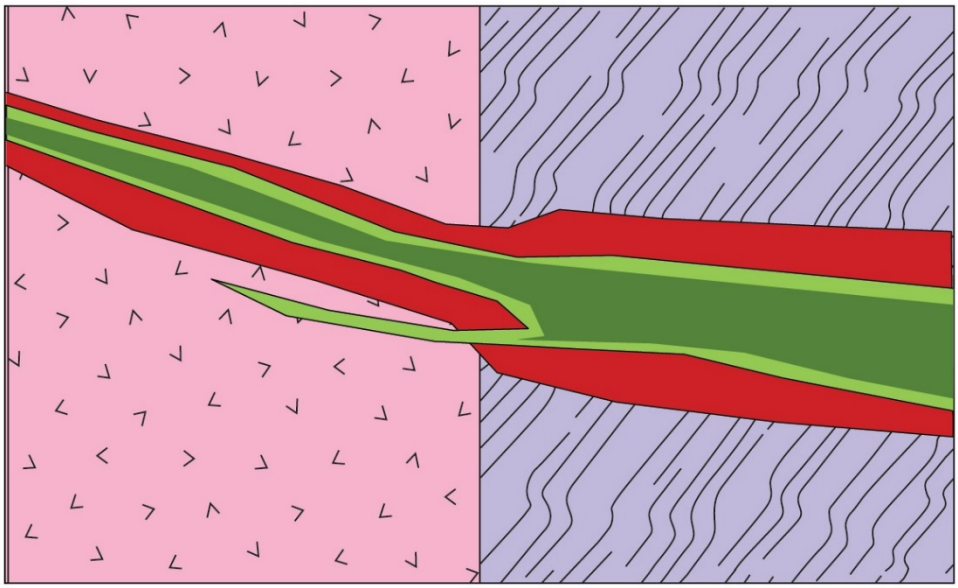

Figure 4.12 – Emplacement model for the formation of the CLIC as the product of two magmatic episodes. A) Granitic and metasedimentary rocks of the CLZ and BLZ prior to the first magmatic pulse; lines illustrate the subhorizontal pre-existing structures thought to exist; B) Emplacement of the first pulse of mafic magma which becomes strongly contaminated and loaded with granitic country

rock inclusions; C) Partial crystallization of HQG unit; D) Composite intrusion second pulse of mafic magma with chilling and contamination of the Melagabbro unit; E) Complete crystallization of the Wehrlite unit.

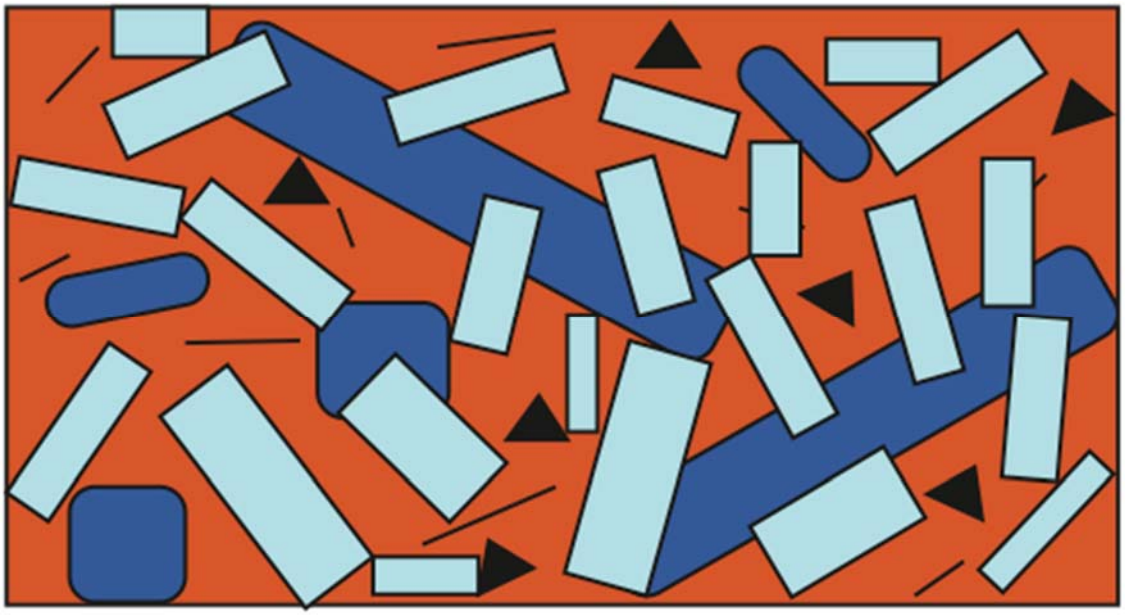

Figure 4.13 – Illustration of HQG crystallization after the formation of plagioclase (light blue)**, clinopyroxene** (dark blue)**, and Fe-Ti oxides** (black)**, prior to crystallization of the residual felsic liquid** (red).

5.0 Conclusions

Taking into consideration of all the evidence gathered through core logging, petrographic, and geochemical analysis, the major conclusions for this study are as follows:

- The “red hybrid” and in some cases the “grey hybrid” units consist of several lithological variations of quartz gabbroic rocks. The dominant rock types include very intensely altered and contaminated potassium feldspar-bearing, quartz gabbro/leucogabbro, quartz monzogabbro, and quartz monzonite. The resultant new terminology for these rock types in this study is the Heterolithic Quartz Gabbro (HQG) unit.
- The remaining “grey hybrid” unit rocks were moderately to intensely altered, fine- to medium fine grained, intergranular to subpoikilitic quartz-bearing feldspathic wehrlite to melagabbro in the BLZ and gabbro to melagabbro in the CLZ. Though mineralogical differences exist between the two zones, they were renamed the Melagabbro unit and the mineralized intrusion was termed the Wehrlite unit.
- Potassium feldspar and quartz are the primary mineral inclusions observed throughout the HQG unit. In both the CLZ and BLZ, quartz and potassium feldspar typically occur as single inclusions, or together as micrographic inclusions that are interstitial to primary mafic phases. Exclusively in parts of the BLZ, large quartz-rich and granitic inclusions are observed. Petrographic and geochemical evidence suggests that these inclusions originated from the adjacent

granitic country rocks of the Quetico Subprovince and are likely the result of partial melting and assimilation.

- The location of the HQG unit at the margins of the mineralized intrusion suggests that it was emplaced first, followed by a comagmatic event which emplaced the Melagabbro and Wehrlite units. This interpretation is further supported by the abrupt mineralogical and textural contact relationships between the HQG and Melagabbro/Wehrlite units.
- The similarities of the HQG and Melagabbro/Wehrlite primitive mantle trace element patterns as well as the $La/Sm_{(cn)}$ vs Nb/Nb* correlations provide strong evidence that the units were derived from the same parental magma source.
- Considering the resemblance between the trace element signatures of the rocks of the CLIC and those of other intrusions associated with the early stages of the MCR, it was concluded that the parental magma of the CLIC was derived from an enriched mantle plume source similar to that of modern OIB.

References

Boudreau, A.E, 1999, PELE – A version of the MELTS software program for the PC platform, Computers and Geosciences, vol. 25, pp. 21-203.

Cannon, W. F., 1994, Closing of the Midcontinent Rift—a far-field effect of Grenvillian compression: Geology, v. 22, p. 155–158.

Card, K.D. and Poulsen, K.H., 1998, Geology and mineral deposits of the Superior province of the Canadian Shield. In *Geology of the Precambrian Superior and Grenville Provinces and Precambrian Fossils of North America*, ed. S.B. Lucas and M.R. St. Onge, Geological Society of America, C1, pp. 13-204.

Cundari, R., 2012, Geology and geochemistry of midcontinent rift-related igneous rocks. M.S. Thesis, Lakehead University, 153 p.

Davis, D.W. and Sutcliffe, R.H. 1985. U-Pb ages from the Nipigon Plate and northern Lake Superior; Geological Society of America Bulletin, v.96, p.1572-1579.

Davis, D.W., Pezzutto, F., and Ojakangas, R.W., 1990. The age and provenance of metasedimentary rocks in the Quetico Subprovince, Ontario, from single zircon analyses: implications for Archean sedimentation and tectonics in the Superior Province. Earth and Planetary Science Letters 99, p. 195-205.

Ding, X., Li, C., Ripley, E.M., Rossell, D., and Kamo, S., 2010, The Eagle and East Eagle sulfide ore-bearing mafic-ultramafic intrusions in the Midcontinent Rift System, upper Michigan: Geochronology and petrologic evolution. G^3-Geochemistry, Geophysics and Geosystems, V. 11, 22 p.

Foley, D.J., 2011, Petrology and Cu-Ni-PGE mineralization of the Bovine Igneous Complex, Baraga County, northern Michigan. M.S. thesis, University of Minnesota Duluth, 109 p.

Fralick, P., Smyk, M., Mailman, M., 2000. Geology and stratigraphy of the Mesoproterozoic Sibley Group: Institute of Lake Superior Geology. 46th Annual Meeting, Thunder Bay, ON, Proceedings and Abstracts, part 2. p. 7-46.

Fralick, P., Purdon, R.H., and Davis, D.W., 2006. Neoarchean trans-subprovince sediment transport in southwestern Superior Province: sedimentological, geochemical, and geochronological evidence: Canadian Journal of Earth Science. 43, p. 1055-1070.

Franklin, J.M., 1978, The Sibley Group, Ontario; in Rubidium-strontium isochron age studies, Report 2, Geological Survey of Canada, Paper 77-14, p.31-34.

Goldner, B.D., 2011. Igneous petrology of the Ni-Cu-PGE mineralized Tamarack intrusion, Aitkin and Carlton Counties, Minnesota. M.S. thesis. University of Minnesota Duluth, Duluth, MN.

Goodgame, V.R., 2010. Initial lithogeochemical study of the Current Lake Intrusive Complex, Ontario, Canada: Taloumba, Inc. Magma Metals (Canada) Limited internal report. 85p.

Goodgame, V.R., J.R. Johnson, A.D. MacTavish, W.E. Stone, K.P. Watkins and G.C. Wilson, 2010, The Thunder Bay North Deposit: Chonolith-Hosted Pt-Pd-Cu-Ni Mineralization Related to the Midcontinent Rift. 11th International Platinum Symposium, Abstract Volume, Sudbury, Ontario. Ontario Geological Survey, Miscellaneous Release–Data 269.

Green, J.C., 1982, Geology of Keweenawan extrusive rocks. In: Wold, R.J. and Hinze, W.J. (eds.) Geology and tectonics of the Lake Superior Basin. Geological Society of America Memoir 156, p. 47-56

Hart, T.R., Hollings, P., Heggie, G., and MacDonald, C.A. 2005. Proterozoic platinum group element mineralization of the Nipigon Embayment, northwest Ontario. In Proceedings of the 10th International Platinum Symposium, Oulu, Finland, 7-11 August 2005. Abstracts Vol., pp. 362-364.

Hart, T.R., and Macdonald, C.A., 2007. Proterozoic and Archean geology of the Nipigon Embayment: implications for the emplacement of the Mesoproterozoic Nipigon diabase sills and mafic to ultramafic intrusions. Canadian Journal of Earth Sciences 44: p. 1021-1040.

Heaman, L.M., Easton, R.M., Hart, T.R., Hollings, P., MacDonald, C.A., and Smyk, M. 2007. Further refinement to the time of Mesoproterozoic magmatism, Lake Nipigon region, Ontario: Canadian Journal of Earth Sciences, 44: p. 1055-1086.

Heggie, G.J. 2005. Whole rock geochemistry, mineral chemistry, petrology and Pt, Pd mineralization of the Seagull intrusion, northwestern Ontario. M.Sc. thesis, Lakehead University, Thunder Bay, Ont.

Heggie, G., MacTavis, A., Johnson, J., Weston, R., and Ma, L., 2012, Structural control on the emplacement of the TBN-Igneous Complex [abstract]: In; Hollings, P. (Ed.), Institute on Lake Superior Geology Proceedings, 58th Annual Meeting, Thunder Bay, Ontario, Part 1 - Proceedings and Abstracts, v. 58, part 1, 1-2

Hollings, P., Fralick, P., Cousens, B., 2007a. Early history of the Midcontinent Rift inferred from geochemistry and sedimentology of the Mesoproterozoic Osler Group, northwestern Ontario. Canadian Journal of Earth Sciences, 44: 389-412.

Hollings, P., Hart, T., Richardson, A., and MacDonald, C.A., 2007b. Geochemistry of the Midproterozoic intrusive rocks of the Nipigon Embayment, Northwestern Ontario. Canadian Journal of Earth Sciences, 44, 1087-1110.

Hollings, P., Richardson, A., Creaser, R., and Franklin, J., 2007c. Radiogenic isotope characteristics of the Midproterozoic intrusive rocks of the Nipigon Embayment, Northwestern Ontario. Canadian Journal of Earth Sciences, 44, 1111-1129.

Hollings, P., Smyk, M., Heaman, L.M., and Halls, H., 2010. The geochemistry, geochronology and paleomagnetism of dikes and sills associated with the Mesoproterozoic Midcontinent Rift near Thunder Bay, Ontario, Canada: Precambrian Research (2010), 19p.

Hollings P., Smyk, M, and Cousens, B., 2012, The radiogenic isotope characteristics of dikes and sills associated with the Mesoproterozoic Midcontinent Rift near Thunder Bay, Ontario, Canada. Precambrian Research 214–215, p. 269-279

Hollings, P. and Heggie, G., 2014, Rethinking the Midcontinent rift – puncturing the “plume paradigm”: Institute on Lake Superior Geology Proceedings v. 60, Part 1, p. 57

Hutchinson, D.R., White, R. W., Cannon, W. F., and Schulz, K.J.,1990. Keweenaw hot spot: geophysical evidence for a 1.1 Ga mantle plume beneath the Midcontinent Rift System. Journal of Geophysical Research, 95: 10,869 – 10,884.

Klewin, K.W. and Berg, J.H., 1990. Geochemistry of the Mamainse Point volcanics, Ontario, and implications for the Keweenawan paleomagnetic record: Canadian Journal of Earth Sciences 27, p. 1194-1199.

Lightfoot, P., Sutcliffe, R., and Doherty, W., 1991. Crustal contamination identified in Keweenawan Osler Group tholeiites, Ontario: a trace element perspective. Journal of Geology, 99, p. 739-760.

MacTavish, A. and Smyk, M.C., 2010, Thunder Bay North Project, Magma Metals Limited. In Miller, J.D., Smyk, M.C. and Hollings, P.N. (eds.).Cu-Ni-PGE deposits in mafic intrusions of the Lake Superior region: A field trip for the 11th International Platinum Symposium; Ontario Geological Survey, Open File Report 6254, 166p.

MacTavis, A.D., Heggie, G.J., Goodgame, V.R., Johnson, J.R., Beswick, A.E., Stone, W.E., Watkins, K.P., 2012, Platinum-Palladium-Copper-Nickel mineralization at the Thunder Bay North Deposit, Ontario [abstract]: Institute on Lake Superior Geology Proceedings, 57th Annual Meeting, Ashland, WI, v. 57, part 1, p. 53-54.

Metsaranta, R., 2006. Sedimentology and geochemistry of the Mesoproterozoic Pass Lake and Rossport formations, Sibley Group. M.Sc. thesis abstract, Lakehead University, Thunder Bay, Ont.

Miller, J.D., Jr., and Vervoort, J.D., 1996. The latent magmatic stage of the Midcontinent rift: a period of magmatic underplating and melting of the lower crust: Institue of Lake Superior Geology, 42nd Annual Meeting, Cable, Wis., Proceedings, v. 42, Program and Abstracts, pt. 1, p. 33-35.

Miller, J.D., Jr., and Green, J.C., 2002. Geology of the Beaver Bay Complex and related hypabyssal intrusions. In: Geology and mineral potential of the Duluth Complex and related rocks of northeastern Minnesota: Minnesota Geological Survey Report of Investigation 58, p. 144-163.

Miller, J.D., Jr., and Severson, M.J., 2002. Geology of the Duluth Complex. In: Geology and mineral potential of the Duluth Complex and related rocks of northeastern Minnesota: Minnesota Geological Survey Report of Investigation 58, p. 106-143.

Miller, J.D., Jr., Green, J.C., Severson, M.J., Chandler, V.W., Hauck, S.A., Peterson, D.M., and Wahl, T.E., 2002. Geology and mineral potential of the Duluth Complex and related rocks of northeastern Minnesota: Minnesota Geological Survey Report of Investigation 58, 207p.

Miller, J.D., 2007, The Midcontinent Rift in the Lake Superior Region: A 1.1 Ga Large Igneous Province. Large Igneous Provinces Commission website (http://www.largeigneousprovinces.org/), Nov. 2007 LIP of the month

Miller, J.D. and Nicholson, S.W., 2013, **T**he Geology and Mineral Deposits of the 1.1Ga Midcontinent Rift in the Lake Superior Region – An Overview; to be submitted to Economic Geology.

Nicholson, S.W., Shirey, S.B., 1990, Midcontinent rift volcanism in the Lake Superior region: Sr, Nd, and Pb isotopic evidence for a mantle plume origin, J. Geophys. Res. 95, 10851-10868.

Nicholson, S.W., Shirey, S.B., Shulz, K.B., Green, J.C., 1997. Rift-wide correlation of 1.1 Ga Midcontinent rift system basalts: implications for multiple mantle sources during rift development. Canadian Journal of Earth Sciences 34, p. 504-520.

Panoramic Resources LTD, 2014, Thunder Bay North PGM Project, http://panoramicresources.com/thunder-bay-north-pgm-project/ (accessed January 2015).

Ripley, E.M., and Li, C., 2009, Ni-Cu-PGE mineralization associated with the Proterozoic Midcontinent Rift System, USA. In Li, C., and Ripley, E.M. (eds.), New Developments in Magmatic Ni-Cu and PGE Deposits, Geological Publishing House, Bejing, China, p. 180-191.

Rossell, Dean, 2008. Geology of the Keeweenawan BIC intrusion: Institute of Lake Superior Geology. 54th Annual Meeting, Marquette, MI, Proceedings and Abstracts, part 2. p. 181-199

Shirey, S.B., 1997, Re-Os isotopic compositions of Midcontinent rift system picrites: implications for plume-lithosphere interaction and enriched mantle sources: Canadian Journal of Earth Sciences, V. 34, p. 489-503.

Sun, S.S. and McDonough, W.F., 1989, Chemical and isotopic systematics of oceanic basalts: implications for mantle composition and processes. In: Saunders, A.D., Norry, M.J. Eds., Magmatism in Ocean Basins. Geol. Soc. Spec. Publ., London, pp. 313–345.

Van Schmus, W. R., 1992, Tectonic setting of the Midcontinent Rift System: Tectonophysics, v. 213, p. 1–15.

Vervoort, J.D., Wirth, K., Kennedy, B., Sandland, T., and Harpp, K.S., 2007. The magmatic evolution of the Midcontinent rift: new geochronologic and geochemical evidence from felsic magmatism. Precambrian Research 157, p. 235-268.

Ware, A., Cherry, J., and Ding, X., 2008. Geology of the Eagle project: Institute of Lake Superior Geology. 54th Annual Meeting, Marquette, MI, Proceedings and Abstracts, part 2. p. 87-111

Appendices

Appendix A

Core Logs

Drill Core Log

page 1 of 11

Project _____ Azimuth _____ Inclination _____

Hole Name IBND-60 - A Elevation _____ Total Depth _____

Location T____, R____, Sec____. ____ of ____ Date Drilled___/___/___ By_____

UTM (83 / 27) _____E_____N Date Logged___/___/___ By _____

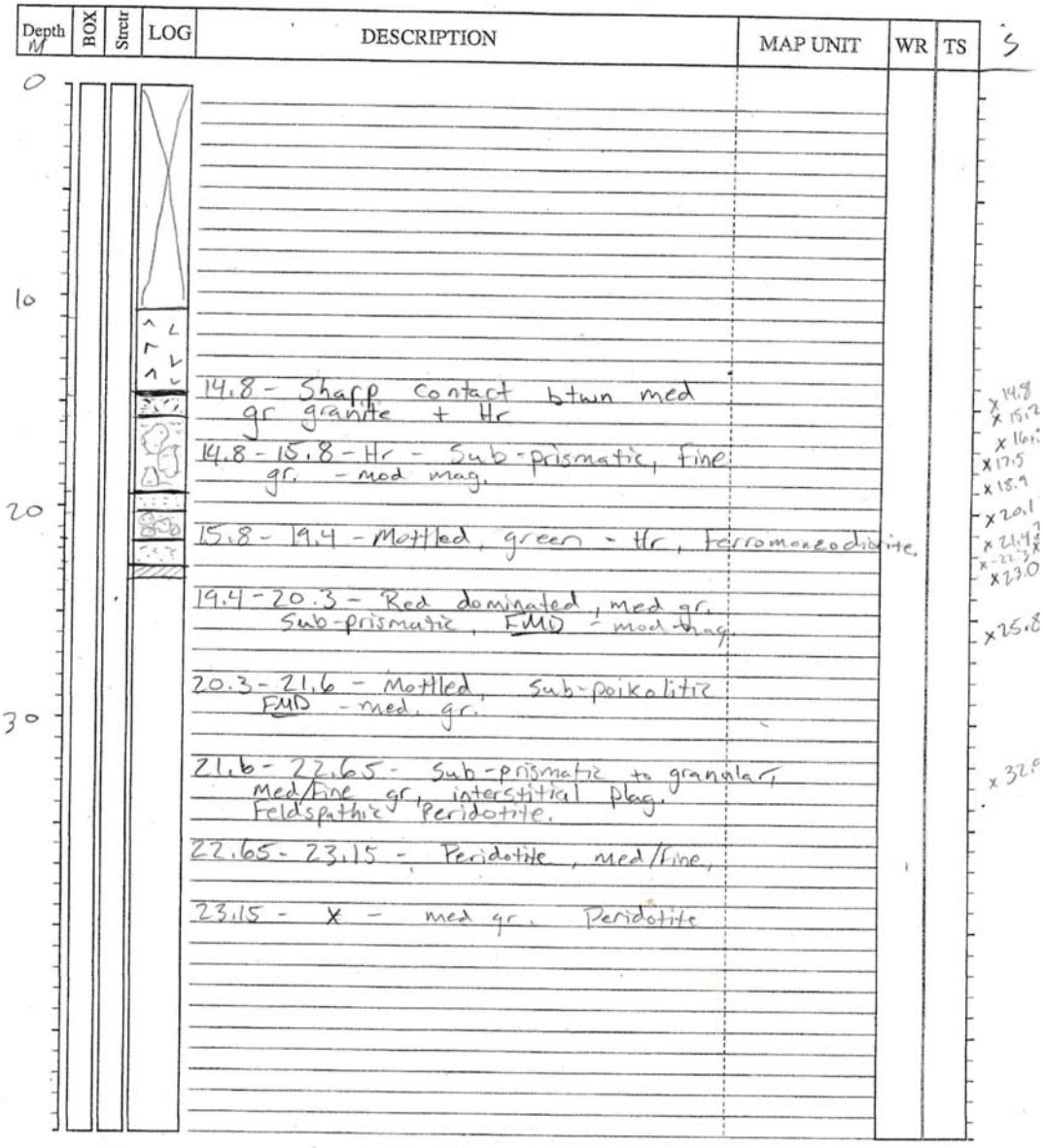

Drill Core Log

page 2 of 11

Project _____ Azimuth _____ Inclination _____

Hole Name IBND-95-13 Elevation _____ Total Depth _____

Location T____, R____, Sec____. ____ of ____ Date Drilled___/___/___ By_____

UTM (83 / 27) _____E_____N Date Logged___/___/___ By _____

+2.4
101.5

Depth	BOX	Strctr	LOG	DESCRIPTION	MAP UNIT	WR	TS
80m							
				Red Granite - 10% QTZ			
90				Sharp Contact			
				HG - 92.1 - 93.2 - Fine grading to Med. grained			
				93.2 - 94.3 - Med grained interval - HG grades down to Med/Fine.			
				94.3 - 97.6 - Med/Fine - HG			
100				97.6 - 99.1 - Med/Fine grades to Aphanitic Chilled Contact (99.1) Sharp Contact			
				99.1 - 102.4 - Bleached / sulfidic granite w/ gossen staining.			
				102.4 - 103.51 - Unaltered ~15% QTZ			
110m							

Drill Core Log

page 3 of 11

Project _____ Azimuth _____ Inclination _____

Hole Name TBND 124C Elevation _____ Total Depth _____

Location T____, R____, Sec____. ____ of ____ Date Drilled___/___/___ By _____

UTM (83 / 27) _____E_____N Date Logged___/___/___ By _____

Depth m	BOX	Strctr	LOG	DESCRIPTION	MAP UNIT	WR	TS
30							
40				37.76 - 40.3 Red Granite 1m missing near contact of RG + Perid. 40.3 - 51.5 - Med/Fine Feld. Peridotite			
50				51.5 - 55.1 - Med/Fine Feld Peridotite w/ Sulfide 55.1 - 58.1 - Med/Fine Feld Peridotite Sharp Contact			
60				58.1 - Red Granite.			
70							
80							

Drill Core Log

Project _____ Azimuth _____ Inclination _____

Hole Name TBND 124 DC Elevation _____ Total Depth _____

Location T____, R____, Sec____. ____ of ____ Date Drilled___/___/___ By_____

UTM (83 / 27) _____E_____N Date Logged___/___/___ By _____

Depth	BOX	Strctr	LOG	DESCRIPTION	MAP UNIT	WR	TS
80				Red Granite - No Mag.			
				86.2 - 86.6 - Non mag., Med/Fine Peridotite Gr/P Contact			
				86.6 - 87 - Red Granite			
				87 - 87.2 - Non mag zone			
90				87.2 - 94 - Mod - Strong Mag, Med/Fine Fold Peridotite grades to aphanitic.			
				94 - 94.9 - Chill zone - Mod mag at top to Non mag. at Contact.			
				94.9 - 101 - Red granite - No mag.			
100							

Drill Core Log

Project _____ Azimuth _____ Inclination _____

Hole Name TBND 136 D Elevation _____ Total Depth _____

Location T____, R____, Sec____. ____ of ____ Date Drilled___/___/___ By_____

UTM (83 / 27) _____E_____N Date Logged___/___/___ By _____

Depth	BOX	Strctr	LOG	DESCRIPTION	MAP UNIT	WR	TS
10				14.8 - 16.2 - Red Granite (gradational contact)			
				16.2 - 16.9 - HG - Ferrodiorite, med/fine, prismatic pyroxene, mod mag			
20				16.9 - 20.8 - Mottled, fine grading to med toward the base of contact, granular pyroxene, sulfide veins, mod mag			
				20.8 - 21.6 - Feldspathic Peridotite: Med/fine, w/ some disseminated sulfide mod, mag.			
				21.65 - 22.8 - Peridotite w/ sulfide med/fine mod, mag			
30				22.8 - 35.6 - peridotite, med/fine mod mag.			
40							

Drill Core Log

Project _____ Azimuth _____ Inclination _____

Hole Name IBND 125 E Elevation _____ Total Depth _____

Location T____, R____, Sec____. ____ of ____ Date Drilled___/___/___ By_____

UTM (83 / 27) _____E_____N Date Logged___/___/___ By _____

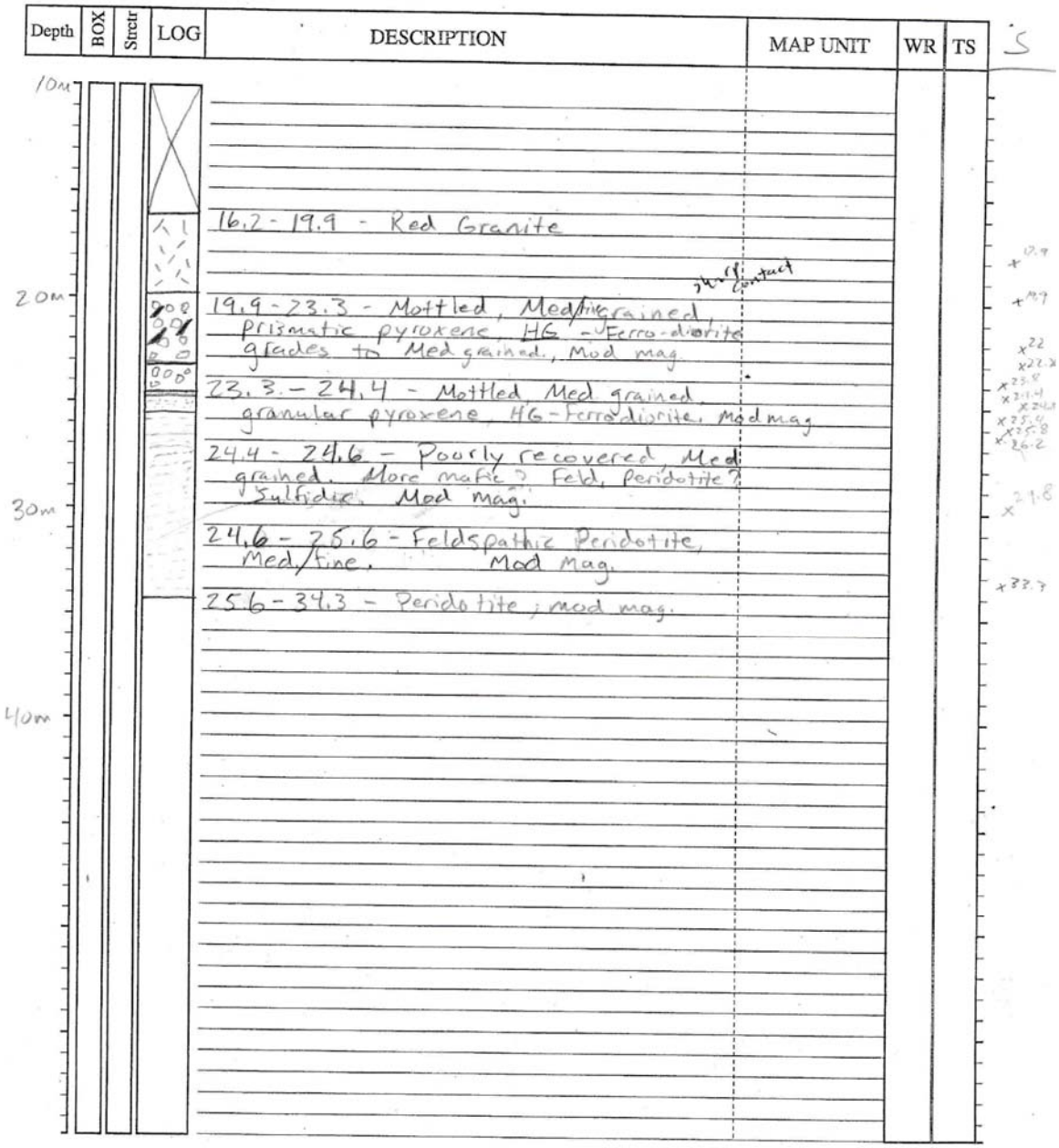

Drill Core Log

page 7 of 11

Project _____ Azimuth _____ Inclination _____

Hole Name TB.ND 023F Elevation _____ Total Depth _____

Location T____, R____, Sec____. ____ of ____ Date Drilled___/___/___ By_____

UTM (83 / 27) _____E_____N Date Logged___/___/___ By _____

Depth	BOX	Strctr	LOG	DESCRIPTION	MAP UNIT	WR	TS
100				104.9 - 107.7 - Bleached/sulfidic granite, med grained.			
110				107.7 - 112.2 - HG - Chilled at top grading to med/fine in center then grading to chilled (Aphanite). Non-weak mag at top, becomes mod mag at bottom			
				112.2 - 115.4 - Med grained Red Granite			
120				115.4 - 117 - Matic, chilled, Aphanitic. Non mag			

Drill Core Log

Project _____ Azimuth _____ Inclination _____

Hole Name BL08-75 G Elevation _____ Total Depth _____

Location T____, R____, Sec____. ____ of ____ Date Drilled___/___/___ By_____

UTM (83 / 27) _____E_____N Date Logged___/___/___ By _____

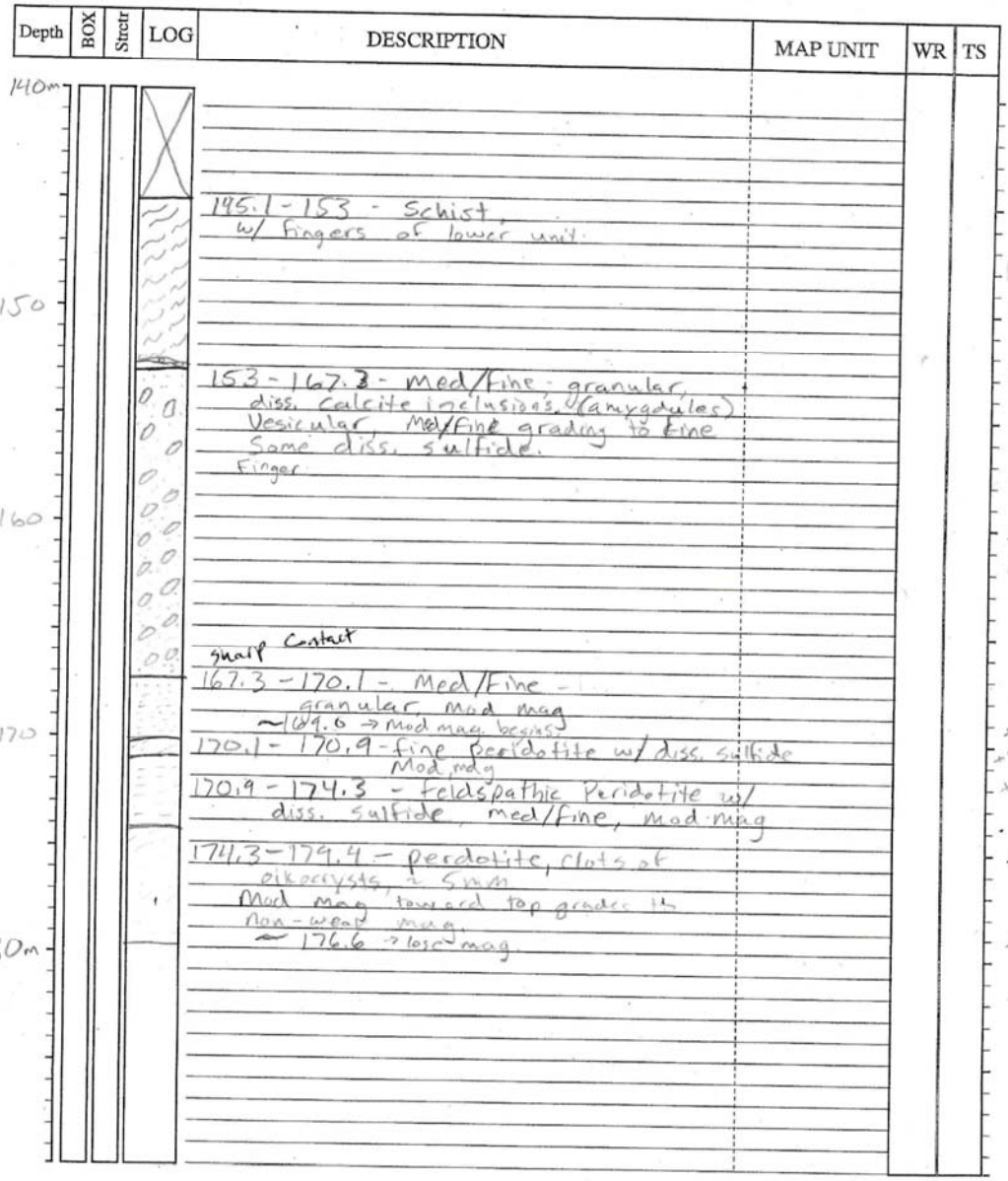

Drill Core Log

Project _____ Azimuth _____ Inclination _____

Hole Name BL08-78 H Elevation _____ Total Depth _____

Location T____, R____, Sec____. ____ of ____ Date Drilled___/___/___ By_____

UTM (83 / 27) _____E_____N Date Logged___/___/___ By _____

Depth	BOX	Strctr	LOG	DESCRIPTION	MAP UNIT	WR	TS
160m				161.15 - 166.0 - Schist w/ some fingers of lower unit.			
				166.0 - 175.8 - Big, mantled qtz inclusions, Red, granular, med/fine.			
170				175.8 - 180 - Prismatic pyroxene, med/fine, few small qtz inclusions, grades to granular texture at contact.			
180				180 - 181.1 - Granular, Med/Fine, Small Calcite/qtz			
				181.1 - 182.3 - More Mafic, granular, med/fine homogeneous. No inclusions.			
				182.3 - 188.4 - granular, med/fine, local large clasts, mantled w/ chlorite?, 5% well dispersed qtz/calcite.			
190				188.4 - 189.2 - red med/fine homogeneous, granular, grading to more mafic			
				189.2 - 191.0 - Mafic, granular, feldspathic peridotite/melagabbro? Sharp contact → Sulfide ~2-5%			
				191.0 - 191.7 - peridotite, med grained.			
200				191.7 - 192.7 - Coarse grained peridotite.			
				192.7 - 204.8 - peridotite, poikolitic, med/fine			
210							

Drill Core Log

page 16 of 11

Project _____ Azimuth _____ Inclination _____

Hole Name BL09-146I Elevation _____ Total Depth _____

Location T____, R____, Sec____. ____ of ____ Date Drilled___/___/___ By _____

UTM (83 / 27) _____E_____N Date Logged___/___/___ By _____

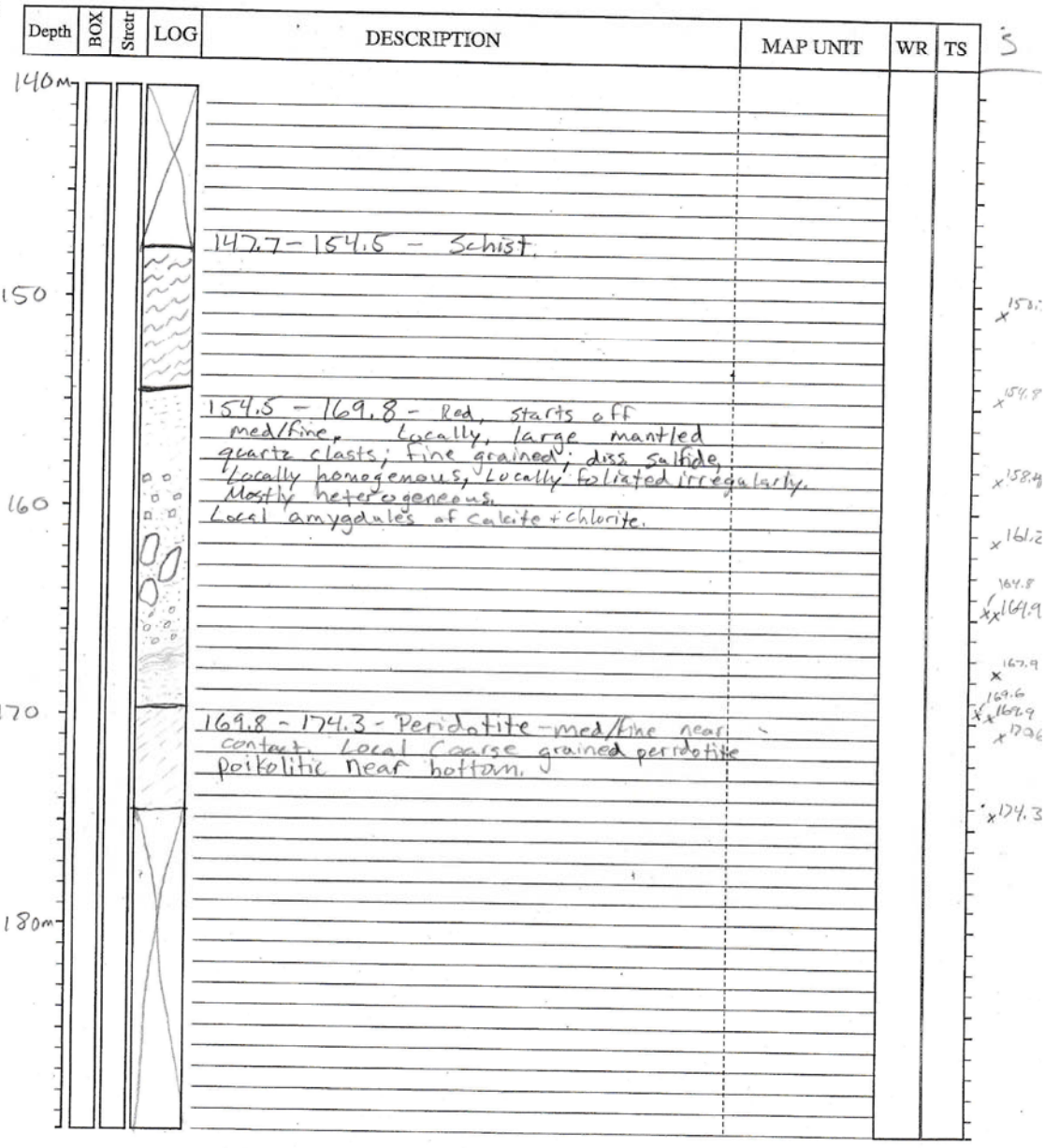

176.8 - 125 / 65

Drill Core Log

page 11 of 11

Project _____ Azimuth _____ Inclination _____

Hole Name BL09 -147 J Elevation _____ Total Depth _____

Location T____, R____, Sec____. ____ of ____ Date Drilled___/___/___ By_____

UTM (83 / 27) _____E_____N Date Logged___/___/___ By _____

Depth	BOX	Strctr	LOG	DESCRIPTION	MAP UNIT	WR	TS

150

152.0 - 155.6 - Siltstone?

156.6 - 160.45 - HG - Med/Fine granular, Sulfidic - disseminated & vn Semi-massive pockets, quartz inclusions are large and elongated. grades to red near basal contact

160

160.45 - 176.8 - Heterogeneous. Local large, mantled quartz inclusions; disseminated sulfide. Locally mottled and prismatic pyroxene. Local homogeneous, Local granular med/fine & Fine grained Granite Inc. Grades to more mafic at basal Contact Mod, Mag. + chlorite inclusions

170

176.8 - 181.0 - peridotite, disseminated sulfide, becomes more poikolitic toward base (less sulfide the more poikolitic), Mod Mag.

180

190m

5

153.1
155.
157.6
161.7
165.2
165.9
166.8
169.8
172.2
174.5
176.7
176.
177.9
180.

Appendix B

Petrographic Descriptions and Lithogeologic Logs

Core	Sample ID	Petrographic Description	Depth (m)	Grain Size	Plagioclase			Clinopyroxene			Olivine			Oxides			Sulfide			Quartz			K-Feldspar		
					Mode	Habit	Alteration	Mode	Habit	Alteration	Mode	Habit	Alteration	Mode	Habit	Habit	Mode	Habit	Type	Mode	Habit	Habit	Mode	Habit	Alteration
TBND-60	*TBND-60-14.8u*	red, coarse gr, granite	14.8		42	LS	C-Ser							1	AG					25	AG	Rutilated	30	AG	S-Ser/Hem
TBND-60	*TBND-60-14.8l*	red hybrid, fine, sub-prismatic, quartz, oxide ferrodiorite	14.8	FF	60	LS	C-Ser	20	SR	C-Url/Chl				10	AG					10	PK				
TBND-60	*TBND-60-15.2*	red hybrid, med/fine, subophitic, oxide, carbonate, quartz-rich leucogabbro	15.2	MF	55	LS	C-Ser	13	SOP	C-Url/Chl				7	AG	Acicular				20	PK		5	AG	S-Ser/Hem
TBND-60	*TBND-60-16.5*	red hyrid, med/fine, subophitic, oxide-carbonate-quartz- bearing gabbro	16.5	MF	55	LS	S-Ser	15	SOP	C-Chl/Url				7	SK	Acicular				10	PK		3	AG	S-Ser/Hem
TBND-60	*TBND-60-17.5*	red, med, subophitic, carbonate-quartz-bearing, oxide leucogabbro	17.5	MM	65	LS	M-Ser	15	SOP	C-Chl/Url				5	AG	SK				5	Pk		3	AG	C-Ser/Hem
TBND-60	*TBND-60-18.9*	red, med, subophitic, carbonate bearing, oxide, quartz gabbro	18.9	MM	55	LS	M-Ser	20	SOP	C-Chl/Crb				10	Sk	Pr	3	AG	Pyr	5	Pk				
TBND-60	*TBND-60-20.1*	red, mottled, med, subprismatic, carbonate, oxide, quartz gabbro	20.1	MM	55	LS	C-Ser	20	SR	C-Chl/Crb				10	AG					7	PK		3	AG	C-Ser/Hem
TBND-60	*TBND-60-21.4*	red, mottled, med, subophitic, oxide bearing, carbonate, quartz gabbro	21.4	MC	50	LS	S-Ser	20	SOP/SR	C-Chl				7	PR	AG				7	PK		5	AG	C-Ser/Hem
TBND-60	*TBND-60-21.65*	red, med/fine, oxide, quartz bearing gabbro	21.65	MM	50	LS	S-Ser	25	SG	M-Chl/Url				15	AG	SK	3	AG	Pyr	5	PK				
TBND-60	*TBND-60-22.3*	grey, med/fine, subpoikilitic quartz bearing gabbro	22.3	MF	50	SP	S-Ser	40	SG	W-Url/Chl				5	PK					5	PK				
TBND-60	*TBND-60-23.0*	grey, med/fine, supboikilitic, feldspathic olivine clinopyroxenite	23	FF	25	SP	M-Ser	45	SG	W-Url/Chl	20	AG	C-Srp/Tlc	3	AG					2	Pk				
TBND-60	*TBND-60-25.8*	black, medium, poikilitic, feldspathic wehrlite	25.8	MM	10	PK	M-Ser	30	SG/PK	W-Url	40	SG	S-Srp/Tlc	5	AG	PR									
TBND-60	*TBND-60-32.9*	black, med gr, pokilitic wehrlite	32.9	MM	5	PK	M-Ser	35	SG/PK	W-Url	45	SG	S-Srp/Tlc	3	Ag		2	Ag	Pyr						
TBND-95	*TBND-95-91.5*		91.5	MM										3	Ag					32	AG		65	AG	S-Ser/Hem
TBND-95	*TBND-95-92.1*	grey, med/fine, intergranular oxide-bearing, olivine melagabbro	92.1	MF	45	AG	C-Ser	20	AG	S-Url/Bi/Chl	20	SG	C-Srp/Tlc	5	PK		trace	Ag	Pyr	trace	Pk				
TBND-95	*TBND-95-93.8*	grey, med/fine, subpoikilitic, feldspathic dunite/wehrlite	93.8	MF	10	PK	S-Ser/???	15	SG	S-Url/Bi/Amp	60	SG	C-Srp/Tlc	7	PK	AG									
TBND-95	*TBND-95-94.9*	grey, med/fine, subpoikilitic werhlite	94.9	MF	5	PK	S-Ser	20	SG	S-Url/BiAmp	40	SG	C-Srp/Tlc/Crb	7	Pk	AG	2	Ag	pyr						
TBND-95	*TBND-95-97.2*	red, fine, subophitic, quartz-bearing oxide gabbro	97.2	FF	65	LS	S-Ser	15	SOP/SR	C-Chl/Crb/Url?				7	PK	AG				5	Pk		3	AG	C-Ser/Hem
TBND-95	*TBND-95-98.1*	grey, fine, subophitic, quartz-bearing, oxide gabbro	98.1	FF	65	LS	S-Ser	15	SOP/SR	C-Chl/Crb/???				7	PK	Ag	3	ag	pyr	5	pk				
TBND-95	*TBND-95-99.1*	grey, very fine, porphyritic, quartz-bearing, oxide gabbro	99.1	VF	60	LS	S-Ser/Crb	20	AG	C-Chl/Crb				10	PR					5					
TBND-95	*TBND-95-99.3*	red, coarse gr, granite	99.3	CC	15	AG	M-Ser							2	AG					15	AG		65	AG	W-Ser/Hem
TBND-95	*TBND-95-100.6*	red, coarse gr, granite	100.6	CC	20	AG	M-Ser													20	AG		55	AG	W-Ser
TBND-95	*TBND-95-101.9*	red, coarse gr, granite	101.9	CC	15	AG	M-Ser													20	AG		60	AG	W-Ser
TBND-124	*TBND-124-38.6*		38.6	CC										2	AG					25	AG		68	AG	S-Ser/Hem
TBND-124	*TBND-124-44.2*	green, med gr, intergranular to subpoikilitic, feldspathic wehrlite	44.2	MF	15	PK	M-Ser	30	SG/PK	W-Bi/Amp	40	SG	S-Srp	3	AG					2	PK				
TBND-124	*TBND-124-49.5*	green, med gr, intergranular to subpoikilitic, feldspathic wehrlite	49.5	MM	15	PK	M-Ser	25	SG/PK	W-Bi/Amp	40	SG	S-Srp/Tlc	3	Ag										
TBND-124	*TBND-124-52.8*	green, med gr, intergranular to subpoikilitic, sulfide-bearing feldspathic wehrlite	52.8	MM	10	PK	W-Ser	30	SG/PK	W-Bi/Amp	35	SG	M-Srp/Tlc	2	Ag		8	PK	Pyr						
TBND-124	*TBND-124-53.9*	green, med gr, intergranular to subpoikilitic, sulfide-bearing feldspathic wehrlite	53.9	MM	20	PK	W-Ser	30	SG/PK	W/Bi/Amp	35	SG	S-Srp/Tlc	2	Ag		5	PK	Pyr						
TBND-124	*TBND-124-55.5*	green, med gr, intergranular to subpoikilitic, feldspathic wehrlite	55.5	MM	20	PK	W-Ser	35	SG/PK	W-Bi/Amp	30	SG	S-Srp/Tlc	5	Ag										
TBND-124	*TBND-124-57.5*	green, med/fine gr, intergranular to subpoikilitic gabbro	57.5	MM	20	PK	W-Ser	35	SG/PK	W-Bi/Amp	30	SG	S-Srp/Tlc?	3	SR										
TBND-124	*TBND-124-58.1u*	green, med/fine gr, intergranular to subpoikilitic gabbro	58.1	MF	50	SP	W-Ser/Alb	40	AG	C-Amp/Chl	5	SG	C-???	3	PR					2	PK				
TBND-124	*TBND-124-58.1l*		58.1	MC										2	AG					25	AG	rutilated	70	AG	S-Ser/Hem
TBND-124	*TBND-124-60.8*		60.8	CC													2	ag	pyr	25	AG	rutilated	65	Ag	S-Ser/Hem
TBND-124	*TBND-124-81.0*		81	CC	5	AG	S-Ser							2	AG					20	AG	Rutilated	68	AG	S-Ser/Hem
TBND-124	*TBND-124-86.5l*	green, med/fine gr, intergranular to subpoikilitic gabbro	86.5	MF	60	SP	M-Ser	25	SG/SOP	C-Chl/Amp				7						3	AG				
TBND-124	*TBND-124-87.2*	green, med/fine gr, intergranular to subpoikilitic gabbro	87.2	FF	60	Pk	S-M-Ser	25	SG	M-Unk/Bi/Amp?				5	PR	Sk				5	PK				
TBND-124	*TBND-124-87.6*	green, med/fine gr, intergranular to subpoikilitic feldspathic wehrlite	87.6	MF	25	PK	W-Ser	30	SG/SP	W-Amp	30	SG	C-Srp/Tlc	3	AG										
TBND-124	*TBND-124-88.9*	green, med/fine gr, intergranular to subpoikilitic feldspathic wehrlite	88.9	MF	25	PK	W-Ser	25	SG	W-Bi/Amp	35	SG	M-Srp/Tlc	5	AG	Corona									
TBND-124	*TBND-124-91.5*	grey, med/fine gr, intergranular, olivine melagabbro	91.5	MF	50	AG/SP	S-Ser/Crb	15	AG	C-???	10	SG	S-Tlc	20	AG	Corona				0.1	PK				
TBND-124	*TBND-124-93.0*	grey, med/fine gr, intergranular, olivine-quartz-bearing gabbro	93	MF	57	LS	S-Ser	15	SOP/PR	S-Bi/Amp	5	SG	S-Tlc	15	AG	SK/Corona				2	PK				
TBND-124	*TBND-124-94.7*	grey, med/fine gr, intergranular, quartz-bearing gabbro	94.7	VF	70	LS	S-Ser	15	....	C-chl				10	PR	Sk				5	PK				
TBND-124	*TBND-124-97.5*		97.5	CC	10	AG	M-Ser							2	AG					20	AG	Rutilated	63	AG	M-Ser/Hem
TBND-136	*TBND-136-16.2*		16.2	CC										1	AG					20	AG	rutilated	77		
TBND-136	*TBND-136-16.6*	red, med/fine, subprismatic, oxide, quartz ferrodiorite	16.6	MF	55	LS	M-Ser	25	SR	C-Chl/Url?				7	AG					10	PK		3	AG	C-Ser/Hem
TBND-136	*TBND-136-18.9*	red, med/fine, equigranular, oxide, quartz leucogabbro	18.9	MF	55	LS	S-Ser	20	SOP	C-Chl/Crb/Unk				7	AG	PR				10	PK		3	AG	S-Ser/Hem
TBND-136	*TBND-136-20.6*	red, med gr, subophitic, carbonate, oxide, quartz leucogabbro	20.6	MM	58	Ls	S-Ser	15	SOP	C-Chl/Crb/Unk				7	AG	SK				10	PK		3	AG	S-Ser/Hem
TBND-136	*TBND-136-20.8*	red, med/fine, intergranular, oxide, quartz gabbro	20.8	MF	55	LS	S-Ser	25	SG	M-Chl/Unk				10	AG	Sk	2	Pk	Pyr	5	Pk		0.5	Ag	S-Ser/Hem
TBND-136	*TBND-136-21.1*	grey, med/fine, prismatic to intergranular, quartz-bearing gabbro	21.1	MF	52	SP	S-Ser	35	SG/PR	W-Chl/Url/Bi				5	Ag					5	PK				
TBND-136	*TBND-136-22.0*	green, med gr, subpoikilitic, feldsparthic werhlite	22	MM	8	Pk	W-Ser	35	SG/PK	W-Amp	35	SG	C-Srp	5	Pk		2	PK	Pyr						
TBND-136	*TBND-136-26.0*	green, med gr, subpoikilitic, feldspathic werhlite	26	MM	15	Pk	M-Ser	35	SG/PK	W-Apm/Chl	35	SG	S-Srp/Tlc	3	AG		2	PK	Pyr/Cpy						
TBND-136	*TBND-136-34.7*	Green, med gr, subpoikilitic werhlite	34.7	MF	5	Pk	M-Ser	30	SG/Pk	W-Apm/Chl	40	SG	M-Srp/Tlc	2	AG		3	PK							
TBND-125	*TBND-125- 17.9*		17.9	CC										2	AG					30	AG		65	AG	S-Hem
TBND-125	*TBND-125- 19.9*	red med/fine gr, subprismatic, quartz ferrodiorite	19.9	MF	60	LS	S-Ser	10	SR/AG	C-Chl				3	AG	SR				20	PK	AG	5	AG	S-Hem/Ser
TBND-125	*TBND-125- 22.0*	red, med gr, subprismatic to subophitic, oxide, quartz gabbroic anorthosite	22	MF	70	LS	M-Ser/Ssr	15	SOP/SR	C-Chl/Url??				8	SR	Acicular				7	PK		0.5	AG	S-Hem/Ser
TBND-125	*TBND-125- 22.8*	red, med gr, intergranular, oxide bearing, quartz leucogabbro	22.8	MF	65	LS	S-Ser	20	AG/SOP	C-Chl/Url??				5	SR					10	PK		0.5	AG	S-Hem/Ser
TBND-125	*TBND-125- 23.8*	red, med gr, subophitic, quartz bearing, oxide gabbroic anorthosite	23.8	MM	70	LS	S-Ser	15	SOP	C-Chl/Url??				7	SK	AG				5	PK				
TBND-125	*TBND-125- 24.4a*	red, med gr, subophitic, quartz bearing, oxide leucogabbro	24.4	MM	65	LS	M-Ser	20	SOP	S-Chl/Url??				10	SK	AG				5	Pk				
TBND-125	*TBND-125- 24.4b*	red, med gr, subophitic, quartz bearing, oxide leucogabbro	24.4	MM	65	LS	S-Ser	15	SOP	C-Chl/Url?				10	PR	SK/AG				5	PK				
TBND-125	*TBND-125- 24.8*	grey, med/fine, intergranular, quartz-bearing melagabbro	24.8	MF	45	PK	S-Ser	45	SG	W-Unk??				5	PK					3	Pk				
TBND-125	*TBND-125- 25.4*	grey, med/fine, intergranular, quartz-bearing gabbro	25.4	MF	50	PK	M-Ser	40	SG	W-Url/Chl				3	PK					2	PK				
TBND-125	*TBND-125- 25.8*	grey, med/fine, prismatic to intergranular, quartz-bearing gabbro	25.8	MF	53	PK	S-Ser	40	SG/PR	W-Url/Chl				3	SK					2	PK				
TBND-125	*TBND-125- 26.2*	green, med gr, subpoikilitic to poikilitic feldspathic wehrlite	26.2	MM	10	PK	W-Ser	30	SG	W-Url/Chl	30	SG	C-Srp	3	PK										
TBND-125	*TBND-125- 29.8*	green, med gr, subpoikilitic to poikilitic feldspathic wehrlite	29.8	MM	10	PK	W-Ser	30	SG	W-Amp	40	SG	S-Srp/Tlc	3	AG										
TBND-125	*TBND-125- 33.3*	green, med gr, subpoikilitic to poikilitic feldspathic wehrlite	33.3	MM	10	PK	S-Ser	30	SG	W-???	40	SG	S-Srp/Tlc	3	AG										
TBND-023	*TBND-023-106.3*		106.3	CC	10	AG	W-Ser							1	AG					20	AG		62	AG	W-Ser
TBND-023	*TBND-023-107.8*	grey, fine gr, ophitic quartz-bearing oxide gabbro	107.8	FF	65	LS	M-Ser	15	AG	C-Chl/Crb				8	AG	PR	2	AG	Pyr	5	PK				
TBND-023	*TBND-023-109.3*	grey, fine gr, ophitic quartz-bearing, oxide gabbro	109.3	MF	60	LS	M-Ser	20	OPH	C-Chl/Crb/Am				7	AG	SK				3	PK		3	AG	S-Ser/Hem
TBND-023	*TBND-023-111*	grey, fine gr, intergranular quartz-bearing oxide gabbro	111	MF	60	LS	S-Ser	18	AG	C-Chl/Url?	2	AG	C-???	15	AG					5	PK				
TBND-023	*TBND-023-112.6*		112.6	CC	40	AG	S-Ser/Hem							2	AG					25	AG		30	AG	W-Ser
TBND-023	*TBND-023-115.9*	grey, v. fine gr, ophitic quartz-bearing oxide leucogabbro	115.9	FF	65	LS	M-Ser	20	AG	C-Chl/Am				10	AG					3	Pk				
BL08-75	*BL08-75-149.6*		149.6	VF	5	AG	S-Ser							2	Ag		3	AG	Pyr	30	AG		15	AG	S-Ser
BL08-75	*BL08-75-152.5*	grey, fine gr, subophitic, quartz gabbro	152.5	FF	65	LS	S-Ser	15	SOP	C-Chl				2	SP		3	AG	Pyr	10	PK	Incl...			
BL08-75	*BL08-75-153.2*	grey, fine gr, subophitic, quartz gabbro	153.2	FF	60	LS	S-Ser	20	SOP	C-Chl				3	SP	SR	2	AG	Pyr	7	Pk	Incl...			
BL08-75	*BL08-75-157.5*	grey, v. fine gr, porphyritic,subprismatic, quartz gabbro	157.5	VF	65	LS	S-Ser	15	SR	C-Chl				5	SP					10	PK				
BL08-75	*BL08-75-160*	grey, v.fine gr, amygdaloydal, subophitic, carbonate-quartz leucogabbro	160	FF	60	LS	S-Ser	10	SR	C-Chl				2	PK		3	PK	Pyr	10	PK	Incl...			

Core	Sample ID	Petrographic Description	Depth (m)	Grain Size	Plagioclase			Clinopyroxene			Olivine			Oxides			Sulfide			Quartz			K-Feldspar		
					Mode	Habit	Alteration	Mode	Habit	Alteration	Mode	Habit	Alteration	Mode	Habit	Habit	Mode	Habit	Type	Mode	Habit	Habit	Mode	Habit	Alteration
BL08-75	*BL08-75-161.5a*	grey, v. fine gr, amygdaloydal, subophitic, carbonate-quartz gabbro	161.5	VF	60	LS	M-Ser	15	AG	C-Chl				3	PK		2	AG	Pyr	10	PK				
BL08-75	*BL08-75-161.5b*	grey, v.fine grey, amygdaloydal, subophitic, carbonate-bearing quartz leucogabbro	161.5	VF	65	LS	M-Ser	15	AG	C-Chl				2	PK		1	AG	Pyr	10	PK				
BL08-75	*BL08-75-167.3u*	grey, v. fine, subohpitic-prismatic, quartz gabbroic anorthosite	167.3	VF	70	LS	M-Ser	15	AG	C-Chl				5	PK	SR				10	PK				
BL08-75	*BL08-75-167.3l*	grey, fine gr, intergranular, quartz gabbro	167.3	MF	55	LS	M-Ser	30	SG	C-Chl				5	AG	SR				10	PK				
BL08-75	*BL08-75-169.2*	red, med/fine, intergranular, quartz-bearing gabbro	169.2	MF	50	LS	S-Ser	25	SG	C-Chl				5	AG		5	AG	Pyr	5	PK		3	Corona	C-Ser/Hem
BL08-75	*BL08-75-170*	red, med/fine gr, intergranular, quartz-bearing gabbro	170	MF	60	LS	S-Ser	25	SG	C-Chl				5	AG		3	AG	Pyr	3	PK		2	Corona	C-Ser/Hem
BL08-75	*BL08-75-170.2*	grey, med/fine gr, intergranular, quartz-bearing werhlite	170.2	MF				25	SG	C-Am/Bi/Chl	30			5	AG		5	AG	Pyr	2	PK				
BL08-75	*BL08-75-171.8a*	grey, med gr, subpoikilitic werhlite	171.8	MM				35	SG	M-Amp/Chl	45	SG	C-Tlc	2	AG		3	AG	pyr						
BL08-75	*BL08-75-171.8b*	grey, med gr, subpoikilitic werhlite	171.8	MM				30	SG	M-Amp/Chl	35	SG	C-Srp/Tlc	3	AG										
BL08-75	*BL08-75-175*	grey, med gr, subpoikilitic werhlite	175	MC				25	SG	W-Url/Chl	50	SG	C-Srp/Tlc	2	AG	SR	3	AG	???						
BL08-75	*BL08-75-179*	grey, med gr, subpoikilitic werhlite	179	MC				30	SG	W-Url/Chl	53	SG	C-Srp/Tlc	2	AG		3	AG	???						
BL08-78	*BL08-78-162.65*		162.65	FF	30	AG	W-Ser							5	AG					20	AG				
BL08-78	*BL08-78-165.34*		165.34	CC	65	SG	S-Ser/Hem							5	Ag					20	AG				
BL08-78	*BL08-78-165.34*		165.34	VF	30	AG	W-Ser							5	AG					20	AG				
BL08-78	*BL08-78-166.28*	red, fine gr, subophitic, oxide-sulfide bearing, quartz gabbro	166.28	FF	60	LS	S-Ser	20	AG	C-Chl				5	AG	SR	5	AG	Pyr	10	PK				
BL08-78	*BL08-78-169.57a*	red, v. fine gr, micrographic, K-feldspar-quartz-inclusion-rich monzonite	169.57	FF	15	AG/LS	S-Ser	20	AG	C-Chl				5	AG		3	AG	Pyr	40	PK	Incl	15	Ag	C-Ser/Hem
BL08-78	*BL08-78-169.57b*	red, v. fine gr, micrographic, K-feldspar-quartz-inclusion-rich monzonite	169.57	FF	20	AG/LS	S-Ser	20	AG	C-Chl/Url				5	Ag	PR	3	AG	Pyr	40	Pk	Incl	10	AG	C_Ser/Hem
BL08-78	*BL08-78-171.92a*	red, v. fine gr, micrographic, K-feldspar-quartz-inclusion-rich monzonite	171.92	MF	20	AG/LS	S-Ser	25	AG	C-Chl				5	PR	Ag	3	AG	Pyr	35	Pk	Incl	5	Ag	C-Ser/Hem
BL08-78	*BL08-78-171.92b*	red, v. fine gr, micrographic, K-feldspar-quartz-inclusion-rich monzonite	171.92	MF	20	AG/LS	M-Ser	20	SR	C-Chl				5	SR	SK	5	AG	Pyr	30	PK	Incl	10	AG	C-Ser
BL08-78	*BL08-78-171.92c*	red, v. fine gr, micrographic, K-feldspar-quartz-inclusion-rich monzonite	171.92	MF	15	AG/LS	S-Ser	15	AG	C-Chl				2	AG		3	AG	Pyr	45	Pk	Incl	20	AG	C-Ser
BL08-78	*BL08-78-171.92d*	red, v. fine gr, micrographic, K-feldspar-quartz-inclusion-rich monzonite	171.92	MF	25	AG/LS	M-Ser	35	SG	C-Chl				3	SR	AG	2	Ag	Pyr	25	PK	Incl	10	AG	C-Ser
BL08-78	*BL08-78-177.1*	red, fine gr, mottled, subophitic-subprismatic, quartz-monzogabbro	177.1	MF	45	LS	S-Ser	15	SOP/SR	C-Chl				3	AG	Sk	2	AG	Pyr	10	PK		20	AG	C-Ser/Hem
BL08-78	*BL08-78-178.7*	red, med/fine gr, mottled, subophitic-subprismatic, quartz-monzogabbro	178.7	MF	48	LS	S-Ser	15	SOP/SR	C-Chl				5	AG	SK				10	Pk	Incl	7	AG	C-Ser/Hem
BL08-78	*BL08-78-181.7*	red, med/fine gr, intergranular, carbonate-quartz gabbro	181.7	MF	45	LS	S-Ser	20	SG	C-Chl				7	AG	PR				10	PK		3	AG	C-Ser/Hem
BL08-78	*BL08-78-183.68*	red, med/fine gr, mottled, carbonate-bearing, quartz-gabbro	183.68	MF	55	LS	S-SER/HEM	15	SG	C-CHL				5	AG	Acicular	3	AG	Pyr	7	PK		10	AG	S-SER
BL08-78	*BL08-78-186.3a*	red, med/fine, subophitic, inclusion-rich, quartz-gabbro	186.3	MF	50	LS	S-Ser/Hem	25	SOP	C-CHL				5	AG	Acicular	3	AG	Pyr	17	PK				
BL08-78	*BL08-78-186.3b*	red, med/fine, mottled, subophitic, quartz-leucogabbro	186.3	MF	60	LS	S-SER/Hem	20	SOP	C-CHL				5	AG	Acicular	3			10	PK		2	AG	S-Ser
BL08-78	*BL08-78-188*	red, fine gr, subophitic, quartz-leucogabbro	188	MF	60	LS	S-Ser/Hem	10	SOP	C-CHL				5	AG					7	PK	Incl..			
BL08-78	*BL08-78-189.9*	red, med/fine, subophitic, quartz-bearing, oxide leucogabbro	189.9	FF	65	LS	M-Ser/Hem	13	SOP	C-CHL				7	AG					5	PK				
BL08-78	*BL08-78-190.3*	red, fine gr, intergranular, oxide-quartz leucogabbro	190.3	FF	65	LS	C-Ser/Hem	15	AG	C-CHL				7	AG					7	PK		3	AG	C-Ser/Hem
BL08-78	*BL08-78-191*	red, med/fine gr, intergranular, quartz-bearing, oxide gabbro	191	FF	55	LS	C-Ser/Hem	30	SG	S-CHL				7	PK	SK				5	PK				
BL08-78	*BL08-78-192.1a*	grey, v. coarse gr, prismatic, quartz-oxide-bearing feldspathic clinopyroxenite	192.1	CC	20	LS/Pk	S-???	64	SG	W-???/Chl				3	PK	SK				8	PK				
BL08-78	*BL08-78-192.1b*	grey, v. coarse gr, prismatic, quartz-oxide-bearing feldspathic clinopyroxenite	192.1	CC	30	LS	S-Ser/???	55	SG/PR	W-???/Chl				5	Sk	PK				2	PK				
BL08-78	*BL08-78-193.9*	grey, med-coarse gr, subpoikilitic, feldspathic wehrlite	193.9	MM	10	PK	W-Ser	30	PK/IGR	W-Chl/Act	30	SG	S-Srp/Tlc	3	PK	Corona									
BL08-78	*BL08-78-204.2*	grey, med-coarse gr, subpoikilitic, feldspathic wehrlite	204.2	MM	5	PK	M-Ser	25	Pk	W-Chl?	45	SG	S-Srp	2	PK	Corona?									
BL09-147	*BL09-147-153.1*		153.1	FF	35	AG	S-Ser										5	AG	Pyr	25	AG		25	AG	S-Ser/Hem
BL09-147	*BL09-147-155.8*	grey, fine gr, prismatic, oxide-sulfide bearing, quartz gabbro	155.8	FF	65	LS	C-Ser	15	PR	C-CHL				3	PK		5	AG/PK	Pyr	7	PK				
BL09-147	*BL09-147-157.6a*	grey, fine gr, intergranular, oxide-sulfide bearing, quartz monzogabbro	157.6	FF	25	AG/LS	S-Ser	25	AG/PR	C-Chl				2	PR	PK	3	AG	Pyr	35	PK	Incl..	10	AG	C-Ser/Hem
BL09-147	*BL09-147-157.6b*	grey, fine, gr, subprismatic, quartz monzonite	157.6	FF	45	AG/LS	S-Ser	25	SR	C-Chl				2	AG		3	AG	Pyr	20	PK	Incl..	5	AG	C-Ser/Hem
BL09-147	*BL09-147-161.7*	grey, fine gr, subprismatic, oxide/sulfide-bearing monzogabbro	161.7	FF	50	LS	S-Ser	20	SR	C-Chl				2	AG	PR	3	AG	Pyr	10	PK		10	AG	C-Ser/Hem
BL09-147	*BL09-147-165.2*	red, med gr, subprismatic, oxide/sulfide-bearing quartz monzogabbro	165.2	MM	40	LS	S-Ser	20	SR	C-Chl				3	AG	SK	2	AG	Pyr	10	Incl..	PK	20	AG	C-Ser/Hem
BL09-147	*BL09-147-165.9au*	red, fine gr. Subprismatic, oxide/sulfide-bearing quartz monzogabbro	165.9	FF	58	LS	S-Ser	15	SR/AG	C-Chl				5	AG	SR	2	AG	Pyr	10	Incl..	PK	7	AG	C-Ser/Hem
BL09-147	*BL09-147-165.9al*	red, med gr, mottled intergranular to prismatic, oxide/sulfide-bearing quartz monzonite	165.9	MF	10	LS	S-Ser	15	SG/PR	C-Chl				3	AG	SR	2	AG	Pyr	7	PK		60	AG/SP?	C-Ser/Hem
BL09-147	*BL09-147-165.9b*	red, med gr, mottled intergranular to prismatic, oxide/sulfide-bearing quartz monzonite	165.9	MF	15	LS	S-Ser	15	SR/AG	C-Chl				3	AG	SR				7	PK	Incl	60	AG/SP	C-Ser/Hem
BL09-147	*BL09-147-166.8a*	red, med gr, mottled, subprismatic to prismatic, oxide-bearing quartz monzogabbro	166.8	MM	25	LS	S-Ser	10	SR/AG	C-Chl				3	AG	SR				7	PK		50	AG/SP	C-Ser/Hem
BL09-147	*BL09-147-166.8b*	red, med gr, mottled, subprismatic, oxide-bearing quartz monzogabbro	166.8	MM	45	LS	S-Ser	20	SR/AG	C-Chl				5	AG	SR				7	PK		20	AG/SP	C-Ser/Hem
BL09-147	*BL09-147-167.8*	red, v.fine gr, intergranular, oxide-bearing, quartz gabbro	167.8	FF	60	LS	S-Ser	20	AG/SOP	C-Chl				5	AG					7	PK	Incl..	5	AG	C-Ser/Hem
BL09-147	*BL09-147-172.2*	Granite	172.2	CC																35	AG	PK...	65	AG	S-Ser/Hem
BL09-147	*BL09-147-174.5*	red, fine gr, intergranular, oxide/sulfide-bearing, quartz gabbro	174.5	MF	55	LS	S-Ser	20	AG/SOP	C-Chl				3	PR	Ag	2	AG	Pyr	12	Pk	Incl..	5	AG	C-Ser/Hem
BL09-147	*BL09-147-176.7*	red, fine gr, subprismatic to intergranular, oxide-bearing quartz gabbro	176.7	MF	50	LS	S-Ser	25	SG/SR	C-Chl				5	AG	SR				10	PK		3	AG	S-Ser/Hem
BL09-147	*BL09-147-176.9*	grey, med/fine gr, subprismatic to intergranular, quartz-bearing feldspathic olivine clinopyroxenite	176.9	MF	15	PK	M-Ser	55	SR/SG	S-Chl/Url/Amph	10	SG	C-Tlc/Srp???	2	Ag		3	AG	Pyr	5	PK				
BL09-147	*BL09-147-177.9*	grey, fine gr/ subprismatic to subpoikilitic, quartz-bearing wehrlite	177.9	MF				20	SR/SG	W-Amp	65	SG	C-Cal?	2	AG		2	AG	Pyr	2	PK				
BL09-147	*BL09-147-180.3*	green, med gr, intergranular to poikilitic, wehrlite	180.3	MC	5	PK	W-Ser	25	SG	W-Amp	45	SG	S-Srp/Tlc	3	AG	Corona	2	AG	Pyr						
BL09-146	*BL09-146-150.3*		150.30	VF	70	AG	S-Ser							trace	AG					20	AG				
BL09-146	*BL09-146-154.8*	grey, fine gr, intergranular, oxide/sulfide-bearing, quartz-rich gabbro	154.8	FF	60	LS	S-Ser	20	AG	C-Chl				2	AG		5	PK/AG	Pyr	10	PK	Incl...	2	AG	S-Ser/Hem
BL09-146	*BL09-146-158.4a*	grey, fine gr, intergranular, oxide/sulfide-bearing, quartz-rich gabbro	158.4	FF	60	Ls	S-Ser	20	AG	C-Chl				3	AG					10	PK	Incl...	3	AG	C-Ser/Hem
BL09-146	*BL09-146-158.4b*	red, fine gr, intergranular, oxide/sulfide-bearing, quartz-rich gabbro	158.4	FF	60	LS	S-Ser	20	Ag	C-Chl				2	AG					10	PK	Incl...	3	Ag	C-Ser/Hem
BL09-146	*BL09-146-161.2*	red, v.fine gr, intergranular, oxide-bearing, quartz gabbro	161.2	VF	60	LS	S-Ser	20	AG/SOP	C-Chl				3	AG	SR				10	PK	Incl...	5	AG	C-Ser/Hem
BL09-146	*BL09-146-164.8au*	red, v.fine gr, subprismatic, oxide-bearing, quartz gabbro	164.8	VF	60	LS	M-Ser	15	SR/AG	C-Chl				3	AG					15	PK	Incl...	7	AG	C-Ser/Hem
BL09-146	*BL09-146-164.8al*	red, med/fine gr, intergranular, oxide-bearing, quartz gabbro	164.8	MF	55	LS	S-Ser	25	SG/AG	C-Chl				7	AG					10	PK				
BL09-146	*BL09-146-164.8b*	red, med/fine gr, intergranular, oxide-bearing quartz melagabbro	164.8	MM	40	AG	S-Ser	35	SG	C-Chl				7	AG					10	PK	Incl...	5	AG	C-Ser/Hem
BL09-146	*BL09-146-164.9au*	red, med/fine gr, intergranular, oxide-bearing quartz gabbro	164.9	FF	55	LS	S-Ser	30	SG	C-Chl				5	AG					7	Pk	Incl	3	AG	
BL09-146	*BL09-146-164.9al*	red, fine gr, intergranular, sulfide/oxide-bearing, quartz leucogabbro	164.9	FF	70	LS	S-Ser	10	AG	C-Chl				2	AG		3	AG	Pyr	10	PK	Incl...	3	AG	C-Ser/Hem
BL09-146	*BL09-146-164.9b*	red, fine gr, intergranular sulfide-bearing, quartz leucogabbro	164.9	FF	65	LS	S-Ser	15	AG	C-Chl				2	AG	SP	5	AG	Pyr	10	PK	Incl...	3	AG	C-Ser/Hem
BL09-146	*BL09-146-167.9a*	red, med/fine gr,subprismatic, oxide-bearing quartz gabbro	167.9	MF	55	LS	S-Ser	25	SR	C-Chl				5	AG		2	AG	Pyr	7	PK	Incl...	3	Ag	C-Ser/Hem
BL09-146	*BL09-146-167.9b*	red, med/fine gr,subprismatic, oxide/sulfide-bearing quartz gabbro	167.9	MF	60	LS	S-Ser	20	AG	C-Chl				2	AG		3	AG	Pyr	7	PK	Incl...	3	AG	C-Ser/Hem
BL09-146	*BL09-146-169.6*	red, med/fine , prismatic to intergranular, oxide-quartz gabbro	169.6	MF	55	LS	S-Ser	25	SG/PR	S-Chl				8	AG		2	AG	Pyr	5	PK		2	AG	C-Ser/Hem
BL09-146	*BL09-146-169.9*	grey, med/fine gr, subpoikilitic, quartz-bearing feldspathic wehrlite	169.9	MF	15	SP	S-ser	30	SP	M-Url/Chl	30	SG	C-Tlc/srp	5	AG		2	AG		3	Pk				
BL09-146	*BL09-146-170.6*	grey, med gr, subpoikilitic, plagioclase-bearing wehrlite	170.6	MF	3	PK	S-Ser/???	25	SG	W-Url/Chl	52	SG	C-Srp/Tlc	3	AG										
BL09-146	*BL09-146-174.3*	grey, med gr, subpoikilitic, plagioclase-bearing wehrlite	174.3	MC	7	PK	W-Ser	30	SG	W-Act/Chl?	43	SG	S-Srp/Tlc	3	AG										

Core	Sample ID	Apatite			Granophyre			Amphibole			Biotite			Carbonate			Other Minerals			Comments
		Mode	Habit	Host	Mode	Habit	Alteration	Mode	Habit	Type	Mode	Habit	Primary?	Mode	Habit	Habit 2	Phase	Mode	Habit	
TBND-60	*TBND-60-14.8u*				2	AG														**Diffuse Contact** between hybrid red and granitic country rock; appears to have experienced partial melting; quartz is deformed and plagioclase occurs as laths between quartz.
TBND-60	*TBND-60-14.8l*																			Dominantly lath to acicular shaped plagioclase completely altered to sericite with hemitite staining; similar in texture to "matrix" of granitic unit; subprismatic pyroxenes completely altered to uralite and chlorite strongly associated with oxides.
TBND-60	*TBND-60-15.2*	Trace	Bl	Pl																
TBND-60	*TBND-60-16.5*													10	Pk					relict pyroxene texturtures are somewhat hard to see, however in some cases the dominant texuture is subophitic; some fine grained hemitized Kfs; some fresh plagioclase
TBND-60	*TBND-60-17.5*	Trace	Bl	Pl										7	AG					relict pyroxene textures include supophitic and anhedral granular; k-feldspar occurs as rims around plagioclase; calcite is very fine grained and occurs with(in) chlorite.
TBND-60	*TBND-60-18.9*	2	Bl	Pl										5	Pk	Ag				Carbonate occurs as interstitial phases with quartz and also as blebs replacing pyroxene with chlorite!
TBND-60	*TBND-60-20.1*	trace	Bl	Pl										5	Pk	Ag				Carbonate occurs as interstitial phases with quartz and also also as blebs with chlorite replacing pyroxene; quartz is very abundant; plagioclase is strongly to completely altered to sericite and mantled by Kfs..
TBND-60	*TBND-60-21.4*	trace	Bl	Pl										13	PK	AG				Large relict pyroxene oikocryst; sample consists of pockets of heavily hemitized plagioclase with quartz (representative of partial melt?)
TBND-60	*TBND-60-21.65*	Trace	Bl	Pl							Trace	SG	No				Sphene	2	AG	Some fresh pyroxene that is altering to chlorite/ uralite and unknown; plagioclase cores altering to sericitie; quartz occurs in interstitial space; some biotite.
TBND-60	*TBND-60-22.3*	Trace	Bl	Pl																Fresh subhedral Cpx altering to uralite and chlorite (similar to chlorite seen in above samples); plagioclase and quartz are interstitial
TBND-60	*TBND-60-23.0*	trace	bl	pl							trace	SG	no	2	Pk		Chl	3	Ag	Abundant fresh Cpx; olivine MAY be present however, possibly completely altered and leave very indistinct trace of relict habits; chlorite occurs in interstitial space and so does carbonate.
TBND-60	*TBND-60-25.8*	tr	bl	pl				15	AG	Act										Actinolite makes up a 'matrix' hosting olivine and Cpx. Some olivine appears to be altering to actinolite matrix??
TBND-60	*TBND-60-32.9*	trace	bl	pl				5	AG	Act	trace	SG					Chl	5	AG	Actinolite and Chlorite make a 'matrix' between cpx, olivine and plagioclase
TBND-95	*TBND-95-91.5*																MS	5		unkown mineral is pale green in plain light and high birefringence colores; quartz appears to be sheared...
TBND-95	*TBND-95-92.1*	2	Bl	Pl										3	AG		Chl	10	AG	Strong biotite and chlorite alteration of granular Cpx; some areas appear to have pockets of chlorite; plagioclase occurs as laths and subpoikilitic habits; some phases appear to be completely altered olivines???
TBND-95	*TBND-95-93.8*	trace	bl	pl										3	AG	Vein	Chl	5	Vein	5mm wide calcite vein mantled by chlorite; Calcite also seen in interstitial space, at times with chlorite; olivine completely altered to serpentine and talc; plagioclase appears in interstitial space.
TBND-95	*TBND-95-94.9*	trace	bl	pl				8	AG	Act	1	AG	no	2	Ag		Chl	15		Chlorite and actinolite serve as a 'matrix'; some biotite appears as alteration of Cpx; some carbonate associated w/ relict Olivines.
TBND-95	*TBND-95-97.2*	trace	bl	pl										5	AG					Completely altered subophitic Cpx to Chlorite, Uralite and Carbonate; oxide strongly associated with chlorites; some hematized K-feldspar rimming plagioclase (some fresh visible).
TBND-95	*TBND-95-98.1*													5	Ag	VEIN				Carbonate occurs as a single vein, as well as alteration of pyroxenes; plagioclase exhibits relict twinning; pyroxenes exhibit relict subophitic and subprismatic textures.
TBND-95	*TBND-95-99.1*													5	AG					CHILL ZONE - Rock is aphanitic; percentages difficult to distinguish. Carbonate appears to be replacing plagioclase and Cpx (chlorite); Oxides occur as both anhedral and prismatic needles.
TBND-95	*TBND-95-99.3*										3	AG	Yes	Trace	AG					Fresh granitic rocks; biottie?? Appears green, no apparent pleocroism, higher birefringence colors in XPL.
TBND-95	*TBND-95-100.6*										3	Ag	Yes				MS	2	AG	Biotite is not as certain; could be something else; K-Feldspar is fresh; plagioclase exhibites sericite alteratoin;
TBND-95	*TBND-95-101.9*										3	AG	Yes				MS	2	AG	Same as above
TBND-124	*TBND-124-38.6*																Unk	5	AG	Strongly hematized K-Feldspar; green unkown mineral assiciated with oxides, low to higher 1st order colors...
TBND-124	*TBND-124-44.2*	trace	Bl	Pl				3	Ag	Act	2	SG	Yes				Chl	5	AG	Poikolitic pyroxene; interstitial plagioclase and chlorite/actinolite make a 'matrix'; biotite alteration of pyroxenes?; some fresh olivine.
TBND-124	*TBND-124-49.5*	trace	Bl	Pl				3	Ag	Act	2	AG	Yes	2	PK		Chl	10	AG	Poikolitic pyroxene; interstitial plagioclase and chlorite/actinolite make a 'matrix'; biotite alteration of pyroxenes?; some fresh olivine; some carbonate present; in some cases it appears that plagioclase is altering to chlorite???
TBND-124	*TBND-124-52.8*	trace	bl	pl				3	Ag	Hbl	2	Ag	Yes	2	PK		chl	5	SG	Poikolitic pyroxene; interstitial plagioclase and chlorite/actinolite make a 'matrix with some calcite'; POSSIBLY SOME OPX!!; biotite alteration of pyroxenes?; some fresh olivine; some carbonate present; in some cases it appears that plagioclase is altering to chlorite???
TBND-124	*TBND-124-53.9*	trace	Bl	Pl				2	Ag	Act	2	Ag	Yes	2	Pk		Chl	2	AG	Same composition as above sample but with more plagioclase; less chlorite/actinolite 'matrix'; and sulfide present
TBND-124	*TBND-124-55.5*	trace	Bl	Pl				5	AG	Hbl	1	AG	Yes				Chl	5	Ag	Some olivine altering to what appears to be actinolite????
TBND-124	*TBND-124-57.5*	trace	BL	Pl				2	AG	Hbl	5	SG	Yes				Unkown	5?	??	Biotite and hornblende;
TBND-124	*TBND-124-58.1u*	trace	BL	Pl	trace	MGR	W-Ser													**Sharp Contact:** plagioclase appears as lath shaped interstitial phase, in some areas it also appears mermikitic with either quartz or k-feldspar?; pyroxene is completely altered to amphibole and possibly biotite?; olivine may be present but completely altered/replaced.
TBND-124	*TBND-124-58.1l*																Mica	3	Ag	Appears to be experiencing partial melting.
TBND-124	*TBND-124-60.8*																Unknown	8	AG	Unknown mineral is pale green to clear in plain light with 2nd order colors; quartz is deformed.
TBND-124	*TBND-124-81.0*																Unkown	5	AG	Quartz deformed, breaking down into smaller graines; unkown greenish mineral associated with oxides.
TBND-124	*TBND-124-86.5l*	trace	bl	pl										5	AG					Grades from subophitic completely altered pyroxene to subhedral granular pyroxene habits; pyroxenes completely altered to amphibole toward top and chlorite/amphibole mix toward bottom; plagioclase is subpoikilitic.
TBND-124	*TBND-124-87.2*	TRACE	BL	PL				3	Ag	Hbl?	2	Sg	???							Fresh Cpx altering to an unkown phase (Sphene????), biottte and some amphibole (Hbl?); plagioclase is lath shaped and appears to be subpoikilitic;
TBND-124	*TBND-124-87.6*	trace	Bl	Pl				5	AG	Act	2	AG	Yes				Chl	5	AG	Chlorite and Actinolite make up matrix, appears to be altering from plagioclase and pyroxene. Plagioclase is interstitial to Olivine and Cpx;
TBND-124	*TBND-124-88.9*	trace	Bl	Pl				2	AG	Act	3	AG	yes/no				Chl	10	AG	Actinolite makes up matrix, strong association with Cpx; olivine is strongly to completely altered to srp and tlc.
TBND-124	*TBND-124-91.5*													5	Veins					Calcite occurs as veins; pyroxenes are completely altered to unknown; olivines appear clear in ppl with oxide coronas, high biref colors in xpl.
TBND-124	*TBND-124-93.0*	trace	Bl	Pl							3	SG		3	Pk					Similar to above; except fresh Cpx appears - altered to biotite and amphibole?-;
TBND-124	*TBND-124-94.7*																			CHILL ZONE - plagioclase laths, acicular to prismatic oxides (ilmenite?) w/ some skeletal magnetite altering to SPHENE!
TBND-124	*TBND-124-97.5*																			
TBND-136	*TBND-136-16.2*																UNK	3	AG	Unkown mineral is green pleocroic with high birefringence colors (2nd order); K-feldspar appears as radial needles.
TBND-136	*TBND-136-16.6*	trace	Bl	pl																Prismatic pyroxenes that are completely altered; plagioclase is moderately altered
TBND-136	*TBND-136-18.9*	trace	bl	pl										5	PK					Consists of pockets of plagioclase and hemitized K-feldspar; Cpx occurs as completely altered to chlorite and carbonate blebs and unkown; oxides are anhedral, prismatic and some skeletal habits.
TBND-136	*TBND-136-20.6*	trace	bl	pl										7	Pk					Chlorite exhibits relict subophitic textures for Cpx (also altering to carbonate and unkown); Hematized K-feldspar occurs as a rim around plagioclase.
TBND-136	*TBND-136-20.8*	trace	bl	pl										3	Pk					From top to bottom, Cpx grades from strongly altered to moderately altered. With a plagioclase rich "vein" in the center of the slide.
TBND-136	*TBND-136-21.1*	trace	bl	pl										3	AG					Plagioclase is interstitial to cumulus pyroxene.
TBND-136	*TBND-136-22.0*	trace	bl	pl					AG	Hbl							Chl/Act	15	AG	Subhedral poikilitic Cpx that is beginning to alter to hornblende; plagioclase is interstitial; olivine and cpx make up cumulus minerals; chlorite and actinolite make up a 'matrix'
TBND-136	*TBND-136-26.0*																Chl/Act	10	AG	Actinolite/Chlorite create a 'matrix'; fresh olivine can be observed within plagioclase; pyroxenes are subhedral and poikilitic with olivine oikicrysts.
TBND-136	*TBND-136-34.7*																Chl/Act	20	AG	
TBND-125	*TBND-125- 17.9*																Unknown	3	SG	Strongly hematized granite; rock has experienced some deformation; appears to contain some biotite that is fine grained and possibly altered to chlorite???; unknown subhedral mineral, dark grey birefringence...
TBND-125	*TBND-125- 19.9*	trace	BL	Pl													Uralite??	2	SG	**Diffuse contact** between granite and hybrid red; granite appears to be partially melted with similar textures to that of the mottled red hybrid.
TBND-125	*TBND-125- 22.0*	trace	Bl	Pl																Some hematized k-feldspar; plagioclase shows zoning with cores being altered to sericite; pyroxenes are completely altered to chlorite and uralite/actinolite??; some relict textures include subprismatic to subophitic pyroxenes...
TBND-125	*TBND-125- 22.8*	trace	Bl	Pl																Some hematized k-feldspar; plagioclase shows zoning with cores being altered to sericite; pyroxenes are completely altered to chlorite and uralite/actinolite??; some relict textures include subophitic to (possibly) anhedral pyroxenes...
TBND-125	*TBND-125- 23.8*	2	Bl	Pl													Unkown	1	AG	Relict subophitic to ophitic pyroxenes (altered to chlorite and possibly uralite/actinolite); plagioclase altering to sericite commonly in core; unkown mineral commonely associated with chlorite.
TBND-125	*TBND-125- 24.4a*	trace	Bl	Pl																Relict subophitic to ophitic pyroxenes (altered to chlorite and possibly uralite/actinolite); plagioclase is weakly foliated and altering to sericite commonly in core; unkown brown mineral commonely associated with chlorite.
TBND-125	*TBND-125- 24.4b*	trace	BL	PL										2	AG					Strongly altered; Very littele (2%) fresh Cpx?, altering to chlorite; carbonate occurs as blobs within chlorite; unknown brown mineral; plagioclase is strongly altered to sericite and fresh plag exhibits zoning.
TBND-125	*TBND-125- 24.8*	trace	Bl	Pl				trace	Ag	Act?				2	AG					Fresh Cpx; some interstitial chlorite; plagioclase is poikilitic; unknown alteration of Cpx (uralite and actinolite?)
TBND-125	*TBND-125- 25.4*	2	Bl	PL										3	PK					Fresh granular Cpx that exhibits uralite and chlorite alteration (possibly some amphibole); some Cpx completely altered to chlorite (AG to SR); plagiclase altering to sericite and exhibits relict lath shape and twinning.
TBND-125	*TBND-125- 25.8*	2	Bl	Pl																Same as above sample except no calcite and more abundant Cpx.
TBND-125	*TBND-125- 26.2*	trace	bl	pl				7	Ag	Act							Chl	20	PK	Chlorite and Actinolite make up a 'Matrix'; serpentinized olivine within Cpx oikocrysts.
TBND-125	*TBND-125- 29.8*	2	Bl	Pl				3	AG	Act				2	AG		Chl	5	PK	Chlorite and Actinolite make up a 'Matrix'; some fresh olivine.
TBND-125	*TBND-125- 33.3*							5	AG	Act							Chl	7	PK	Chlorite and Actinolite make up a 'Matrix'; some fresh olivine; some plagioclase appears to be altering to sericite.
TBND-023	*TBND-023-106.3*										2	SG	Yes				Ms	5	SG	
TBND-023	*TBND-023-107.8*													5	AG					Chill - lath to acicular plagioclase; prismatic oxides; Cpx altering to chlorite and carbonate (carbonate modal percentage is additional and is also part of the modal % for Cpx)
TBND-023	*TBND-023-109.3*							2	AG	Hbl?				5	AG	PK				Lath shaped plagioclase in relict ophitic Cpx (altered to chlorite and amphibole?); unkown mineral exhibits similar habit to that of skeletal oxides
TBND-023	*TBND-023-111*	trace	bl	pl										trace	AG					Some chlorite shapes exhibit relict pyroxene habits; in some cases one could argue that some olivine is represented???; unkown mineral phase appears to be altered oxides
TBND-023	*TBND-023-112.6*										3	AG	Yes							
TBND-023	*TBND-023-115.9*													2	AG					Chill - similar to 107.8 except less calcite and oxides appear to be altering to unkown mineral phase.
BL08-75	*BL08-75-149.6*																Ms	45	SG	Well foliated muscovites; plagiocalse and k-feldspars are altering to sericite; pyrite ocurs in veins.
BL08-75	*BL08-75-152.5*	2	BL	PL										3	AG	Amygdule	UNK(MS??)	trace	SG	Very fine grained; quartz shows up in interstitial space and as amygdules with calcite; some fresh plagioclase is observed with twinning; unkown mineral associated with amydules appears to be muscovite????; BOTH Fe and Mg Chlorite observed
BL08-75	*BL08-75-153.2*	3	BL	PL										5	AG	Amygdule				Very fine grained; quartz shows up in interstitial space and as amygdules with calcite; some fresh plagioclase is observed with twinning; BOTH Fe and Mg Chlorite observed
BL08-75	*BL08-75-157.5*																Sphene	5	SG	aphanitic to very fine grained; plagioclase is lath shaped to acicular in shape; both Fe and Mg chlorite replace pyroxene.
BL08-75	*BL08-75-160*	trace	BL	PL										15	AG	Amydule				Very fine grained; Coarse grained calcite amygdules with quartz XTL's; both Fe and Mg chlorite appear with amygdules and as relict anhedral and subprismatic pyroxenes.

Core	Sample ID	Apatite			Granophyre			Amphibole			Biotite			Carbonate			Other Minerals			Comments
		Mode	Habit	Host	Mode	Habit	Alteration	Mode	Habit	Type	Mode	Habit	Primary?	Mode	Habit	Habit 2	Phase	Mode	Habit	
BL08-75	*BL08-75-161.5a*	trace	BL	PL										10	PK/AG	Amygdule	UNK	Trace	???	Very fine grained; Coarse vesicles, some filled w/ calcite and quartz; both Fe and Mg chlorite observed as interstitial and anhedral; UNKOWN mineral found in the core of some oxides???
BL08-75	*BL08-75-161.5b*	2	BL	PL										5	PK	Amygdule				Very fine grained; both Fe and Mg chlorite present; occurs as rim around amygdules; plagioclase appears to be foliated in localize areas in the section.
BL08-75	*BL08-75-167.3u*	Trace	BL	PL																**Sharp Contact:** similar to upper unit minus the calcite.
BL08-75	*BL08-75-167.3l*	Trace	BL	PL																Similar mineralogy than upper unit; Medium fine grained; both Fe and Mg chlorite which becmes coarser grained and more "granular".
BL08-75	*BL08-75-169.2*	Trace	BL	PL										7	PK					Plagioclase appears to be rimmed by hematized K-feldspar. Calcite appears as interstial and as blebs within Fe-Chlorite; Both Fe and trace Mg chlorite present.
BL08-75	*BL08-75-170*	Trace	BL	PL										2	PK					
BL08-75	*BL08-75-170.2*							5	AG	Act/Trm	3	AG	No	25	PK	AG				Abundant Carbonate replacing chlorite???; some relict grain shapes preserved - some possibly olivine?? - biotite alteration from pyroxene. Completely BLITZED!!
BL08-75	*BL08-75-171.8a*																chl	15	Matrix	
BL08-75	*BL08-75-171.8b*													2	pk		Chl	20	Matrix	Chlorite makes up a 'matrix' that possibly replaced plagioclase; some fresh olivine, but mostly altered to talc/serpentine and possibly replaced by calcite?
BL08-75	*BL08-75-175*	Trace?	BL	??				2	AG	Act				3	pk		Chl	15	Matrix..	Poikilitic Cpx hosting completely altered olivines; matrix consists of chlorite and actinolite.
BL08-75	*BL08-75-179*							2	AG	Act							Chl	10	Matrix	Poikilitic Cpx hosting completely altered olivines; matrix consists of chlorite and actinolite.
BL08-78	*BL08-78-162.65*										40	AG	Yes	5	Vein					Foliated, biotite appears as cruddy green color w/ 2nd order birefringence.
BL08-78	*BL08-78-165.34*										10	AG	Yes							Appears to be granitic inclusion, plagioclase appears hemitized and sericitized (relict twinning); some areas of the sample appear to be experiencing brittle breakdown of feldspars.
BL08-78	*BL08-78-165.34*										5	AG	Yes				Chl	40	AG	
BL08-78	*BL08-78-166.28*	trace	BL	PL										3	Vein					Plagioclase appears to be hemitized (and sericitized); pyroxenes completely altered to chlorite but exhibit relict anhedral and subprismatic textures and possibly some subophitic textures.
BL08-78	*BL08-78-169.57a*	Trace	Bl	PI										2	AG					Granophyre consists of micrographic quartz and sericitized feldspar (possibly also hematized); most of the quartz occurs as large inclusions rimmed by chlorite and granophyre.
BL08-78	*BL08-78-169.57b*	Trace	Bl	PI										2	Ag					Granophyre appears to be subpoikolitic with sericitized plagioclase (some fresh) primocrysts; chlorite exhibits relict subprismatic to anhedral pyroxene textures as well as mantling quartzite incl. w/ calcite?
BL08-78	*BL08-78-171.92a*				5	MGr	M-Ser							2	Ag		Ep?	Trace	AG	Inclusions include Quartz and Granitic rock compositions mantled by chlorite, K-feldspar and granophyre; Epidote appears as v. fine grained anhedral cyrstals.
BL08-78	*BL08-78-171.92b*				5	MGR	M-Ser							2	AG		Sph	3	AG	Similar to Above sample, quartz inclusion is mantled by K-feldspar and granophyre; sphene is prevelant
BL08-78	*BL08-78-171.92c*																			
BL08-78	*BL08-78-171.92d*																			
BL08-78	*BL08-78-177.1*	Trace	Bl	PI										5	AG					Sericitized plagioclase w/ relict twinning and habit; relict ophitic/diabasic texture; calcite appears w/in chlorite and plagioclase; hematization of feldspars
BL08-78	*BL08-78-178.7*	Trace	Bl	PI										5	AG	Amyg				Sericitized plagioclase w/ relict twinning and habit; calcite appears w/ chlorite; relict subprismatic and granular textures, some subophitic; hematization of feldspars
BL08-78	*BL08-78-181.7*	Trace	Bl	PI										15	AG	Amyg				Abundant subpoikolitic-anhedral calcite; sericitized plagioclase laths; K-feldspar occurs as a hematized rim around plagioclase; chlorite exhibits anhedral, subprismatic and subophitic pyroxene textures.
BL08-78	*BL08-78-183.68*													5	AG					Contains both Fe and Mg chlorite alteration (Cpx). Calcite amygdules mantled by strong hematized plagioclase.
BL08-78	*BL08-78-186.3a*																			Contains quartzite inclusions mantled by Fe-Chlorite. Moderate hemitization of plagioclase.
BL08-78	*BL08-78-186.3b*																			Contains both Fe and Mg chlorite (Cpx). alteration (Cpx
BL08-78	*BL08-78-188*	Trace	BL	PL										8	AG	Amygdules				Carbonate occurs as amygdules w/ quartz and is mantled by Fe-chlorite and also as blebs w/in chlorite; Apatite appears as inclusions in plagioclase.
BL08-78	*BL08-78-189.9*													10	AG	PK				Carbonate occurs as interstitial along with quartz.
BL08-78	*BL08-78-190.3*	Trace	BL	PI										3	PK					Looks similar to Red Hybrid. Some feldspars that didn't exhibit twinning were interpreted to be Kfs.
BL08-78	*BL08-78-191*													3	PK					**Contact –** Calcite/Chlorite/quartz vein ~1cm wide through middle of the section
BL08-78	*BL08-78-192.1a*	trace	BL	PL										5	PK					Very Coarse grained pyroxenes with some chlorite and unkown alteration. Plagioclase appears interstitial with sericite and UNKNOWN alteration.
BL08-78	*BL08-78-192.1b*													2	PK		Chl	5	Pk	Very Coarse grained pyroxenes. Same mineralogy as above sample except w/ more plagioclase and quartz!
BL08-78	*BL08-78-193.9*	Trace	BL	PL				3	AG?	Act	2	SG	No	2	PK		CHL	20	PK	Chlorite/Actinolite make up interstitial alteration minerals (matrix...); some primary olivine present
BL08-78	*BL08-78-204.2*							3	Interstitial	Act				2	Amygdules		CHL	18	PK	Same as above
BL09-147	*BL09-147-153.1*																MS/Chl	10	AG	Fine grained rock consisting of felspar grains (plagioclase and K-Feldspar), quartz grains, and muscovite and chlorite.
BL09-147	*BL09-147-155.8*													5	PK	Vein/Amygdule				
BL09-147	*BL09-147-157.6a*																			Fine grained rock with very coarse quartzite inclusions mantled by chlorite and granophyre.
BL09-147	*BL09-147-157.6b*													3	AG	Amygdule				
BL09-147	*BL09-147-161.7*	2	BL	PL										3	AG	Amygdule				Contains pockets of strongly hematized K-feldspar.
BL09-147	*BL09-147-165.2*	2	BL	PL?										3	AG					Pockets of "fibrous", strongly hematized K-Feldspar. Some plagioclase laths appear to be contributing to the Fe-Chlorite alteration. In some cases, there appears to be both Fe and Mg chlorite.
BL09-147	*BL09-147-165.9au*													3	AG	Amygdule				**Sharp Contact**- sharp textural contact, transition to mottled texture. Calcite and small quartz inclusions mantled by Fe-Chlorite occur throughout.
BL09-147	*BL09-147-165.9al*													3	Amygdule					**Sharp Contact-** sharp textural contact to mottled texture. K-Feldspars appear as a hematized matrix and exhibits anhedral to acicular habits.
BL09-147	*BL09-147-165.9b*													trace	AG					Same as above except more plagioclase and no sulfide and only trace calcite. K-Feldspar is hematized and anhedral to acicular habit..
BL09-147	*BL09-147-166.8a*	2	BL	PL/Kfs										2	AG	pk				Mottled texture, pockets of hematized anhedral to radiating acicular K-feldspar. Calcite occurs in interstictial space as well as "blobs" associated with chlorite.
BL09-147	*BL09-147-166.8b*													3	AG	PK				Mottled texture, pockets of hematized anhedral to radiating acicular K-feldspar; in some areas Kfs appears to be radiating from plagioclase laths. Chlorite alteration of sub-ophitic pyroxenes, calcite blobs appear to be associated within Fe-chlorite, along with some sericite??.
BL09-147	*BL09-147-167.8*													3	AG	Amygdules				Fine grained; hematized K-feldspar appears to rim plagiocalse and also as interstitial. Calcite observed with Fe-Chlorite. Also, trace Mg-Chlorite seen with Fe-chlorite. ONE large quartz inclusion mantled by Kfs, Fe-Chl and Cal.
BL09-147	*BL09-147-172.2*																			Quartz grains appear strained. Strong hematization of Kfs, relict microcline twinning.
BL09-147	*BL09-147-174.5*	Trace	Bl	PI										3	AG					Quartz inclusions occur with chlorite and Kfs rims; plagioclase is lath shaped with hematitzed K-Feldspar rims.
BL09-147	*BL09-147-176.7*	trace	BL	PL										7	AG	Amyg/Vein	Ep??	2	AG	Hematized Kfs rims plagioclase; calcite appears as a vein and as blobs in chlorite.
BL09-147	*BL09-147-176.9*													5	AG		5	AG	PK	Subhedral to sub-prismatic clinopyroxenes altering to Fe-chlorite and amphibole (Act/Tremolite??). Olivine appears to be completely altered to talc (possibly some serpentine) and has an oxide corona.
BL09-147	*BL09-147-177.9*							2	AG	Tremolite	2	SG	No	2	AG	Amygdule	CHL	5	PK	Clinopyroxene has amphibole coronas; olivine appears completely altered to talc??; calcite shows up as amygdules; chlorite occurs in interstitial space.
BL09-147	*BL09-147-180.3*	Trace	BL	PL				3	AG	Act	2	SG	No				Chl	15	PK	Cpx is poikolitic with olivine primocrysts; olivine is strong to completely altered to Srp and Tlc with oxide corona; Fe-Chlorite appears in interstitial space along with biotite and actinolite?
BL09-146	*BL09-146-150.3*																Garnet	5	AG	Ms and Chl make up ~ 5%; garnets are breaking down; dominant feldspar is plagioclase.
BL09-146	*BL09-146-154.8*	3	BL	PL										3	AG	Amygdule				Carbonate occurs in interstitial space, amygdules, and as blobs within chlorite; chlorite exhibits relict pyroxene habits; K-feldspar occurs as a hematized rim around plagioclase. Large inclusions are mantled by chlorite, carbonate and Kfs and consist of quartz and carbonate.
BL09-146	*BL09-146-158.4a*	2	BL	PL										2	AG	Amydule				Carbonate occurs as amygdules and blobs within chlorite; chlorite exhibits relict pyroxene habits; K-Feldspar occurs as a hematized rim around plagioclase. Large quartz inclusion mantled by chlorite and Kfs and also contains some carbonate and plagioclase and K-feldspar blob.
BL09-146	*BL09-146-158.4b*	trace	BL	PL										5	AG	Amygdule				Carbonate occurs with quartz as amydules and in interstitial space; chlorite shows relict pyroxene habits; K-feldspar occurs as hematized rims around plagioclase.
BL09-146	*BL09-146-161.2*													2	AG					Very Fine grained, almost aphanitic; K-feldspar occurs as hematized rims around plagioclase and as a vein with quartz; quartz occurs as small inclusions and as interstitial material; plagioclase is lath shaped to acicular.
BL09-146	*BL09-146-164.8au*	trace	BL	PI																**Contact-** sharp textural and compositional contact between hybrid subunits. Hematized K-Feldspar rims plagioclase and forms anhedral crystals surrounding quartz near contact. Chlorite less abundant.
BL09-146	*BL09-146-164.8al*													3	SP					Consists of pockets of fine grained upper unit; relict anhedral granular and sub ophitic Cpx textures in Chlorites.
BL09-146	*BL09-146-164.8b*													3	SP					Abundand Chlorite (relict Cpx textures) and mantles small quartz inclusions; consists of small pockets of strongly altered plagioclase with some K-Feldspar; also, a 1cm wide "vein" of fine grained chlorite, quartz and plagioclase through the section.
BL09-146	*BL09-146-164.9au*													trace	SP					**Contact** - diffuse textural contact.
BL09-146	*BL09-146-164.9al*													2	SP					Chlorites grade to finer grained from one end of the section to the other, also mantles small quartz inclusions. Very little hematite staining.
BL09-146	*BL09-146-164.9b*													3	SP					Chlorite less abundant that above sample; plagioclase is rimmed by hematized K-Feldspar; some K-Feldspar is associated with quartz inclusions;
BL09-146	*BL09-146-167.9a*													3	Sp	Amygdule				Completely altered K-Feldspar that is anhedral crystals and rims around plagioclase;
BL09-146	*BL09-146-167.9b*													5	SP	Amygdule				Completely altered K-Feldspar that is anhedral crystals and rims around plagioclase; Chlorite exhibits relict subophitic textures and is less abundant.
BL09-146	*BL09-146-169.6*													3	SP					Completely altered K-Feldspar to sericite and hemitite, forms anhedral grains and some rimming plagioclase??; some fresh Clinopyroxene going to chlorite.
BL09-146	*BL09-146-169.9*																Chl	20		
BL09-146	*BL09-146-170.6*													2	AG		Chl	15	PK	Some relict olivines are now calcite; chlorite appears in interstitial space as a "matrix"
BL09-146	*BL09-146-174.3*	2	BL	PI				3	AG	Act?				2	PK		Chl	10	PK	Chlorite occurs as 'matrix' along with actinolite?; interstitial plagioclase and calcite; poikilitic clinopyroxene hosting cumulus olivine.

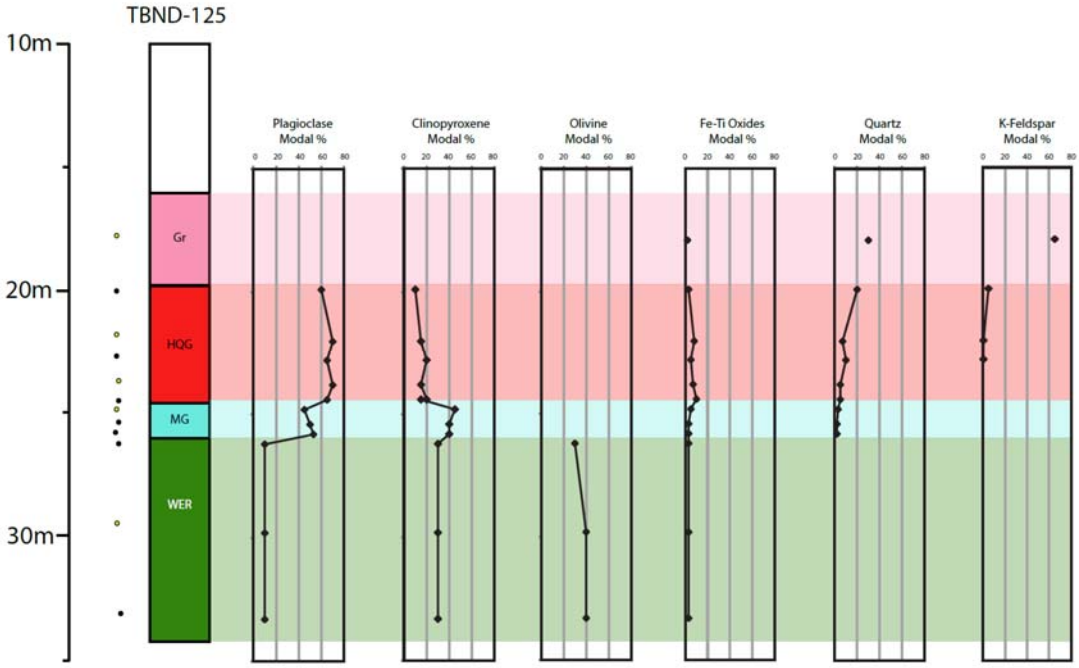
TBND-125
10m
20m
30m
Gr
HQG
MG
WER
Plagioclase Modal %
Clinopyroxene Modal %
Olivine Modal %
Fe-Ti Oxides Modal %
Quartz Modal %
K-Feldspar Modal %
0 20 40 60 80

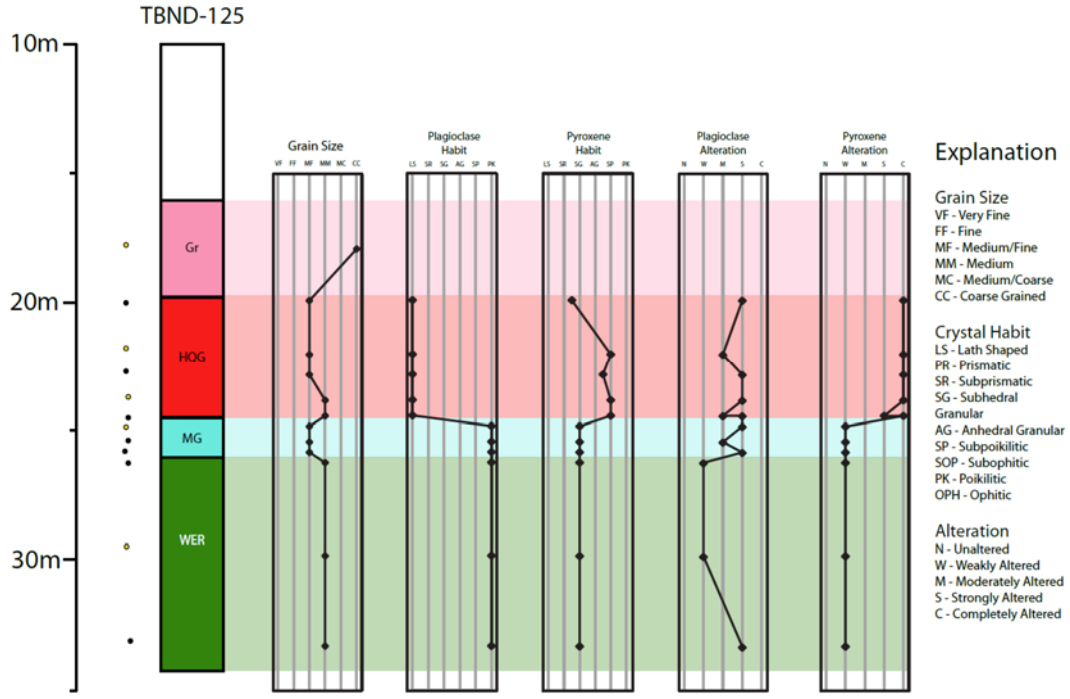
TBND-125
10m
20m
30m
Gr
HQG
MG
WER
Grain Size
VF FF MF MM MC CC
Plagioclase Habit
LS SR SG AG SP PK
Pyroxene Habit
LS SR SG AG SP PK
Plagioclase Alteration
N W M S C
Pyroxene Alteration
N W M S C
Explanation
Grain Size
VF - Very Fine
FF - Fine
MF - Medium/Fine
MM - Medium
MC - Medium/Coarse
CC - Coarse Grained
Crystal Habit
LS - Lath Shaped
PR - Prismatic
SR - Subprismatic
SG - Subhedral Granular
AG - Anhedral Granular
SP - Subpoikilitic
SOP - Subophitic
PK - Poikilitic
OPH - Ophitic
Alteration
N - Unaltered
W - Weakly Altered
M - Moderately Altered
S - Strongly Altered
C - Completely Altered

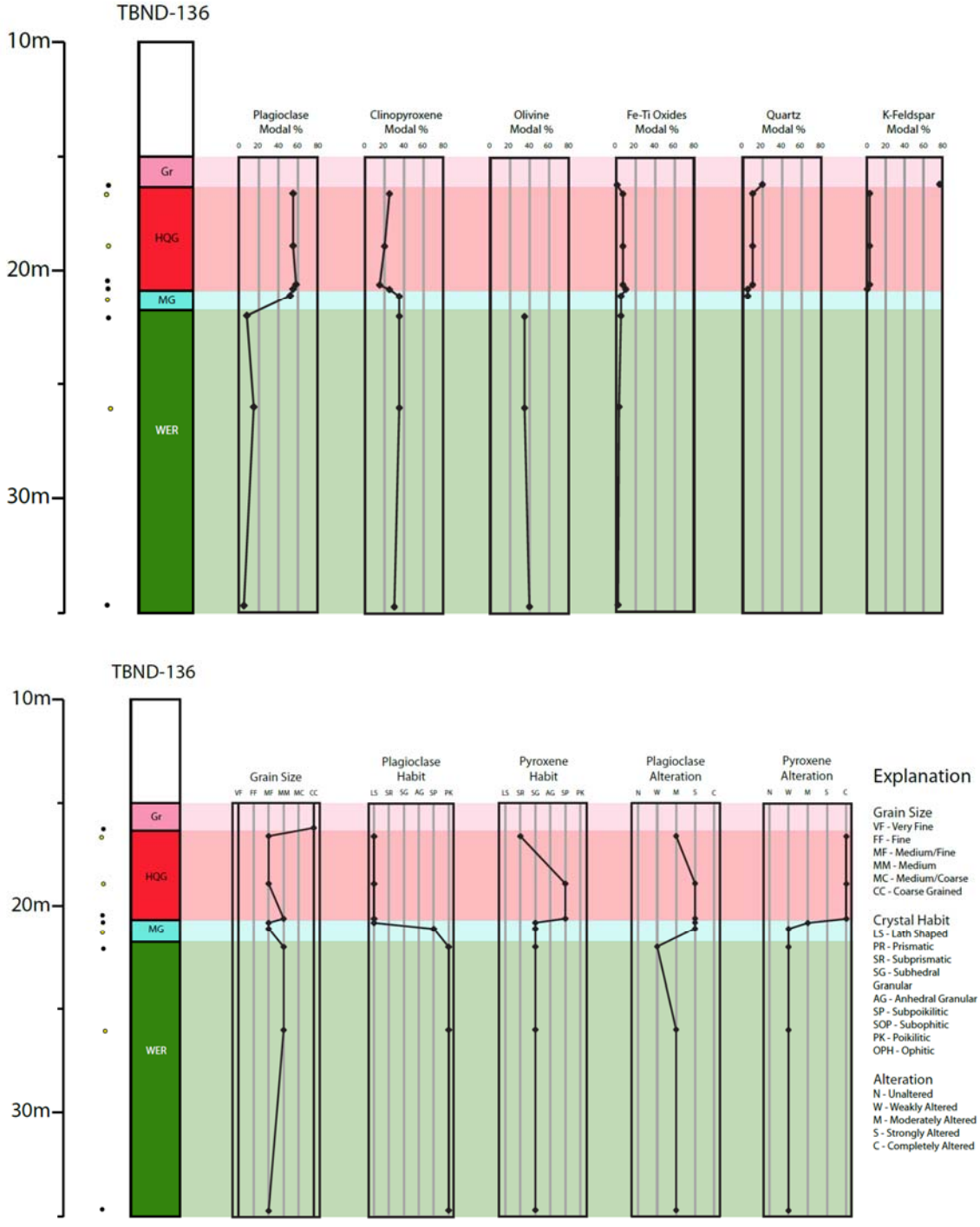
TBND-136
10m
20m
30m
Gr
HQG
MG
WER
Plagioclase Modal %
Clinopyroxene Modal %
Olivine Modal %
Fe-Ti Oxides Modal %
Quartz Modal %
K-Feldspar Modal %
0 20 40 60 80
TBND-136
Grain Size
VF FF MF MM MC CC
Plagioclase Habit
LS SR SG AG SP PK
Pyroxene Habit
LS SR SG AG SP PK
Plagioclase Alteration
N W M S C
Pyroxene Alteration
N W M S C
Explanation
Grain Size
VF - Very Fine
FF - Fine
MF - Medium/Fine
MM - Medium
MC - Medium/Coarse
CC - Coarse Grained
Crystal Habit
LS - Lath Shaped
PR - Prismatic
SR - Subprismatic
SG - Subhedral Granular
AG - Anhedral Granular
SP - Subpoikilitic
SOP - Subophitic
PK - Poikilitic
OPH - Ophitic
Alteration
N - Unaltered
W - Weakly Altered
M - Moderately Altered
S - Strongly Altered
C - Completely Altered

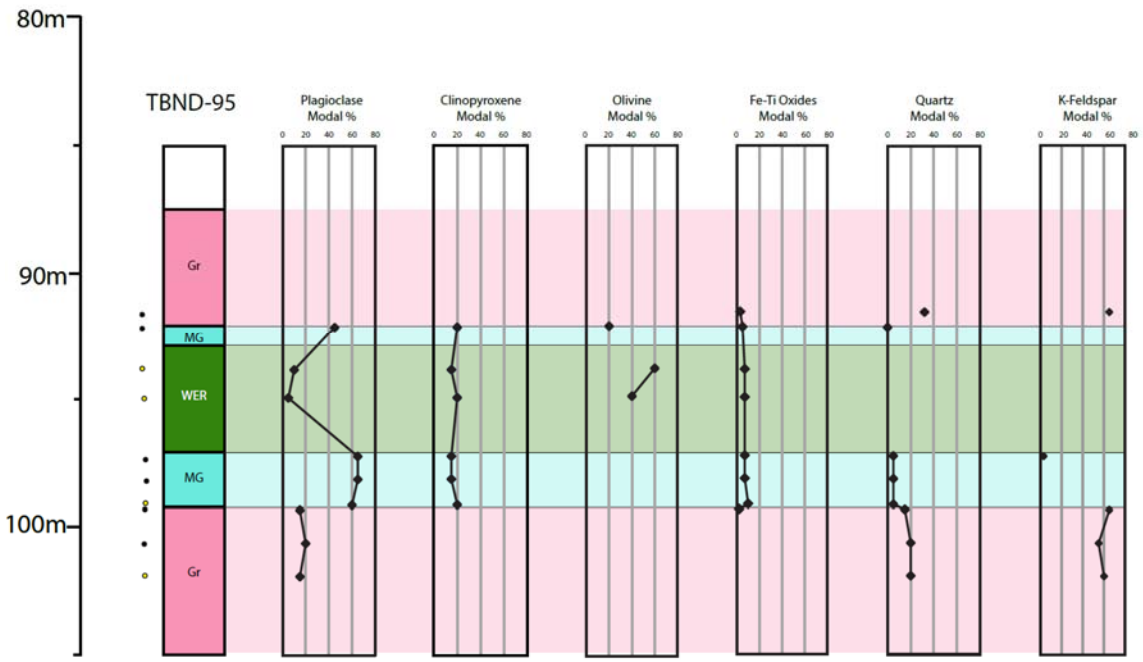
80m
90m
100m
TBND-95
Plagioclase Modal %
Clinopyroxene Modal %
Olivine Modal %
Fe-Ti Oxides Modal %
Quartz Modal %
K-Feldspar Modal %
0 20 40 60 80
Gr
MG
WER
MG
Gr

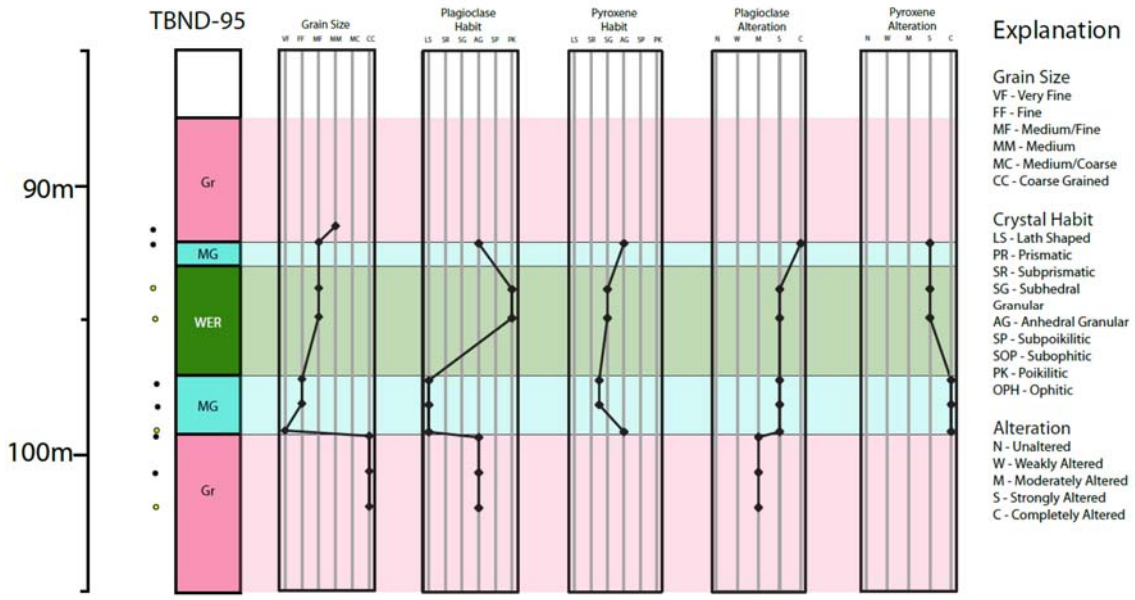
90m
100m
TBND-95
Grain Size
VF FF MF MM MC CC
Plagioclase Habit
Pyroxene Habit
LS SR SG AG SP PK
Plagioclase Alteration
Pyroxene Alteration
N W M S C
Gr
MG
WER
MG
Gr
Explanation
Grain Size
VF - Very Fine
FF - Fine
MF - Medium/Fine
MM - Medium
MC - Medium/Coarse
CC - Coarse Grained
Crystal Habit
LS - Lath Shaped
PR - Prismatic
SR - Subprismatic
SG - Subhedral Granular
AG - Anhedral Granular
SP - Subpoikilitic
SOP - Subophitic
PK - Poikilitic
OPH - Ophitic
Alteration
N - Unaltered
W - Weakly Altered
M - Moderately Altered
S - Strongly Altered
C - Completely Altered

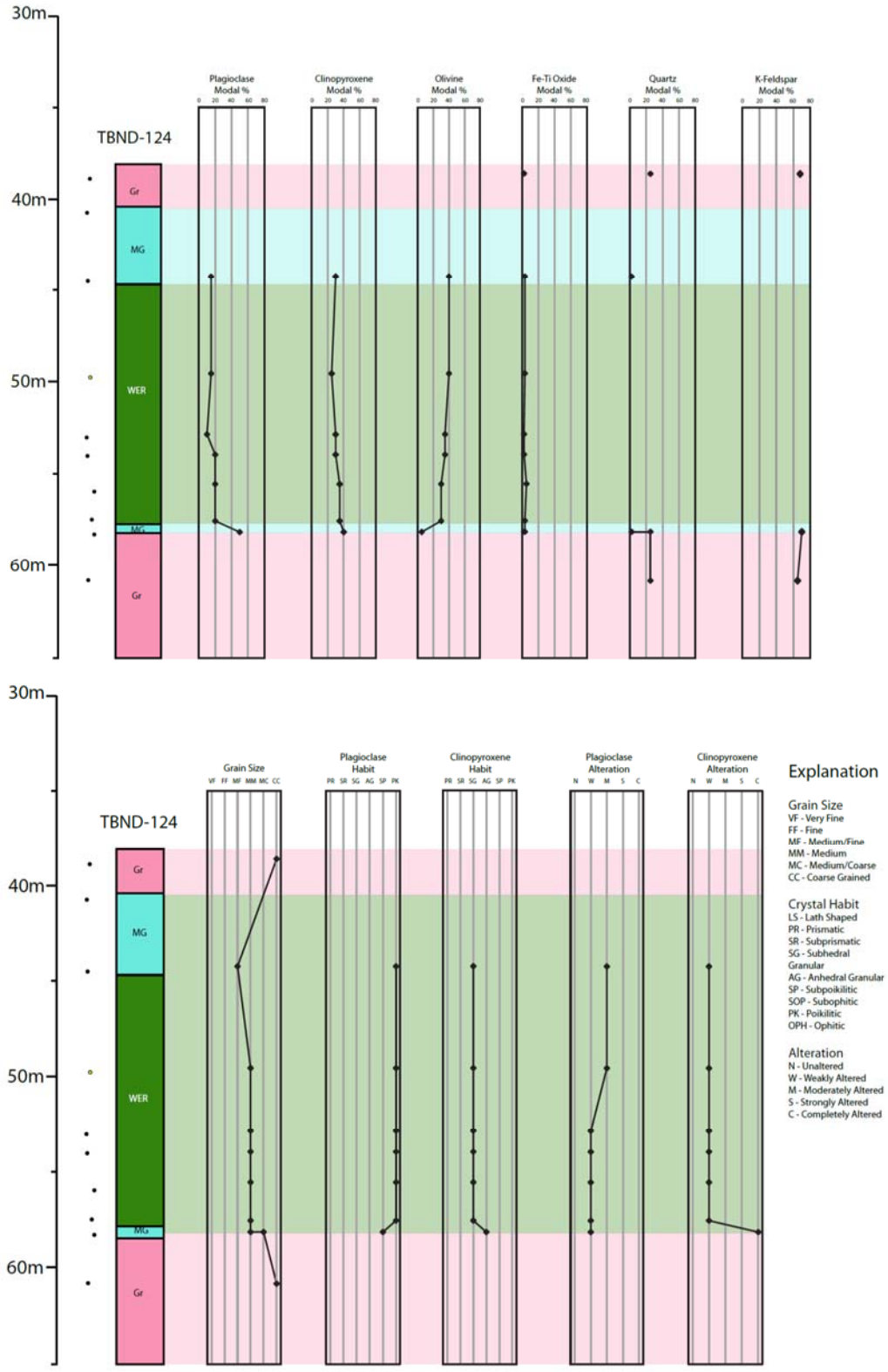
30m
40m
50m
60m
TBND-124
Gr
MG
WER
MG
Gr
Plagioclase Modal %
Clinopyroxene Modal %
Olivine Modal %
Fe-Ti Oxide Modal %
Quartz Modal %
K-Feldspar Modal %
0 20 40 60 80
Grain Size
VF FF MF MM MC CC
Plagioclase Habit
PR SR SG AG SP PK
Clinopyroxene Habit
PR SR SG AG SP PK
Plagioclase Alteration
N W M S C
Clinopyroxene Alteration
N W M S C
Explanation
Grain Size
VF - Very Fine
FF - Fine
MF - Medium/Fine
MM - Medium
MC - Medium/Coarse
CC - Coarse Grained
Crystal Habit
LS - Lath Shaped
PR - Prismatic
SR - Subprismatic
SG - Subhedral Granular
AG - Anhedral Granular
SP - Subpoikilitic
SOP - Subophitic
PK - Poikilitic
OPH - Ophitic
Alteration
N - Unaltered
W - Weakly Altered
M - Moderately Altered
S - Strongly Altered
C - Completely Altered

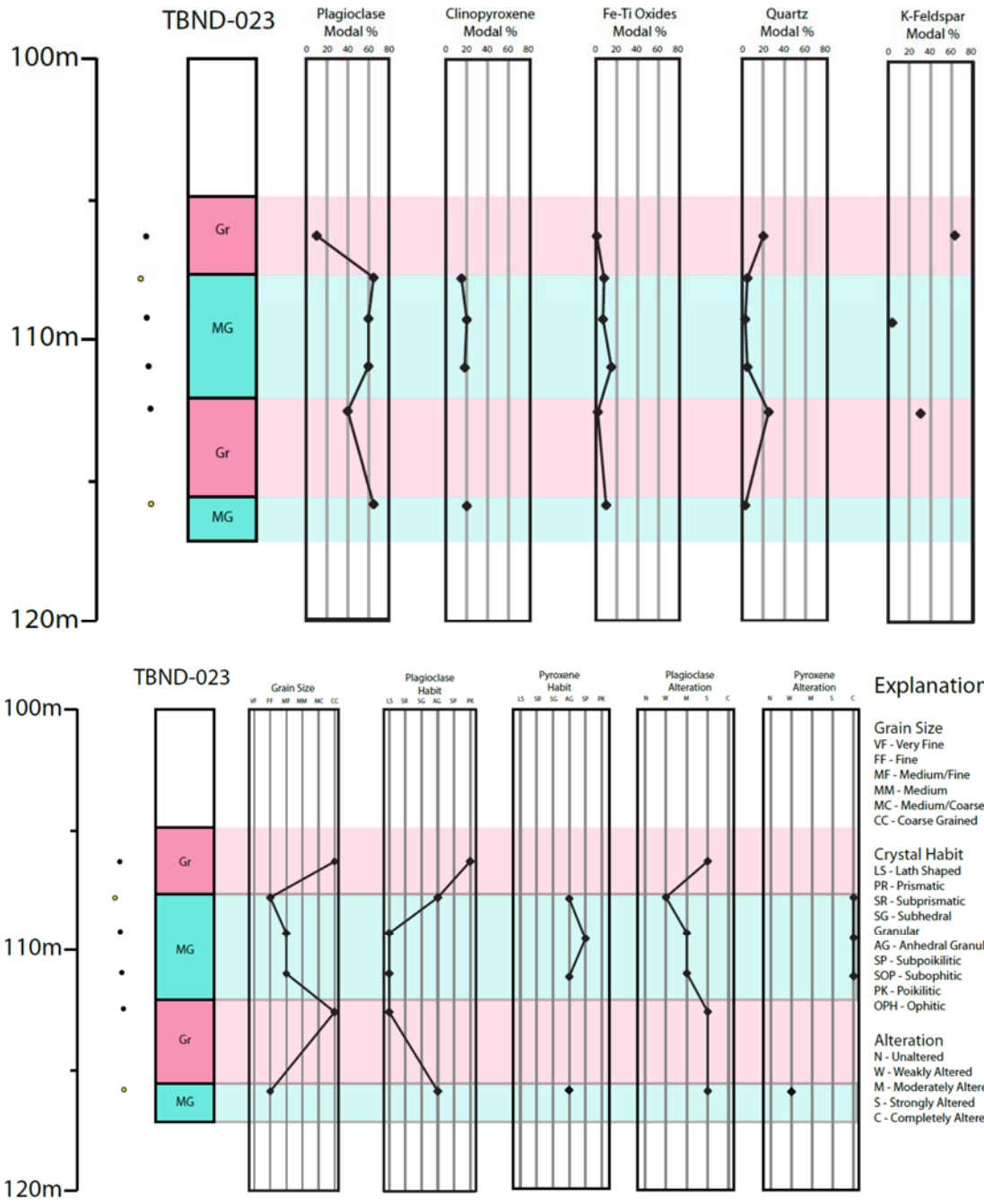
TBND-023
Plagioclase Modal %
Clinopyroxene Modal %
Fe-Ti Oxides Modal %
Quartz Modal %
K-Feldspar Modal %
0 20 40 60 80
100m
110m
120m
Gr
MG
Gr
MG
TBND-023
Grain Size
VF FF MF MM MC CC
Plagioclase Habit
LS SR SG AG SP PK
Pyroxene Habit
Plagioclase Alteration
N W M S C
Pyroxene Alteration
Explanation
Grain Size
VF - Very Fine
FF - Fine
MF - Medium/Fine
MM - Medium
MC - Medium/Coarse
CC - Coarse Grained
Crystal Habit
LS - Lath Shaped
PR - Prismatic
SR - Subprismatic
SG - Subhedral Granular
AG - Anhedral Granular
SP - Subpoikilitic
SOP - Subophitic
PK - Poikilitic
OPH - Ophitic
Alteration
N - Unaltered
W - Weakly Altered
M - Moderately Altered
S - Strongly Altered
C - Completely Altered

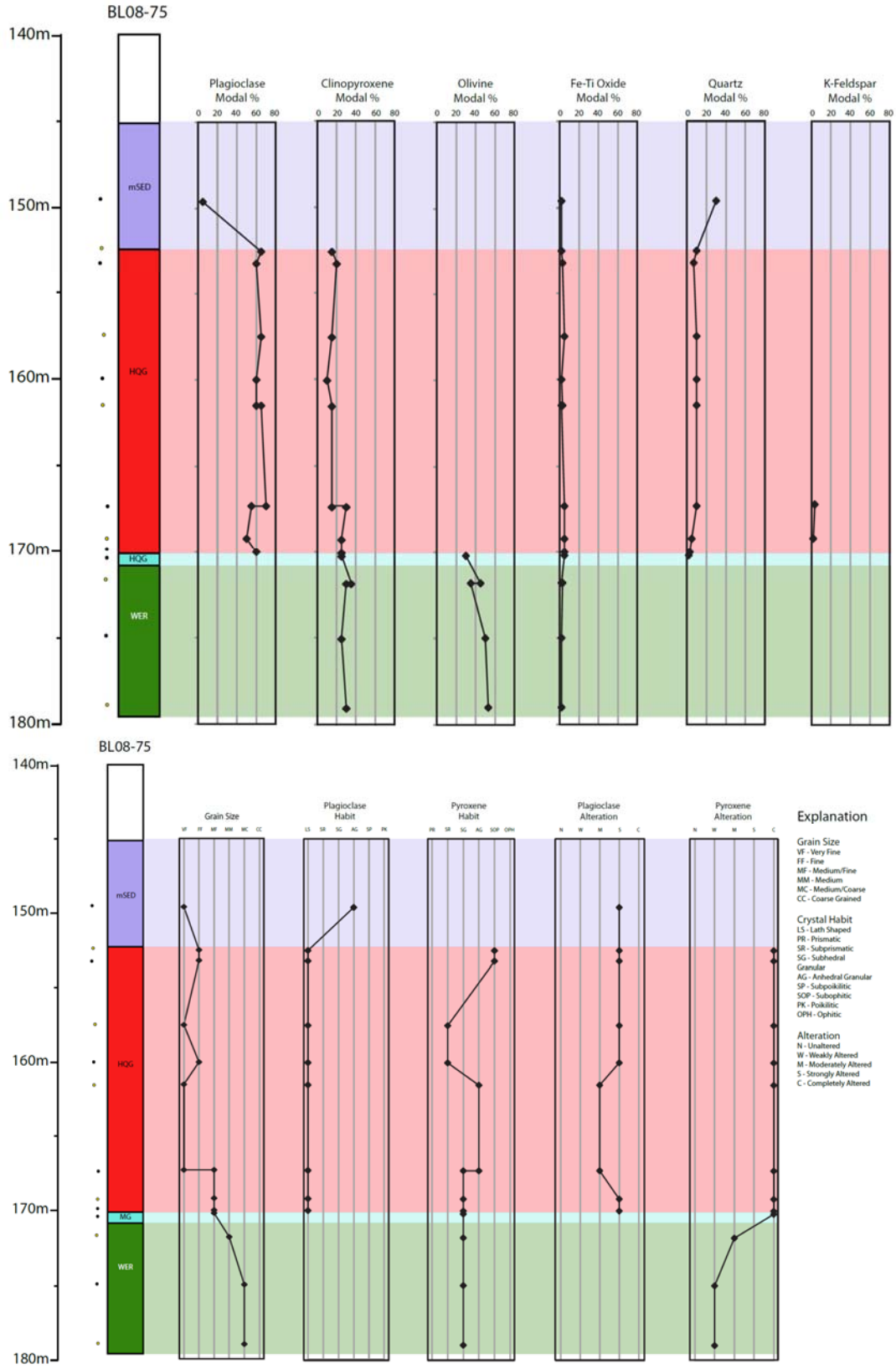
BL08-75
140m
150m
160m
170m
180m
mSED
HQG
HQG
WER
Plagioclase Modal %
Clinopyroxene Modal %
Olivine Modal %
Fe-Ti Oxide Modal %
Quartz Modal %
K-Feldspar Modal %
0 20 40 60 80
BL08-75
140m
150m
160m
170m
180m
mSED
HQG
MG
WER
Grain Size
Plagioclase Habit
Pyroxene Habit
Plagioclase Alteration
Pyroxene Alteration
Explanation
Grain Size
VF - Very Fine
FF - Fine
MF - Medium/Fine
MM - Medium
MC - Medium/Coarse
CC - Coarse Grained
Crystal Habit
LS - Lath Shaped
PR - Prismatic
SR - Subprismatic
SG - Subhedral Granular
AG - Anhedral Granular
SP - Subpoikilitic
SOP - Subophitic
PK - Poikilitic
OPH - Ophitic
Alteration
N - Unaltered
W - Weakly Altered
M - Moderately Altered
S - Strongly Altered
C - Completely Altered

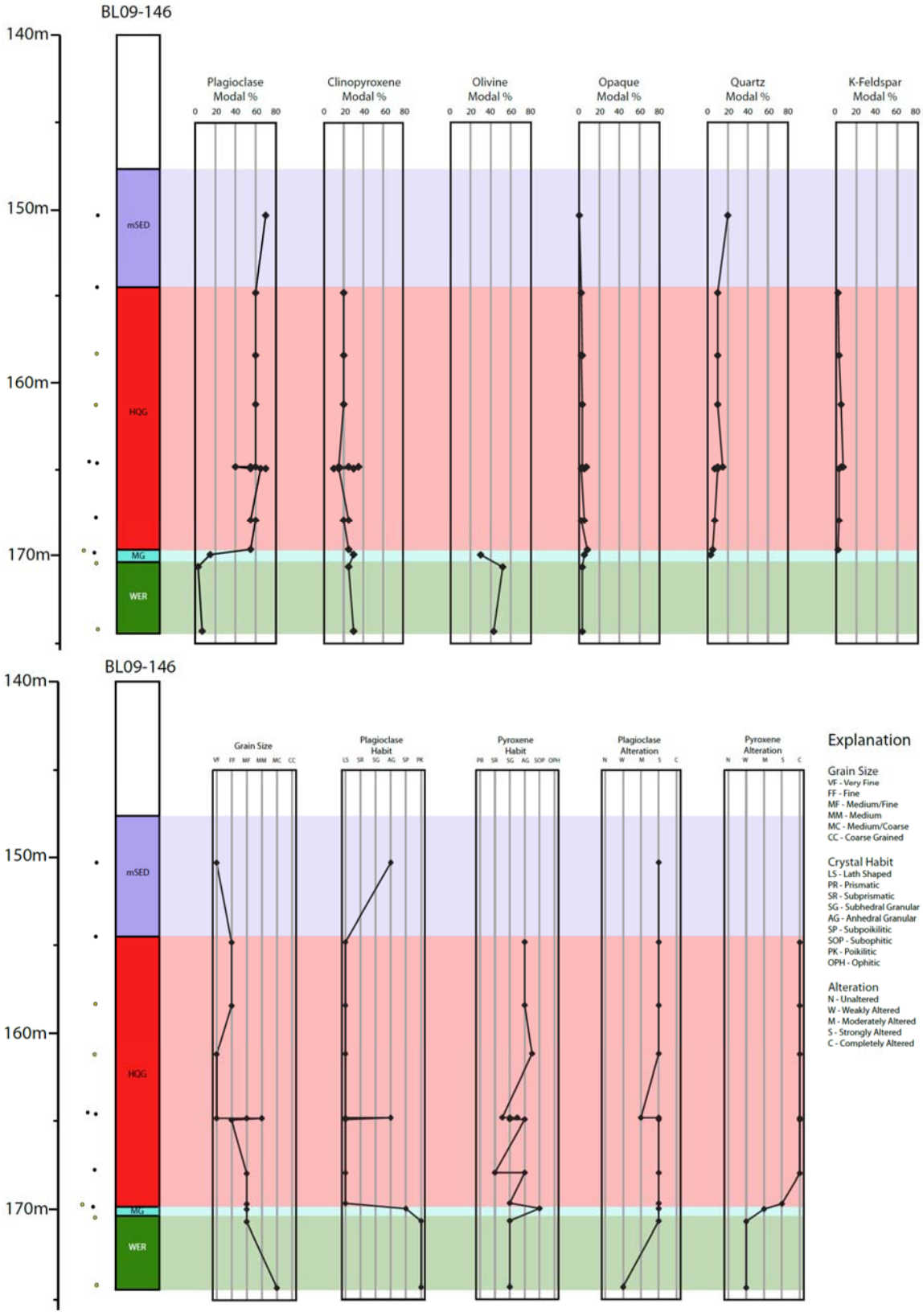
BL09-146
140m
150m
160m
170m
mSED
HQG
MG
WER
Plagioclase Modal %
Clinopyroxene Modal %
Olivine Modal %
Opaque Modal %
Quartz Modal %
K-Feldspar Modal %
0 20 40 60 80
BL09-146
Grain Size
VF FF MF MM MC CC
Plagioclase Habit
LS SR SG AG SP PK
Pyroxene Habit
PRI SR SG AG SOP OPH
Plagioclase Alteration
N W M S C
Pyroxene Alteration
N W M S C
Explanation
Grain Size
VF - Very Fine
FF - Fine
MF - Medium/Fine
MM - Medium
MC - Medium/Coarse
CC - Coarse Grained
Crystal Habit
LS - Lath Shaped
PR - Prismatic
SR - Subprismatic
SG - Subhedral Granular
AG - Anhedral Granular
SP - Subpoikilitic
SOP - Subophitic
PK - Poikilitic
OPH - Ophitic
Alteration
N - Unaltered
W - Weakly Altered
M - Moderately Altered
S - Strongly Altered
C - Completely Altered

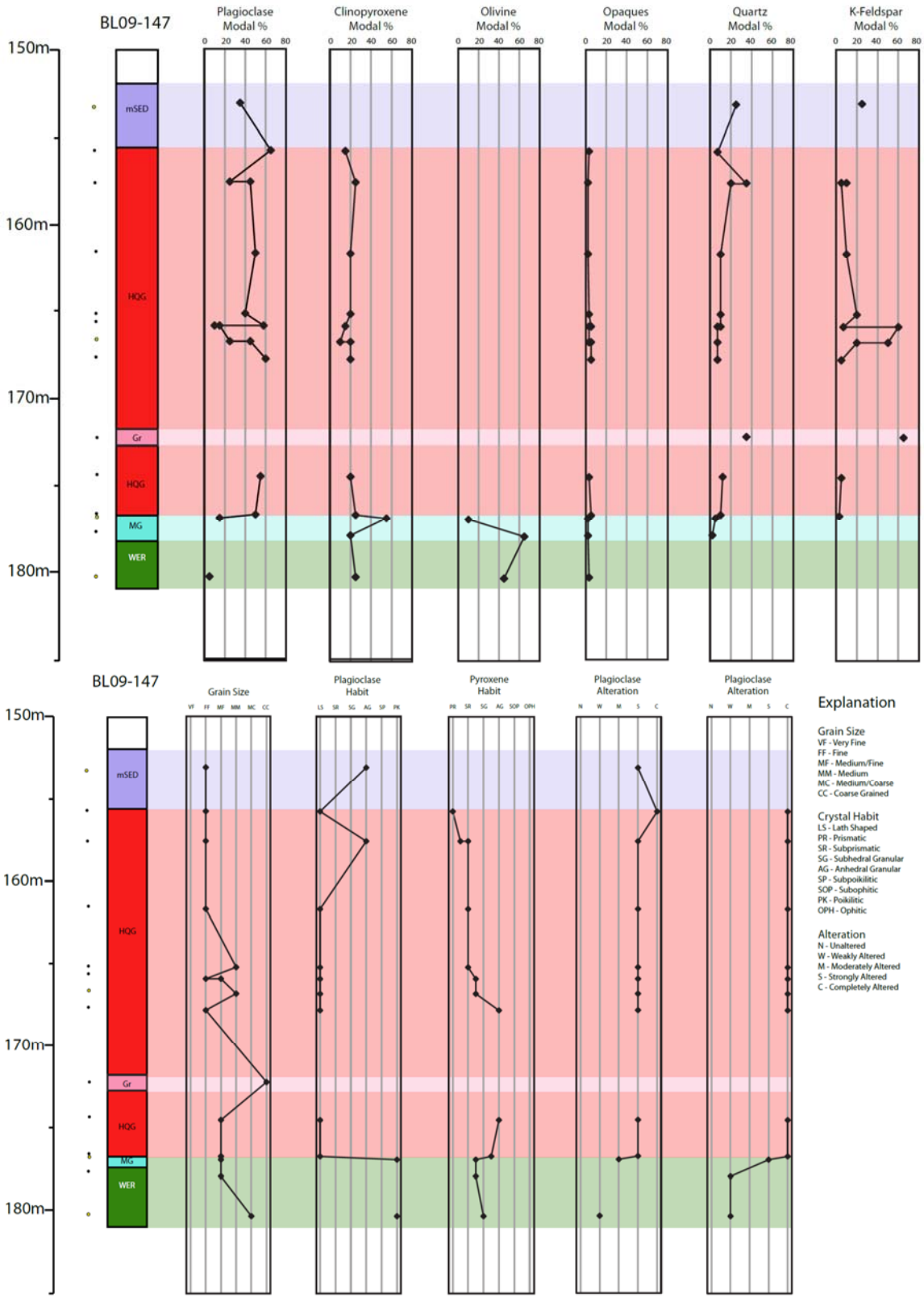
BL09-147
Plagioclase Modal %
Clinopyroxene Modal %
Olivine Modal %
Opaques Modal %
Quartz Modal %
K-Feldspar Modal %
0 20 40 60 80
150m
160m
170m
180m
mSED
HQG
Gr
HQG
MG
WER
BL09-147
Grain Size
VF FF MF MM MC CC
Plagioclase Habit
LS SR SG AG SP PK
Pyroxene Habit
PR SR SG AG SOP OPH
Plagioclase Alteration
N W M S C
Plagioclase Alteration
N W M S C
Explanation
Grain Size
VF - Very Fine
FF - Fine
MF - Medium/Fine
MM - Medium
MC - Medium/Coarse
CC - Coarse Grained
Crystal Habit
LS - Lath Shaped
PR - Prismatic
SR - Subprismatic
SG - Subhedral Granular
AG - Anhedral Granular
SP - Subpoikilitic
SOP - Subophitic
PK - Poikilitic
OPH - Ophitic
Alteration
N - Unaltered
W - Weakly Altered
M - Moderately Altered
S - Strongly Altered
C - Completely Altered

Appendix C

Mineral Chemistry

Appendix C - Mineral Chemistry

Sample: TBND-60 21.65
Pyroxene

	Raw										Normalized												
Spectrum	SiO2	TiO2	Al2O3	FeO	MnO	MgO	CaO	Na2O	Cr2O3	Total	SiO2	TiO2	Al2O3	FeO	MnO	MgO	CaO	Na2O	Cr2O3	Total	En	Fs	Wo	En'
Spectrum 1	64.41005	1.099748	2.876155	9.798889		18.81914	23.24504	0.4749773		120.7	53.4	0.9	2.4	8.1	0.0	15.6	19.3	0.4	0.0	100.0	45.9	13.4	40.7	77.4
Spectrum 2	63.41842	1.334337	3.275561	9.996177		18.43774	23.01817	0.4021957		119.9	52.9	1.1	2.7	8.3	0.0	15.4	19.2	0.3	0.0	100.0	45.4	13.8	40.8	76.7
Spectrum 3	64.20665	1.296166	3.07479	9.776808		18.56154	23.18016	0.4232914		120.5	53.3	1.1	2.6	8.1	0.0	15.4	19.2	0.4	0.0	100.0	45.6	13.5	40.9	77.2
Spectrum 4	63.6368	1.489063	3.714436	10.62073		18.42553	22.29659	0.5006548		120.7	52.7	1.2	3.1	8.8	0.0	15.3	18.5	0.4	0.0	100.0	45.6	14.7	39.7	75.6
Spectrum 5	64.31644	1.231934	3.022441	10.00446		18.57494	23.4034	0.3780826		120.9	53.2	1.0	2.5	8.3	0.0	15.4	19.4	0.3	0.0	100.0	45.3	13.7	41.0	76.8
Spectrum 6	64.98985	1.303355	3.119874	9.848219		18.65483	23.1215	0.3870593		121.4	53.5	1.1	2.6	8.1	0.0	15.4	19.0	0.3	0.0	100.0	45.7	13.5	40.7	77.1
Spectrum 7	64.55695	1.348256	3.028162	9.952847		18.70708	23.38698	0.3972805		121.4	53.2	1.1	2.5	8.2	0.0	15.4	19.3	0.3	0.0	100.0	45.5	13.6	40.9	77.0
Spectrum 8	65.14875	1.257693	2.807804	9.868841		18.841	23.14314	0.4327756		121.5	53.6	1.0	2.3	8.1	0.0	15.5	19.0	0.4	0.0	100.0	45.9	13.5	40.6	77.3
Spectrum 9	63.97073	1.519297	3.474758	10.28863		18.41201	23.0516	0.4428843		121.2	52.8	1.3	2.9	8.5	0.0	15.2	19.0	0.4	0.0	100.0	45.2	14.2	40.7	76.1
Spectrum 10	66.20858	0.9660108	1.892046	9.892341		19.64556	22.63692	0.3977995		121.6	54.4	0.8	1.6	8.1	0.0	16.2	18.6	0.3	0.0	100.0	47.4	13.4	39.2	78.0
																				Average	45.7	13.7	40.5	76.9

Sample: TBND-60 23.0
Pyroxene

	Raw										Normalized												
Spectrum	SiO2	TiO2	Al2O3	FeO	MnO	MgO	CaO	Na2O	Cr2O3	Total	SiO2	TiO2	Al2O3	FeO	MnO	MgO	CaO	Na2O	Cr2O3	Total	En	Fs	Wo	En'
Spectrum 1	65.43717	1.172366	2.778258	7.940991		20.29354	23.53144	0.4119978		121.6	53.8	1.0	2.3	6.5	0.0	16.7	19.4	0.3	0.0	100.0	48.7	10.7	40.6	82.0
Spectrum 2	66.33902	1.043371	2.649461	7.660128		20.37447	23.40607	0.4390192	0.6696601	122.6	54.1	0.9	2.2	6.2	0.0	16.6	19.1	0.4	0.5	100.0	49.1	10.4	40.5	82.6
Spectrum 3	66.60272	0.8510194	2.01432	7.144014		20.54102	23.82336	0.3968575	0.8811345	122.3	54.5	0.7	1.6	5.8	0.0	16.8	19.5	0.3	0.7	100.0	49.3	9.6	41.1	83.7
Spectrum 4	67.61057	0.7108688	1.5732	7.398875		21.71529	22.41732	0.3747217	0.5433226	122.3	55.3	0.6	1.3	6.0	0.0	17.7	18.3	0.3	0.4	100.0	51.7	9.9	38.4	83.9
Spectrum 5	66.2766	0.9394906	2.178661	7.349921		21.07651	22.42005	0.5171723	0.8626866	121.6	54.5	0.8	1.8	6.0	0.0	17.3	18.4	0.4	0.7	100.0	51.0	10.0	39.0	83.6
Spectrum 6	66.4449	0.9538142	2.224082	7.738698		21.26002	22.61707	0.3566126	0.6813308	122.3	54.3	0.8	1.8	6.3	0.0	17.4	18.5	0.3	0.6	100.0	50.8	10.4	38.8	83.0
Spectrum 7	66.51988	1.053446	2.464568	7.52516		20.69692	23.30436	0.4123556		122.0	54.5	0.9	2.0	6.2	0.0	17.0	19.1	0.3	0.0	100.0	49.7	10.1	40.2	83.1
Spectrum 8	66.99763	0.9404126	2.245099	6.633511		20.69316	23.75193	0.4423061	0.988304	122.7	54.6	0.8	1.8	5.4	0.0	16.9	19.4	0.4	0.8	100.0	49.9	9.0	41.2	84.8
Spectrum 9	66.66008	0.7668222	1.961202	7.109925		21.24824	23.20644	0.3863704	0.9831359	122.3	54.5	0.6	1.6	5.8	0.0	17.4	19.0	0.3	0.8	100.0	50.7	9.5	39.8	84.2
Spectrum 10	65.82893	1.140659	2.820214	7.891963		20.53057	23.22712	0.3705419	0.4738631	122.3	53.8	0.9	2.3	6.5	0.0	16.8	19.0	0.3	0.4	100.0	49.3	10.6	40.1	82.3
																				Average	50.0	10.0	40.0	83.3

Sample: TBND-60 32.9
Pyroxene

	Raw										Normalized												
Spectrum	SiO2	TiO2	Al2O3	FeO	MnO	MgO	CaO	Na2O	Cr2O3	Total	SiO2	TiO2	Al2O3	FeO	MnO	MgO	CaO	Na2O	Cr2O3	Total	En	Fs	Wo	En'
Spectrum 1	67.08267	0.887184	1.763716	6.169837		20.8225	24.45736		0.6301709	121.8	55.1	0.7	1.4	5.1	0.0	17.1	20.1	0.0	0.5	100.0	49.7	8.3	42.0	85.7
Spectrum 2	66.48416	0.8743408	1.868912	6.006163		20.55395	24.44523	0.3973799	0.9152605	121.5	54.7	0.7	1.5	4.9	0.0	16.9	20.1	0.3	0.8	100.0	49.5	8.1	42.4	85.9
Spectrum 3	67.54517	0.7307896	1.333707	5.752501		21.44563	23.98814	0.3916888	0.7586849	121.9	55.4	0.6	1.1	4.7	0.0	17.6	19.7	0.3	0.6	100.0	51.2	7.7	41.1	86.9
Spectrum 4	65.7746		2.22814	5.687743		21.15545	24.96674			119.8	54.9	0.0	1.9	4.7	0.0	17.7	20.8	0.0	0.0	100.0	50.0	7.5	42.4	86.9
Spectrum 5	66.51902	1.007202	2.111826	6.175715		20.47131	24.48631	0.3915051	0.7914526	122.0	54.5	0.8	1.7	5.1	0.0	16.8	20.1	0.3	0.6	100.0	49.3	8.3	42.4	85.5
Spectrum 6	67.75307	0.6541692	1.270866	6.02467		21.61115	23.95799	0.3964313	0.6395321	122.3	55.4	0.5	1.0	4.9	0.0	17.7	19.6	0.3	0.5	100.0	51.2	8.0	40.8	86.5
Spectrum 7	66.22102	0.9608214	2.130736	6.429508		20.7036	24.7457	0.4184332	0.8613638	122.5	54.1	0.8	1.7	5.2	0.0	16.9	20.2	0.3	0.7	100.0	49.2	8.6	42.3	85.2
Spectrum 8	66.64606	0.8374249	2.023356	6.194823		20.74736	24.33776	0.3941466	0.926607	122.1	54.6	0.7	1.7	5.1	0.0	17.0	19.9	0.3	0.8	100.0	49.7	8.3	41.9	85.6
Spectrum 9	63.25146	1.975118	4.467395	7.17713		18.84576	24.77056	0.5784473	0.4787275	121.5	52.0	1.6	3.7	5.9	0.0	15.5	20.4	0.5	0.4	100.0	46.3	9.9	43.8	82.4
Spectrum 10	67.08048	0.7945962	1.586618	5.737927		20.81227	24.43646	0.3698929	0.7934531	121.6	55.2	0.7	1.3	4.7	0.0	17.1	20.1	0.3	0.7	100.0	50.0	7.7	42.2	86.6
																				Average	49.6	8.3	42.1	85.7

Sample: TBND-125 24.4b
Pyroxene

	Raw											Normalized													
Spectrum	SiO2	TiO2	Al2O3	FeO	MnO	MgO	CaO	K2O	Na2O	Cr2O3	Total	SiO2	TiO2	Al2O3	FeO	MnO	MgO	CaO	Na2O	Cr2O3	Total	En	Fs	Wo	En'
Spectrum 1	60.58449	1.120184	3.428581	13.90853		17.91983	11.38791	0.8399558	2.747743		111.9	54.1	1.0	3.1	12.4	0.0	16.0	10.2	0.8	2.5	100.0	52.8	23.0	24.1	69.7
Spectrum 2	60.32698	0.9753041	3.475652	14.12901		18.10649	11.15604	0.7376775	2.686736		111.6	54.1	0.9	3.1	12.7	0.0	16.2	10.0	0.7	2.4	100.0	53.2	23.3	23.6	69.5
Spectrum 3	61.83175	0.7898628	2.675416	13.10661	0.4447846	18.80077	10.57132	0.7003698	2.526753		111.4	55.5	0.7	2.4	11.8	0.4	16.9	9.5	0.6	2.3	100.0	55.7	21.8	22.5	71.9
Spectrum 4	57.9788	1.247906	5.04756	15.02807	0.3870129	17.04509	11.45214	0.8826326	2.830773		111.9	51.8	1.1	4.5	13.4	0.3	15.2	10.2	0.8	2.5	100.0	50.6	25.0	24.4	66.9
Spectrum 5	60.02808	1.009896	3.528859	14.22662	0.5100812	17.55811	10.93898	0.6041827	2.79744		111.2	54.0	0.9	3.2	12.8	0.5	15.8	9.8	0.5	2.5	100.0	52.6	23.9	23.5	68.7
Spectrum 6	62.82018	0.9342962	3.21321	14.22268		19.10683	10.55028	0.7026419	2.529288		114.1	55.1	0.8	2.8	12.5	0.0	16.7	9.2	0.6	2.2	100.0	55.1	23.0	21.9	70.5
																						Average	53.3	23.3	23.3	69.5

Sample: TBND-125 25.4

Pyroxene

	Raw											Normalized												
Spectrum	SiO2	TiO2	Al2O3	FeO	MnO	MgO	CaO	K2O	Na2O	Cr2O3	Total	SiO2	TiO2	Al2O3	FeO	MnO	MgO	CaO	Na2O	Cr2O3	Total	En	Fs	Wo	En'
Spectrum 1	61.34324	0.9356214	2.090743	7.428817		19.34075	21.31039			0.5243686	113.0	54.3	0.8	1.9	6.6	0.5	17.1	18.9	0.0	0.5	100.0	49.8	10.7	39.5	82.3
Spectrum 2	61.38226	0.7673016	1.891062	7.159019		19.54172	21.29751		0.3694303	0.528468	112.9	54.4	0.7	1.7	6.3	0.5	17.3	18.9	0.3	0.5	100.0	50.3	10.3	39.4	82.9
Spectrum 3	61.43436	0.8118567	1.8024	7.178462		19.89266	20.51203		0.371075	0.6529688	112.7	54.5	0.7	1.6	6.4	0.6	17.7	18.2	0.3	0.6	100.0	51.4	10.4	38.1	83.2
Spectrum 4	61.20369	0.8948913	2.368182	7.442613		19.0395	21.47472		0.4128573	0.4861993	113.3	54.0	0.8	2.1	6.6	0.4	16.8	19.0	0.4	0.4	100.0	49.3	10.8	39.9	82.0
Spectrum 5	60.9341	0.8077852	1.837488	7.125542		19.02173	21.20145		0.3237125	0.3779052	111.6	54.6	0.7	1.6	6.4	0.3	17.0	19.0	0.3	0.3	100.0	49.7	10.5	39.8	82.6
Spectrum 6	60.51249	0.8569776	2.016009	7.196435		19.09845	20.83797		0.3621192	0.4022555	111.3	54.4	0.8	1.8	6.5	0.4	17.2	18.7	0.3	0.4	100.0	50.1	10.6	39.3	82.5
Spectrum 7	60.58492	0.8805465	1.994344	7.270736		19.10459	20.84618		0.3634441	0.5323724	111.6	54.3	0.8	1.8	6.5	0.5	17.1	18.7	0.3	0.5	100.0	50.0	10.7	39.3	82.4
Spectrum 8	59.66917	0.9203979	2.114769	6.676667		18.29421	21.69737		0.3284897	0.5351265	110.2	54.1	0.8	1.9	6.1	0.5	16.6	19.7	0.3	0.5	100.0	48.6	10.0	41.4	83.0
Spectrum 9	60.20645	0.9192182	1.891298	6.828001		18.70175	21.15405		0.3470048	0.505188	110.6	54.5	0.8	1.7	6.2	0.5	16.9	19.1	0.3	0.5	100.0	49.6	10.2	40.3	83.0
Spectrum 10	60.13647	0.9331135	2.052216	7.107099		18.79266	20.79222		0.3682993	0.6152124	110.8	54.3	0.8	1.9	6.4	0.6	17.0	18.8	0.3	0.6	100.0	49.8	10.6	39.6	82.5
																					Average	49.9	10.5	39.7	82.6

Sample: TBND-125 25.8

Pyroxene

	Raw											Normalized												
Spectrum	SiO2	TiO2	Al2O3	FeO	MnO	MgO	CaO	K2O	Na2O	Cr2O3	Total	SiO2	TiO2	Al2O3	FeO	MnO	MgO	CaO	Na2O	Cr2O3	Total	En	Fs	Wo	En'
Spectrum 1	60.22201	0.7969127	1.804695	6.509778		19.04807	21.10787		0.3437863	0.6766087	110.5	54.5	0.7	1.6	5.9	0.0	17.2	19.1	0.3	0.6	100.0	50.3	9.6	40.1	83.9
Spectrum 2	59.82853	0.7069975	1.986414	6.472664		19.16852	20.81141		0.3657857	0.7833617	110.1	54.3	0.6	1.8	5.9	0.0	17.4	18.9	0.3	0.7	100.0	50.8	9.6	39.6	84.1
Spectrum 3	59.04497	1.08402	2.286302	7.126202		18.06975	21.15371		0.4074403	0.4273161	109.6	53.9	1.0	2.1	6.5	0.0	16.5	19.3	0.4	0.4	100.0	48.5	10.7	40.8	81.9
Spectrum 4	59.74529	0.716374	1.924717	6.572847		18.87397	21.03039		0.395406	0.7605311	110.0	54.3	0.7	1.7	6.0	0.0	17.2	19.1	0.4	0.7	100.0	50.1	9.8	40.1	83.7
Spectrum 5	59.34796	0.7965894	1.905921	6.705472		18.8134	20.8629		0.3220575	0.5828888	109.3	54.3	0.7	1.7	6.1	0.0	17.2	19.1	0.3	0.5	100.0	50.1	10.0	39.9	83.3
Spectrum 6	59.25472	0.8857536	2.244859	6.905141		18.4369	20.89958		0.3588558	0.523403	109.5	54.1	0.8	2.0	6.3	0.0	16.8	19.1	0.3	0.5	100.0	49.4	10.4	40.2	82.6
Spectrum 7	59.06393	1.045299	2.569224	7.243887		18.14146	20.94711				109.0	54.2	1.0	2.4	6.6	0.0	16.6	19.2	0.0	0.0	100.0	48.7	10.9	40.4	81.7
Spectrum 8	58.75068	1.040893	2.267888	7.151771		18.50508	20.38547		0.3500821		108.5	54.2	1.0	2.1	6.6	0.0	17.1	18.8	0.3	0.0	100.0	49.8	10.8	39.4	82.2
Spectrum 9	59.03699	1.105662	2.156307	7.199824		18.68947	20.07385		0.3726556	0.6648535	109.3	54.0	1.0	2.0	6.6	0.0	17.1	18.4	0.3	0.6	100.0	50.3	10.9	38.8	82.2
Spectrum 10	58.8825	0.9841363	2.185068	6.901945		18.96391	20.13349		0.3613597	0.5431821	109.0	54.0	0.9	2.0	6.3	0.0	17.4	18.5	0.3	0.5	100.0	50.8	10.4	38.8	83.0
																					Average	49.9	10.3	39.8	82.9

Sample: TBND-125 29.8

Pyroxene

	Raw											Normalized												
Spectrum	SiO2	TiO2	Al2O3	FeO	MnO	MgO	CaO	K2O	Na2O	Cr2O3	Total	SiO2	TiO2	Al2O3	FeO	MnO	MgO	CaO	Na2O	Cr2O3	Total	En	Fs	Wo	En'
Spectrum 1	58.71956	1.129239	2.689906	6.277414		17.61713	21.84096		0.4357108	0.6412677	109.4	53.7	1.0	2.5	5.7	0.0	16.1	20.0	0.4	0.6	100.0	47.8	9.6	42.6	83.3
Spectrum 2	60.67896	0.6182919	1.233637	5.348595		19.08009	22.00046		0.4019961	0.6799185	110.0	55.1	0.6	1.1	4.9	0.0	17.3	20.0	0.4	0.6	100.0	50.3	7.9	41.7	86.4
Spectrum 3	59.71254	0.715479	1.687184	5.358975		18.70536	22.15968		0.3879074	0.8620448	109.6	54.5	0.7	1.5	4.9	0.0	17.1	20.2	0.4	0.8	100.0	49.7	8.0	42.3	86.1
Spectrum 4	59.81191	0.8088264	1.73527	5.685888		18.61796	21.78951		0.4517688	0.8182848	109.7	54.5	0.7	1.6	5.2	0.0	17.0	19.9	0.4	0.7	100.0	49.7	8.5	41.8	85.4
Spectrum 5	59.90561	0.7265404	1.330356	5.507464		18.87494	21.71656		0.3567447	0.6344288	109.1	54.9	0.7	1.2	5.1	0.0	17.3	19.9	0.3	0.6	100.0	50.2	8.2	41.5	85.9
Spectrum 6	60.47301	0.6427769	1.309052	5.551487		18.96497	21.79183		0.3468929	0.6305181	109.7	55.1	0.6	1.2	5.1	0.0	17.3	19.9	0.3	0.6	100.0	50.2	8.3	41.5	85.9
Spectrum 7	59.18823	0.9670105	2.071333	5.766527		18.13612	22.20194		0.4250676	0.7436444	109.5	54.1	0.9	1.9	5.3	0.0	16.6	20.3	0.4	0.7	100.0	48.6	8.7	42.8	84.9
Spectrum 8	59.70131	0.8210499	1.467411	5.849788		18.59742	21.84882		0.3645212	0.5708278	109.2	54.7	0.8	1.3	5.4	0.0	17.0	20.0	0.3	0.5	100.0	49.5	8.7	41.8	85.0
Spectrum 9	59.77069	0.8318489	1.576168	5.574627		18.3832	21.85566		0.4043427	0.6051121	109.0	54.8	0.8	1.4	5.1	0.0	16.9	20.1	0.4	0.6	100.0	49.4	8.4	42.2	85.5
Spectrum 10	59.64781	0.7049147	1.743497	5.722463		18.81163	21.77423		0.3710898	0.904375	109.7	54.4	0.6	1.6	5.2	0.0	17.2	19.9	0.3	0.8	100.0	49.9	8.5	41.5	85.4
																					Average	49.5	8.5	42.0	85.4

Sample: BL08-78 191.0

Pyroxene

	Raw										Normalized													
Spectrum	SiO2	TiO2	Al2O3	FeO	MnO	MgO	CaO	Na2O	Cr2O3	Total	SiO2	TiO2	Al2O3	FeO	MnO	MgO	CaO	Na2O	Cr2O3	Total	En	Fs	Wo	En'
Spectrum 1	58.65398	1.230395	2.831545	8.438115		17.08611	21.51933	0.376351		110.1	53.3	1.1	2.6	7.7	0.0	15.5	19.5	0.3	0.0	100.0	45.8	12.7	41.5	78.3
Spectrum 2	59.48829	0.9973212	2.411777	8.927449		17.55039	20.48992	0.3520332		110.2	54.0	0.9	2.2	8.1	0.0	15.9	18.6	0.3	0.0	100.0	47.1	13.4	39.5	77.8
Spectrum 3	58.17429	1.120838	3.114101	9.979188		17.1111	20.09026	0.3607021		110.0	52.9	1.0	2.8	9.1	0.0	15.6	18.3	0.3	0.0	100.0	46.1	15.1	38.9	75.3
Spectrum 4	59.15536	1.045009	2.363123	8.237385		17.36704	21.35751	0.3811173		109.9	53.8	1.0	2.2	7.5	0.0	15.8	19.4	0.3	0.0	100.0	46.5	12.4	41.1	79.0
Spectrum 5	59.09064	1.145798	2.630082	8.59649		17.26721	21.44385	0.3586011		110.5	53.5	1.0	2.4	7.8	0.0	15.6	19.4	0.3	0.0	100.0	46.0	12.9	41.1	78.2
Spectrum 6	59.17275	0.9753671	2.202219	9.024881		17.35751	20.70711	0.3387735		109.8	53.9	0.9	2.0	8.2	0.0	15.8	18.9	0.3	0.0	100.0	46.5	13.6	39.9	77.4
Spectrum 7	58.29819	1.323416	2.870116	8.674272		16.79545	21.60894	0.3845564		110.0	53.0	1.2	2.6	7.9	0.0	15.3	19.7	0.3	0.0	100.0	45.1	13.1	41.8	77.5
Spectrum 8	58.44188	1.070135	2.893854	9.436567		17.18955	20.48505	0.3669504		109.9	53.2	1.0	2.6	8.6	0.0	15.6	18.6	0.3	0.0	100.0	46.2	14.2	39.6	76.4
Spectrum 9	57.94277	1.332901	2.865083	8.728057		16.80159	21.54813	0.3376991		109.6	52.9	1.2	2.6	8.0	0.0	15.3	19.7	0.3	0.0	100.0	45.2	13.2	41.7	77.4
Spectrum 10	57.6437	1.213733	2.848639	8.432802		17.05304	21.10892	0.3601431		108.7	53.0	1.1	2.6	7.8	0.0	15.7	19.4	0.3	0.0	100.0	46.1	12.8	41.1	78.3
																				Average	46.1	13.3	40.6	77.6

Appendix C - Mineral Chemistry

Sample: BL08-78 192.1b
Pyroxene

	Raw										Normalized												
Spectrum	SiO2	TiO2	Al2O3	FeO	MnO	MgO	CaO	Na2O	Cr2O3	Total	SiO2	TiO2	Al2O3	FeO	MnO	MgO	CaO	Na2O	Cr2O3	Total	En	Fs	Wo	En'
Spectrum 1	59.00828	0.9880978	2.392259	6.993919		17.68093	21.60796	0.3834006		109.1	54.1	0.9	2.2	6.4	0.0	16.2	19.8	0.4	0.0	100.0	47.6	10.6	41.8	81.8
Spectrum 2	58.87716	1.069508	2.473101	7.37106		17.58443	21.51863	0.3274212		109.2	53.9	1.0	2.3	6.7	0.0	16.1	19.7	0.3	0.0	100.0	47.3	11.1	41.6	81.0
Spectrum 3	59.90564	1.014476	1.712473	6.932529		18.22383	21.74959	0.3703935		109.9	54.5	0.9	1.6	6.3	0.0	16.6	19.8	0.3	0.0	100.0	48.3	10.3	41.4	82.4
Spectrum 4	58.38808	1.191986	2.409063	7.187387		17.58503	21.87198	0.4831023		109.1	53.5	1.1	2.2	6.6	0.0	16.1	20.0	0.4	0.0	100.0	47.1	10.8	42.1	81.3
Spectrum 5	58.52692	1.081472	2.49159	7.536899		17.69915	21.17685	0.3650839		108.9	53.8	1.0	2.3	6.9	0.0	16.3	19.5	0.3	0.0	100.0	47.6	11.4	41.0	80.7
Spectrum 6	60.08485	0.8238475	1.414134	7.043553		18.52234	21.38914	0.398248		109.7	54.8	0.8	1.3	6.4	0.0	16.9	19.5	0.4	0.0	100.0	48.9	10.4	40.6	82.4
Spectrum 7	58.4981	1.186898	2.136256	7.008768		17.64603	21.78144	0.3352841		108.6	53.9	1.1	2.0	6.5	0.0	16.2	20.1	0.3	0.0	100.0	47.4	10.6	42.1	81.8
Spectrum 8	58.61539	1.22505	2.516851	7.334462		17.33064	21.28574	0.409148		108.7	53.9	1.1	2.3	6.7	0.0	15.9	19.6	0.4	0.0	100.0	47.2	11.2	41.6	80.8
Spectrum 9	58.56177	1.035177	2.352335	6.982739		17.58137	21.77203	0.3993427		108.7	53.9	1.0	2.2	6.4	0.0	16.2	20.0	0.4	0.0	100.0	47.3	10.5	42.1	81.8
Spectrum 10	58.55494	1.082904	2.248091	7.106434		17.63056	21.63898	0.4161696		108.7	53.9	1.0	2.1	6.5	0.0	16.2	19.9	0.4	0.0	100.0	47.4	10.7	41.8	81.6
																				Average	47.6	10.8	41.6	81.6

Sample: BL08-78 193.9
Pyroxene

	Raw										Normalized												
Spectrum	SiO2	TiO2	Al2O3	FeO	MnO	MgO	CaO	Na2O	Cr2O3	Total	SiO2	TiO2	Al2O3	FeO	MnO	MgO	CaO	Na2O	Cr2O3	Total	En	Fs	Wo	En'
Spectrum 1	58.935	0.7884374	1.904042	5.942335		18.07938	22.09408	0.3716722	0.7931143	108.9	54.1	0.7	1.7	5.5	0.0	16.6	20.3	0.3	0.7	100.0	48.5	8.9	42.6	84.4
Spectrum 2	59.22964	0.6597439	1.636461	5.523807		18.40109	21.53358	0.4351933	0.8110157	108.2	54.7	0.6	1.5	5.1	0.0	17.0	19.9	0.4	0.7	100.0	49.8	8.4	41.9	85.6
Spectrum 3	59.80262	0.7124031	1.683578	5.953275		18.41945	21.92991	0.3963638	0.6854703	109.6	54.6	0.7	1.5	5.4	0.0	16.8	20.0	0.4	0.6	100.0	49.1	8.9	42.0	84.6
Spectrum 4	59.62292	0.8447492	1.546301	5.876833		18.37586	22.0569	0.3508098	0.6568574	109.3	54.5	0.8	1.4	5.4	0.0	16.8	20.2	0.3	0.6	100.0	49.0	8.8	42.3	84.8
Spectrum 5	59.37221	0.7769408	1.816166	5.908699		18.86565	21.11964	0.4433094	0.9447833	109.2	54.3	0.7	1.7	5.4	0.0	17.3	19.3	0.4	0.9	100.0	50.5	8.9	40.6	85.1
Spectrum 6	59.54885	0.7724993	1.696589	5.619644		18.68457	21.18719	0.3814896	0.941547	108.8	54.7	0.7	1.6	5.2	0.0	17.2	19.5	0.4	0.9	100.0	50.4	8.5	41.1	85.6
Spectrum 7	59.21432	0.7929638	1.760565	5.815486		18.47014	20.92675	0.3918027	0.9210694	108.3	54.7	0.7	1.6	5.4	0.0	17.1	19.3	0.4	0.9	100.0	50.2	8.9	40.9	85.0
Spectrum 8	59.21857	0.8358293	1.958791	6.101841	0.3219881	18.12963	21.79864	0.3899983	0.7301057	109.5	54.1	0.8	1.8	5.6	0.3	16.6	19.9	0.4	0.7	100.0	48.7	9.2	42.1	84.1
Spectrum 9	59.40882	0.8673267	1.471776	5.821885		18.38885	22.14848	0.3748887	0.6353319	109.1	54.4	0.8	1.3	5.3	0.0	16.9	20.3	0.3	0.6	100.0	48.9	8.7	42.4	84.9
Spectrum 10	58.86125	0.7983387	1.839674	5.975659		17.88608	21.89933	0.4038369	0.547744	108.2	54.4	0.7	1.7	5.5	0.0	16.5	20.2	0.4	0.5	100.0	48.4	9.1	42.6	84.2
Spectrum 11	59.57328	0.817325	1.5477	6.011213		18.32367	21.99727	0.3681702	0.8095019	109.4	54.4	0.7	1.4	5.5	0.0	16.7	20.1	0.3	0.7	100.0	48.8	9.0	42.2	84.5
																				Average	49.3	8.8	41.9	84.8

Sample: BL09-146 169.6
Pyroxene

	Raw										Normalized												
Spectrum	SiO2	TiO2	Al2O3	FeO	MnO	MgO	CaO	Na2O	Cr2O3	Total	SiO2	TiO2	Al2O3	FeO	MnO	MgO	CaO	Na2O	Cr2O3	Total	En	Fs	Wo	En'
Spectrum 1	59.29309	1.457713	3.058078	8.537192		17.22741	22.49578	0.4214279		112.5	52.7	1.3	2.7	7.6	0.0	15.3	20.0	0.4	0.0	100.0	45.1	12.5	42.3	78.2
Spectrum 2	59.38271	1.448105	3.068238	8.864231		17.43341	22.59609	0.4716544		113.3	52.4	1.3	2.7	7.8	0.0	15.4	19.9	0.4	0.0	100.0	45.1	12.9	42.0	77.8
Spectrum 3	60.2686	1.087431	2.506142	9.569777		17.5314	21.98114	0.4046064		113.3	53.2	1.0	2.2	8.4	0.0	15.5	19.4	0.4	0.0	100.0	45.3	13.9	40.8	76.6
Spectrum 4	59.2089	1.522018	3.232634	8.925119		17.36976	22.36343	0.4003729		113.0	52.4	1.3	2.9	7.9	0.0	15.4	19.8	0.4	0.0	100.0	45.2	13.0	41.8	77.6
Spectrum 5	59.34284	1.301564	2.808196	8.489885		17.5722	22.56647	0.4179581		112.5	52.7	1.2	2.5	7.5	0.0	15.6	20.1	0.4	0.0	100.0	45.6	12.4	42.1	78.7
Spectrum 6	58.76303	1.588439	3.0569	8.386932		17.12759	22.47718	0.4421593		111.8	52.5	1.4	2.7	7.5	0.0	15.3	20.1	0.4	0.0	100.0	45.1	12.4	42.5	78.4
Spectrum 7	58.7579	1.481915	3.18195	8.706545		17.21351	22.05996	0.3945434		111.8	52.6	1.3	2.8	7.8	0.0	15.4	19.7	0.4	0.0	100.0	45.3	12.9	41.8	77.9
Spectrum 8	59.14351	1.438404	3.027019	8.484093		17.41782	22.69657	0.4754731		112.7	52.5	1.3	2.7	7.5	0.0	15.5	20.1	0.4	0.0	100.0	45.2	12.4	42.4	78.5
Spectrum 9	59.41164	1.330449	3.063233	9.065811		17.46357	21.78059	0.3915941		112.5	52.8	1.2	2.7	8.1	0.0	15.5	19.4	0.3	0.0	100.0	45.7	13.3	41.0	77.4
Spectrum 10	59.0386	1.435241	2.999498	8.584775		17.42283	22.22952	0.4117871		112.1	52.7	1.3	2.7	7.7	0.0	15.5	19.8	0.4	0.0	100.0	45.6	12.6	41.8	78.3
																				Average	45.3	12.8	41.9	78.0

Sample: BL09-146 169.9
Pyroxene

	Raw										Normalized												
Spectrum	SiO2	TiO2	Al2O3	FeO	MnO	MgO	CaO	Na2O	Cr2O3	Total	SiO2	TiO2	Al2O3	FeO	MnO	MgO	CaO	Na2O	Cr2O3	Total	En	Fs	Wo	En'
Spectrum 1	59.8648	1.365136	2.768626	7.890759		17.83297	22.37715	0.4731011		112.6	53.2	1.2	2.5	7.0	0.0	15.8	19.9	0.4	0.0	100.0	46.5	11.5	42.0	80.1
Spectrum 2	59.29516	1.299904	3.178561	7.875913		17.24053	22.221	0.4764178	0.4049474	112.0	52.9	1.2	2.8	7.0	0.0	15.4	19.8	0.4	0.4	100.0	45.8	11.7	42.4	79.6
Spectrum 3	59.51522	1.169952	2.766415	7.927439		17.93848	22.29613	0.4514872		112.1	53.1	1.0	2.5	7.1	0.0	16.0	19.9	0.4	0.0	100.0	46.7	11.6	41.7	80.1
Spectrum 4	59.74785	1.282023	2.623177	7.819146		18.04501	21.98739	0.3797466		111.9	53.4	1.1	2.3	7.0	0.0	16.1	19.7	0.3	0.0	100.0	47.2	11.5	41.3	80.4
Spectrum 5	59.44107	1.245342	2.642807	7.816109		17.56391	22.46569	0.4255457		111.6	53.3	1.1	2.4	7.0	0.0	15.7	20.1	0.4	0.0	100.0	46.1	11.5	42.4	80.0
Spectrum 6	59.64624	1.396917	2.993113	7.955653		17.34795	22.66397	0.3804968		112.4	53.1	1.2	2.7	7.1	0.0	15.4	20.2	0.3	0.0	100.0	45.5	11.7	42.8	79.5
Spectrum 7	59.56352	1.252106	2.634245	7.772586		17.69245	22.41972	0.4128392		111.7	53.3	1.1	2.4	7.0	0.0	15.8	20.1	0.4	0.0	100.0	46.3	11.4	42.2	80.2
Spectrum 8	58.97509	1.42597	3.018634	7.835311		17.37791	22.38004	0.4633482		111.5	52.9	1.3	2.7	7.0	0.0	15.6	20.1	0.4	0.0	100.0	45.9	11.6	42.5	79.8
Spectrum 9	59.97698	1.22985	2.686033	7.917996		17.74691	22.22866	0.407063		112.2	53.5	1.1	2.4	7.1	0.0	15.8	19.8	0.4	0.0	100.0	46.5	11.6	41.9	80.0
Spectrum 10	59.71491	1.198972	2.859826	7.730956		17.76929	22.38617	0.4396454		112.1	53.3	1.1	2.6	6.9	0.0	15.9	20.0	0.4	0.0	100.0	46.5	11.4	42.1	80.4
																				Average	46.3	11.6	42.1	80.0

Appendix C - Mineral Chemistry

Sample: BL09-146 174.3
Pyroxene

	Raw										Normalized											
Spectrum	SiO2	TiO2	Al2O3	FeO	MnO	MgO	CaO	Na2O	Cr2O3	Total	SiO2	TiO2	Al2O3	FeO	MnO	MgO	CaO	Na2O	Cr2O3	Total	En	Fs	Wo	En'
Spectrum 1	61.27816	0.8924217	2.004685	5.958344		19.14579	22.7793	0.3898057	0.8682319	113.3	54.1	0.8	1.8	5.3	0.0	16.9	20.1	0.3	0.8	100.0	49.3	8.6	42.1	85.1
Spectrum 2	61.3349	0.7425867	1.788962	5.905208		19.59401	22.67321	0.4093556	0.8987692	113.3	54.1	0.7	1.6	5.2	0.0	17.3	20.0	0.4	0.8	100.0	50.0	8.5	41.6	85.5
Spectrum 3	61.93327	0.7212491	1.60111	5.492281		19.46958	23.00261	0.4300931	1.000917	113.7	54.5	0.6	1.4	4.8	0.0	17.1	20.2	0.4	0.9	100.0	49.8	7.9	42.3	86.3
Spectrum 4	61.43323	0.6859288	1.730214	5.810064		19.63964	22.31578	0.4197825	0.8874958	112.9	54.4	0.6	1.5	5.1	0.0	17.4	19.8	0.4	0.8	100.0	50.4	8.4	41.2	85.8
Spectrum 5	61.53026	0.7438742	1.605559	5.407767		19.6217	22.75381	0.3897583	0.9362931	113.0	54.5	0.7	1.4	4.8	0.0	17.4	20.1	0.3	0.8	100.0	50.3	7.8	41.9	86.6
Spectrum 6	61.87496	0.4889185	0.9308941	5.404347		20.02323	22.48682		0.5498507	111.8	55.4	0.4	0.8	4.8	0.0	17.9	20.1	0.0	0.5	100.0	51.0	7.7	41.2	86.8
Spectrum 7	62.01038	0.7032035	1.395004	5.48353		19.62405	22.72837	0.410169	0.6890933	113.0	54.9	0.6	1.2	4.9	0.0	17.4	20.1	0.4	0.6	100.0	50.3	7.9	41.9	86.4
Spectrum 8	61.60232	0.8369585	1.609217	5.551647		19.561	22.51554	0.4220491	0.9406757	113.0	54.5	0.7	1.4	4.9	0.0	17.3	19.9	0.4	0.8	100.0	50.3	8.0	41.7	86.3
Spectrum 9	61.37246	0.8358525	1.857063	6.029116		19.03308	22.80424	0.402494	0.8074746	113.1	54.2	0.7	1.6	5.3	0.0	16.8	20.2	0.4	0.7	100.0	49.0	8.7	42.2	84.9
Spectrum 10	62.16254	0.5669074	1.335609	5.48893		19.85178	22.57706	0.3858558	0.8636009	113.2	54.9	0.5	1.2	4.8	0.0	17.5	19.9	0.3	0.8	100.0	50.7	7.9	41.4	86.6
																				Average	50.1	8.1	41.8	86.0

Sample: TBND-60 32.9
Olivine

	Raw						Normalized						
Spectrum	SiO2	FeO	MnO	MgO	CaO	Total	SiO2	FeO	MnO	MgO	CaO	Total	Fo
Spectrum 1	49.95749	18.31363		51.9062	0.3107458	120.5	41.5	15.2	0.0	43.1	0.3	100.0	83.5
Spectrum 2	49.61508	20.25993		50.78275		120.7	41.1	16.8	0.0	42.1	0.0	100.0	81.7
Spectrum 3	49.63014	20.37574		50.86723	0.348227	121.2	40.9	16.8	0.0	42.0	0.3	100.0	81.6
Spectrum 4	50.12116	19.49097		51.94186	0.313126	121.9	41.1	16.0	0.0	42.6	0.3	100.0	82.6
Spectrum 5	50.03157	20.25433	0.4095835	51.27615	0.3449109	122.3	40.9	16.6	0.3	41.9	0.3	100.0	81.9
Spectrum 6	49.93471	20.19366		51.41953	0.3775231	121.9	41.0	16.6	0.0	42.2	0.3	100.0	81.9
Spectrum 7	49.52222	21.13252	0.3819439	50.45763		121.5	40.8	17.4	0.3	41.5	0.0	100.0	81.0
Spectrum 8	49.76795	20.29684	0.3497453	51.06969	0.3387466	121.8	40.9	16.7	0.3	41.9	0.3	100.0	81.8
Spectrum 9	49.33011	20.50796	0.3456462	50.5196	0.2997386	121.0	40.8	16.9	0.3	41.8	0.2	100.0	81.4
Spectrum 10	49.88844	19.8576		51.54194	0.3659785	121.7	41.0	16.3	0.0	42.4	0.3	100.0	82.2
												Average	82.0

Sample: TBND-125 29.8
Olivine

	Raw						Normalized						
Spectrum	SiO2	FeO	MnO	MgO	CaO	Total	SiO2	FeO	MnO	MgO	CaO	Total	Fo
Spectrum 1	45.11129	17.6125		47.06948	0.3131787	110.1	41.0	16.0	0.0	42.7	0.3	100.0	82.6
Spectrum 2	44.55043	19.30493	0.3449652	45.31589		109.5	40.7	17.6	0.3	41.4	0.0	100.0	80.7
Spectrum 3	44.37892	19.16295		45.05822		108.6	40.9	17.6	0.0	41.5	0.0	100.0	80.7
Spectrum 4	43.99998	20.67386		43.87159		108.5	40.5	19.0	0.0	40.4	0.0	100.0	79.1
Spectrum 5	44.42991	19.23547	0.3329711	45.08468	0.2883214	109.4	40.6	17.6	0.3	41.2	0.3	100.0	80.7
Spectrum 6	44.96819	16.83921	0.3274355	47.62518	0.3018337	110.1	40.9	15.3	0.3	43.3	0.3	100.0	83.4
Spectrum 7	44.43703	19.79482		45.12376	0.2990128	109.7	40.5	18.1	0.0	41.2	0.3	100.0	80.2
Spectrum 8	44.06086	21.07673		43.40981	0.2824267	108.8	40.5	19.4	0.0	39.9	0.3	100.0	78.6
Spectrum 9	44.93436	18.83543		46.40237		110.2	40.8	17.1	0.0	42.1	0.0	100.0	81.4
Spectrum 10	44.86653	18.07117		46.39762		109.3	41.0	16.5	0.0	42.4	0.0	100.0	82.1
												Average	81.0

Sample: BL08-78 193.9
Olivine

	Raw						Normalized						
Spectrum	SiO2	FeO	MnO	MgO	CaO	Total	SiO2	FeO	MnO	MgO	CaO	Total	Fo
Spectrum 1	43.37782	22.45021	0.3801981	41.77882	0.2571476	108.2	40.1	20.7	0.4	38.6	0.2	100.0	76.8
Spectrum 2	43.63581	23.1337		41.16803		107.9	40.4	21.4	0.0	38.1	0.0	100.0	76.0
Spectrum 3	43.31324	23.46472	0.345144	41.08586	0.241369	108.5	39.9	21.6	0.3	37.9	0.2	100.0	75.7
Spectrum 4	43.26549	23.18331	0.4213959	41.26882		108.1	40.0	21.4	0.4	38.2	0.0	100.0	76.0
Spectrum 5	43.53114	23.0502	0.3745857	41.55956		108.5	40.1	21.2	0.3	38.3	0.0	100.0	76.3
Spectrum 6	57.03686	7.065942		16.70639	21.89848	102.7	55.5	6.9	0.0	16.3	21.3	100.0	80.8
Spectrum 7	43.43206	23.00796	0.4476397	41.34826		108.2	40.1	21.3	0.4	38.2	0.0	100.0	76.2
Spectrum 8	43.30507	23.28559		41.08731		107.7	40.2	21.6	0.0	38.2	0.0	100.0	75.9
Spectrum 9	43.37552	23.4567		41.45102		108.3	40.1	21.7	0.0	38.3	0.0	100.0	75.9
Spectrum 10	43.68722	23.51683	0.3752587	41.57444		109.2	40.0	21.5	0.3	38.1	0.0	100.0	75.9
												Average	76.6

Sample: BL09-146 174.3

Olivine

Appendix C - Mineral Chemistry

	Raw						Normalized						
Spectrum	SiO2	FeO	MnO	MgO	CaO	Total	SiO2	FeO	MnO	MgO	CaO	Total	Fo
Spectrum 1	44.62517	20.75509		46.51786	0.2800834	112.1782034	39.8	18.5	0.0	41.5	0.2	100.0	80.0
Spectrum 2	44.10643	22.78843	0.3498126	44.60194		111.8466126	39.4	20.4	0.3	39.9	0.0	100.0	77.7
Spectrum 3	43.98479	22.29617		44.75741	0.2704634	111.3088334	39.5	20.0	0.0	40.2	0.2	100.0	78.2
Spectrum 4	44.19274	21.91672		45.19968		111.30914	39.7	19.7	0.0	40.6	0.0	100.0	78.6
Spectrum 5	44.54071	20.57003	0.4174405	46.70268		112.2308605	39.7	18.3	0.4	41.6	0.0	100.0	80.2
Spectrum 6	44.56385	21.80202		45.61246		111.97833	39.8	19.5	0.0	40.7	0.0	100.0	78.9
Spectrum 7	44.24592	22.43025	0.3561381	44.82226		111.8545681	39.6	20.1	0.3	40.1	0.0	100.0	78.1
Spectrum 8	43.7938	23.23901		44.50613		111.53894	39.3	20.8	0.0	39.9	0.0	100.0	77.3
Spectrum 9	43.95188	23.15043	0.3858677	44.69383		112.1820077	39.2	20.6	0.3	39.8	0.0	100.0	77.5
Spectrum 10	44.24039	23.15068		44.59172		111.98279	39.5	20.7	0.0	39.8	0.0	100.0	77.4
												Average	78.4

Appendix D

Raw Lithogeochemistry Data

ACME ANALYTICAL LABORATORIES LTD.
Client: University of Minnesota Duluth
File Created: February 1, 2012
Job Number: VAN11006524
Number of Samples: 52
Project: Thunder Bay North - MS
Shipment ID:
P.O. Number:
Received: Novermber 24, 2011

Appendix D - Raw Lithogeochemical Data

	Method	WGHT	1EX	1EX	1EX	1EX	1EX	1EX	1EX	1EX	1EX	1EX	1EX	1EX	1EX	1EX	1EX	1EX	1EX	1EX	1EX	1EX	1EX
	Analyte	Wgt	Ti	Al	Fe	Mn	Mg	Ca	Na	K	P	S	Mo	Cu	Pb	Zn	Ag	Ni	Co	As	U	Au	Th
	Unit	KG	%	%	%	PPM	%	%	%	%	%	%	PPM	PPM	PPM	PPM	PPM	PPM	PPM	PPM	PPM	PPM	PPM
	MDL	0.01	0.001	0.01	0.01	1	0.01	0.01	0.001	0.01	0.001	0.1	0.1	0.1	0.1	1	0.1	0.1	0.2	1	0.1	0.1	0.1
Sample	Type																						
TBND-60 15.2	Drill Core	0.07	1.094	6.83	4.63	363	1.77	0.35	3.235	1.5	0.152	0.7	1.9	9.2	2.5	21	0.1	15.8	20.6	10	16.6	<0.1	11.1
TBND-60 17.5	Drill Core	0.09	1.339	7.02	7.37	937	1.87	4.39	3.17	1.08	0.147	0.3	1.5	14.6	4.2	55	0.1	10.5	32.2	6	2.8	<0.1	5.2
TBND-60 20.1	Drill Core	0.04	1.215	6.85	5.29	596	1.22	3.94	4.788	0.47	0.198	0.3	1.4	3.7	1.8	36	<0.1	1.4	16	5	2.6	<0.1	5.7
TBND-60 21.4	Drill Core	0.06	1.139	6.54	7.04	981	3.2	3.16	2.99	0.95	0.162	0.7	1.3	56.8	4.1	87	0.1	23.1	38.2	43	1.5	<0.1	4.3
TBND-60 22.3	Drill Core	0.05	1.138	5.01	6.97	1375	5.74	5.84	2.373	0.34	0.106	0.8	0.6	134.1	2.1	86	<0.1	87.7	39.8	8	0.8	<0.1	2.1
TBND-60 23.0	Drill Core	0.1	0.883	4.27	6.95	1992	7.11	6.5	1.505	0.23	0.08	1.3	0.6	154.1	8.8	105	0.1	137.7	48	22	1	<0.1	2
TBND-60 25.8	Drill Core	0.12	0.748	3.02	8.76	1392	12.32	3.1	0.658	0.35	0.065	0.2	0.4	259.5	2.9	94	0.2	853.8	106.8	3	0.4	<0.1	1.4
TBND-60 32.9	Drill Core	0.1	0.587	2.37	9.41	1485	14.4	2.88	0.391	0.27	0.062	0.6	0.5	633.8	5.1	107	0.5	1202.2	126.1	10	0.5	<0.1	1.3
TBND-95 93.8	Drill Core	0.14	0.551	3.06	10.95	1419	11.08	3.55	0.197	0.15	0.069	4.7	0.6	94.9	13.6	143	0.3	860.2	121.3	23	0.3	<0.1	1.3
TBND-95 94.9	Drill Core	0.04	1.436	4.53	11.99	2438	9.72	2.25	0.898	0.3	0.108	0.4	0.8	52.6	1.9	166	0.1	524.4	115.1	6	0.6	<0.1	2
TBND-95 99.1	Drill Core	0.03	1.402	6.97	9.13	811	4.14	3.29	2.585	0.23	0.178	3	1.3	222.6	64	146	0.8	33.4	36.7	7	1.8	<0.1	3.9
TBND-95 101.9	Drill Core	0.1	0.072	5.5	0.79	62	0.23	0.22	2.13	4.04	0.027	0.3	0.9	3	33.1	5	0.2	6.3	2.4	1	5	<0.1	22.9
TBND-124 49.5	Drill Core	0.13	0.858	3.31	9.17	1444	12	3.38	0.696	0.44	0.078	0.3	0.6	290	3.5	96	0.2	898.5	104.2	5	0.5	<0.1	1.8
TBND-124 88.9	Drill Core	0.05	1.067	3.74	11.34	1530	11.51	2.56	0.845	0.5	0.078	0.2	0.6	78.3	2.8	118	0.1	824	124.3	2	0.5	<0.1	2
TBND-124 91.5	Drill Core	0.07	1.641	6.41	11.87	1178	2.89	4.21	1.996	1.18	0.214	2.4	0.7	21.2	3.9	129	0.1	74.7	66.4	8	0.6	<0.1	2.3
TBND-124 94.7	Drill Core	0.1	1.506	7.19	7.93	842	2.72	5.01	3.369	0.41	0.177	2.1	1.1	36.6	11.7	93	0.2	22.8	39	8	2.9	<0.1	4
TBND-136 16.6	Drill Core	0.1	0.897	6.73	8.02	1066	3.22	1.08	2.817	1.19	0.137	0.5	1.3	38.6	6.5	92	<0.1	35.1	33.7	5	2.3	<0.1	4.4
TBND-136 18.9	Drill Core	0.09	1.401	6.81	7.09	897	2.36	3.17	3.181	0.65	0.165	3.3	1.2	16.6	16.2	72	0.1	10.6	31.4	13	7.2	<0.1	4.5
TBND-136 21.1	Drill Core	0.17	1.091	4.66	8.2	1927	5.88	6.46	1.949	0.41	0.087	0.7	0.8	542	4.8	101	0.2	157.4	54	9	0.8	<0.1	2.5
TBND-125 22.0	Drill Core	0.08	1.177	7.47	8.14	1321	1.84	1.11	3.864	1.46	0.182	0.7	2.1	36.2	5.7	98	0.1	12	34.7	5	5.9	<0.1	5.5
TBND-125 23.8	Drill Core	0.05	1.364	7.08	9.07	1466	2.58	1.41	3.134	0.98	0.155	0.5	1.5	51	3	81	<0.1	16.4	44.4	4	4.5	<0.1	3.9
TBND-125 24.8	Drill Core	0.09	1.043	4.17	9.09	3527	6.31	6.14	1.939	0.14	0.078	0.5	0.8	264.9	2.2	86	0.1	140.5	53	10	0.7	<0.1	2.1
TBND-125 29.8	Drill Core	0.12	0.785	3.01	9.12	1437	12.91	3.15	0.568	0.33	0.065	0.2	0.4	132.7	3.3	94	0.1	812.3	106.5	4	0.4	<0.1	1.5
TBND-023 107.8	Drill Core	0.07	1.749	7.65	6.66	1113	2.72	3.9	3.971	0.61	0.194	0.9	1	65.4	5.4	76	0.1	24.2	32.6	14	4.3	<0.1	4.5
TBND-023 112.6	Drill Core	0.1	0.084	6.04	1.29	101	0.26	0.2	1.781	3.14	0.027	0.6	0.7	5.4	23.9	7	0.2	9.7	2.6	10	9.4	<0.1	21.4
TBND-023 115.9	Drill Core	0.03	1.815	7.67	7.75	1099	2.44	4.14	3.948	0.33	0.204	1.9	1.1	10.3	33.1	92	0.5	15	33.2	7	6	<0.1	5.2
BL08-75 152.5	Drill Core	0.03	1.501	7.1	6.2	491	3.28	0.42	2.277	1.72	0.157	1.3	1.4	6.6	2.8	34	0.1	14.9	29.1	9	2.8	<0.1	5.7
BL08-75 157.5	Drill Core	0.08	0.975	6.8	5.84	590	3.37	0.68	2.497	1.18	0.229	0.2	0.7	3.2	2.6	63	0.1	11.6	17.3	4	2.2	<0.1	4.8
BL08-75 161.5	Drill Core	0.08	1.015	6.8	4.58	732	2.88	2.11	2.779	1.39	0.227	0.3	0.6	6.7	1.2	54	<0.1	3.9	14.8	7	1.8	<0.1	6.2
BL08-75 169.2	Drill Core	0.15	1.335	6.49	9.71	855	4.2	3.28	2.576	0.42	0.072	0.9	0.4	4.1	1.6	78	<0.1	17.6	40.3	25	0.7	<0.1	2.5
BL08-75 171.8	Drill Core	0.06	0.572	1.94	6.34	1489	11.52	5.8	0.097	0.02	0.052	0.5	0.9	1308.7	42.5	65	0.6	823.7	63.5	18	0.3	<0.1	1.1
BL08-75 179.0	Drill Core	0.07	0.517	1.75	9.99	1530	14.98	2.84	0.143	0.28	0.05	0.3	0.3	772.4	2.1	101	0.5	1295.2	136	5	0.3	<0.1	1
BL08-78 162.65	Drill Core	0.07	0.39	6.37	5.69	1776	5.07	5.36	1.719	0.25	0.343	0.5	0.8	90	22.2	92	0.1	143.5	35.2	23	4.6	<0.1	18.3
BL08-78 166.28	Drill Core	0.1	0.849	6.67	5.95	764	3.78	1.1	2.622	1.55	0.111	0.3	0.7	349.7	6.4	81	<0.1	116.1	27.5	13	1.3	<0.1	5
BL08-78 169.57	Drill Core	0.06	0.551	6.02	4.97	525	3.12	0.82	1.753	1.19	0.112	0.8	1.3	153	2	46	<0.1	54.8	26.2	20	4.1	<0.1	3.3
BL08-78 178.7	Drill Core	0.18	1.081	7.42	6.83	892	1.78	3.78	3.561	2.25	0.133	0.2	0.8	54	2.4	63	<0.1	9.6	24.5	7	1.8	<0.1	5
BL08-78 181.7	Drill Core	0.13	1.41	7.13	9.51	1262	3.39	4.08	3.289	0.74	0.086	0.1	0.7	36	2.9	100	<0.1	14.2	44.2	7	0.9	<0.1	2.9
BL08-78 186.3	Drill Core	0.08	1.152	7.28	7.18	871	3.35	1.24	3.393	1.47	0.185	0.4	0.7	5.5	1.8	79	<0.1	10.7	28.7	13	1.4	<0.1	4.4
BL08-78 188.0	Drill Core	0.09	1.28	7.54	6.62	879	2.45	2.82	3.948	1.48	0.21	<0.1	1.2	6	1.9	62	<0.1	1.7	22.8	3	1.3	<0.1	4.8
BL08-78 190.3	Drill Core	0.16	1.802	7.61	7.64	1738	3.42	3.02	3.488	0.89	0.096	<0.1	0.7	93.5	3.3	86	<0.1	5	29.7	7	1	<0.1	3
BL08-78 192.1	Drill Core	0.09	1.08	5	6.15	3153	5.24	8.83	0.84	0.27	0.119	0.2	0.9	105	15.7	33	<0.1	93.3	39.9	32	1	<0.1	3.1
BL08-78 193.9	Drill Core	0.18	0.756	2.86	9.44	1537	13.15	5.26	0.519	0.29	0.065	<0.1	0.3	187.8	2.2	99	0.2	784.4	111.3	4	0.4	<0.1	1.4
BL08-78 204.2	Drill Core	0.1	0.543	2	10.35	1603	17.33	2.81	0.322	0.25	0.052	<0.1	0.2	87.1	1.6	108	<0.1	1186.1	139.5	5	0.3	<0.1	1
BL08-146 158.4	Drill Core	0.03	1.095	6.28	6.29	725	2.97	1.33	2.891	0.9	0.188	<0.1	0.3	7.6	1.1	63	<0.1	18.7	19.6	3	1.2	<0.1	4.5
BL08-146 161.2	Drill Core	0.06	1.155	6.76	6.71	680	3.48	1.13	3.112	1.05	0.204	<0.1	0.3	5.7	1.2	49	<0.1	10.3	19.8	3	1.2	<0.1	4.3
BL08-146 169.6	Drill Core	0.1	1.537	6.85	10.14	1359	4.64	3.11	2.87	0.75	0.066	0.5	0.4	150.1	2.2	111	<0.1	30.7	53.5	17	0.7	<0.1	2.3
BL08-146 174.3	Drill Core	0.1	0.65	2.78	9.91	1643	12.96	4.41	0.41	0.23	0.059	0.2	0.3	160	2.8	107	0.1	786.4	110.4	6	0.4	<0.1	1.4
BL08-147 153.1	Drill Core	0.11	0.269	7.29	3.35	515	1.8	0.34	3.819	2.27	0.065	0.3	0.7	5.6	2.3	51	<0.1	49.1	15.8	7	1.2	<0.1	3.3
BL08-147 166.8	Drill Core	0.11	0.932	7.72	6.36	872	3.08	2.48	3.312	1.63	0.127	<0.1	1.8	7.2	3.4	51	<0.1	26.8	27.6	4	1.3	<0.1	4
BL08-147 174.5	Drill Core	0.16	1.167	7.26	6.71	665	4.05	0.86	2.566	1.48	0.149	1.4	0.4	6	1.7	58	<0.1	8.8	33.5	33	1.4	<0.1	4.1
BL08-147 176.7	Drill Core	0.1	1.25	7.01	8.85	1445	4.35	3.77	2.929	0.58	0.082	0.3	0.6	204.6	1.8	105	<0.1	73.8	53.8	8	0.8	<0.1	2.5
BL08-147 177.9	Drill Core	0.07	0.855	3.18	9.3	1862	11.2	3.79	0.442	0.14	0.059	0.7	0.6	1573.6	451.7	595	2.7	1037.8	124.9	111	0.4	<0.1	1.4

	1EX Sr PPM 1	1EX Cd PPM 0.1	1EX Sb PPM 0.1	1EX Bi PPM 0.1	1EX V PPM 1	1EX La PPM 0.1	1EX Cr PPM 1	1EX Ba PPM 1	1EX W PPM 0.1	1EX Zr PPM 0.1	1EX Ce PPM 1	1EX Sn PPM 0.1	1EX Y PPM 0.1	1EX Nb PPM 0.1	1EX Ta PPM 0.1	1EX Be PPM 1	1EX Sc PPM 1	1EX Li PPM 0.1	1EX Rb PPM 0.1	1EX Hf PPM 0.1	4B Ba PPM 1	4B Be PPM 1	4B Co PPM 0.2	4B Cs PPM 0.1	4B Ga PPM 0.5
Sample																									
TBND-60 15.2	61	<0.1	<0.1	0.1	185	47.4	2	231	0.8	261.4	98	2.3	26.9	23.1	1.6	3	11	63.2	52.4	7	238	3	20.7	1	22.2
TBND-60 17.5	420	0.2	<0.1	<0.1	255	50.1	2	327	0.8	264	102	2.2	25.2	25.3	1.8	2	16	56.2	37.6	6.8	323	3	32.6	1.2	20.6
TBND-60 20.1	176	<0.1	<0.1	<0.1	136	52.9	1	131	0.9	303.1	112	2.7	29.6	36	2.2	3	11	38.9	10.8	7.9	139	<1	17.3	0.5	22.3
TBND-60 21.4	351	0.2	<0.1	<0.1	226	44.3	2	388	0.5	231.7	92	1.5	24.1	20.9	1.4	2	14	66.8	36.4	6.1	390	2	39.7	1.2	18.7
TBND-60 22.3	252	<0.1	<0.1	0.1	257	23.2	248	120	0.3	128.9	51	1.2	17.3	13.3	0.9	1	37	38.8	13.2	3.5	125	1	40.7	0.3	12.8
TBND-60 23.0	220	0.2	<0.1	0.2	242	22.4	897	115	0.3	123.2	49	1.8	16.3	10	0.7	1	40	69.1	9.8	3.3	114	<1	48.7	0.6	13.4
TBND-60 25.8	291	<0.1	<0.1	0.1	158	18.2	1783	143	0.1	100.8	39	0.7	10.7	10.5	0.6	1	16	31.6	19.8	2.7	150	<1	113.5	3.4	9.6
TBND-60 32.9	293	0.2	<0.1	0.4	145	17.3	2148	209	0.2	101.1	38	0.6	10.4	7.9	0.5	<1	14	26.6	17.6	2.5	213	<1	129	2.8	7.8
TBND-95 93.8	109	<0.1	<0.1	2.6	166	19.5	1620	59	0.1	99.4	42	0.9	10.7	6.6	0.4	<1	12	90.3	8.3	2.5	64	<1	124.6	1.3	10.1
TBND-95 94.9	162	<0.1	<0.1	<0.1	270	28.5	997	174	0.2	184.7	62	1.4	16.1	18.2	1	1	14	131.1	15.7	4.8	189	1	123.8	2.2	16.2
TBND-95 99.1	52	0.3	0.1	0.6	206	48.9	36	92	0.8	286	100	5.6	55.5	26.1	1.6	3	15	200.4	10.6	7.3	96	2	37.2	1	22
TBND-95 101.9	79	<0.1	<0.1	0.3	9	44.4	6	412	0.2	107.8	90	2.2	16.6	5.4	0.5	1	3	9.4	165.2	4	421	<1	2.1	2.1	15.9
TBND-124 49.5	305	<0.1	<0.1	0.1	185	22.1	1911	187	0.2	132.7	49	0.9	13.3	11.7	0.7	<1	17	57.6	35.4	3.5	206	<1	111.5	6.5	11
TBND-124 88.9	330	0.2	<0.1	<0.1	214	23.6	2185	182	0.2	166.3	51	1.1	13.3	14.7	0.9	<1	12	38.2	20.1	4.4	184	<1	135	3.7	12.2
TBND-124 91.5	550	<0.1	<0.1	<0.1	411	36.7	85	337	0.1	156.1	81	1.1	19.6	9.9	0.8	1	15	70.3	52.5	4	364	1	65.4	0.4	21
TBND-124 94.7	183	0.1	<0.1	0.3	216	51.5	17	86	0.3	273.3	112	2	29.2	28.8	1.7	2	15	87.6	24.8	7	78	2	38.5	1.2	17.7
TBND-136 16.6	310	<0.1	<0.1	<0.1	250	38.8	46	857	0.6	228.2	83	1.4	22	15.2	1.3	3	20	102	38.8	6.1	3540	<1	32.3	1.3	18.1
TBND-136 18.9	208	0.2	0.1	0.1	275	45.3	8	171	0.6	253.8	95	2.1	25.8	23.7	1.7	3	17	83.8	22.1	6.6	181	2	31.5	0.6	19.2
TBND-136 21.1	211	0.2	<0.1	<0.1	302	28.4	90	149	0.4	156.4	62	1.2	20.7	12.9	0.9	1	43	45.6	14.7	4.2	146	<1	49.8	0.4	14
TBND-125 22.0	468	0.2	<0.1	<0.1	285	55.3	3	499	0.7	302.5	116	1.8	28.2	22.2	1.6	2	18	36	64.4	8	493	<1	33.2	0.5	23.4
TBND-125 23.8	410	<0.1	<0.1	<0.1	323	42.5	3	374	0.5	226.7	93	1.6	23.6	19.5	1.4	2	21	60.2	37.9	6.1	379	2	43.4	0.8	19.6
TBND-125 24.8	158	<0.1	<0.1	<0.1	284	22.5	272	74	0.3	133.3	49	1.2	18.9	11.7	0.8	1	46	30.4	3.5	3.6	78	<1	52.5	<0.1	12.2
TBND-125 29.8	302	0.2	<0.1	0.1	164	18.8	1811	119	0.1	108.7	40	0.7	10.9	10.9	0.6	<1	14	30.1	18.9	2.8	129	<1	109.3	3.7	10
TBND-023 107.8	131	0.2	<0.1	0.2	219	53.1	19	261	1.1	345.7	115	2.4	37.6	34.8	2.1	2	16	84.6	29.9	9	249	2	33.1	0.6	21.7
TBND-023 112.6	158	<0.1	<0.1	0.5	6	25.5	12	1053	0.1	118.7	53	1.9	12.9	5	0.4	1	3	7.6	110.8	3.7	1141	3	2.1	2	14.3
TBND-023 115.9	103	0.3	<0.1	0.5	223	51.7	9	290	0.7	337.1	106	2.4	48.1	35.1	2.1	2	16	94.5	12.2	9	307	3	33.8	0.3	21.5
BL08-75 152.5	56	<0.1	0.1	0.1	188	29.1	5	348	2.4	384.8	65	2.5	34.5	33.5	2.1	3	14	74.5	36.5	10.1	359	1	30.3	1.2	19.3
BL08-75 157.5	48	<0.1	<0.1	<0.1	126	13.4	2	246	1.2	363.2	34	1.7	31.8	31.6	2.1	2	9	83.2	13.5	9.5	252	3	17.6	0.3	18.8
BL08-75 161.5	59	0.1	<0.1	<0.1	105	64.7	3	528	0.9	363.1	142	2.5	41.7	33	2.1	2	10	66.8	25.2	9.4	543	2	16	0.3	18.9
BL08-75 169.2	67	<0.1	<0.1	<0.1	467	31.2	14	172	0.9	130	65	1.3	18.8	10.6	0.8	2	25	75	8.6	3.4	175	1	40.6	0.4	17.3
BL08-75 171.8	74	0.2	<0.1	0.1	137	11.7	1135	69	0.2	85.5	29	0.7	10.7	7.6	0.4	1	28	55.3	0.3	2.3	74	1	66.5	0.3	7.1
BL08-75 179.0	196	0.2	<0.1	<0.1	123	13.1	2326	147	<0.1	80.6	29	0.7	8.3	7.1	0.4	<1	11	46.9	18.1	2.1	147	<1	141.5	4.8	6.5
BL08-78 162.65	1102	0.2	0.1	0.3	139	102	209	1480	0.4	212.1	202	1.9	28.5	8.1	0.3	1	20	49.5	8.4	5.2	1655	<1	34.6	0.7	15.3
BL08-78 166.28	306	<0.1	<0.1	0.1	192	30.1	142	1136	2.7	183.9	69	1.5	18.1	14.6	0.9	3	18	59.2	30.2	4.8	1174	5	25.8	2.2	17.1
BL08-78 169.57	148	<0.1	<0.1	0.3	126	11.6	84	345	8	135.9	28	1.6	14.2	14.1	1.4	4	12	56.5	38	3.4	337	5	26.8	1.6	14.7
BL08-78 178.7	235	<0.1	<0.1	<0.1	264	45.8	12	845	1.3	222.3	99	1.8	23	19	1.7	3	20	32.6	46.4	5.7	816	6	22.4	0.7	18.5
BL08-78 181.7	248	<0.1	<0.1	<0.1	450	28.9	10	333	1	157	64	1.4	16.1	12.2	0.9	2	25	51.6	22.4	4	312	7	43	0.8	18.8
BL08-78 186.3	174	<0.1	<0.1	<0.1	160	41.7	16	584	1.3	313.6	99	2.2	24.9	29.7	1.9	3	12	47.6	18.9	8	598	1	27.9	0.4	19.5
BL08-78 188.0	120	0.1	<0.1	<0.1	169	52.6	<1	436	0.9	310.6	118	2.3	26.8	28.9	1.9	2	13	37.2	22.9	7.9	404	3	23.1	0.3	20.3
BL08-78 190.3	205	<0.1	<0.1	<0.1	303	29.6	7	319	0.8	180.2	67	1.6	18.5	17.2	1.3	2	21	52.9	17	4.7	312	3	29.4	0.9	19.7
BL08-78 192.1	111	0.1	0.1	<0.1	199	35.6	171	797	0.4	209.9	80	1.6	21.7	20.2	1.2	2	33	42.1	4.8	5.6	788	1	42.8	0.4	14.4
BL08-78 193.9	305	0.2	<0.1	<0.1	168	18.4	1509	161	0.1	114.1	42	0.8	11.6	10.4	0.6	<1	24	40.3	12.9	3	158	2	115.4	4.6	9.7
BL08-78 204.2	264	0.1	<0.1	<0.1	130	12.8	2359	116	<0.1	79.5	29	0.5	8.1	6.8	0.4	<1	15	12.5	10	2.1	104	3	147.4	2	7.5
BL08-146 158.4	116	<0.1	<0.1	<0.1	153	62.4	25	1571	2.3	260.8	134	2	22.8	27.4	1.8	1	11	47.5	14.1	6.7	1770	7	22	0.4	17.3
BL08-146 161.2	111	<0.1	<0.1	<0.1	141	35	16	546	0.9	318.7	87	2.2	21	30.9	2	2	11	63	9.6	8.3	617	7	22.7	0.5	21.2
BL08-146 169.6	251	<0.1	<0.1	<0.1	561	20.4	15	409	0.4	128.4	48	1.3	15.1	11	0.9	2	27	72.8	18.4	3.5	433	3	61	1.6	20.9
BL08-146 174.3	246	0.2	<0.1	<0.1	141	15.7	1644	92	0.1	90.1	37	0.6	9.9	9.1	0.6	<1	20	55.3	10.5	2.3	98	1	120.7	4.1	8.7
BL08-147 153.1	216	<0.1	<0.1	0.1	83	2.6	88	637	1.1	76.2	6	0.8	4.6	4.2	0.3	2	9	45.3	70.2	2.1	723	4	17.7	2.9	17.7
BL08-147 166.8	194	<0.1	0.1	<0.1	225	36.2	41	426	1.6	209.8	83	1.6	20.6	19	1.5	2	19	59.9	38.9	5.3	452	3	27.7	0.9	22.1
BL08-147 174.5	125	<0.1	<0.1	0.4	199	45.1	7	265	5.3	273.1	101	2	25.9	24.7	1.6	2	16	70.5	24.9	6.8	776	4	35.2	0.7	19.9
BL08-147 176.7	304	<0.1	<0.1	0.2	308	24.7	122	953	1	146.4	56	1.2	16.2	13.1	0.9	2	22	53.4	17.8	3.6	1016	1	62.6	1.4	19.2
BL08-147 177.9	83	2.2	0.2	0.6	192	17.6	964	34	0.2	116.3	40	1.7	11.8	10.6	0.6	<1	21	61.7	6.1	3	36	1	142.4	1.9	10.4

	4B Hf PPM 0.1	4B Nb PPM 0.1	4B Rb PPM 0.1	4B Sn PPM 1	4B Sr PPM 0.5	4B Ta PPM 0.1	4B Th PPM 0.2	4B U PPM 0.1	4B V PPM 8	4B W PPM 0.5	4B Zr PPM 0.1	4B Y PPM 0.1	4B La PPM 0.1	4B Ce PPM 0.1	4B Pr PPM 0.02	4B Nd PPM 0.3	4B Sm PPM 0.05	4B Eu PPM 0.02	4B Gd PPM 0.05	4B Tb PPM 0.01	4B Dy PPM 0.05	4B Ho PPM 0.02	4B Er PPM 0.03	4B Tm PPM 0.01	4B Yb PPM 0.05
Sample																									
TBND-60 15.2	8	23.7	62.6	2	71.1	1.5	10.5	17.3	184	<0.5	274.2	27.7	53.5	116.5	14.5	62.1	10.31	3.01	8.13	1.25	5.6	1.06	2.44	0.33	1.79
TBND-60 17.5	6.9	26.2	35.3	3	446.7	1.9	4.2	2.5	236	0.9	271.6	22.1	40.3	89.6	11.83	55.9	9.01	2.79	7.29	1.07	4.44	0.8	2.02	0.31	2.26
TBND-60 20.1	8.1	36.8	11.5	2	194.8	2.5	5.4	2.5	134	1.1	329	28.6	47.4	112.8	14.5	66.7	11.24	3.68	8.9	1.34	6.3	1.15	3.07	0.41	2.25
TBND-60 21.4	6.7	25.6	35.2	2	384.3	1.7	3.7	1.1	226	0.5	257.6	21.2	37.5	86.9	11.28	52	9.09	2.44	7.32	1.02	4.27	0.91	2.33	0.34	1.59
TBND-60 22.3	4.6	15.1	12.5	2	278	1.1	1.8	0.9	254	<0.5	168.1	15	20.1	48.5	6.59	31.9	6	2.05	5.15	0.8	3.34	0.68	1.77	0.26	1.5
TBND-60 23.0	5.2	11.3	9.7	2	243.1	0.9	1.7	0.8	245	<0.5	199.5	13.7	20.3	47.8	6.3	31.3	5.75	1.51	4.7	0.7	3.2	0.59	1.67	0.25	1.47
TBND-60 25.8	2.5	12.1	19.9	2	317.5	0.7	1.3	0.4	169	<0.5	111.9	11	14.8	36.9	4.82	19	3.78	1.28	3.47	0.51	2.48	0.4	1.15	0.13	0.88
TBND-60 32.9	2.4	8.5	16.6	1	313.7	0.5	1.1	0.4	141	<0.5	99.3	9.7	14	34.4	4.56	23.7	3.7	1.11	3.03	0.45	1.96	0.39	1	0.15	0.66
TBND-95 93.8	3.3	11.4	9.1	3	117.5	0.3	1.1	0.4	186	<0.5	125.1	10.4	17.2	39.2	5.46	21.4	4.68	1.26	3.56	0.51	2.34	0.41	1.03	0.14	0.75
TBND-95 94.9	5.3	18.8	16.6	2	183.5	1	1.9	0.5	286	<0.5	200.4	14.7	25.5	61.3	8.46	37.4	6.94	2.01	5.15	0.75	3.61	0.62	1.69	0.19	1.25
TBND-95 99.1	8.6	29.8	10.6	5	52.8	1.8	3.3	1.6	228	1	315.7	51.6	42.9	95.8	12.71	49.3	10.69	1.88	10.23	1.79	9.71	1.97	5.22	0.6	3.97
TBND-95 101.9	4	8.2	196.1	2	85.5	0.8	19.8	4.5	15	<0.5	109.6	23.1	43.2	95.8	11.12	38.8	7.04	0.67	5.2	0.78	4.2	0.78	2.23	0.37	2.21
TBND-124 49.5	4	12.5	36.2	<1	340.8	0.6	1.6	0.5	205	<0.5	142.9	12.8	19.6	45.9	6.26	28.4	5.38	1.52	4.16	0.6	2.74	0.5	1.18	0.17	1.17
TBND-124 88.9	4.2	15.5	19.8	2	371.4	0.9	1.9	0.5	220	<0.5	182	12.3	20.6	49.6	6.74	28.7	5.52	1.5	4.13	0.6	2.89	0.53	1.22	0.15	1.07
TBND-124 91.5	6.2	22.2	52	2	603.4	1.6	2.1	0.6	494	<0.5	211.1	18.7	32	78.1	10.64	54.9	8.77	2.6	6.97	0.97	3.67	0.81	1.87	0.24	1.17
TBND-124 94.7	7.6	29.9	20.9	2	172.2	1.8	3.5	2.7	224	<0.5	297.1	25.4	40.8	98.4	13.2	57.1	10.52	3.09	8.68	1.24	4.78	0.96	2.52	0.35	1.96
TBND-136 16.6	6.3	18.7	41.9	2	326	1.7	4.1	2	243	1.1	229	18.8	33.5	80	10.29	48.7	8	2.03	6.57	0.96	4.31	0.8	2.07	0.26	1.49
TBND-136 18.9	6.8	25.3	20.7	2	208.3	1.6	3.5	6.5	267	<0.5	263.4	21.9	36.5	86.1	10.98	51.8	9.65	2.75	7.31	1.1	4.77	0.84	2.38	0.36	2.11
TBND-136 21.1	4.7	15.5	13.8	1	217.2	0.9	1.9	0.9	297	<0.5	172.4	17.1	22.9	53.9	7.43	39.3	7.24	2.17	5.58	0.86	4.03	0.68	1.66	0.23	1.57
TBND-125 22.0	7.9	28.2	62.4	2	468.4	2.1	4.4	5.6	286	0.6	319.7	22.3	44.6	103.5	13.4	59.1	10.21	3.02	7.71	1.22	5.39	0.98	2.53	0.36	2.18
TBND-125 23.8	5.8	25.5	40.5	2	435	1.6	3.3	4.3	328	0.5	239.2	20.4	37.3	90.9	11.56	54.4	9.07	2.93	7.14	1.11	5.33	0.91	2.25	0.3	1.96
TBND-125 24.8	3.3	12.7	3.4	1	154	0.7	1.5	0.5	287	<0.5	134	15.2	19	43.3	6.3	27.5	5.93	1.87	5.12	0.81	4.31	0.75	1.75	0.25	1.42
TBND-125 29.8	2.9	10.4	19.2	<1	329.8	0.9	1.4	0.4	164	<0.5	116.2	8.6	15.9	37.8	4.82	24.7	4.12	1.18	3.34	0.5	2.31	0.46	0.92	0.13	0.85
TBND-023 107.8	9.1	34.5	27.8	2	132.2	2.3	3.5	3.6	215	0.6	362.4	33.1	44.3	107	14.31	60	12.88	3.24	9.77	1.51	6.81	1.35	3.21	0.45	2.54
TBND-023 112.6	3.4	4.4	183.7	<1	161.1	0.8	17.7	8	<8	<0.5	135.8	11.5	21.1	49.9	5.68	19.1	3.65	0.47	2.89	0.52	2.53	0.47	1.56	0.24	1.71
TBND-023 115.9	8.7	35.3	11.3	2	107.3	2.3	3.8	5.3	232	<0.5	353.8	43.9	42.7	98.1	13.26	62.6	12.77	3.13	10.99	1.78	8.67	1.56	4.08	0.54	3.19
BL08-75 152.5	10.5	37	48.1	3	55.8	2.4	5.5	2.6	193	2	407.4	30.7	29.7	72.8	9.4	36.3	8.27	1.8	7.43	1.23	6.18	1.31	3.65	0.52	2.8
BL08-75 157.5	8.5	36.5	21.8	1	45.1	2.5	4.6	2.3	133	0.9	360.8	31.2	13.3	35.7	5.14	21.5	5.42	1.46	5.59	1.05	5.49	1.29	3.41	0.54	3.19
BL08-75 161.5	8.7	38.1	24.1	3	55.5	2.1	5	1.6	110	0.9	377.6	33.7	54.8	129.6	16.71	75.7	13.65	3.26	10.85	1.62	7.52	1.37	4.46	0.48	3.49
BL08-75 169.2	3.8	12.6	8.1	<1	63.5	0.8	1.8	0.7	462	1.3	139.6	15.3	24.5	53.2	7.32	35.1	5.92	1.91	5.41	0.76	3.89	0.65	1.67	0.19	1.12
BL08-75 171.8	2.2	7.4	0.7	<1	73.1	0.5	0.9	0.3	142	<0.5	104.2	9.1	9.6	27.3	3.63	15.4	3.55	0.99	3.15	0.47	2.25	0.4	1.18	0.14	0.61
BL08-75 179.0	2.1	6.6	17.5	1	195.9	0.5	0.8	0.3	123	<0.5	96.1	6.3	10.4	26.2	3.51	14.7	3.21	0.92	2.53	0.37	1.62	0.32	0.81	0.11	0.48
BL08-78 162.65	6.1	9.2	7.8	2	1136.8	0.5	14.4	4.3	143	0.7	258	25.3	85.8	192	24.62	110.8	18.54	4.39	13.6	1.55	5.65	1.02	2.42	0.33	2.08
BL08-78 166.28	4.2	17.5	38.3	1	326.5	1.9	4.7	1.4	182	2.6	185	19.2	32.9	73.2	9.3	33.2	6.86	1.95	5.65	0.74	4.14	0.66	1.8	0.28	1.56
BL08-78 169.57	3.1	13.7	41.4	3	151.5	1.8	2.9	4	130	6.7	130.4	15.2	10.5	26.8	3.74	14.4	4	1.19	3.29	0.52	2.4	0.45	1.19	0.2	1.11
BL08-78 178.7	5.1	21.4	42.9	2	234.9	2.7	4.5	1.7	254	1	208.2	20.7	42.2	91.2	11.7	45.9	9.31	2.66	7.11	0.91	4.74	0.8	2.08	0.26	1.75
BL08-78 181.7	3.5	13.1	19.3	2	239.2	1.2	2.3	0.9	425	0.9	137.9	14.9	24	54.7	7.39	31.6	6.11	1.77	4.88	0.66	3.26	0.55	1.61	0.2	1
BL08-78 186.3	7.1	28.1	23.7	3	173.7	1.9	4.5	1.4	147	1.7	293.2	27.4	51	109.1	14.64	57.9	11.34	3.14	8.43	1.14	6.5	0.95	2.61	0.38	1.99
BL08-78 188.0	8.5	28.7	24.5	1	120.1	1.7	4.6	1.2	174	1	303.7	28.2	50.8	112.6	14.46	58.9	10.67	2.92	9.14	1.15	5.21	1	2.35	0.3	2.35
BL08-78 190.3	5.4	18.4	18.6	<1	204.4	1.4	2.8	1	297	1.2	173.1	17.6	29.5	65.1	8.21	34.9	6.46	2.09	5.61	0.76	3.5	0.67	1.71	0.22	1.39
BL08-78 192.1	5.7	18	4.5	2	113.1	1.3	2.8	0.9	206	0.6	211.1	21.8	33	75.2	9.8	41.3	8.56	2.56	6.74	1	4.8	0.8	2.1	0.26	1.61
BL08-78 193.9	3	11.2	12.9	<1	311.1	0.7	1.2	0.5	173	<0.5	112.3	11.4	16.4	39.1	5.13	20.7	4.44	1.19	3.82	0.52	2.63	0.45	1.08	0.13	0.96
BL08-78 204.2	2.2	6.6	9.3	<1	272.3	0.4	0.8	0.3	145	0.7	79.9	8.5	11.4	26.2	3.56	14.5	3.12	0.86	2.66	0.37	1.81	0.37	0.74	0.1	0.6
BL08-146 158.4	8.1	26.5	16.5	3	127.2	1.8	4.3	1.4	170	1.9	308.3	24.3	69.7	151.3	18.07	71.3	12.63	3.42	9.43	1.21	5.11	0.9	2.47	0.3	1.99
BL08-146 161.2	10.5	33.7	19.1	2	126.1	2.1	5	1.6	159	1.4	372.2	27.9	50.3	116.8	15.75	69.3	11.94	2.94	9.69	1.27	5.85	1.1	2.65	0.35	2.26
BL08-146 169.6	4.4	12.6	19.3	<1	276	1	2.1	0.6	611	<0.5	135.9	15.8	20.8	46.5	6.21	29.7	5.26	1.57	4.58	0.67	3.3	0.62	1.31	0.16	1.03
BL08-146 174.3	3	8.4	10.1	1	263.1	0.7	1	0.4	157	<0.5	91	9.6	15.3	32.9	4.56	19	3.66	1.24	3.2	0.46	1.75	0.34	1	0.12	0.81
BL08-147 153.1	3.2	4	87.9	<1	276.3	0.4	4.1	1.5	91	1.2	118.5	6.8	4.2	9.1	1.25	6	1.23	0.28	1.09	0.21	0.99	0.27	0.69	0.1	0.66
BL08-147 166.8	6.1	17.6	52.4	<1	212.2	1.5	4.2	1.4	238	1.6	219.9	22.4	40.3	88.9	10.92	45.5	8.5	2.24	6.78	0.95	4.94	0.89	2.06	0.26	1.6
BL08-147 174.5	9.6	23.7	30	2	134.7	1.6	3.6	1.4	210	6	288.1	26.3	47.9	108.9	13.3	51	10.99	2.92	8.76	1.13	5.7	1.06	2.79	0.33	2.17
BL08-147 176.7	4	14.5	18.9	<1	343	1	2.4	0.7	339	1	159.5	16.9	23.4	54.4	7.38	31.7	6.28	2.04	5.41	0.76	3.59	0.7	1.63	0.2	1.19
BL08-147 177.9	3.6	10.8	6.4	1	94.9	0.5	1.1	0.5	218	<0.5	124	12.5	18.3	41	5.43	22.1	4.71	1.36	3.84	0.55	2.46	0.54	1.02	0.16	0.86

Sample	4B Lu PPM 0.01	3BMS Au PPB 1	3BMS Pt PPB 0.1	3BMS Pd PPB 0.5
TBND-60 15.2	0.28	<1	0.8	<0.5
TBND-60 17.5	0.28	<1	<0.1	<0.5
TBND-60 20.1	0.33	<1	<0.1	<0.5
TBND-60 21.4	0.27	<1	<0.1	<0.5
TBND-60 22.3	0.19	<1	6.8	0.8
TBND-60 23.0	0.19	1	28.3	12.1
TBND-60 25.8	0.15	1	59	52.5
TBND-60 32.9	0.12	5	151.5	147.9
TBND-95 93.8	0.12	<1	9	27.1
TBND-95 94.9	0.17	<1	3.6	2.1
TBND-95 99.1	0.5	<1	0.4	<0.5
TBND-95 101.9	0.32	<1	0.5	<0.5
TBND-124 49.5	0.14	4	106.3	97.3
TBND-124 88.9	0.13	<1	9.8	10.5
TBND-124 91.5	0.2	<1	0.2	<0.5
TBND-124 94.7	0.28	<1	0.4	<0.5
TBND-136 16.6	0.26	<1	1	<0.5
TBND-136 18.9	0.23	<1	<0.1	<0.5
TBND-136 21.1	0.24	5	32.1	4.2
TBND-125 22.0	0.29	<1	<0.1	<0.5
TBND-125 23.8	0.25	<1	<0.1	<0.5
TBND-125 24.8	0.2	2	24.8	3.1
TBND-125 29.8	0.11	<1	33.1	28.2
TBND-023 107.8	0.34	<1	<0.1	<0.5
TBND-023 112.6	0.21	<1	<0.1	<0.5
TBND-023 115.9	0.4	<1	<0.1	<0.5
BL08-75 152.5	0.46	<1	<0.1	<0.5
BL08-75 157.5	0.48	<1	<0.1	<0.5
BL08-75 161.5	0.43	<1	<0.1	<0.5
BL08-75 169.2	0.16	<1	0.5	<0.5
BL08-75 171.8	0.09	13	146.3	108.3
BL08-75 179.0	0.09	14	242.8	240.9
BL08-78 162.65	0.27	20	3.8	3.6
BL08-78 166.28	0.24	12	143.6	120
BL08-78 169.57	0.16	6	11.1	4.8
BL08-78 178.7	0.26	1	0.6	0.6
BL08-78 181.7	0.17	1	0.4	<0.5
BL08-78 186.3	0.31	1	0.6	0.7
BL08-78 188.0	0.3	<1	<0.1	<0.5
BL08-78 190.3	0.19	<1	1.1	0.8
BL08-78 192.1	0.22	1	0.1	<0.5
BL08-78 193.9	0.13	3	32	25.1
BL08-78 204.2	0.1	<1	7.6	8
BL08-146 158.4	0.25	1	0.8	0.6
BL08-146 161.2	0.31	<1	0.4	<0.5
BL08-146 169.6	0.19	<1	0.1	<0.5
BL08-146 174.3	0.13	2	26.7	21.6
BL08-147 153.1	0.13	<1	1.2	1.1
BL08-147 166.8	0.25	<1	0.1	<0.5
BL08-147 174.5	0.29	<1	0.2	<0.5
BL08-147 176.7	0.22	<1	3.9	1.8
BL08-147 177.9	0.15	54	557	407.2

Appendix E

Raw XRF Data

Appendix E - Raw XRF Data

Sample ID	Depth (m)	SiO_2	TiO_2	Al_2O_3	Fe_2O_3	MnO	MgO	CaO	Na_2O	K_2O	P_2O_5	LOI	Sum
TBND-60 15.2	15.2	62.5	2.2	15.2	7.2	0.1	3.0	0.6	4.4	1.8	0.3	2.7	99.8
TBND-60 17.5	17.5	52.6	2.3	13.9	11.3	0.1	3.2	6.5	3.6	1.3	0.4	5.2	100.5
TBND-60 20.1	20.1	55.4	2.0	14.9	8.1	0.1	2.0	5.9	5.5	0.6	0.5	4.6	99.4
TBND-60 21.4	21.4	49.3	2.2	13.3	11.1	0.1	5.0	4.6	3.6	1.2	0.4	4.9	95.6
TBND-60 22.3	22.3	48.3	2.0	9.4	10.8	0.1	9.1	8.8	2.7	0.4	0.2	2.8	94.6
TBND-60 23.0	23	49.9	1.6	8.0	10.6	0.2	11.9	9.8	1.8	0.3	0.2	3.8	98.1
TBND-60 25.8	25.8	43.0	1.3	6.0	14.3	0.2	22.2	4.9	1.0	0.5	0.2	5.8	99.1
TBND-60 32.9	32.9	41.9	1.1	4.5	15.3	0.2	23.6	4.5	0.6	0.3	0.2	7.0	99.0
TBND-95 93.8	93.8	37.3	1.6	6.2	17.3	0.2	20.2	5.5	0.3	0.2	0.2	9.6	98.5
TBND-95 94.9	94.9	40.7	2.4	8.8	18.9	0.3	16.6	3.4	1.2	0.4	0.3	6.0	99.0
TBND-95 99.1	99.1	45.6	2.7	15.1	14.6	0.1	6.8	5.1	3.1	0.3	0.4	8.7	102.4
TBND-95 101.9	101.9	75.3	0.1	13.5	1.2	0.0	0.8	0.4	3.1	5.8	0.1	0.8	101.0
TBND-124 49.5	49.5	43.8	1.5	6.3	14.0	0.2	20.6	5.2	1.0	0.5	0.2	5.5	98.8
TBND-124 88.9	88.9	40.7	1.8	7.2	17.3	0.2	20.1	3.9	1.1	0.6	0.2	4.6	97.7
TBND-124 91.5	91.5	34.4	4.5	12.8	20.2	0.1	4.5	6.3	2.5	1.4	0.5	3.8	90.9
TBND-124 94.7	94.7	45.7	2.7	14.8	12.3	0.1	4.3	7.4	4.0	0.5	0.4	7.1	99.3
TBND-136 16.6	16.6	55.3	2.2	13.5	11.9	0.1	5.3	1.6	3.3	1.4	0.3	3.2	98.1
TBND-136 18.9	18.9	52.7	2.6	14.1	11.2	0.1	4.1	4.6	3.8	0.8	0.4	6.0	100.4
TBND-136 21.1	21.1	50.2	1.9	8.8	12.0	0.2	9.4	9.7	2.4	0.5	0.2	3.5	98.8
TBND-125 22.0	22	54.6	2.7	15.4	11.4	0.0	3.1	1.7	4.3	1.6	0.4	3.0	98.1
TBND-125 23.8	23.8	54.0	3.0	14.8	13.9	0.1	4.5	2.2	3.7	1.2	0.4	3.3	101.0
TBND-125 24.8	24.8	49.0	1.8	7.8	13.9	0.4	10.0	9.2	2.3	0.2	0.2	4.0	98.7
TBND-125 29.8	29.8	42.8	1.4	5.9	14.3	0.2	23.0	4.9	0.8	0.4	0.2	6.9	100.8
TBND-023 107.8	107.8	50.6	3.1	16.3	10.9	0.2	4.9	6.0	4.6	0.8	0.5	5.6	103.4
TBND-023 112.6	112.6	70.1	0.1	12.6	1.8	0.0	0.8	0.3	2.5	6.9	0.1	1.1	96.3
TBND-023 115.9	115.9	47.3	2.8	15.6	12.0	0.1	3.9	6.0	4.5	0.4	0.5	5.1	98.2
BL08-75 152.5	152.5	57.7	2.8	15.1	9.0	0.1	5.8	0.6	2.8	2.0	0.3	4.2	100.3
BL08-75 157.5	157.5	59.3	2.0	14.7	8.5	0.1	5.9	1.0	3.1	1.4	0.5	3.5	99.8
BL08-75 161.5	161.5	58.3	2.0	14.5	6.8	0.0	5.2	3.1	3.5	1.6	0.5	4.3	99.7
BL08-75 169.2	169.2	46.2	2.6	13.6	15.5	0.1	6.6	4.9	3.1	0.5	0.2	5.3	98.6
BL08-75 171.8	171.8	46.1	1.0	3.9	10.2	0.2	22.1	9.7	0.1	0.0	0.1	9.3	102.8
BL08-75 179.0	179	41.1	0.9	3.6	16.0	0.2	25.7	4.4	0.2	0.3	0.1	7.7	100.3
BL08-78 162.65	162.65	55.5	0.7	12.9	8.7	0.2	9.1	8.3	2.2	0.3	0.9	2.9	101.8
BL08-78 166.28	166.28	59.3	1.4	13.5	8.3	0.0	6.4	1.6	3.1	1.8	0.2	3.2	98.8
BL08-78 169.57	169.57	69.8	1.0	11.5	7.4	0.1	5.3	1.2	2.4	1.4	0.3	3.5	103.8
BL08-78 178.7	178.7	54.2	2.1	14.7	10.3	0.1	3.1	5.5	4.0	2.6	0.3	4.7	101.6
BL08-78 181.7	181.7	47.6	2.5	14.1	14.5	0.1	5.1	5.9	3.7	0.9	0.2	6.1	100.7
BL08-78 186.3	186.3	54.4	2.1	15.1	10.4	0.0	5.7	1.9	3.9	1.7	0.4	3.1	98.8
BL08-78 188.0	188	54.9	2.5	14.9	10.4	0.1	4.3	4.0	4.3	1.9	0.5	4.3	101.9
BL08-78 190.3	190.3	52.5	3.4	15.3	12.4	0.2	6.0	4.5	4.0	1.2	0.3	4.9	104.7
BL08-78 192.1	192.1	52.3	1.6	9.3	9.0	0.3	8.1	13.1	1.1	0.3	0.3	3.7	99.1
BL08-78 193.9	193.9	44.2	1.2	5.0	13.8	0.2	20.9	7.5	0.7	0.4	0.1	5.7	99.7
BL08-78 204.2	204.2	41.5	0.9	3.5	16.3	0.2	25.4	4.0	0.4	0.3	0.1	5.9	98.5
BL09-146 158.4	158.4	59.8	2.1	12.5	9.2	0.0	5.4	2.0	3.4	1.1	0.4	3.5	99.3
BL09-146 161.2	161.2	55.3	2.2	14.7	10.1	0.0	6.2	1.8	3.7	1.3	0.5	3.9	99.6
BL09-146 169.6	169.6	45.4	2.7	13.7	15.8	0.1	7.1	4.6	3.3	1.0	0.2	5.6	99.4
BL09-146 174.3	174.3	43.4	1.1	5.1	15.0	0.2	21.3	6.6	0.6	0.3	0.1	6.1	99.8
BL09-147 153.1	153.1	63.8	0.5	16.8	5.0	0.1	3.1	0.6	4.9	2.6	0.1	2.6	100.0
BL09-147 166.8	166.8	54.8	1.8	15.3	9.0	0.0	5.2	3.4	3.7	1.9	0.3	5.0	100.4
BL09-147 174.5	174.5	56.2	2.2	14.2	9.7	0.0	6.9	1.3	3.0	1.7	0.3	4.2	99.7
BL09-147 176.7	176.7	47.7	2.3	13.8	13.6	0.2	6.6	5.6	3.3	0.7	0.2	6.2	100.1
BL09-147 177.9	177.9	43.5	1.5	6.2	14.8	0.3	19.2	5.9	0.7	0.2	0.2	6.5	98.9